Fabrication, characterisation, and application of functional protein aggregates derived from faba bean protein isolates

A thesis presented in partial fulfilment of the requirements

for the degree of

Doctor of Philosophy in Food Technology

at Massey University, Auckland, New Zealand

Yinxuan Hu

2025

Abstract

This thesis explores the preparation, characterisation, and applications of plant protein aggregates, derived from faba bean protein isolate (FPI). The formation of FPI aggregates was accomplished by various methods, including pH adjustments, salt addition, heat treatment, sonication, and thermosonication (TS). The physico-chemical properties and technofunctional characteristics of FPI aggregates formed by different treatments, such as ζ-potential, solubility, emulsification capability, and particle sizes, were also characterised in this study. Furthermore, the microstructure of the FPI aggregates in solutions was examined using various techniques, including light scattering, microscopies (TEM and SEM), and small angle neutron scattering. Additionally, this project further developed the TS method for formation of FPI fibrillar aggregates at pH 2 and amorphous aggregates at pH 7. The characteristics of FPI aggregates formed by TS and conventional heat treatment (CH) were analysed by sodium dodecyl sulfate-polyacrylamide gel electrophoresis (SDS-PAGE) and liquid chromatography linked to tandem mass spectrometry (LC-MS/MS). In addition, Thioflavin T (ThT) fluorescence, Fourier-transform infrared spectroscopy (FTIR) and circular dichroism (CD) were applied to investigate the differences in secondary structure between CH-treated FPI and TS-treated FPI, indicating that TS effectively converted FPI structures to be enriched in β-sheets. The gelation behaviours of different FPI aggregates at 10 wt% were studied by examining their rheological properties and observing the microstructure using scanning electron microscopy (SEM), indicating that TS-treatment of FPI at pH 7 facilitated the formation of stronger protein hydrogels.

The functionality of FPI aggregates fabricated from various treatments at the oil-water and oil-air-water interfaces was also characterised. Emulsions (O/W) with various oil factions (ϕ) ranging from 0.2 (dilute emulsions) to 0.75 (high internal phase emulsions, HIPEs), were stabilised by suitable FPI aggregates selected based on their different physico-chemical properties. The findings indicate that higher FPI concentrations (~5 wt%) and pH

values (~pH 9) result in better emulsification capabilities. Among all FPI aggregates studied in this project, fibrillar aggregates exhibited the best emulsification performance as they could stabilise emulsions with oil content up to 75% (v/v). However, emulsions stabilised by FPI aggregates induced from TS at pH 7 had the greatest application potential due to their long-term stability (up to 28 days) and compatibility with a neutral pH environment. Therefore, another study in this thesis was to investigate the application of FPI aggregates in stabilising vegetable oil-based whipped creams. TS-treated FPI at pH 7 exhibited superior functional properties compared to other treatments, such as CH and ultrasonication (US), in terms of visual appearance, overrun, and stability of whipped cream.

Overall, this project provides fundamental insights into the physical-chemical and techno-functional properties of FPI aggregates, including their ability to stabilise and form emulsions, gels, and foams, with an emphasis on their potential applications in innovative food products such as 3D-printed emulsion gels and plant based whipped cream. The enhanced physicochemical and techno-functional properties of FPI aggregates fabricated in this study showed a great application potential as novel food ingredients for formulation of plant-based food products.

Acknowledgement

With unwavering determination and belief, I have completed the most important part in my PhD journey, which began in March 2022 and concluded in January 2025. This journey was filled with the challenges of the restructuring of Massey University and moments of disappointment. Besides these various obstacles, I also experienced many moments of joy, success, and support that made the journey memorable. When I write this acknowledgement, I am overwhelmed with gratitude toward all who have been part of this remarkable chapter of my life.

First and foremost, I owe my deepest thanks to my incredible supervisory team: Dr Zhi Yang, Professor Aiqian Ye, Dr Lirong Cheng, Dr Sung Je Lee, and Professor Marie Wong. Their invaluable guidance, generous support, constructive feedback, and shared wisdom have been fundamental to my research and have greatly influenced my growth as an independent researcher. I am especially grateful to my supervisors, Prof. Aiqian Ye and Dr Zhi Yang, for offering me and supporting me with this invaluable opportunity to pursue my PhD degree. Their kind support was not only in academia but also in various aspects of my personal journey. I extend my heartfelt appreciation to Dr Lirong Cheng and Dr Sung Je Lee for their dedicated time and insightful discussions. Their expertise has been instrumental in shaping my research approach and career aspirations. My sincere gratitude goes to Professor Maire Wong for her strong support when we were facing the “cut off” situation at the Albany campus. She gave me the opportunity and workspace I needed in my lab work, thesis writing, and presentations.

I deeply appreciate Riddet Institute for continuously funding my conference travel grants. I am also grateful to Massey University for offering me the doctoral scholarship. Without it, I would not have had the opportunity to start chasing my degree. Australian Neutron Science and Technology Organisation (ANSTO) also provided crucial support during my research journey.

My heartfelt thanks also go to the staff and colleagues at Massey University, the Riddet Institute, the Manawatu Microscopy and Imaging Centre, and ANSTO. I am immensely grateful to the laboratory managers and staff for their expert guidance and extensive training, which were crucial for the successful completion of this project. Special thanks go to the Miss Ruth Brooks for her unwavering assistance. I also want to thank Dr Yanyu He, Dr Matthew Savoian, Arthur Xu, Rachel Liu, and Michelle Tamehena; their support was vital in completing my research.

This journey was made even more meaningful by the support and companionship of friends who lifted my spirits through challenging times. My heartfelt gratitude goes to my friends: Cheng Cheng, Yang Li, Peizhen Li, Rong Cong, Peng Jin, Yuchen Lin, and Shu Yang for sharing countless joyful moments. I am also grateful to my office mates and study mates who encouraged and inspired me, especially Dr Mengxiao Yang, Dr Boying Wang, Dr Jia Sun, Youwei Wang and many other incredible people.

Finally, I extend my deepest gratitude to my dear parents, grandparents, and my partner Ms Tingting Yang, for their unconditional support, encouragement, and love. Their presence has been my anchor throughout this journey, and I am truly grateful for everything they have done to support me.

Table of Contents

List of Figures

List of Tables

List of Abbreviations

AFM	Atomic force microscopy
AI	Artificial intelligence
ANOVA	Analysis of variance
ANS	8-anilino-1-naphthalene sulphonate
CD	Circular dichroism
CH	Conventional heat treatment
CLSM	Confocal laser scanning microscopy
DLS	Dynamic light scattering
DTT	Dithiothreitol
FPC	Faba bean protein concentrate
FPI	Faba bean protein isolate
FTIR	Fourier-transform infrared spectroscopy
GDL	Glucono-δ-lactone
G′	Storage modulus
G″	Loss modulus
HIPEs	High-internal phase emulsions
HPH	High-pressure homogenisation
HPP	High hydrostatic pressure processing
H_0	Surface hydrophobicity
IFT	Interfacial tension
IDA	Iodoacetamide
LC-MS/MS	Liquid chromatography linked to tandem mass spectrometry
LPI	Lentil protein isolate
LVR	Linear viscoelastic region
ML	Machine learning
MMIC	Manawatu Microscopy and Imaging Centre
MPI	Mung bean protein isolates

OH	Ohmic heat treatment
PEF	Pulsed electric field
pI	Isoelectric point
PPI	Pea protein isolate
PoPI	Potato protein isolate
PSD	Particle size distribution
QPI	Quinoa protein isolates
SAXS	Small-angle X-ray scattering
SANS	Small-angle neutron scattering
SD	Standard deviation
SDS	Sodium dodecyl sulphate
SDS-PAGE	Sodium dodecyl sulphate-polyacrylamide gel electrophoresis
SLD	Scattering length density
SPI	Soybean protein isolate
TEM	Transmission electron microscopy
ThT	Thioflavin T
TS	Thermosonication
US	Ultrasonication
UV	Ultraviolet
WPI	Whey protein isolates
γ_b	Breaking strain
σ_b	Breaking stress
ϕ	Oil fraction

List of Publications

Hu, Y., Cheng, L., & Yang, Z. (2025). Impact of various physical treatments on physicochemical and microstructural characteristics of vegetable oil-based whipped cream stabilised by faba bean protein isolate. *Food Hydrocolloids, 163*, 111084. https://doi.org/10.1016/j.foodhyd.2025.111084

Hu, Y., Cheng, L., Gilbert, E. P., Lee, S. J., & Yang, Z. (2024). Impact of thermosonication at neutral pH on the structural characteristics of faba bean protein isolate dispersions and their physicochemical and techno-functional properties. *Food Hydrocolloids*, *154*, 110140. https://doi.org/10.1016/j.foodhyd.2024.110140

Hu, Y., Cheng, L., Gilbert, E. P., Loo, T. S., Lee, S. J., Harrison, J., & Yang, Z. (2024). Fibrillisation of faba bean protein isolate by thermosonication for process efficacy: Microstructural characteristics, assembly behaviour, and physicochemical properties. *Food Hydrocolloids*, *154*, 110127. https://doi.org/10.1016/j.foodhyd.2024.110127

Hu, Y., Cheng, L., Lee, S. J., & Yang, Z. (2023). Formation and characterisation of concentrated emulsion gels stabilised by faba bean protein isolate and its applications for 3D food printing. *Colloids and Surfaces A: Physicochemical and Engineering Aspects*, *671*, 131622. https://doi.org/10.1016/j.colsurfa.2023.131622

Hu, Y., Ye, A, Cheng, L., Lee, S. J., & Yang, Z. (2025). Recent progress on fabrication, characterisation and application of functional protein aggregates derived from plant proteins. *Critical Reviews in Food Science and Nutrition.* (Under peer-review).

Conference presentations

Hu, Y., Cheng, L., Gilbert, E. P., Loo, T. S., Lee, S. J., Harrison, J., & Yang, Z. (Nov 2023) Fibrillisation of faba bean protein isolate by thermosonication for process efficacy: microstructural characteristics, assembly behaviour, and physicochemical properties. Oral presentation at *the 7th International Conference on Food Structures, Digestion and Health*. Queenstown, New Zealand.

Hu, Y., Ye, A., Cheng, L., Gilbert, E. P., Lee, S. J., & Yang, Z. (Aug 2024). Impact of thermosonication at neutral pH on the structural characteristics of faba bean protein isolate dispersions and their physicochemical and techno-functional properties. Oral presentation at *Riddet Institute Conference and Student Colloquium*. Palmerston North, New Zealand.

Hu, Y., Ye, A., Yang, Z., Cheng, L., Gilbert, E. P., Lee, S. J., & Wong, M. (Nov 2024). Impact of thermosonication at neutral pH on structures and functionalities of faba bean protein isolate. Oral presentation at *the 17th International Hydrocolloids Conference (IHC)*. Palmerston North, New Zealand.

Chapter 1 Introduction

Currently, the world is potentially facing a food crisis due to environment-related challenges (e.g., climate change and water scarcity) (Amiri, et al., 2024; Karabulut, et al., 2024), and the rapidly increasing world population (approximately 9.7 billion by 2050) (Karabulut, et al., 2024). As a result, in the expansive field of food science, plant proteins have emerged as important components due to their abundant availability, cost-effectiveness, and sustainability (Akyazi, et al., 2020). Recently, plant proteins have become popular worldwide, and the plant-based foods market is predicted to account for approximately 7.7 % of the global protein market by 2030, with a market value exceeding 162 billion USD (De Angelis, et al., 2023; Karabulut, et al., 2024; Veronika & Samantha, 2021).

Nowadays, plant proteins are widely applied in the food industry because of their versatility, nutritional benefits, and eco-friendly characteristics. There are many products developed from plant-based proteins, including burgers (De Marchi, et al., 2021), sausages (Flores & Piornos, 2021), and dairy alternatives (Beegum, et al., 2022). Most of these applications rely on the technofunctionality of plant proteins, which facilitates their use in food systems as ingredients, such as emulsifiers (Nivala, et al., 2021), gelling agents (Luo, et al., 2021), and foaming agents (Ye, et al., 2021). However, plant proteins have limited technofunctionality compared to animal-sourced proteins, making further application and commercialisation of plant protein products difficult in the food industry (Karabulut, et al., 2024). Therefore, several innovative methods and technologies have been recently implemented to produce different types of functional plant protein aggregates to improve the limited functionalities of plant proteins (Akharume, et al., 2021; Nasrabadi, et al., 2021).

Among various plant proteins, plant protein extracted from faba beans (*Vicia faba*) is one of the most important plant protein sources. Faba beans, also known as broad beans, fava

beans, horse beans, and field beans, contain a large amount of protein (~27-34 % of dry weight depending on varieties) (Samaei, et al., 2020). It is ranked as the third most important grain legume in the world after soybean and chickpea (Gu, et al., 2020). The major proteins present in faba beans are 11S globulin, 7S globulin, accounting for 69.5-78.1% of the total protein, followed by glutelin (~12.0-18.4%), prolamin (~1.83-3.57%), and albumin (1.41-3.01%) (Alghamdi, 2009). Although faba bean protein is a promising food ingredient, it still has far less research and application compared to other plant-based proteins such as soy and pea (Rahate, et al., 2021).

Protein aggregation from food proteins can be frequently observed in our daily lives, including in tofu and cheese making, egg cooking, and bread making. Additionally, functional protein aggregates in the food industry, characterised by their specific and controllable physicochemical properties, play a crucial role in determining the texture, stability, and nutritional quality of final products (Zhu, Bassey, et al., 2022). For plant proteins, the general strategy for inducing plant protein aggregates is usually based on physical, chemical, enzymatic, fermentative, and combined processes to form plant protein aggregates ranging from nano to macro scale (Nasrabadi, et al., 2021). There are many external factors that can affect plant protein aggregation, including temperature (Bühler, et al., 2020), pressure (Luo, et al., 2021), pH (Hu, et al., 2023), ions (Langton, et al., 2020), and processing time (Zhong & Xiong, 2020). These factors can influence the thermodynamic state, structure, and conformations of proteins (Karabulut, et al., 2024).

There are many methods that have been applied to characterise the formed plant protein aggregates, and most of them are based on two aspects (i.e. physicochemical and microstructural properties). Physicochemical properties, such as solubility, particle size, and surface hydrophobicity, can be determined by spectrophotometry (Luo, Yang, et al., 2022), dynamic light scattering (DLS) (Hu, Cheng, Gilbert, Lee, et al., 2024), and fluorescence spectrometry (Yan, et al., 2021). Moreover, the physicochemical properties of

proteins are closely related to their microstructural conformation. Therefore, advanced instruments are used to observe the microstructure of formed plant protein aggregates, including light microscopy, transmission electron microscopy (TEM) (Hu, Cheng, Gilbert, Loo, et al., 2024), atomic force microscopy (AFM) (Herneke, Karkehabadi, et al., 2023), and small-angle neutron scattering (SANS) (Hu, Cheng, Gilbert, Loo, et al., 2024).

From a functionality point of view, plant protein aggregates have been widely studied recently. Researchers are working to find the potential of functional plant protein aggregates for broader applications in the food industry. For example, Wynnychuk, et al. (2021) formed lentil protein fibrillar/particulate aggregates through heat treatment (90 °C for 2 h), which had better emulsifying ability than the native state of lentil proteins. Additionally, Li, Dai, et al. (2024) found that stirred media milling transforms the aggregate state of pea proteins, enhancing their physicochemical properties and significantly improving gelation behaviour. Both studies emphasise the preparation of plant protein aggregates with higher functional performance and applicability than native proteins, enabling their future application in sustainable and innovative food products.

Therefore, the overall aim of this project was to provide an in-depth characterisation of the physiochemical properties of plant protein aggregates, such as solubility, particle size, microstructure, and ζ-potential, taking faba bean protein as an example. Additionally, the techno-functional properties (e.g. emulsifying ability, gelling behaviour, and foaming ability) of variously faba bean protein aggregates were determined. Different protein aggregate structures were also investigated for their use in designing different types of new food systems.

This thesis consists of 6 chapters, including **Chapter 1**: Introduction, **Chapter 2**: Literature Review, Experimental Chapters **(Chapters 3-6**), and **Chapters 7**: Overall Conclusions and Recommendation.

Besides this Chapter (**Chapter 1**), **Chapter 2** is a literature review of recent progress on fabrication, characterisation and application of functional protein aggregates derived from plant proteins. This review summarises the current research progress on plant protein aggregates, focusing on recent developments in the mechanisms, fabrication, physicochemical properties, microstructure, functional properties, and emerging applications of plant protein aggregates. By highlighting the latest research trends and identifying gaps in the current knowledge, this review will provide insights for future research that could further unlock the potential of plant protein aggregates and commercial applications.

Chapter 3 discusses the formation of various faba bean protein isolate (FPI) aggregates at different protein concentrations, pH values and salts (NaCl and $CaCl_2$), demonstrating that the effectiveness of FPI aggregates in stabilizing concentrated oil-in-water emulsions (oil fraction: ϕ=0.5) for 3D food printing. This chapter provides a new route to fabricate FPI aggregates that could sufficiently stabilise concentrated emulsion gels, Furthermore, effect of different factors such as protein concentrations and pHs on formation, characteristics and 3D printability of FPI aggregates stabilised emulsion gels were systematically studied.

Chapter 4 describes the formation of FPI fibrillar aggregates by thermosonication (TS) and/or conventional heat (CH) treatments and their use for the formation of FPI fibrillar thermoreversible gels and high-internal phase emulsions (HIPEs). In this chapter, our work demonstrated that TS could significantly accelerate the fibrillisation process of plant proteins, producing fibrillar aggregates with superior gelation and emulsification properties compared to conventional heating (CH). This chapter suggests that TS is an efficient method for producing functional FPI aggregates with promising applications in food processing.

Chapter 5 investigates the formation of a new type of FPI amorphous aggregates acquired by TS for their application in stabilising emulsion systems with a long-term storage (four weeks). In Chapter 5, TS was applied to FPI under a neutral pH value (pH 7) to observe the differences of FPI aggregates. This work showed that TS treatment significantly enhanced the formation of FPI protein aggregates rich in β-sheet secondary structures, resulting in improved solubility, reduced particle size, and the formation of a thermoreversible viscoelastic gel network. Furthermore, emulsions stabilised by TS-treated FPI exhibited smaller oil droplet sizes, greater mechanical strength, and better storage stability than those stabilised by native FPI.

Chapter 6 discusses the preparation of a novel plant-based whipped cream stabilised by FPI amorphous aggregates based on TS technology identified in Chapters 4 and 5. This was aimed to produce a new plant-based whipped cream with superior foaming abilities, which is comparable to commercial whipped cream products. Chapter 6 evaluates the impact of TS on the quality and stability of FPI, and its application in a novel plant-based whipped cream. This chapter provides insights into producing high-quality plant-based whipped cream using TS-treated FPI, offering a potential clean label alternative to animal fats and hydrogenated vegetable oils. This study proved that TS-induced FPI aggregates not only exhibited superior emulsification ability than native proteins, but also had better foaming ability. All these works have pointed out that the potential of TS treatment on the formation of functional plant protein aggregates.

Chapter 7 concludes that the microstructure and technofunctional properties of FPI aggregates are important in stabilising emulsions, gels, and foams. By controlling the formation of different FPI aggregates by various treatments (e.g. pH adjustments, CH, and TS), the functionalities of FPI aggregates can be significantly enhanced. In addition, few future research directions based on findings of this thesis were also provided. Therefore, future work related to the development of plant protein aggregates that can be used in daily

diets can be benefited from the information gained from this project.

MASSEY UNIVERSITY
TE KUNENGA KI PŪREHUROA
UNIVERSITY OF NEW ZEALAND

GRADUATE RESEARCH SCHOOL

STATEMENT OF CONTRIBUTION DOCTORATE WITH PUBLICATIONS/MANUSCRIPTS

We, the student and the student's main supervisor, certify that all co-authors have consented to their work being included in the thesis and they have accepted the student's contribution as indicated below in the Statement of Originality.

Student name:	Yinxuan Hu
Name and title of main supervisor:	Prof. Aiqian Ye
In which chapter is the manuscript/published work?	Chapter 2

Describe the contribution that the student and members of the supervisory team have made to the manuscript/published work:[1]

Yinxuan Hu: Methodology, Investigation, Data curation, Formal analysis, Writing-original draft. Aiqian Ye: Supervision, Funding acquisition, Writing-review & editing. Lirong Cheng: Supervision, Writing-review & editing. Sung Je Lee: Supervision, Writing-review & editing. Zhi Yang: Conceptualization, Investigation, Methodology Supervision, Project administration, Writing-original draft, Writing-review & editing, Funding acquisition.

Please select one of the following three options:

○ The manuscript/published work is published or in press

Please provide the full reference of the research output:

◉ The manuscript is currently under review for publication

Please provide the name of the journal:

Critical Reviews in Food Science and Nutrition

○ It is intended that the manuscript will be published, but it has not yet been submitted to a journal

Student's signature:	Yinxuan Hu Digitally signed by Yinxuan Hu Date: 2025.01.21 20:00:02 +13'00'	Main supervisor's signature:	Aiqian Ye Digitally signed by Aiqian Ye DN: cn=Aiqian Ye, c=NZ, o=Massey University, ou=Riddet Institute, email=A.M.YE@massey.ac.nz Reason: I am approving this document Date: 2025.01.22 10:02:26 +13'00'

This form should be placed at the beginning of each relevant thesis chapter.

[1] Refer to the Massey University Publishing and Authorship guidelines (OneMassey for staff, Stream for students) and/ or Contributor Roles Taxonomy (CRediT) guidelines for guidance.

Chapter 2 Literature review- Recent progress on fabrication, characterisation and application of functional protein aggregates derived from plant proteins[1]

Abstract

This review highlights recent advancements in fabrication, characterisation, and applications of functional plant protein aggregates, emphasizing their growing importance in the food industry because of their sustainability as well as cost-effectiveness compared to animal proteins. While native plant proteins often exhibit limited technofunctional properties, the formation of protein aggregates offers a promising solution. This review explores various aggregation methods, including physical methods (e.g., heat treatment, ultrasonication), chemical modifications (e.g., glycation, acylation), and biological processes (e.g., enzymatic hydrolysis, fermentation), and structural and functional properties changes after these treatments. Advanced characterisation techniques such as spectroscopy, microscopy, and rheological methods, are discussed to assess microstructures and key properties like emulsification, gelation, and foaming. Applications of these aggregates in products like beverages, mayonnaise, and whipped cream are highlighted. The review concludes with future research directions to enhance industrial applications and nutritional benefits, providing insights into the potential of plant protein aggregates for developing innovative and sustainable plant-based food and non-food products.

Keywords: Plant proteins; Protein aggregates; Technofunctional properties; Microstructures; Fat mimics.

[1] This chapter has been submitted for publication: Recent progress on fabrication, characterisation and application of functional protein aggregates derived from plant proteins. *Critical Reviews in Food Science and Nutrition*. (Under peer-review).

2.1 Introduction

Currently, the world is facing a food security challenge because of environmental problems, including climate change and water scarcity (Amiri, et al., 2024; Karabulut, et al., 2024), and a rapidly growing global population (~9.7 billion by 2050) (Karabulut, et al., 2024). Growing awareness of environmental challenges and food security has encouraged researchers to find more sustainable as well as eco-friendly protein sources, which can be achieved by using plant proteins to substitute animal-sourced proteins. Plant proteins are considered more sustainable due to their lower cost, minimal environmental impact, and greater accessibility. (Boland, et al., 2013; Wu, et al., 2014). Therefore, plant proteins have emerged as pivotal food ingredients because of their abundant availability, cost-effectiveness, and sustainability (Akyazi, et al., 2020). By 2023, the plant-based food market is projected to account for approximately7.7 % of the global protein market, with an estimated market value exceeding $162 billion (De Angelis, et al., 2023; Karabulut, et al., 2024; Veronika & Samantha, 2021).

Plant proteins (e.g. soybean and pea proteins) are increasingly used as food ingredients because of their characteristics, including high versatility, desired nutritional benefits, and sustainable properties. There are many products (e.g. burgers) developed from plant-based proteins, including, dairy alternatives (Beegum, et al., 2022), sausages (Flores & Piornos, 2021), and burgers (De Marchi, et al., 2021). These applications primarily rely on the technofunctionality of plant proteins, enabling their effective use as emulsifiers (Nivala, et al., 2021), gelling agents (Luo, et al., 2021), and foaming agents (Ye, et al., 2021). Moreover, the technofunctionality of plant proteins (e.g. gelation behaviour, foaming ability, and emulsifying property), often fall short than those of animal proteins, posing significant challenges for broader applications and commercialisation in the food industry (Karabulut, et al., 2024). To address this, innovative methods and technologies have been researched to create functional plant protein aggregates, significantly improving their functionalities (Nasrabadi, et al., 2021).

Protein aggregates are commonly encountered in everyday life during processes such as tofu and cheese manufacturing, and egg cooking, all of which involve protein aggregation. In addition, protein aggregation can enhance protein functionalities, leading to the formation of functional aggregates (Foegeding & Davis, 2011). Technofunctional properties of protein aggregates are typically related to their physicochemical properties, which impact the nutritional quality, texture, and stability of commercial products (Zhu, Bassey, et al., 2022). For plant proteins, the general strategy for inducing aggregates, ranging from the nano to macro scale, usually involve physical, chemical, enzymatic, fermentative, or combined methods (Nasrabadi, et al., 2021). There are many external factors that can influence plant protein aggregation, such as temperature (Bühler, et al., 2020), pressure (Luo, et al., 2021), pH (Hu, et al., 2023), ionic strength (Langton, et al., 2020), and processing time (Zhong & Xiong, 2020). These factors affect the thermodynamic state, structure, and conformational properties of proteins (Karabulut, et al., 2024).

Various methods have been employed to characterise plant protein aggregates, focusing on their physiochemical and microstructural properties. Physiochemical properties, such as solubility, hydrophobicity, and particle size, are normally determined using techniques like spectroscopy (Luo, Yang, et al., 2022), static and dynamic light scattering (Hu, Cheng, Gilbert, Lee, et al., 2024), and fluorescence spectroscopy (Yan, et al., 2021). Also, the microstructural characteristics of protein aggregates, closely linked to their physicochemical properties, is mainly probed using microscopies such as light microscopy (LM), transmission and scanning electron microscopies (TEM and SEM), confocal laser scanning microscopy (CLSM) (Hu, Cheng, Gilbert, Loo, et al., 2024), atomic force microscopy (AFM) (Herneke, Karkehabadi, et al., 2023), and scattering methods, including small-angle X-ray (SAXS) and neutron scattering (SANS) (Gilbert, 2023).

Recent research has concentrated on improving the functionality of plant protein aggregates andexploring their potential applications as food products. For instance, Wynnychuk, et al. (2021) demonstrated that lentil protein fibrillar/particulate aggregates formed through heat treatment (90 °C for 2 h) exhibited superior emulsification capability compared to native lentil proteins. Similarly, Li, Dai, et al. (2024) reported that stirred media milling altered the aggregation state of pea proteins, significantly improving gelation behaviour. These studies highlight the development of plant protein aggregates with superior technofunctional properties and applicability compared to their native counterparts, paving the way for their integration into sustainable and innovative food products.

This review summarises recent advancements in plant protein aggregates, focusing on their fabrication, physicochemical properties, microstructure, functional properties, and emerging applications. By highlighting current research trends and identifying existing gaps, it aims to provide valuable insights to guide future studies that can unlock the full of plant protein aggregates in various food applications.

2.2 Fabrication of plant protein aggregates

2.2.1 Pre-existing plant protein aggregates from manufacturing

Plant proteins often exhibit varying extents of pre-existing aggregation following their extraction and manufacturing process. These aggregates range from natural oligomers (e.g. trimers or hexamers) to large, microscopic aggregates induced during the conventional wet extraction process, which is widely used to obtain high-purity plant protein materials (Schmitt & Wanasundara, 2024). Wet extraction involves dispersing plant material in water, followed by fractionation to isolate the desired protein components. Various fractionation techniques such as the use of organic solvents, pH adjustments, and heat treatments, are employed to remove non-protein components (Sari, et al., 2015). These processing conditions often lead to significant chemical changes on protein molecules, such as promoting phenol-protein interaction from

alkaline pH shifts (Keppler, et al., 2020), and structural changes such as denaturation induced by heat treatment (Yang & Sagis, 2021). As a result, larger aggregated structures are formed, including insoluble protein aggregates (Kornet, Veenemans, et al., 2021). In addition, spray drying, a common method used to manufacture plant protein powders (e.g. concentrates and isolates), can also induce protein denaturation and aggregation. The high temperatures and rapid dehydration during this process alter protein structures, promoting the formation of aggregated structures (Loveday & Halim, 2024).

For instance, alkaline extraction followed by isoelectric precipitation is a commonly used method to obtain plant proteins with high purity, including pea proteins (Tanger, et al., 2022), soybean proteins (Zhao, et al., 2023), and quinoa proteins (Luo, Yang, et al., 2022), to name a few. However, irreversible aggregation often occurs during the isoelectric precipitation in this process, and the size of these aggregates are larger in extensively purified plant protein extracts (Kornet, et al., 2020; Yang & Sagis, 2021). These large aggregates can significantly reduce plant protein solubility. For example, a recent study on yellow pea protein research reported a ~20% decrease in solubility after isoelectric precipitation compared to proteins isolated through diafiltration (Kornet, Shek, et al., 2021). Similarly, a study on soybean proteins found that precipitation based extraction resulted in lower solubility precipitation (~30%) compared to membrane-based extraction methods (Rao, et al., 2002).

2.2.2 Physical methods for fabrication of functional plant protein aggregates

Recently, researchers have sought to improve the technofunctionalities of plant proteins by formation of new functional aggregates or modifying the pre-existing aggregates through various modification techniques including physical, chemical, and biological treatments. Among these treatments, physical approaches stand out as relatively straightforward, simple, and effective approaches for inducing and manipulating plant protein aggregation. Recent studies from the past 5 years on the fabrication of plant

protein aggregates using physical methods over the past five years are listed in **Table 2.1**.

Table 2.1 Summary of recent studies on the formation of plant protein aggregates using various physical methods over the past 5 years.

Approaches	Protein sources	Formulations	Conditions	Results	References
Conventional heat treatment	**Faba bean**	2-15 wt % of faba protein isolates (FPI) at pH =7.3	90 °C for 5 or 30 min	FPI aggregates with increased hydrophobicity formed after heat treatment. FPI formed gels at high concentration (>10 wt%)	Nivala, et al. (2021)
(All studies in this category were conducted under the heat treatment without shearing)		1 wt% of FPI at pH=2.0	85 °C for 24 h	Formation of straight semi-flexible nanofibrillar aggregates of ~10 nm in diameter	Herneke, Lendel, et al. (2023)
	Soybean	5-9 wt % of soybean protein isolates (SPI) at pH=7.0	50–95 °C for 0-6000 min	Formation of flexible self-similar aggregates independent of temperature (50–85 °C) and protein concentrations (50–90 g/L).	Chen, Zhao, et al. (2016)
		3.5 wt% of SPI at pH=7.0	95 °C for 15 min with/without $CaCl_2$ (0–10 mM)	Homogeneous aggregates formed after heating with $CaCl_2$ and particle diameter increased form ~0.2 μm to ~100 μm	Amagliani, et al. (2023)
		1-9 wt% SPI at pH=7.0	121 °C for 15 min	Formation of SPI soluble aggregates and the average sizes D [3,2] increased from ~125 nm to ~174 nm with increasing SPI concentrations	Fu, et al. (2023)
		1 wt% SPI at pH=2.0 with 100 mM NaCl	85 °C for 0.5 – 24 h	Formation of amyloid-like fibrillar aggregates after long time heating (> 8 h) with a particle size of ~35 μm	Wang, et al. (2020)
	Pea	5 wt% pea protein isolates	50–100 °C for 30 min	Formation of highly aggregated PPI at a	Chao and

		(PPI) at pH=7.0		high temperature (80–100 °C)	Aluko (2018)
		3.5 wt% of PPI at pH=7.0	95 °C for 15 min with/without $CaCl_2$ (0–10 mM)	Formation of PPI aggregates in the presence of $CaCl_2$ and particle diameter increased form ~0.2 μm (native PPI) to ~100 μm (PPI with $CaCl_2$)	Amagliani, et al. (2023)
	Hemp	2 wt% of hemp protein concentrate (HPC) at pH=2.0	95 °C for 0-5 h	Formation of fibrillar aggregates with the average fibril height of ~7.8 nm and length of ~1.8 μm	Kutzli, et al. (2023)
Sonication	**Faba bean**	1 wt% of FPI at pH=7.4	50%-70% amplitude of 750 W for 15-30 min	The smallest FPI aggregates with particle size (~225 nm) and greatest solubility (~45%) observed after treatment (70% amplitude for 15 min)	Martínez-Velasco, et al. (2018)
(All studies used a temperature control system (e.g. ice bath) to avoid the overheating of proteins during the sonication)		5 wt% of FPI at pH=7.0	50% amplitude of 250 W for 1-10 min	Formation of FPI aggregates with particle size decreased from ~370 nm to ~188 nm and increased solubility from ~1.15% to ~89.11% with increasing sonication time	Adal (2024)
	Quinoa	1 wt% of quinoa protein isolate (QPI) at pH 5, 7, and 9	50% amplitude of 750 W for 5 and 15 min	Formation of QPI aggregates with smaller particle sizes decreasing from ~750 nm to ~210 nm with increasing sonication time at pH 7, and similar trend could be observed at all pH ranges	Luo, Yang, et al. (2022)
	Buckwheat	4 wt% of buckwheat protein isolates at pH=7.0	60% amplitude of 120 W for 5-30 min plus 10-min further sonication at 40-100% amplitude	Formation of large buckwheat protein aggregates after long-time sonication (>10 min) at ~2000 nm particle size than native state with ~427 nm particle size	Jin, et al. (2021)
	Soybean	1 wt% of SPI at pH=3-11	50% amplitude of 2000 W	Formation of SPI aggregates with	Rahman, et

			for 1-4 min	increased solubility than native state at all pH ranges	al. (2022)
	Pea	3 wt% of PPI at pH=7.0	600 W ultrasonic power for 20-120 min in the primary ultrasound and for 20-50 min in the secondary ultrasound	Formation of PPI aggregates (~91 nm) after 120 min sonication	Liu, et al. (2024)
		1 wt% of PPI at pH=7.0	400 W ultrasonic power for 20 min	Formation of PPI aggregates (~200 nm) with increased solubility ~35%	Yan, Zhao, et al. (2024)
High pressure homogenisation (HPH) at temperature	**Faba bean**	1 wt% FPI at pH=7.0	103 MPa and 207 MPa, respectively for 6 cycles	Formation of supramolecular aggregates at a major particle size peak of ~12 nm after HPH treatment at both pressure	Yang, Liu, et al. (2018)
	Quinoa	5 wt% QPI at pH=7.0	10 MPa, 30MPa, and 50 MPa for 5 cycles, respectively	Formation of smaller aggregates with D [4,3] value around 0.2 μm and great solubility (~98%) after homogenisation at 50 MPa for 5 cycles	Luo, Cheng, et al. (2022)
High hydrostatic pressure processing (HHP)	**Pea, Lentil, and Faba bean**	5-15 wt% pulse proteins at pH=7.0	200-600 MPa for 4 min	Forming of pulse protein aggregates Forming gels at high concentration (>10 wt%)	Hall and Moraru (2021)
	Quinoa	1 wt% QPI at pH=5-9	100-600 MPa for 15 min	Formation of heterogenous QPI aggregates at all pH ranges and the solubility of QPI significantly increased at from ~15% to ~23% at pH 7 and from ~32% to ~40% at pH 9 after treated at 600 MPa for 15 min	Luo, Yang, et al. (2022) and Luo, et al. (2021)
Cold plasma	**Soybean**	5 wt% SPI at pH=7.0	170 V, 200 V, and 230 V at 5, 10, and 15 min	Formation of SPI aggregates with improved solubility (14%) and water holding capability (~62%) compared to native SPI after treatment at all conditions	Dabade, et al. (2023)
	Pea	12 wt% pea protein	Under 0-30 kV at 10 μs	Formation of fibrillar aggregates with a	Zhang,

		concentrate (PPC) at pH=6.9	pulse time for 2 min and 5 times.	network structure	Huang, et al. (2021)
High shear at room temperature	**Lentil**	5 wt% lentil protein isolates (LPI) at pH=6.8	Shearing at 10200 rpm for 1-15 min at room temperature	Formation of smaller LPI aggregates from ~5 to ~1.7 µm and greater solubility from ~46% to ~68% with the increase of shearing time from 0 to 15 min	Malterre, et al. (2024)
Combination of HPH with heat treatment	**Faba bean**	5 wt% of FPI at pH=6.8 and FPC at pH=6.3, respectively	60- 90 °C for 30 min for the primary heat treatment combining then treated by HPH for 6 cycles at 103.4 MPa	FPI heated after 90 °C for 30 min at pH 6.8 combining with HPH formed the smallest aggregates with D [4,3] value of ~0.2 µm and good dispersibility (~93.7%)	Coker, et al. (2024)
Combination of HPH with sonication	**Pea**	1 wt% of PPI at pH=7.0	400 W ultrasonic power for 20 min combining with three cycles of HPH at 50 MPa	Formation of smaller PPI aggregates with particle size of ~180 nm, and significantly higher solubility at ~40% after combination of HPH and US treatment	Yan, Zhao, et al. (2024)
Combination of heat treatment with sonication	**Soybean**	10 wt% of SPI dispersed in 30% v/v acetic acid aqueous solution	Sonicated at 40% amplitude for 30 min at 90 °C	Formation of amyloid-like fibrillar aggregates with smaller particle size (~29 nm) than native SPI (~148 nm)	Kamada, et al. (2021)
	Faba bean	2.5 and 10 wt% of FPI at pH=2.0	Sonicated at 50% amplitude for 30 min at 90 °C	Formation of amyloid-like fibrillar aggregates at 2.5wt% with radius at ~5 nm Gels were formed at 10 wt%	Hu, Cheng, Gilbert, Loo, et al. (2024)
		2.5 and 10 wt% of FPI at pH=7.0	Sonicated at 50% amplitude for 30 min at 90 °C	Formation of amorphous aggregates with radius at ~12 nm and formed gels at 10 wt%	Hu, Cheng, Gilbert, Lee, et al. (2024)
Combination of heat treatment with shear	**Potato and pea**	10 wt% of potato protein (pH= 6.9) and pea protein (pH=7.5)	Heat-treated at 95 °C of 30 min then treated by shearing from 100 to 1500	Formation of smaller aggregates for pea proteins had smaller particle size (~29 µm) distributions with increasing shear rate	Tanger, Quintana Ramos, et

			s^{-1}	than native state (~50 µm)	al. (2021)
Extrusion	**Pea**	PPI powder	Extruded using an intermeshing twin-screw extruder (25 mm diameter; total length of the screw of 28D) at screw speed varied from 200 rpm to 1200 rpm under 30 °C to 150 °C	Largest PPI aggregates (~250 µm) formed when the screw speeds at 1200 rpm at 150 °C, and the variation in screw speed did not influence the particle size of PPI aggregates	Tanger, Schmidt, et al. (2021)

2.2.2.1 Heat treatment

Conventional heat treatment

Conventional heat treatment is a common method to modify food proteins (Sharif, et al., 2018). This process increases the thermal mobility within peptide chains, disrupting inter- and/or intra-molecular hydrophobic interactions, and electrostatic, disulfide as well as hydrogen bonds. Initially, these disruptions can induce reversible unfolding of proteins. However, when the temperature exceeds the denaturation threshold, protein unfolding becomes irreversible (Akharume, et al., 2021), leading to the loss of the secondary and tertiary structures (Davis & Williams, 1998; Peng, et al., 2016). During denaturation, the protein would expose the hydrophobic core, promoting crosslinking through hydrophobic interactions (Dabade, et al., 2023; Zink, et al., 2016). These structural changes significantly influence the functionality and aggregation behaviour of proteins.

Heat treatment can result in the formation of various types of plant protein aggregates, influenced by environmental factors, such as protein concentration, ionic strength, pH values, and heating conditions (e.g., time and temperature) (Hu, Cheng, Gilbert, Loo, et al., 2024; Nivala, et al., 2021; Zink, et al., 2016). Generally, three types of plant protein aggregates can be formed through conventional heat treatment: spherical particles, flexible strands, and fibrillar aggregates (Amagliani & Schmitt, 2017; Nicolai & Durand, 2013). Spherical particles, with diameters ranging from ~ 50 nm to several microns, typically aggregate at the pH near the protein's isoelectric point (pI). For instance, spherical particles were observed in heat-treated SPI dispersion at pH 5.8 heated at 80 °C for 24 h (Chen, et al., 2017). Additionally, when the pH is significantly different from the isoelectric point (pI), long and flexible strands (length from ~10 nm to ~100 μm) are formed due to strong electrostatic repulsions between protein molecules. Ju, et al. (2023) reported the formation of a flexible stranded network after heating β-conglycinin/glycinin (5 wt%) dispersion at pH 7 at 90 °C for 30 min. Further aggregation of flexible strands and spherical particles can lead to fractal aggregates with larger sizes, and gels may form at hi/gher concentrations, resulted by different protein types and environmental conditions (Langton, et al., 2020; Nicolai & Durand, 2013; Nivala, et al., 2021). Fibrillar aggregates (i.e. amyloid fibrils) are characterised by their

high aspect ratio, and typically form under extensive heating at low pH (<2.5) (Xu, Ma, et al., 2023). For instance, Herneke, Lendel, et al. (2023) treated faba bean protein isolates (FPI) (1 wt%, pH 2) at 85 °C for 24 h, producing fibrillar aggregates from peptides released during protein hydrolysis. Such conditions involving acidic pH and high temperature are typically required for fibrillation (Amagliani & Schmitt, 2017).

Heat treatment is also considered as an effective method to reduce or eliminate anti-nutritional compounds in plant proteins. For example, heating chickpeas and soybean flours at 80 °C for 2 h with the addition of a reducing agent metabisulfite, achieved approximately 99% reduction in trypsin inhibitors (Avilés-Gaxiola, et al., 2018). Furthermore, heat treatment will make plant proteins easy to digest. For example, album seed proteins digestibility increased to ~88% after heating at 100 °C for 30 min (Mir, et al., 2020). However, heat treatment also has drawbacks, including degradation and loss of thermolabile nutrients in plant proteins, such as antioxidants, vitamins, essential oils, and flavours (Bigi, et al., 2023). These effects highlight the trade-offs in using heat treatment to enhance the technofunctional characteristics and nutritional qualities of plant proteins.

Microwave heat treatment

Microwave heat treatment is a technology that utilizes electromagnetic waves, with wavelengths ranging from ~1 mm to ~1 m and frequencies between 300 MHz and 300 GHz frequencies as illustrated in **Fig. 2.1A** (Karabulut, et al., 2024).When microwaves are applied, the polar or charged protein particles align rapidly with electric fields of the microwaves, causing a shift in the direction of the microwave energy (Galema, 1997). However, if the charged or polar particles in the reaction medium are unable to align rapidly enough with the fluctuating microwave electric field, the resulting friction generate heat within the medium. This technique can effectively disrupt disulfide and hydrogen bonds in protein molecules, resulting in protein unfolding and hydrophobic groups exposing, which enhance protein interactions and promote protein aggregation (Meng, et al., 2019). Thus, microwave heat treatment has gained increasing attentions because of its distinct advantages, including high heating rates and uniform heating.

Recently, a number of studies have worked on the impact of microwave heat treatment on plant protein aggregation. For example, Mu, et al. (2020) treated a 10 wt% SPI dispersion at pH 6.5 with different power levels (0–600 W), overserving enhanced SPI aggregation with stronger gel strength and improved water-holding capacity than native SPI. Cao et al. (2023) induced highly ordered quinoa protein aggregates by microwaving quinoa proteins (90 °C for 30 min) at varying concentrations (0.2 wt%-1.0 wt%, pH7). Xiang, et al. (2020) reported that microwave treatment (1000 W for 5 min) significantly changed the secondary structure of gluten, increasing aggregation and promoting formation of α-helix and β-turn structures. Microwave treatment offers the advantages of shorter processing time and significantly lower energy consumption compared to conventional heat treatment, making it an efficient alternative for modifying plant proteins.

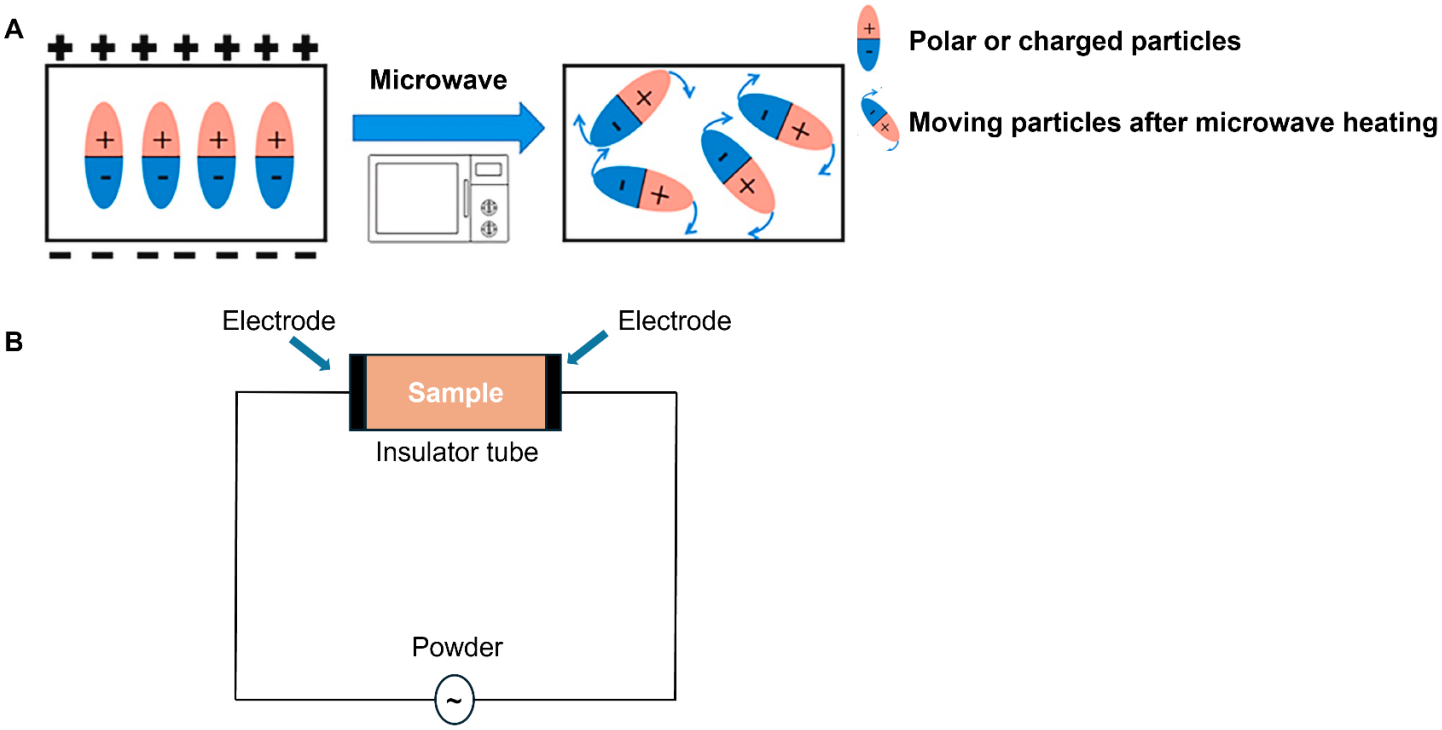

Fig. 2.1 Schematic diagram of the (A) microwave heat treatment thermal effects and (B) a typical ohmic heater. Fig. 2.1A was repreduced from Chen, et al. (2022) with permission from Elsevier, copyright 2022.

Ohmic heat treatment (OH)

Ohmic heating is a thermal approach that offers heat by passing electrical currents through a conductive or semi-conductive medium (**Fig. 2.1B**). This technique was first employed for milk pasteurisation in the 1920s (Nasrabadi, et al., 2021). When protein suspensions are subjected to OH, a thermo-electric process unfolds proteins, induces denaturation, and promotes aggregates formation (Miranda, et al., 2023). Recently, some research has displayed the effectiveness of OH in modifying plant proteins. For instance, Li, et al. (2018) researched that OH (17, 23, 30, and 37 V/cm; 96 °C for 1-8 min) formed soybean protein aggregates with significantly increased free amino groups compared to those formed via conventional heat treatment. Similarly, Miranda, et al. (2023) reported that lentil proteins treated with OH (5 and 37 V/cm; 80 °C for 20 min) formed aggregates with higher β -sheet content (~5% increase) and greater hydrophobicity when treated at pH 9 than pH 7. These findings suggest that OH is highly effective alternative to conventional heat treatment for inducing plant protein aggregation. It offers advantages such as rapid, uniform heating and easy process control (Makroo, et al., 2020).

2.2.2.2 Ultrasonication

Ultrasonication (US) is a non-thermal technique widely applied for modifying plant proteins (Wen, et al., 2019). Its primary mechanism, cavitation generates mechanical waves in a liquid, producing localised turbulence, high shear forces, and extreme temperature and pressure fluctuations in the cavitation zone (**Fig. 2.2A**) (Chavrier, et al., 2000; Gogate & Kabadi, 2009; Wen, et al., 2019). These effects enhance mass transfer and induce radical and superoxide formation, (Jambrak, et al., 2008), promoting cross-linking of plant protein molecules (Nasrabadi, et al., 2021; Wen, et al., 2019). US also modifies the structure of plant proteins by breaking non-covalent bonds while preserving covalent bonds, alternating secondary structures and partially change tertiary and quaternary structures without affecting the primary structure (Gharibzahedi & Smith, 2020). Unfolded proteins can aggregate via weak covalent and non-covalent bonds during sonication (Abd El-Salam, et al., 2009). In heat-sensitive plant proteins, such as glutelin, the heating effects induced during sonication can lead to full protein denaturation at moderate temperatures (~ 60 °C) (Shirsath, et al., 2012).

Despite its advantages, excessive sonication can cause uncontrollable cavitation, leading to the production of free radicals and destructive oxidation (Gharibzahedi & Smith, 2020; Hu, et al., 2015). A good example was from Gülseren, et al. (2007), in which they found a decreased free sulfhydryl (SH) groups in bovine serum albumin due to oxidation into disulfide bonds, caused by hydrogen peroxide generated during prolonged sonication. Such oxidative changes highlight the need for precise optimisation of parameters, including frequency, power, time, temperature, and amplitude to balance beneficial effects and avoid undesirable alterations.

2.2.2.3 High pressure treatments

High hydrostatic pressure processing

High hydrostatic pressure processing (HPP) has emerged as a versatile non-thermal novel technique (**Fig. 2.2B**) with applications extending beyond its original application for microbial pasteurisation in dairy products (Hite, 1899). The treatment pressures are ranging from 100 to 800 MPa for up to 30 min inducing significant structural and functional modifications in proteins. HHP facilitates plant protein aggregation through mechanisms rooted in Le Chateliers' principle: increased pressure results in a decrease in volume, causing protein molecules to undergo structural compression, cavity rupture, and denaturation (Lv, et al., 2020; Messens, et al.; 1997Nasrabadi, et al., 2021). These changes, in turn, drive the formation of aggregates through newly established interaction, including hydrophobic and electrostatic interactions (Akharume, et al., 2021; Galazka, et al., 2000; Messens, et al., 1997). On the other hand, HPP barely affects hydrogen bonds unless the protein solutions are exposed to extremely high pressures (≥1,000 MPa) (Akharume, et al., 2021).

The effect of HPP on plant protein structure and aggregation depends on factors such as pressure, time, and the intrinsic properties of the plant proteins (Queirós, et al., 2018). Many studies have indicated that HPP can lead to a decrease in protein solubility for SPI (200-600 MPa for 15 min) (Wang, et al., 2008), PPI (600 MPa for 5 min) (Chao, et al., 2018), QPI (250-600 MPa for 15 min) (Luo, Yang, et al., 2022; Luo, et al., 2021), and cumin protein isolate (200-600 MPa for 15 min) (Chen, Mu, et al., 2019), because of insoluble aggregates formed after HHP treatment. Conversely, certain proteins like

pine nut proteins, exhibit increased solubility following HPP treatment (200 and 400 MPa for 10 min), suggesting that the response varies depending on protein type and molecular structure (Cao, et al. (2018).

High pressure homogenisation

High pressure homogenisation (HPH) is a promising physical non-thermal treatment that has also been recently used to form and further modify plant protein aggregates (Hall & Moraru, 2021). Originally established for milk homogenisation in the dairy industry, HPH operates at pressures typically between 100 and 400 MPa (Georget, et al., 2014), forcing plant protein dispersions passing through narrow gaps within seconds as indicated in **Fig. 2.2C**. This high-pressure dynamic process enhances protein dispersion and facilitates the formation of small, functional aggregates without the need for chemical additives (Ahmad, et al., 2019). During HPH, the intense mechanical forces disrupt large protein aggregates, resulting in smaller particle sizes and increased solubility (Georget, et al., 2014; Levy, Okun, & Shpigelman, 2021; Messens, et al., 1997). This fragmentation improves interactions between protein particles and solvents, enhancing key technofunctional characteristics, such as solubility, water/oil holding capabilities. (Nasrabadi, et al., 2021). For instance, Levy, Okun, Davidovich-Pinhas, et al. (2021) reported that HPH processing of potato protein isolate (PoPI) at 30–200 MPa significantly reduced particle size and increased solubility after just one cycle, with higher pressures yielding smaller aggregates. (D'Alessio, et al., 2023) found that PoPI dispersions treated at 60 MPa and 100 MPa for five cycles exhibited enhanced solubility and emulsification capabilities, with greater improvements observed at higher pressures.

2.2.2.4 Cold plasma technology

Cold plasma technology is another non-thermal technique with diverse applications in food science (**Fig. 2.2D**), initially developed for food sterilisation but now increasingly used for inducing plant protein aggregates (Akharume, et al., 2021; Karabulut, et al., 2024). This technique is generated from an electric field to gas, partially ionizing it into a quasi-neutral plasma state, containing reactive species (e.g. free radicals, ions, and excited molecules) (Olatunde, et al., 2023). These reactive species interact with proteins, disputing covalent bonds and macro clusters inside the protein structures, leading reduced particle sizes and the formation of nanoaggregates (Basak & Annapure, 2022).

For instance, Mehr and Koocheki (2020) applied short-duration cold plasma treatments (9.4 and 18.6 kV for 30-60 s) to grass PPI, resulting in the formation of uniform PPI aggregates. This treatment resulted in an approximate 2% increase in solubility and a notable enhancement in surface charge (~10 mV). Similarly, Ji, et al. (2018) found that the peanut protein aggregates formed after cold plasma treatment (35 V for 3 min), which exhibited improved water holding capacity with highly ordered secondary structures.

2.2.2.5 Pulsed-electrical field

Pulsed electric field (PEF) technology is a novel and eco-friendly technique gradually used in the food industry, particularly for pasteurisation. As indicated in **Fig. 2.2E**, this technique utilizes high-voltage electric pulses applied for extremely short durations ranging from nanoseconds to milliseconds between two electrodes, inducing polarisation in plant proteins. This polarisation, exposes hydrophobic amino acids, and generates free radicals, resulting in changing the protein structures (Giteru, et al., 2018; Jin, et al., 2020). The PEF has shown that it could partially unfold large plant protein aggregates and modify their secondary and tertiary structures (Lee, et al., 2022; Zhao, et al., 2014). This process induces plant protein denaturation and aggregation, primarily by hydrophobic interactions, affecting their technofunctional properties (Zhao, et al., 2014). In particular, studies have indicated that effectiveness of PEF in enhancing the plant protein solubility and technofunctional properties. Zhang et al. (2017) reported that canola protein aggregates formed after the PEF treatment (10-35 kV, 60-180 s), exhibiting improved solubility as along with enhanced water- and oil-holding capacities. In addition, Zhang, Yang, et al. (2021) applied PEF (5-25 kV at 100-900 Hz for 1-9 min) to wheat gluten, forming highly soluble gluten aggregates with a more uniform microstructure.

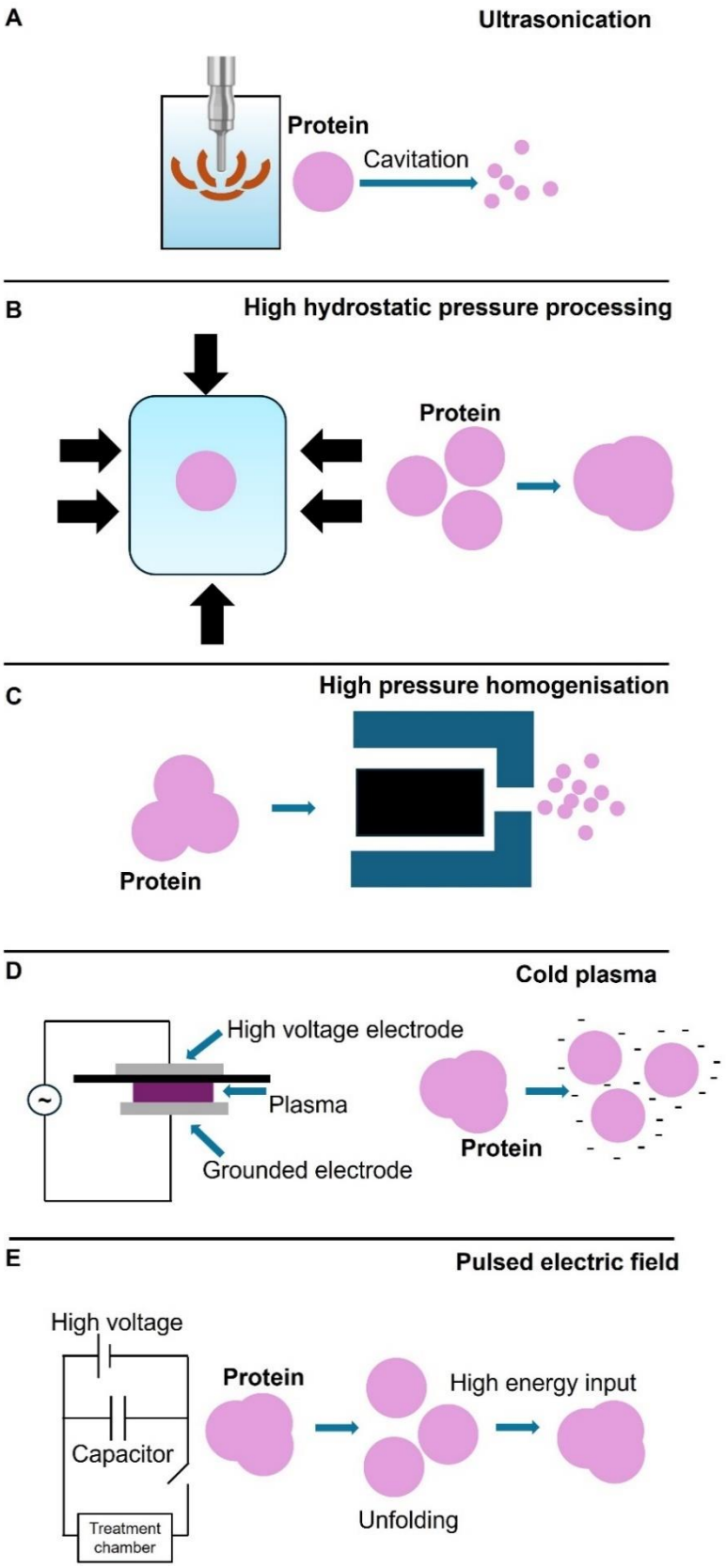

Fig. 2.2 Schematic diagram showing effects of non-thermal physical modifications on plant protein aggregation :(A) ultrasonication, (B) high hydrostatic pressure processing, (C) high pressure homogenisation, (D) cold plasma, and (E) pulsed electric fields.

2.2.3 Chemical modification methods

The chemical approach has also been explored for forming various plant protein aggregates, owning to its high specificity, efficiency, cost-effectiveness, and simplicity of operation (Karabulut, et al., 2024; Nasrabadi, et al., 2021). This method is based on the interaction of chemical agents with proteins, which either break existing bonds or form new ones, resulting protein structures changes (Akharume, et al., 2021). This treatment typically leverages the reactivity of various protein side chains, including amino, carboxyl, disulfide/sulfhydryl, indole, phenolic, and thioester groups, to facilitate chemical reactions that promote protein aggregation (Akharume, et al., 2021; Rojas, et al., 2010). However, the commercial application of chemical techniques is limited in the food industry. This limitation is primarily because of concerns over the uncontrolled formation of toxic chemical by-products during the reactions, consumer safety concerns, and regulatory challenges (Zhang, et al., 2019). A few typical chemical processes that are applied to induce plant protein aggregation are discussed below.

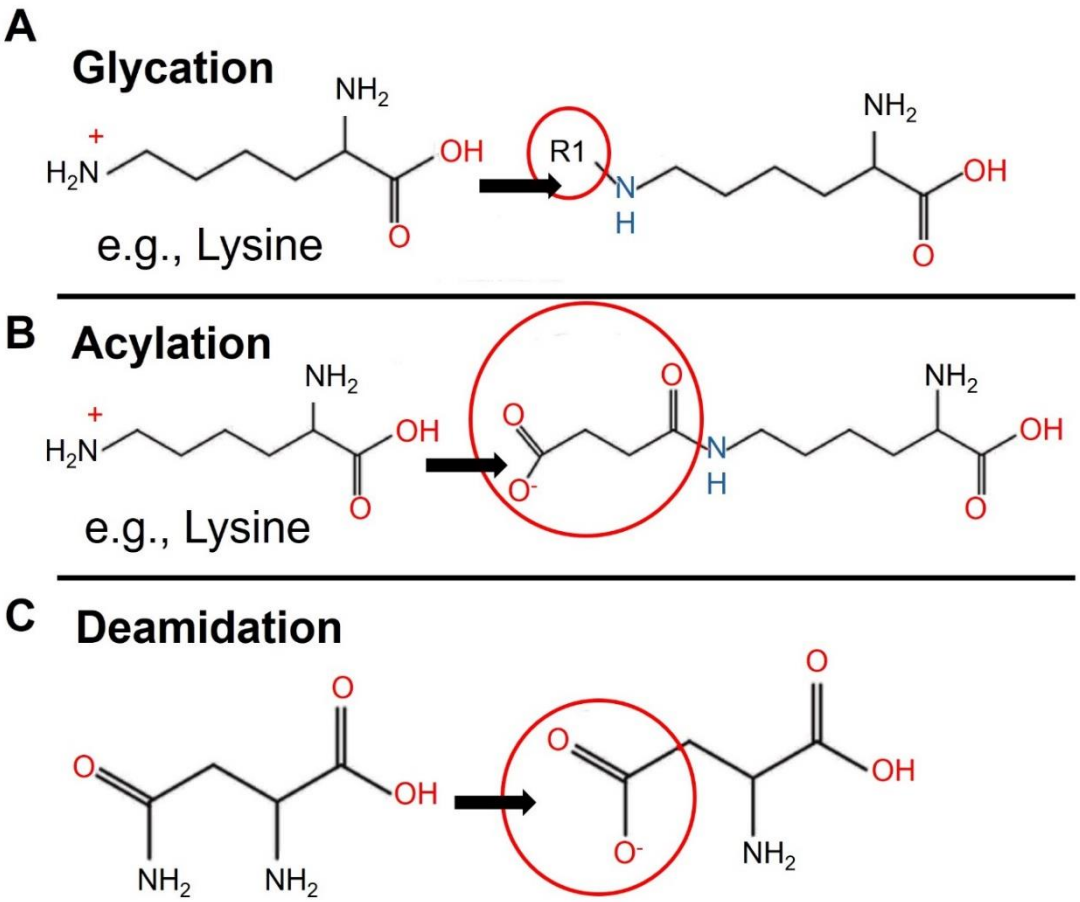

Fig. 2.3 Effect of chemical modifications on proteins using lysine as an example: (A) glycation, (B) acylation, and (C) deamidation. Figure was repreduced from Grossmann and McClements (2023) with permission from Elsevier, copyright 2023.

2.2.3.1 Glycation

Glycation (or glycosylation) is an important chemical reaction in the food industry because it is considered safe for consumers without requiring the use of exogenous chemicals (Doost, et al., 2019; Zhao, et al., 2018). **Fig. 2.3A** indicates the scheme glycation using lysine as an example. Glycation involves the covalent bonding of ε-amino groups in proteins with carbonyl groups from reducing sugars, a process commonly associated with the Maillard reaction. This reaction can lead to forming protein–polysaccharide complexes and/or other glycoconjugates, which can significantly alter the protein's properties (Higa & Nickerson, 2023; Zhang, et al., 2019). Plant protein aggregates formed via glycation highly depends on the actual reaction conditions during the early stages of the Maillard reaction. Key factors include temperature, type of sugar used, processing time, pH, and the ratio of glucans to protein (Akıllıoğlu & Gökmen, 2016; Zhang, et al., 2019). For instance, a recent study on the formation of SPI-Gum Arabic conjugates investigated wet-heating at 95 °C for 1 to 6 h and dry heating at 60 °C for 3-48 h (Feng, et al., 2023). It was found that the SPI aggregates formed through the dry-heating process exhibited reduced interfacial tension and greater electronegativity compared to native SPI, suggesting enhanced functional properties. Recently, Sun, et al. (2022) studied the glycation of PPI in a natural deep eutectic solvent at 80 °C for 2 h. The resulting PPI aggregates had smaller particle sizes and higher hydrophobicity than those formed in a water system. These finding highlight how the selection of glycation conditions, such as temperature, sugar type, and solvent, can greatly impact the functionalities and structural properties of protein aggregates.

2.2.3.2 Acylation

Acylation is another chemical process used to induce plant protein aggregates (**Fig. 2.3B**). This reaction transfers the acyl group to the amino or hydroxyl groups in the amino acid residues within the protein structure (Ferjancic-Biagini, et al., 1998). This modification exposes previously concealed hydrophobic as well as hydrophilic groups, potentially altering the protein's functional properties (Shen & Li, 2021). Miedzianka, et al. (2023) researched the effects of acetylation on rice protein concentrates with acetic anhydride. Their finding showed that acetylation caused the formation of rice protein aggregates with improved water-binding capability and emulsification ability. However,

the water solubility of these aggregates decreased compared to native rice proteins. This reduced solubility could significantly impact extensive aggregation of rice proteins through the interactions of SH groups during acylation process, which caused the proteins aggregate more tightly and reduce their ability to dissolve in water (El-Adawy, 2000; Miedzianka, et al., 2023).

2.2.3.3 Deamidation

Deamidation is a chemical process (**Fig. 2.3C**), which can transform the glutamine amide groups (δ-groups) and asparagine (γ-groups) residues in proteins into carboxyl groups, thereby increasing the negative charge of the protein and enhance its solubility while promoting functional aggregation (Nasrabadi, et al., 2021; Riha III, et al., 1996). This process can occur through chemical or enzymatic pathways, with chemical deamidation involving reactions under mild or strong acid/alkaline environments at higher temperatures, resulting in releasing ammonia molecules (Hamada & Swanson, 1994). The efficiency and outcomes of deamidation are dependent on different factors, such as protein sources, amino acid sequence, temperature, pH, and water activity (Riha III, et al., 1996). For example, Cabra, et al. (2007) demonstrated that alkaline deamidation of α-zein using 0.5 M NaOH for 12 h 0.5 M NaOH for 12 h at 70 °C produced functional aggregates capable of forming stable emulsions, outperforming other methods such as enzymatic or acidic deamidation. Similarly, Zhao, et al. (2010) showed that deamidation of barley hordein under acidic conditions (pH 3-7) formed aggregates with improved solubility, foaming capacity, and emulsification ability compared to its native form. In the food industry, mild alkaline or acidic deamidation methods are preferred due to their ability to enhance protein functionality while maintaining consumer appeal, as strong acid or alkaline treatments can lead to excessive protein denaturation or peptide hydrolysis, reducing suitability of commercialisation (Hamada & Swanson, 1994).

2.2.3.4 pH shifting

The principle of pH-shifting involves inducing significant electrostatic repulsion in plant proteins under extremely acidic or alkaline pH environments, causing partial unfolding of their structures (Nasrabadi, et al., 2021). When the pH value is subsequently readjusted to pH 7, the proteins refold and aggregate rapidly (Liang &

Kristinsson, 2007). The pH level is essential factor to determine the protein structural behaviours (Nasrabadi, et al., 2021). Under extreme acidic (e.g., pH 2) or alkaline conditions (e.g., pH 12), proteins posse strong charges, leading to repulsion and structural unfolding, which in turn exposes sulfhydryl groups and hydrophobic regions (Tang, et al., 2021). (Lee, et al., 2016; Yang, Duan, et al., 2022). Upon returning to neutral pH, these unfolded proteins refold and reorganise into aggregates (Figueroa-González, et al., 2022; Jiang, et al., 2018).

Tang, et al. (2023) investigated the effects of pH-shifting on plant proteins sourced from pea, rice, oat, and hemp and found that treatments at pH 10 or pH 2 for 1 h at room temperature remarkedly enhanced solubility and foaming capability compared to untreated proteins. Among these, oat protein pH shifted to 10 exhibited the greatest water-holding capacity after heat treatment, suggesting desirable rheological properties for gelation (Tang, et al., 2023). Additionally, Nissen, et al. (2021) researched the effects of alkaline (pH 11) and acid pH (pH 2) shifting on alfalfa proteins. They reported that alkaline pH shifting produced protein aggregates with significantly enhanced water solubility to ~90% and improved gelation properties while acid pH shifting resulted in only slight solubility improvement. These findings indicate that pH-shifting holds significant potential as a technique for modifying plant protein structures and enhancing technofunctional properties.

2.2.4 Biochemical methods

Biochemical methods involve enzymatic and/or fermentation processes, with enzymatic process typically classified into enzymatic hydrolysis and/or enzymatic cross-linking (Karabulut, et al., 2024; Nasrabadi, et al., 2021). These methods require lower energy consumption compared to some physical methods (e.g. heat treatment), and they tend to avoid toxic by-products often that often associated with chemical treatments (Alrosan, et al., 2023; Gouseti, et al., 2023). However, the high cost of enzymes and the prolonged processing time, particularly for large-scale plant protein modification (Akharume, et al., 2021), making these methods more expensive than others.

2.2.4.1 Enzymatic modifications

Enzymatic hydrolysis

Enzymatic hydrolysis of plant proteins involves a catalytic reaction between protein substrates and proteolytic enzymes, which breaks down peptide bonds to form peptides and amino acids with reduced molecular size (Eckert, et al., 2019). This hydrolysis method induces protein molecules unfolding and exposing hidden hydrophobic groups, thereby promoting hydrophobic interactions and the protein aggregation (Bučko, et al., 2016; Eckert, et al., 2019). Controlled hydrolysis, maintained within a 10% degree of hydrolysis (DH), can facilitate the generation of plant protein aggregates (Austin, et al., 2024; Wang, Cheng, et al., 2022). However, when the extend of hydrolysis is excessive (DH > 10%), the molecular weight of proteins is significantly reduced, resulting in much smaller peptides and protein fragments (Singh, et al., 2019). Several factors affect the protein enzymatic hydrolysis and aggregation, including enzyme type (e.g. Alcalase, trypsin, neutrase, pepsin, flavoenzyme, etc.), the nature of protein substrate, the ratio of enzyme and protein, awe well as environmental factors such as pH and temperature (Ahmadifard, et al., 2016). Some previous studies have investigated that Alcalase is particularly effective in forming soluble plant protein aggregates with enhanced emulsification properties when hydrolysis occurs under alkaline pH conditions. Examples include chickpea protein isolates (del Mar Yust, et al., 2010), quinoa protein concentrates (Aluko & Monu, 2003), as well as rice, pea, hemp, and oat proteins (Shahbal, et al., 2023).

Enzymatic cross-linking

The principle of enzymatic cross-linking lies in forming covalent bonds between protein molecules by enzymes such as transglutaminase, tyrosinase, and laccase. These enzymes facilitate acyl transfer reaction between the γ-carboxamide groups of glutamine residues on proteins and lysine residues (Nasrabadi, et al., 2021). Among cross-linking enzymes, transglutaminase is one of the most widely used enzymes, which can be sourced from specific bacteria (e.g. *Streptoverticillium mobaraense*) (Nivala, et al., 2017). This enzyme facilitates acyl transfer reactions, crosslinking inter- or intra-chain glutamines as well as lysine side chain residues in proteins (Gaspar & de Góes-Favoni, 2015). Enzymatic crosslinking generally produces protein aggregates with stronger mechanical strength by building up the polypeptides (Akharume, et al.,

2021). A recent study showed the effects of transglutaminase on SPI aggregates, and they found the formation of increased particle size aggregates (from ~105 μm for native SPI to ~140 μm for treated SPI) with significantly improved emulsification ability and stability gelation behaviour (Liu, et al., 2021).

2.2.4.2 Fermentation modification

Fermentation modification is a microorganisms-driven process that transforms plant proteins into aggregates with improved functionalities (Shiferaw Terefe & Augustin, 2020). Different starter cultures are used in plant protein fermentation, including *Bacillus* strains, lactic acid bacteria, yeast, and mould (Schlegel, et al., 2019). Two main process techniques are used for food fermentation, which are solid-state fermentation (SSF) as well as submerged fermentation (SMF). SSF takes place in environments with little to no free water, while SMF occurs in the presence of free water (Singhania, et al., 2009). SSF is particularly suitable for plant protein fermentation due to its higher product yield, lower cost, and superior product characteristics (Couto & Sanromán, 2006). One significant applications of plant protein fermentations are the development of proteinaceous products, where protein aggregation and/or gelation are induced. Examples include plant-based cheese, yoghurt, and beverages (Alrosan, et al., 2023). For instance, lupin protein aggregates formed though SSF using *Pediococcus pentosaceus* at 35 °C for 72 h exhibited enhanced solubility, emulsification ability, and foaming properties than untreated proteins (Klupsaite, et al., 2017). Recently, Dai, Hou, et al. (2022) used three different *Bacillus* species (*Bacillus licheniformis* YYC4 and *Geobacillus stearothermophilus* A75, and *mesophilic Bacillus subtilis* 10 160) to induce soybean protein aggregates through SSF. Their findings revealed a significant secondary structure change, with an approximate 20% increase in β-sheet content across all species. The soybean protein aggregates were mainly formed through SH bonds and hydrophobic interactions. Therefore, they thought that fermentation induced protein group change because of the degradation of proteins by proteases formed from selected strains (Dai, Hou, et al., 2022).

2.2.5 Combination of different methods for inducing protein aggregation

In recent years, researchers have explored combining different modification strategies to achieve a synergistic improvement in the technofunctional properties of plant protein

aggregates. Some notable examples are discussed below.

2.2.5.1 Thermosonication (TS)

Thermosonication (TS) is a novel technique that integrates ultrasonication with traditional heat treatment. A typical TS batch system consist of a sonicator probe connecting with an external circulator water bath for temperature control. Typically, TS involves ultrasonication performed at temperatures exceeding 50 °C (Costa, et al., 2013). The TS was firstly used as an emerging pasteurisation method, due to its ability to effectively destroy harmful microorganisms in food products while preserving their nutritional and sensory properties (Xu, Feng, et al., 2023). In recent years, TS has gained popularity for modifying plant proteins, leveraging its capability to alter protein conformations through the combined effects of ultrasound-induced cavitation and thermal energy (Su, et al., 2022). As reported, TS holds great promise for inducing plant protein aggregates. For example, Zhong and Xiong (2020) applied TS treatment (30-70 °C, 5-30 min, pH 7) to mung bean protein isolate (MPI) dispersions, resulting in plant protein aggregates with enhanced solubility (~90%) and improved heat stability. Furthermore, compared to conventional heat treatment at pH 2 (90 °C for 1-8 h), TS treatment (90 °C, 10-30 min, pH 2) significantly accelerates the formation of fibrillar protein aggregates from faba bean protein isolates (FPI) (Hu, Cheng, Gilbert, Loo, et al., 2024).

2.2.5.2 Thermo-mechanical treatments

The combination of mechanical treatments and heat treatment has been recently used for formation of protein aggregates and enhance their technofunctional properties, including emulsification and gelation properties. For instance, Spiegel and Huss (2002) demonstrated microparticulate whey protein aggregates formed by the combined application of heating (80 or 110 °C for 0-80 s) and controlled mechanical shear (1200 min^{-1}). For plant proteins, Tanger, et al. (2022) processed pea proteins at different shear rates between 100 s^{-1} and 1500 s^{-1} at 88 °C or 98 °C using a rheometer. They observed the formation of smaller pea protein aggregates with increasing shear rate, as high shear forces broke down the aggregates during processing. Similarly, Tanger, Quintana Ramos, et al. (2021) achieved microparticulation of pea and potato proteins by applying shear rates of 100 s^{-1} and 1500 s^{-1} at 95 °C for 30 min in a rheometer. They found that

the aggregate sizes of these proteins significantly decreased when higher shear rate (> 500 s^{-1}) was conducted. The resulting microparticulated pea and potato proteins had enhanced solubility and gelation properties, making them promising ingredients for fat replacement and emulsion stabilisation (Tanger, Quintana Ramos, et al., 2021; Tanger, Schmidt, et al., 2021). Furthermore, Coker, et al. (2024) combined heat treatment (60-90 °C for 30 min) with HPH at 103.4 MPa for six cycles to form FPI aggregates. They concluded that the FPI aggregates exhibited improved dispersion stability, significantly smaller particle sizes, and reduced interfacial tension compared to native and solely heat-treated FPI.

2.2.5.3 Ultrasonic-assisted pH shifting

Recently, the integration of pH shifting and the US on the formation of plant protein aggregates has been increasingly studied. Jiang, et al. (2017) found that ultrasonication (10 min) combined with pH shifting facilitated forming of nano-sized aggregates from PPI with significantly increased surface hydrophobicity. Similarly, Li, Cheng, et al. (2020) found the the combination pH shifting (adjusting pH to 1.5, 2.5, 11.5 and 12.5 for 1 h before readjusting to 7.0) with 10 min of ultrasonication on rapeseed protein isolates (RPI). Their findings showed that this dual treatment led to the generation of highly soluble protein aggregates. Furthermore, Yang, Duan, et al. (2022) explored the effects of ultrasonic-assisted (20 min) pH shifting (pH 10 or 12) on PPI. They observed that this treatment produced soluble protein aggregates with 99% solubility and induced the secondary structure changes in PPI, leading to increased β-sheet content. This combined approach has also been applied to form aggregates in other plant proteins including pea protein aggregates (Jiang, Yildiz, et al., 2019) and soybean protein aggregates (Yildiz, et al., 2017).

2.2.6 Microgel particles

Protein microgels are assembled through protein aggregation and are characterised as highly hydrated, surface-active, and porous particles with superior stability, making them ideal as stabilisers and/or emulsifiers (Ma, et al., 2023). These microgels exhibit excellent emulsification properties due to their deformability, which allows them to absorb at the oil-water interface and create a physical barrier that prevents the coalescence of oil droplets, thereby enhancing the stability of emulsions (Wang, et al.,

2018). In addition to their emulsifying capability, protein microgels have three-dimensional network structure cross-linked by numerous colloidal particles, making them a key component as an internal structure of macroscopic gels (Li & Ngai, 2013). The stability of microgel particles in aqueous solutions is influenced by steric and electrostatic repulsions (Dickinson, 2017).

Microgel particles are usually prepared by breaking down macroscopic protein gels. These gels are firstly formed by physical, chemical, or biological approaches and then processed using various mechanical methods, such as shearing (Dai, et al., 2012), HPH (Yan, Bai, et al., 2024), and sonication (Yang, Zhu, et al., 2023). This process yields solutions having micron- or nano-sized gel particles (Dai, et al., 2012). A summary of recent studies regarding the formation of plant protein microgels is listed in **Table 2.2**.

Table 2.2 Summary of recent studies on the formation of plant protein microgels over the past 5 years.

Protein sources	Microgel formation methods	Microgel formation methods	Particle sizes	References
Pea protein concentrate	• Heated at 90 °C for 1 h (15 wt%, pH 7)	• Gel was homogenised by a hand blender for 5 min • Further passing through HPH at 25 MPa for 1 pass	~232 nm	Zhang, Holmes, et al. (2020)
PPI	• Heated at 85 °C for 30 min (10 wt%, pH 7) • Incubation with 20 U/g transglutaminase at 45 °C for 4 h	• Gel was homogenised by Ultra-Turrax at 10000 rpm for 2 min • Further passing through HPH at 50 MPa for three passes	~176 nm	Yan, Bai, et al. (2024)
SPI	• Heated at 90 °C for 30 min (15-20 wt%, pH 7)	• Gel was homogenised by Ultra-Turrax at 24000 rpm for 5 min • Further sonicated the gel at 100% amplitude for 5 min at ambient temperature or passed the gel once through HPH at 24 MPa	~258 nm after sonication; ~84 nm after HPH	Matsumiya and Murray (2016)
SPI	• Heated at 90 °C for 30 min (10 wt%, pH 7)	• Gel was homogenised by Ultra-Turrax at 23000 rpm for 2 min • Further passing through HPH at 30 MPa for 1 cycle • Or sonicated the gel for 3 min (20 kHz, 400 W) at ambient temperature for 1 cycle	~321 nm after sonication; ~394 nm after HPH	Benetti, et al. (2019)
SPC	• Heated at 95 °C for 25 min (15 wt%, pH 3-9)	• Gel was homogenised by Ultra-Turrax at 10000 rpm for 2 min • Further sonicated the gel at 300 W for 5 min at ambient temperature	Deceased form ~110 nm (pH 3) to ~15 nm (pH 9)	Yang, Zhu, et al. (2023)
FPI	• incubation with 20 U/g transglutaminase at 40 °C for 3 h (10 wt%, pH 7)	• Gel was homogenised by Ultra-Turrax at 12000 rpm for 2 min	N/A	Zhang, et al. (2024)

		• Further passed it through HPH at 60 MPa for 2 cycles		
Oat protein isolates	• Mixed with κ-carrageenan at mass ratios of 10:0.5, 10:1, and 10: 2 respectively (pH 7) • Heated at 100 °C for 60 min	• Gel was homogenised by Ultra-Turrax at 13000 rpm for 3min • Further passed it through HPH at 60 MPa	~433 nm	Du and Meng (2024)
Potato protein isolates	• Heated at 80 °C for 30 min (5-10 wt%, pH 7)	• Gel was homogenised by a hand blender for 5 min • Further passed it through HPH at 25 MPa for 3 cycles	~132 nm	Kew, et al. (2023)
Chickpea protein isolates	• Heated at 90 °C for 30 min (10 wt%, pH 7)	• Gel was homogenised by Ultra-Turrax at 10000 rpm for 3 min • Further passing through HPH at 50 MPa for 3 cycles	~91 nm	Xu, et al. (2024)
Peanut protein isolates	• Heated at 80 °C for 20 min (10 wt%, pH 7) • Incubated with 20 U/g transglutaminase at 45 °C for 4 h	• Gel was homogenised by Ultra-Turrax at 10000 rpm for 2 min • Further passing through HPH at 110 MPa for 2 min	~250 nm	Jiao, et al. (2018)
	• Heated at 90 °C for 30 min (10 wt%, pH 7) • Incubated with 2 U/g transglutaminase at 40 °C for 2 h • Further heated at 80 °C for 20 min	• Gel was homogenised by Ultra-Turrax at 15000 rpm for 1 min • Further passing through HPH at 100 MPa for 1 pass	~186 nm	Du, et al. (2024)

2.3 Characterisation of plant protein aggregates

Plant protein aggregation can occur during extraction, processing, and storage (Zhu, Bassey, et al., 2022). The physicochemical characteristics and technofunctionalities of protein aggregates are influenced by different factors, including intrinsic properties and processing methods. Understanding the microstructural characteristics and physicochemical properties of plant protein aggregates is imperative for their applications (Hu, Cheng, Gilbert, Lee, et al., 2024; Xu, Ma, et al., 2023).

There are many techniques available for characterising plant protein aggregates, including differential scanning calorimetry (DSC), sodium dodecyl sulfate–polyacrylamide gel electrophoresis (SDS-PAGE), dynamic light scattering (DLS), high performance liquid chromatography (HPLC), nuclear magnetic resonance (NMR), circular dichroism (CD), Fourier transform infrared spectroscopy (FTIR), fluorescence spectroscopy, among others (Andreescu & Vasilescu, 2021; Zhu, Bassey, et al., 2022).

2.3.1 Physiochemical properties of plant protein aggregates

2.3.1.1 Particle size

Plant protein particle sizes can range from nanometres to micrometres, and the aggregate size distribution is an important characteristic for protein aggregates (Ndoye, et al., 2013). It has been reported that plant protein particle sizes are closely related to their technofunctionalities (e.g. solubility), with smaller protein aggregates often exhibiting a greater capacity to adsorb or bind water (Schmitt & Wanasundara, 2024). Therefore, it is essential to choose a suitable technique to determine particle sizes of plant protein aggregates as shown in **Fig. 2.4**. Several common techniques are widely used, depending on the size range of plant protein aggregates, including Mastersizer (O′ Flynn, et al., 2021), Zetasizer (Hu, Cheng, Gilbert, Lee, et al., 2024), SAXS/SANS (Hu, Cheng, Gilbert, Loo, et al., 2024), and microscopic methods (Ge, et al., 2022).

It is essential for researchers to determine representative plant protein particle size based on the overall characteristics of the sample. For example, the Zetasizer is able to determine the size and polydispersity of plant protein aggregates within sizes ranging from 0.3 nm to 10 μm. However, this technique is not suitable for samples with sizes

in the tens of microns, as protein sedimentation can affect the measurements (Zhu, Bassey, et al., 2022). In addition, another widely applied instrument for determining the particle sizes of protein aggregates is Mastersizer, which is more suitable for protein aggregates with the size range of 0.01 μm to3500 μm (Sun, et al., 2011; Zhu, Bassey, et al., 2022).

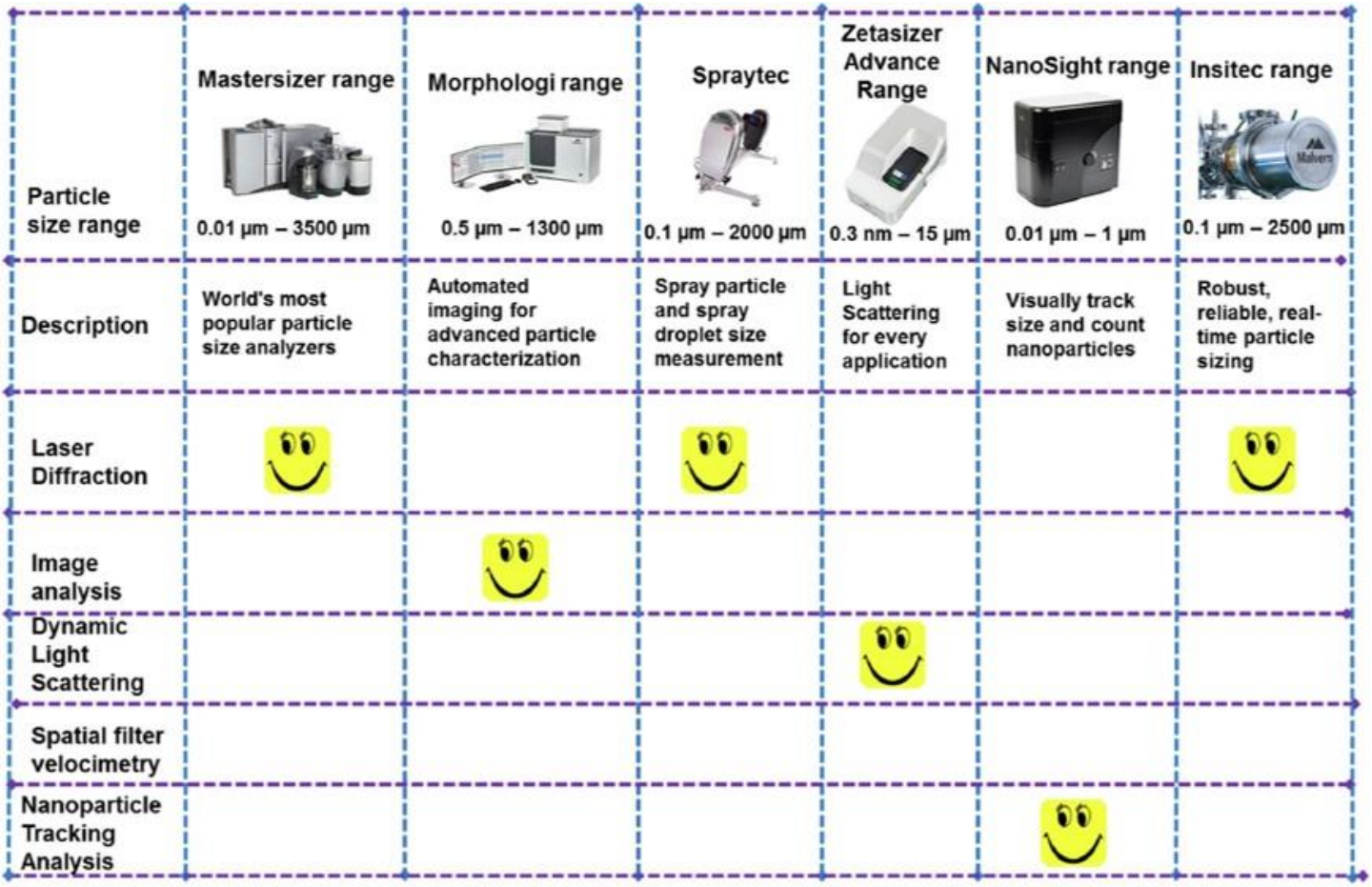

Fig. 2.4 Comparative characteristics of different particle sizing instruments in the characterisation of plant protein aggregates. Figure was repreduced from Zhu, Bassey, et al. (2022) with permisstion Elsevier, copyright 2022.

2.3.1.2 Secondary structures

Studying the secondary structures of plant proteins is essential for understanding the mechanism of protein aggregation (Housmans, et al., 2023). For instance, fibrillar aggregates formed by plant proteins are typically enriched in β-sheets, with small amounts of other secondary structures (Hu, Cheng, Gilbert, Loo, et al., 2024; Nelson, et al., 2005).

There are two most common techniques applied to probe the secondary structures of native plant proteins and aggregates, including CD and FTIR. Both spectroscopic techniques have distinct advantages and can complement each other. FTIR is more versatile and can be applied to samples in either solution or solid state, while CD is limited to liquid samples (Housmans, et al., 2023). However, FTIR results can be significantly affected by the inherent signal of water, necessitating higher sample concentrations compared to CD (Tranter, 2017). Therefore, both CD and FTIR techniques are often used together to examine the secondary structural changes in plant proteins, allowing for a more comprehensive analysis. For example, Kutzli, et al. (2023) used CD and FTIR to examine the conformational changes in hemp seed proteins during fibrillisation, obtaining detailed information that revealed the β-sheet formation. Similar results were reported in a recent fibrillisation research on FPI, which increased the contents of random coils and β-sheets during the process, as analysed by CD and FTIR (Hu, Cheng, Gilbert, Loo, et al., 2024).

2.3.1.3 Fluorescent spectroscopy for aggregates identification

Various fluorescence dyes are used to identify plant protein aggregates by indicating an greater fluorescence intensity and a spectral shift after binding to the protein aggregates (Tranter, 2017). Among these dyes, the most commonly used exogenous fluorescent probes are Thioflavin T (ThT) (Naiki, et al., 1989), Congo Red (Carrió, et al., 2005), and ANS (1,8-anilinonaphthalene-sulfonate) (Guliyeva & Gasymov, 2020). However, these dyes should be used with caution and in combination with other characterisation methods such as microscopy, as they can disrupt the aggregation process and change the microstructure of the protein aggregates, potentially leading to artefactual results (Di Carlo, et al., 2015; Hudson, et al., 2009).

ThT is considered the 'gold standard' dye for detecting and quantifying fibrillar aggregates of proteins *in vitro*, and it is widely used for studying aggregation kinetics (Naiki, et al., 1989; Wang, et al., 2020; Zhou, et al., 2012). ThT binds to amyloid fibrils that are enriched in β-sheets and enhances the fluorescence intensity at 480 nm (Fernandez-Flores, 2011; Hu, Cheng, Gilbert, Loo, et al., 2024). Congo red is another dye used for detecting amyloid fibrils for decades (Carrió, et al., 2005). It binds to amyloid fibrils and shows anomalous colours under polarised light, such as apple-green birefringence (Louros, et al., 2020). Additionally, after Congo Red binds to fibrillar aggregates, it increases the fluorescence intensity of the solution at approximately 614 nm (Fernandez-Flores, 2011; Yakupova, et al., 2019). However, Congo Red has some limitations, including, inconsistent staining results due to variations in sample thickness and a lack of sensitivity for detecting minimal amyloid fragments (Bély & Makovitzky, 2006).

ANS is another commonly used fluorescence dye in plant protein aggregation studies, as it binds to exposed hydrophobic sites of protein molecules (Housmans, et al., 2023). Surface hydrophobicity is an indicator of the number of hydrophobic groups present on the protein surface, which can provide insight into conformation and flexibility of protein aggregates (Dai, Lian, et al., 2022; Yan, et al., 2021). Recently, ANS has become a standard method for monitoring the surface hydrophobicity changes before and after plant protein aggregation, as demonstrated in studies on SPI (Yan, et al., 2021), FPI (Hu, Cheng, Gilbert, Lee, et al., 2024), QPI (Luo, Yang, et al., 2022), and PPI (Shen, et al., 2022). After ANS binding to exposed hydrophobic regions, it shifts emission from 520 nm to 480 nm, along with a significant enhancement in fluorescence intensity at 480 nm, which is used to calculate the surface hydrophobicity (Guliyeva & Gasymov, 2020; Stryer, 1965).

2.3.2 Microstructures of plant protein aggregates

2.3.2.1 Microscopic methods

Although the presence of plant protein aggregates is typically determined by particle size characterisation, structural changes, and the use of fluorescence spectroscopy, advanced misccopies, such as TEM, AFM, CLSM, and SEM, can provide direct visual

information (e.g. size and shape) of protein aggregates and offer detailed insights into their morphology (e.g. fibrils or amorphous aggregates) (Kutzli, et al., 2023; Liamas, et al., 2023). **Table 2.3** outlines the advantages and disadvantages of these techniques. Among them, TEM provides superior resolution (~0.07 nm) compared to CLSM (~140 nm×140 nm× 1 μm) and SEM (~2-10 nm). AFM complements TEM by providing more information, such as the height and topography of protein aggregates. (Rigacci, et al., 2008).

However, these microscopic methods cannot provide comprehensive quantitative information about protein aggregates (Promeyrat, et al., 2010). One limitation is the difficulty in capturing statistically representative structural information (Ruggeri, et al., 2018). To address this, scattering techniques, such as small angle scattering (SAS) has been used to more comprehensively detect and analyse protein aggregates.

Table 2.3 Summary for applying different microscopic methods in characterisation plant protein aggregates.

Techniques	Advantages	Major Disadvantages	Maximum Magnification	Resolution Limit	Reference
TEM	• Morphology/structural characterisation • High resolution and magnification • Visualising the details of nanostructures	• Complicated sample preparation • Vacuum condition required • Non-three-dimensional structures observation • Image overlapping	1000000 ×	~0.07 nm	Jackson, et al. (1998), Harris (2015), Zhu, Bassey, et al. (2022), and Housmans, et al. (2023)
AFM	• High resolution visualisation • Versatile • Three-dimensional imaging • Ease of sample preparation	• High dependency of reported size on the tip radius • Destruction Imaging	Dependent on sample states, imaging mode, environment, etc.	~0.5 nm	Meyer (2003), Dufrêne, et al. (2017), Herneke, et al. (2021), and Zhu, Bassey, et al. (2022)
SEM	• High magnification • Versatile • Three-dimensional imaging • Large depth of field	• Vacuum condition required • Only observe the surface of samples • Complicated sample preparation.	100000 ×	~2–10 nm	Dudkiewicz, et al. (2011), Goldstein, et al. (2017), and Relucenti, et al. (2021)
CLSM	• High-resolution imaging • Non-destructive • Versatile • Imaging horizontally and vertically	• Slow imaging • Fluorescence probes are required	100 ×	Lateral resolution: ~140 nm and axial resolution: ~1 μm	Schmitt, et al. (2021), Lyu, et al. (2022), and Schmitt and Wanasundara (2024)

2.3.2.2 Small-angle X-ray and neutron scattering

SAS techniques are increasingly applied to detect the nanostructure and interactions of protein aggregates scaling from angstrom to micron length. A typical SAS setup is shown in **Fig. 2.5A** (Gilbert, 2019). This method complements microscopic techniques by providing detailed insights into the size, shape, and scale of plant protein aggregates (Hu, Cheng, Gilbert, Loo, et al., 2024; Yang, Cheng, et al., 2023). According to Guinier, et al. (1956) and Gilbert (2019), SAS is conducted by measuring the scattered radiation intensity (i.e. I(Q)) versus the magnitude of the scattering vector Q; with Q is

$$Q = \frac{4\pi\sin\theta}{\lambda} \tag{2.1}$$

where θ is the scattering angle and λ is the incident radiation wavelength. In some cases, ultra-small-angle scattering (USAS) is required to achieve lower Q values, allowing researchers to obtain information on larger length scales (Gilbert, 2019). The probing length scale (d) and its inverse relationship to the Q can be expressed as follows:

$$d = \frac{2\pi}{Q} \tag{2.2}$$

The measured intensity can be written as

$$I(Q) = \Delta\rho^2 V_P \emptyset_P F(Q) S(Q) \tag{2.3}$$

where $\Delta\rho$ represents the differences in density between the surroundings and the scattering particle; V_P denotes the volume of the scattering particle; $\emptyset_P$ refers to the dimensionless particle volume fraction. $F(Q)$ and $S(Q)$ describe the form factor and the structure factor, which are related to the correlation between the colloidal particles, respectively.

Based on the principle of SAS (Guinier, et al., 1956), a contrast must exist between the surrounding solvent and the scattering particles. The scattering contrast ($\Delta\rho$) can be calculated from $\Delta\rho = \rho_p - \rho_m$, where ρ_p and ρ_m are the scattering length densities (SLDs)

related to scattering particle and surroundings, respectively. The SLD, ρ, of a molecule with i atoms, is calculated as below.

$$\frac{\delta N_A \Sigma b_i}{M} \tag{2.4}$$

where δ is the bulk physical density of the molecule (g/cm^{-3}), and M is the molecular weight. N_A represents Avogadro's number, and b_i is the X-ray or neutron scattering length of the ith atom in the molecule.

Molecular contrast can be calculated from the chemical formula and physical density of the molecules. The type of radiation used influences this contrast: for X-rays, it is determined by the electron count, while for neutron scattering, it is based on the atomic nucleus structure. Therefore, SAXS and SANS provide complementary insights into microstructures (Gilbert, 2019). In SANS, the concept of 'contrast variation' is often employed in food colloids research to manipulate the contrast by leveraging the different neutron scattering lengths of hydrogen and deuterium. This is because the scattering length density (SLD) value of H_2O is negative, whereas for D_2O is positive. By carefully mixing of H_2O and D_2O at different ratios, researchers can strategically adjust the contrast of specific components, rendering them effectively transparent to neutrons (Blazek & Gilbert, 2011).

When measuring the structure of plant protein aggregates, it is beneficial to detect them as close to their "native" state (i.e. without altering the samples). In this context, SAS is particularly useful because it is a non-invasive technique compared to AFM and/or TEM (Blazek & Gilbert, 2011; Lee, et al., 2019). Unlike these microscopy techniques, SAS requires minimal sample preparation (e.g. no staining or sectioning), which helps reduce the risk of introducing artefacts (Gilbert, 2019; Hu, Cheng, Gilbert, Lee, et al., 2024). However, unlike microscopy, SAS does not produce visual images (Gilbert, 2019). This requires researchers to convert the scattering data to a real space representation or fitting it to a reciprocal space model, while being constrained by the established parameters of the system. Therefore, complementary structural information from other techniques, such as microscopy, is essential for fully characterising protein

aggregates.

In practice, researchers commonly use both microscopy and SAS techniques to investigate the microstructure of plant protein aggregates. For example, Hu, Cheng, Gilbert, Loo, et al. (2024) employed TEM and SANS techniques to comprehensively examine the microstructure of FPI fibrils. TEM was used to observe the fibril shape, while SANS confirmed the existence of fibrillar aggregates and quantified the thickness of fibrils. In addition, Li, Yang, et al. (2024) employed SAXS to probe the conformation of thermally induced SPI gels, demonstrating that SPI particles form dense spherical particles upon aggregation. In another study on quinoa protein gels (**Fig. 2.5B and 2.5C**), Yang, de Campo, et al. (2022) comprehensively explored the microstructure of QPI gels formed after heat treatment in the presence of NaCl and $CaCl_2$ at different concentrations, using CLSM and SAS (SAXS and SANS). They found the QPI gel strength was significantly improved after the addition of NaCl (0–200 mM) while the addition of $CaCl_2$ (20 and 50 mM) would form observe separation due to the formation of large micron scaled protein agglomerates.

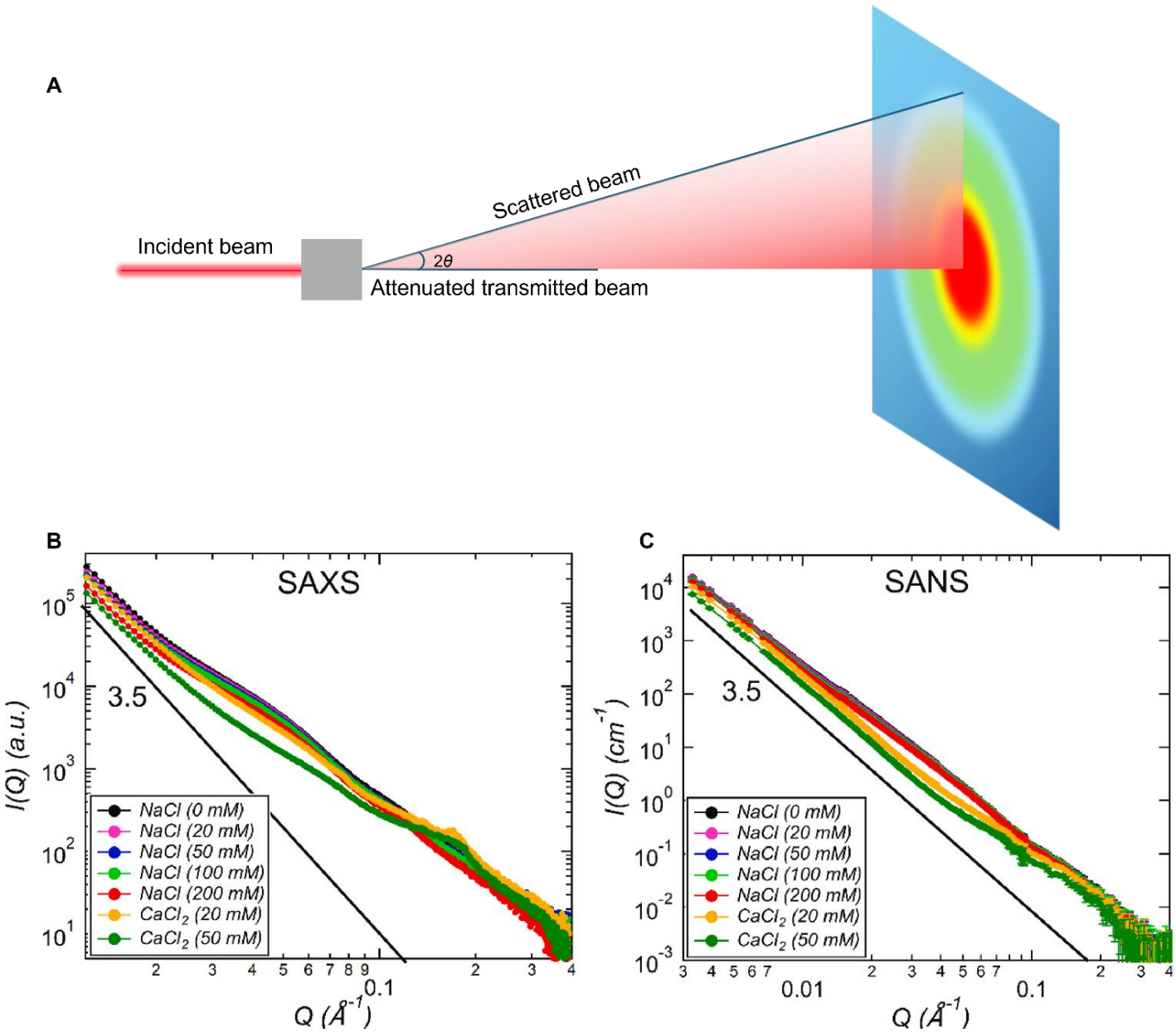

Fig. 2.5 (A) A typical scattering geometry for a SAXS or SANS measurement. (C) SAXS and SANS (D) profiles of quinoa protein isolates (QPI) gels that formed in the presence of various concentrations of NaCl and CaCl2. The power-law scattering found in different Q regions are indicated with a power-law exponent. Figure (A) reproduced from Gilbert (2019) with slight modifications from Elsevier, copyright 2019. Figure (B) reproduced from Yang, de Campo, et al. (2022) with slight modifications from Elsevier, copyright 2022.

2.3.3 Interfacial tension

Interfacial tension is the force required to minimise the interface between two immiscible phases (e.g. water and oil) (McClements, 2004a). When a solute adsorbs from one phase to another at the interface, it will lead to the free energy change at the interface. Thus, interfacial tension can be understood as energy change requirement per unit area, expressed in J/m^2 or N/m (Schmitt & Wanasundara, 2024). The interfacial tension of protein aggregates can be measured using a tensiometer. There are many different types of tensiometers based on different measurement principles (Schmitt & Wanasundara, 2024). A commonly used instrument for measuring static interfacial tension in emulsions is the force tensiometer. It measures the force required to detach a droplet from a ring or to hold a plate at the oil-water interface (McClements, 2004a). Another instrument is the optical tensiometer, which allows protein aggregates in the aqueous phase to diffuse into a pendant oil droplet located at the end of a J-shaped needle as shown in **Fig. 2.6A** (Schmitt & Wanasundara, 2024). The principle of this method is based on the equilibrium between gravitational force and surface force, which governs the shape of the pendant droplet. As the gravitational force pulls the oil droplet downward, the interfacial force maintains the droplet's shape (Schmitt & Wanasundara, 2024). During the adsorption process, the droplet's changing shape is captured by a camera, and the interfacial tension is calculated by a computer (Berry, et al., 2015).

Generally, protein aggregates with low interfacial tension can reduce the energy needed for new surface formation by adsorbing at the interface. This, in turn lowers the energy required to prepare emulsions stabilised by protein aggregates, decreasing the oil droplets sizes during the formation of emulsions (McClements, 2004a). Keivaninahr, et al. (2021) found a relationship between the interfacial tension and plant protein aggregates (pea and faba) at various pH conditions (pH 2 and 7) and their emulsifying ability. The protein aggregates with lower interfacial tension can form emulsions with smaller oil droplet sizes. For instance, potato protein aggregates were found the greatest interfacial value at pH 5 as shown in **Fig. 2.6B**, and the emulsions prepared by potato protein aggregates at pH 5 exhibited the largest and most flocculated oil droplets compared to emulsions prepared at other pHs (da Silva, et al., 2021).

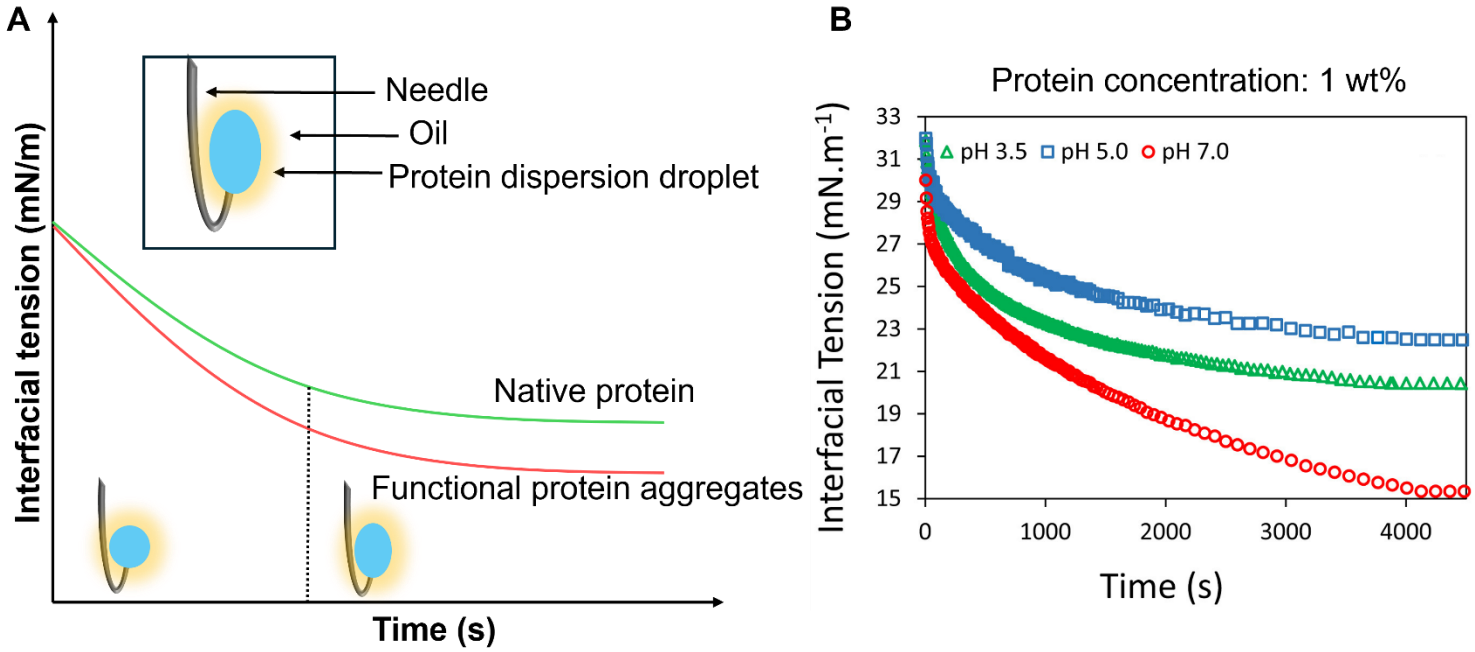

Fig. 2.6 (A) Schematic diagram of the interfacial tension measured over time and the shape change of the droplet. (B) Time dependence of oil-water interfacial tension of potato protein concentrate dispersions at pH 3.5, 5.0, and 7.0. Figure 2.6B was reproduced from da Silva, et al. (2021) with permission from Elsevier, copyright 2021.

2.3.4 Rheological measurement

Rheological studies are important for understanding the deformation and flow of protein aggregates under external forces. These studies measure how protein aggregates respond to deformation, providing valuable information about their mechanical strength and internal structure (Zhu, et al., 2024). Rheological properties are usually characterised using rheometers, which can provide their viscosities and viscoelastic behaviours (Clarke, 2004). Rheometers can also monitor the gelation process, where protein dispersion transforms a liquid state to a semisolid structure at specific protein concentrations during aggregation (Schmitt & Wanasundara, 2024). In general G' reflects the elastic properties, while G'' corresponds to the viscous properties (Barnes, 1994). The ratio of G''/G' yields the value of Tan δ, which provides the information about the protein aggregates, with values ranging from 0.01 (solid gel) to 0.1 (weak gel). A lower Tan δ indicates a more elastic property (Ross-Murphy, 1994).

2.4 Technofunctionalities of plant protein aggregates

Plant proteins are increasingly utilised as key ingredients due to the growing consumer demand for plant-based products in the food industry. The formation of different types of plant protein aggregates is closely associated with changes in the technofunctionalities of plant proteins (Wu, et al., 2021). For example, the emulsifying capability and solubility of plant protein aggregates are essential for beverage production (Sethi, et al., 2016). Gelation behaviour is critical in dough preparation and the manufacturing of plant-based meat products (Drakos, et al., 2007; Villarino, et al., 2016), while the foaming properties of plant protein aggregates are vital for producing whipped toppings (Lu, et al., 2020).

2.4.1 Solubility

Protein solubility is ability that proteins solute dissolving into a solvent forming a homogeneous solution because of the interactions of protein-protein and protein-solvent (Gao, et al., 2023). It is very important in the real-world food industry because it will decide the food type that can be produced (i.e. solid state or liquid state) (Hellebois, et al., 2021). This function also defines the phases that can be stabilised (e.g. oil or air) and the processing method that is needed (e.g. heat treatment, mixing, etc)

(Hellebois, et al., 2021). Protein solubility will also significantly affect the quality characteristics, including visual appearance, viscosity, and flavour after manufacture (Cosson, et al., 2022). The solubility of proteins will also have impacts on mouthfeel and digestibility when the food was consumed (Deng, et al., 2020).

For most plant proteins, the protein powder (e.g. concentrate or isolate) was extracted from raw materials, and this processes usually include fractionation, extraction, purification, and dehydration processes. Thus, the aggregation state (e.g. monomers, dimers, oligomers, aggregates, etc.) and molecular structure (e.g. native or denatured) of plant proteins can also be significantly affected over the processing (Grossmann & McClements, 2023). Further, the solubility characteristics of a protein could be highly related to the processing parameters (e.g. solvent type, pH, ionic strength, and temperature) applied for extraction (McClements & Grossmann, 2021). However, for most plant proteins, a number of other components may present in extracted protein that can further impact its solubility as well, including starch, dietary fibres, and minerals. For this reason, the extracted plant proteins usually have poor solubility than animal proteins, so the highly soluble plant proteins are preferred in the food industry, especially for beverage products (Gao, et al., 2023).

It is an ongoing challenge to improve the solubility of plant protein. Thus, some modifications including, physical, chemical, or biological process and further combined hybrid processes have been used to improve the solubility of plant protein aggregates. According to de Oliveira, et al. (2016), the mechanism to improve the plant proteins solubility can be involved with size reduction, electrostatic repulsion, manipulating the pI and net charge, etc. Some methods to form plant protein aggregates that have been reviewed above in **Section 3.2.2**, such as pH shifting, homogenisation, ultrasonication, and hydrolysis, could most likely enhance proteins solubility, by restructuring protein and forming aggregates with greatly improved solubility (Akharume, et al., 2021). For instance, the solubility walnut proteins were significantly increased from ~ 76.4% to ~93.2% after US treatment at 600 W (pH 7, 15 min) (Zhu, Zhu, et al., 2018). Moll, et al. (2021) conducted HPH (150 MPa for five cycles) to increase the solubility of pea proteins from ~ 22.6% to ~86.3%.

2.4.2 Emulsification

Food emulsions are systems consisting of two or more immiscible liquids, where one liquid is dispersed as droplets within another (McClements, 2004a). The most common type of food emulsion is oil-in-water (O/W) emulsions such as mayonnaise, creams, and soups, where the oil phase is dispersed into the aqueous phase (i.e. water) (Tan, et al., 2023). The emulsifying capability of plant protein aggregates plays a crucial role in the food industry, as they aid in homogenisation and stabilise emulsions (Padial-Domínguez, et al., 2020; Wu, et al., 2021). Plant proteins function as natural emulsifiers by reducing the interfacial tension, which lowers the energy required for homogenisation and enhance the stability of emulsions (Kim, Wang, et al., 2020). Additionally, because of their amphiphilic nature, plant protein aggregates can adsorb at the O/W interface of oil droplets, forming a protective layer that prevents further aggregation (Liu, Pei, et al., 2022).

Recently, many types of food emulsions have been widely researched, such as Pickering emulsions and high internal phase emulsions (HIPEs). Pickering emulsions are emulsions stabilised by solid particles (e.g. microgels and/or nanoparticles) (Pickering, 1907). Compared to conventional surfactant-stabilised emulsions, Pickering emulsions are good at resisting the coalescence of the dispersed phase, leading to a more stable emulsion system (Xiao, Li, et al., 2016). Different research has focused on Pickering emulsions stabilised by plant proteins, including SPI (Wu, Liu, et al., 2023) and PPI (Li, Jiao, et al., 2022). HIPE is another type of emulsion that has been widely researched in recent years because of their semi-solid texture, and the ability to encapsulate bioactive substances due to their high oil phase content (typically > 74%) (Liu, Gao, et al., 2019). These unique features make HIPEs suitable for applications in the food industry that require a solid-like texture and high oil content. Thus, HIPEs have a number of food applications, such as plant-based mayonnaise (Liu, Guo, et al., 2018) and 3D food printer inks (Li, Xu, et al., 2020).

The physiochemical properties of plant protein aggregates are significant to their emulsification abilities. For example, the solubility of plant protein aggregates in the dispersion phase is essential when preparing emulsions, with higher solubility generally linked to better emulsification ability (Nawaz, et al., 2021). Thus, several studies have

examined how plant protein aggregates improve plant protein emulsification ability (Alavi, Chen, & Emam-Djomeh, 2021; Tan, et al., 2023). For instance, Afkhami, et al. (2024) indicated that SPI fibrillar aggregates enhanced the emulsification ability of SPI in stabilisation of 10 %v/v soybean oil using an Ultra-Turrax (10,000 rpm for 2 min). The oil droplet size was significantly reduced when emulsions were formed by SPI fibrillar aggregates, and the ability against environmental stresses (e.g. pH, salt, and heat) was also enhanced. The enhanced emulsification ability of SPI fibrillar aggregates compared to native SPI can increased β-sheet content and fibril length. The formation of long protein fibrils forms a thicker and more continuous coat around the oil droplets, becoming an effective barrier against further coalescence (Hu, Cheng, Gilbert, Loo, et al., 2024; Pang, et al., 2020; Yue, et al., 2022).

Many other plant proteins, such as pea (Zhang, Zhao, et al., 2023), soybean proteins (Xia, Lu, et al., 2021), mung bean (Hei, et al., 2024), and rice proteins (Pan, et al., 2019), that have been used to form functional aggregates which facilitate emulsion preparation through physical, chemical, or biological methods. **Table 2.4** shows some recent studies related to the application of plant protein aggregates in emulsion formation.

Table 2.4 Summary of recent studies in utilisation plant protein aggregates as emulsifiers in formulating O/W emulsions over the past 5 years.

Proteins	Aggregation methods	Oil fractions	Aqueous phase	Emulsification methods	Conclusions	References
Faba bean proteins	untreated	1% v/v sunflower oil	FPC concentrations ranged from 5%-8%, w/w at pH 8	High-shear mixer at 10000 rpm for 20 min followed by a single-stage homogeniser at 80 MPa for 1 pass	• Emulsions prepared with higher protein concentrations result in better emulsification ability. • Oil droplet size decreased from ~11 μm to ~9 μm when the FPC concentration increased from 5% to 8% (w/w).	Nawaz, et al. (2021)
	Highly soluble faba bean protein aggregates were induced by HPH at103 MPa or 207 MPa.	25% v/v canola oil	1% (w/v) of faba bean protein at pH 7	Ultra Turrax at 25,000 rpm for 2 min	• Native FPI showed better emulsification ability than HPH-induced FPI aggregates. • The emulsifying activity index of untreated FPI (~27 m^2/g) were significantly greater than HPH treated FPI (~22.7 m^2/g for 103 MPa and ~19.7 m^2/g for 207 MPa).	Yang, Liu, et al. (2018)
	FPI aggregates induced by pH_{11} shifting assisted by ultrasonication for 10 – 20 min	10% v/v canola oil	1% (w/v) of faba bean protein at pH 7	Ultra-Turrax at 12,000 rpm for 2 min, followed by HPH at 138 MPa for 4 cycles.	• FPI aggregates formed by combined pH shifting and ultrasonication led to better emulsification ability with smaller oil droplet sizes (decreased from ~623 nm to~376 nm).	Alavi, Chen, and Emam-Djomeh (2021)
	Fibrillar FPI aggregates formed by	75% v/v soybean oil	1% (w/w) of faba bean protein at pH 2	Ultra Turrax at 14,500 rpm for 2 min	• Fibrillar FPI aggregates had better emulsification ability	Hu, Cheng, Gilbert,

	TS (90 °C, 10 – 30 min) or heat treatment (90 °C, 1 – 8 h) at pH 2.				• compared to the native FPI. • The oil droplet sizes of fibrillar FPI stabilised emulsions decreased to ~17.6 μm compared to ~21.2 μm (native FPI).	Loo, et al. (2024)
Soybean proteins	SPI was acylated by ethylenediaminetetraacetic dianhydride at ratio from 5 wt% to 30 wt%	25% v/v soybean oil	4% (w/v) of SPI at pH 7	High-speed shearing at 9021 rpm for 2 min	• Emulsions stabilised by acylated SPI aggregates had smaller oil droplet sizes (~15 μm) than native SPI (~28 μm).	Xia, Lu, et al. (2021)
	The pH of SPI was adjusted to pH 10 for 30 min, followed by centrifugation at 10,000 rpm for 30 min after neutralisation, and then heating at 95 °C for 15 min	33%, 50%, 66%, and 75% v/v vegetable oil	4% (w/w) of SPI at pH 7	Ultra-Turrax at 10,000 rpm for 20 s	• SPI nanoparticles had better interfacial activity and can stabilise O/W emulsions with higher oil content than untreated SPI. • HIPEs stabilised by SPI nanoparticles had better stability (>14 d) and greater elastic modulus (>900 Pa) than emulsions stabilised by native SPI.	Wang, Guan, et al. (2023)
	SPI fibrillar aggregates were formed after heating at 85 °C for 90 min	10% v/v soy oil	1.5% (w/v) of SPI fibrillar aggregates at pH 2	Ultra-Turrax at 10,000 rpm for 2 min	• Emulsions stabilised by SPI fibrillar aggregates had significantly smaller oil droplet size distribution than emulsions stabilised by native SPI	Afkhami, et al. (2024)
Pea proteins	PPI was treated by the combination of pH-shifting (pH 12) and sonication (500 W for	75 % v/v sunflower seed oil	5% (w/w) of PPI aggregates at pH 7	Ultra-Turrax at 15,000 rpm for 2.5 min	• PPI aggregates had more flexible structure and better emulsifying ability than native PPI. • Native PPI was unable to form	Zhang, Zhao, et al. (2023)

	10 min)				HIPEs, unlike the treated PPI.	
Rice proteins	Rice proteins were hydrolysed by neutrase, trypsin, and alcalase at a ratio of 1:250 followed by heat treatment at 90 °C for 10 min.	10 % v/v soybean oi	2% (w/v) of rice proteins at pH 7	Ultra-Turrax at 10000 rpm for 2 min, followed by HPH at 60 MPa for three cycles	• Hydrolysed rice protein aggregates had improved surface hydrophobicity and emulsification ability than native proteins. • Trypsin hydrolysates had the best emulsification ability and stability, resulting in emulsions with the smallest particle size (~0.27 μm)	Pan, et al. (2019)
Quinoa protein	QPI was treated by an ultra-Turrax at 15,000 rpm for 5 min and sonication (950 W for 25 min) at pH 7.	20%, 40%, and 60% v/v soybean oil	3% (w/v) of QPI at pH 3, 5, 7, and 9	Ultra-Turrax at 10000 rpm for 7 s, followed by sonication at 950 W for 5 s	• Emulsions formed by QPI suspensions at pH 5 had the largest size and loose packing of oil droplets compared to QPI at other pHs ad oil fractions. • Emulsions stabilised by QPI at pH 7 and 9 had thinner interfacial layers compared to those at pH 3 and 5.	Yang and Cheng (2024)
	QPI was treated by HPH at 10 MPa, 30 MPa, and 50 MPa for 3 cycles at pH 7.	80% v/v soybean oil	1% (w/w) QPI at pH 7	Ultra-Turrax at 10000 rpm for 1 min	• The emulsifying capacity of QPI were improved after HPH. The emulsifying activity index was increased from ~105 m^2/g for native QPI to ~135 m^2/g for the 50 MPa treated sample.	Luo, Cheng, et al. (2022)
Sugar beet	Sugar beet leaves proteins was prepared	10% w/w sunflower	0.2%, 0.5%, and 1% sugar beet leaves	Ultra-Turrax at 9500 rpm for 1 min,	• Oil droplet size decreased from ~2 μm to ~1 μm when the sugar	Martin, et al. (2019)

leaves proteins	at pH 7 and pH 4.	oil	proteins at pH 4 and pH 7	followed by 100 bar HPH for 10 cycles	beet leaves proteins concentration increased from 0.2% to 1% at pH 7. • The emulsions stabilised by sugar beet leaves proteins had slightly smaller oil droplet sizes at pH 4 (~1.8 μm) than pH 7 (~2 μm).	

2.4.3 Gelation behaviour

Gelation behaviour is another essential techno-functional property of plant protein aggregates, which can usually be observed after heat treatment (Zhu, Bassey, et al., 2022). This property affects the textural and organoleptic characteristics of food products, which is important in food formulation design (Tang, Roos, & Miao, 2024). For common globular plant proteins, they denature and unfold upon heating, then interacting with each other to form protein aggregates in size ranging from nano- to micrometres (Nicolai, 2019). In general, a three-dimensional gel network structure can be observed when the protein concentration reaches a specific level (e.g. > 10 wt% for FPI) (Nivala, et al., 2021; Wu, et al., 2021). However, the gelation behaviour of plant proteins is influenced by many factors, such as the source and structure of proteins, ionic strength, pH, and temperature (Tang, Roos, & Miao, 2024). For example, as indicated in **Fig. 2.7**, when the pH value of plant protein solutions shifts away from the pI, protein gels are transformed from a disordered, opaque gel (particulate type) into a translucent and more homogeneous gel (strand type) (Tang, Roos, Vahedikia, et al., 2024).

Further, the gelation behaviour of plant proteins may display diverse responses when being heated under varying pH conditions and times. Under extreme acidic pH conditions, plant proteins may form fibrillar aggregates upon heating, which can subsequently create a gel network. These fibrillar aggregates, characterised by their high aspect ratio, distinguish the gel formed from different from those produced by globular proteins, offering unique structural and functional properties (Hu, Cheng, Gilbert, Lee, et al., 2024; Hu, Cheng, Gilbert, Loo, et al., 2024). Additionally, the presence of plant protein fibrillar aggregates can increase gel viscosity, primarily due to the fibril entanglement from their dense accumulation within the structural domains (Meng, et al., 2022). This phenomenon was also confirmed by Zhang, et al. (2014), who observed that the gelling strength of fibrillar aggregates formed by rice bran proteins at pH 2 was stronger than the gels formed at pH 7.

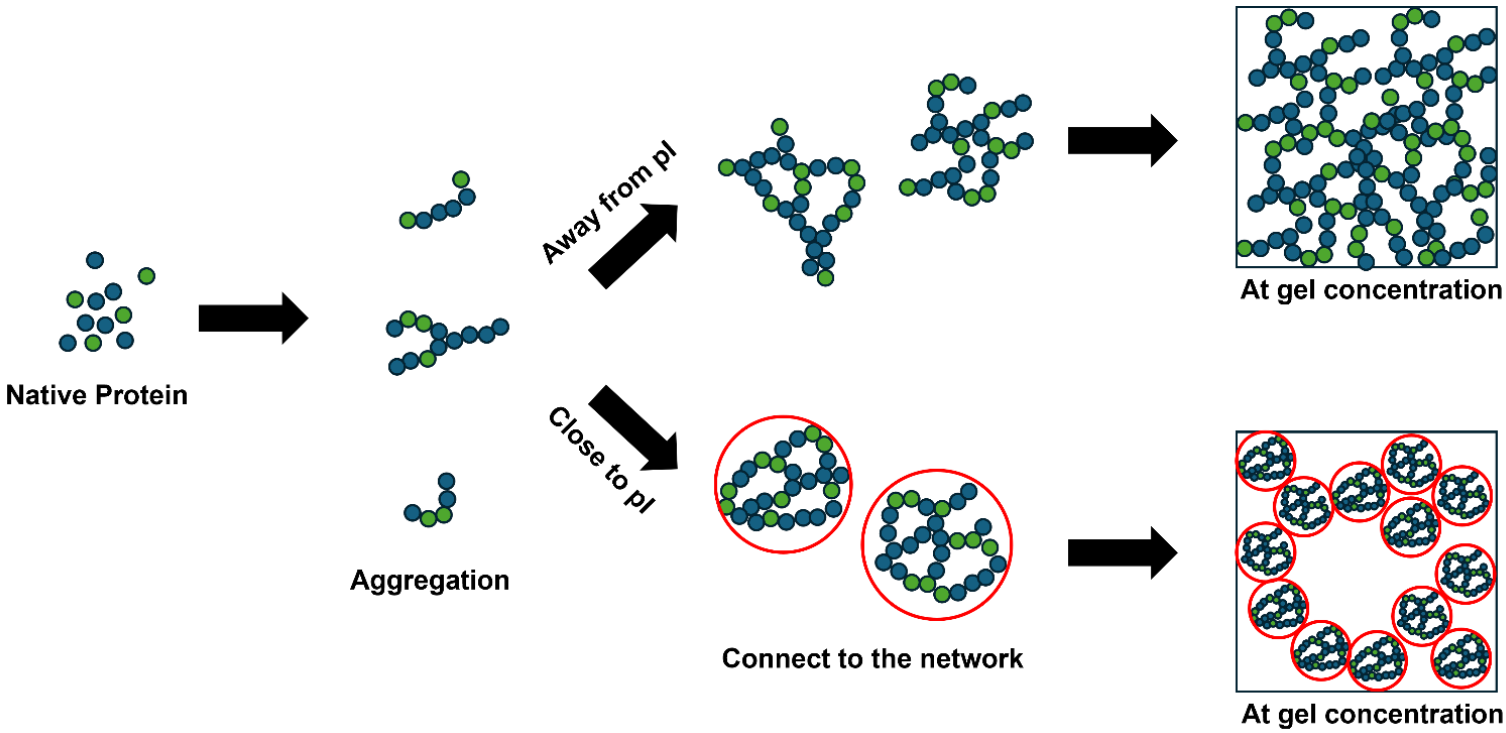

Fig. 2.7 Schematic representation of random aggregation and gelation of globular plant proteins. When the protein concentration exceeds the critical gel concentration, a percolating network is formed. The protein aggregates can form either a fine strand-like or particulate type network, depending on envrironmental factors (e.g. pH).

2.4.4 Foaming

Foams are systems dispersing air bubbles into an aqueous phase (Tan, et al., 2023). The foaming capability and stability of proteins are crucial factors in determining the density, texture, and rheology of food products, thereby influencing their sensory characteristics (Tan, et al., 2023). Proteins are ideal for stabilising foams due to their amphiphilic properties, having both hydrophobic and hydrophilic regions. These characteristics enable proteins to absorb at the air-water interface, facilitating foam formation and stability. (Damodaran, 2005). During aeration, proteins unfold and reorient at the air-water interface. Their hydrophilic groups move toward the aqueous phase, and hydrophobic groups migrate toward the air phase, leading to a decrease in air-water interfacial tension (Alleoni, 2006). At the interface, protein molecules form a film-like barrier around air bubbles, stabilised by electrostatic interactions, hydrophobic bonds, and hydrogen bonds, which collectively protect and maintain the foam structure (Damodaran, 2005; Murray, 2007).

Native plant proteins often exhibit inferior foaming properties because of their compact structure, which limits them unfolding and adsorbing effectively at the air-water interface (Amagliani & Schmitt, 2017). To overcome this issue, functional aggregates are commonly formed to improve the foaming properties of plant proteins. This process involves forming plant protein aggregates with various secondary, tertiary, and quaternary structures that expose more hydrophobic/hydrophilic regions of proteins (Wouters, et al., 2016). Various treatments, including heat treatment (Wang, et al., 2019), ultrasonication (Martínez-Velasco, et al., 2018; Xiong, et al., 2018), high pressure (Chao, et al., 2018), and chemical methods (Alavi, Chen, Wang, et al., 2021; Shao, et al., 2024), have been applied to induce functional aggregates in plant proteins such as soybean proteins and pea proteins. He, et al. (2015) treated SPI (5 wt%, pH 7) at 90 °C for 60 min, resulting in a significant improvement of foaming capability (~1.5 folds of increase after heating) because of greater solubility and hydrophobicity of SPI. Similarly, Xiong, et al. (2018) applied ultrasonication to PPI (5 wt%, pH 7) at amplitudes 30%, 60%, 90% for 30 min, producing PPI aggregates with reduced particle sizes and increased hydrophobicity, leading to enhanced foaming properties (i.e. foaming ability increased from 150% to 200 % after 30-min treatment).

As discussed, plant protein fibrillar aggregates have better foaming capability and stability compared to native plant proteins, primarily due to their large aspect ratios (Meng, et al., 2022). This structural advantage has led to extensive research into their application as foaming agents. For example, soybean protein fibrillar aggregates have demonstrated superior interfacial adsorption, providing enhanced stability against air bubble coalescence (Yu, et al., 2024). Pang, et al. (2020) also found that rice protein fibrillar aggregates could prevent oil droplets flocculation, contributing to stabilising foams and enhance the proteins' coverage around the oil droplets. Specifically, mung bean protein fibrillar aggregates have shown significantly improved foam stability and capability compared to non-fibrillar aggregates (Herneke, Karkehabadi, et al., 2023). These findings align with research on whey protein fibrillar aggregates, which have been shown to remarkably enhance both foaming capacity and stability than native proteins (Oboroceanu, et al., 2014).

2.5 Application of plant protein aggregates in food formulations

2.5.1 Beverages

Beverage products are typically O/W emulsions, which could provide a convenient way for people to consume plant proteins (Jeske, et al., 2018). Recently, plant-based beverages have gained increased popularity, especially among individuals who suffer from lactose intolerance or coronary cardiac disease (Nawaz, et al., 2022). In general, plant proteins used in beverages are in the form of concentrates or isolates extracted from plant resources (Tan, et al., 2023). These proteins are used to create a uniform emulsion by blending them with other ingredients, followed by pasteurisation and commercial packaging for consumer use (Arbach, et al., 2021). Typically, plant proteins are the primary protein sources in the beverage, while some additives such as minerals, fibre, starch, stabilizers, and emulsifiers, are included to improve stability, enhance nutritional values and the sensory attributes (Tan, et al., 2023).

However, due to the increasing consumer demand for "clean-label" food products, plant-based beverage formulations now rely on highly functional plant proteins as essential ingredients to create stable emulsions (Higa & Nickerson, 2023; McClements, 2004a). Therefore, the formation of highly functional plant protein aggregates via

various methods has gradually become a solution to solve this problem. For example, Flores-Jiménez, et al. (2022) demonstrated that ultrasonication treatment could form soluble aggregates from guamuchil-seed protein isolates, which exhibited greater molecular flexibility and surface hydrophobicity. These changes resulted in a significant enhancement in emulsifying, foaming, and gelation properties, offering potential for use in "clean label" beverages. Furthermore, several studies have shown the successful stabilisation of beverages with plant protein aggregates, highlighting their significant market potential, as detailed reviewed by Rojas, et al. (2022) as well as Penha, et al. (2021).

2.5.2 Plant-based mayonnaise

As a popular food product in many countries, mayonnaise is usually consumed with other foods, including sushi, burgers, and salads. Traditionally, egg yolk serves as the primary emulsifier in mayonnaise production, facilitating the formation of an O/W emulsion (Li, Jiao, et al., 2022). However, with the growing demand for plant-based food, plant proteins are increasingly being explored as alternatives to egg yolk, enabling the production of cholesterol-free mayonnaise products (Huang, et al., 2022). Mayonnaise is regarded as a semi-solid concentrated emulsion (oil fraction >0.5, v/v) and a HIPE (Su, et al., 2023).

Studies have indicated that various plant protein aggregates can be used to create mayonnaise-like emulsions, including SPI (Tian, et al., 2023), PPI (Li, Jiao, et al., 2022), and FPI (Augustin & Cole, 2022). For example, Li, Jiao, et al. (2022) developed a plant-based mayonnaise using a Pickering emulsion stabilised by PPI microgel aggregates. These aggregates were formed after heat treatment (95 ℃ for 30 min), followed by incubation at 45 °C for 4 h for gel formation, and then homogenised at 50 MPa for three cycles. This method resulted in a concentrated emulsion containing 50% oil v/v, achieving a viscosity similar to that of commercial mayonnaise. Furthermore, plant-based mayonnaise formulations have demonstrated potential for 3D printing applications. As described in **Fig. 2.8**, Hu, et al. (2023) demonstrated that mayonnaise-like emulsions stabilised by FPI aggregates, at an oil fraction of 0.5 (v/v) and different pH values, improved 3D printability, especially when prepared at higher pH values (e.g. pH 7 and pH 9) and after heat treatment (90 ℃ for 30 min).

Previous studies showed that fibrillar plant protein aggregates can form HIPEs systems due to their large aspect ratios, which significantly enhance emulsification than native proteins (Leng, et al., 2022; Tian, et al., 2023). These fibrillar aggregates exhibit better interfacial adsorption, efficient coverage, and greater ability to prevent aggregation, making them effective emulsifiers in stabilising mayonnaise (Wei, et al., 2019). Hu, Cheng, Gilbert, Loo, et al. (2024) successfully prepared mayonnaise-like HIPEs with an oil fraction of 75% (v/v) stabilised by FPI fibrils. This study demonstrated that HIPEs stabilised by FPI fibrils exhibited stronger mechanical strength compared to the HIPEs stabilised by untreated FPI. Similarly, Tian, et al. (2023) developed a nutrient-rich plant-based HIPE mayonnaise stabilised by SPI fibrils at an oil fraction of 0.75 and fortified with β-carotene. This formulation resulted in higher viscosity and smaller oil droplet sizes than mayonnaise prepared using native SPI particles.

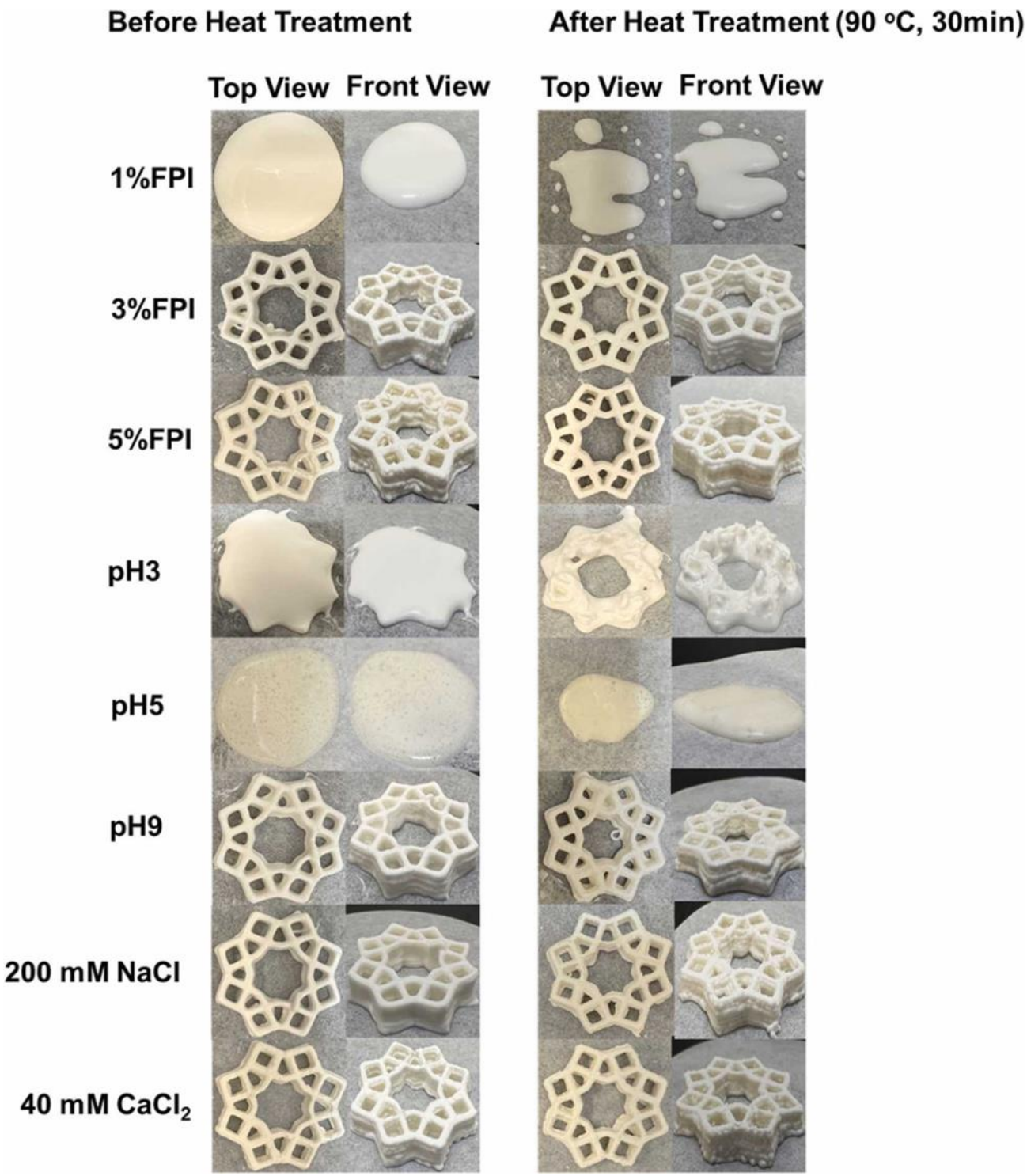

Fig. 2.8 The visual appearance of 5 mm high geometric shapes 3D-printed by plant-based mayonnaises. The mayonnaises were stabilised by FPI at different formulations before and after the heat treatment (90 °C, 30 min). Figure was repreduced from Hu, et al. (2023) with permisstion Elsevier, copyright 2023.

2.5.3 Plant-based whipped cream

Whipped cream, such as hydrogenated vegetable oil cream and milk fat cream, is an O/W emulsion with an oil fraction of 30–40%, typically made from emulsifiers, sugars, and fats/oil (Fu, et al., 2020). Traditional plant-based whipped cream is often produced from hydrogenated palm kernel oil, which is high in trans fatty acids and saturated fatty acids, posing health risks linked to cancer, coronary heart disease, and type *II* diabetes (Islam, et al., 2019; Shin, et al., 2021). Additionally, dairy whipped creams are also unsuitable for consumers having dairy allergies or lactose intolerance (Fu, et al., 2020). Given the growing demand for healthier and more sustainable food products, developing plant-based whipped cream using non-hydrogenated vegetable oils and plant protein aggregates is important for improving diet nutritional quality (Wang, Ma, et al., 2022). For examples, Wu, Zhang, et al. (2023) utilised fibrillar kidney protein aggregates to stabilise whipped cream at an oil fraction of ~0.14 (v/v), resulting in a product with higher overrun, mechanical strength, and structural stability than whipped cream stabilised by native kidney bean protein aggregates. In another study, Zhang, et al. (2024) developed FPI microgels by a combination of heat treatment (90 °C for 30 min), transglutaminase (20 U/g) crosslinking following by HPH treatment at 60 MPa. Whipped cream made from these FPI microgels showed significantly better emulsification ability compared to native FPI (Zhang, et al., 2024).

2.5.4 Fat substitutes

Although animal fat and fat products are important in the human diet, providing essential nutrients, including fatty acids and oil-soluble vitamins, they also contain significantly higher concentrations of saturated fatty acids (Wood & Enser, 2017). These high levels of saturated fats have been associated with various health concerns, including an risk of cardiovascular diseases (Murillo, et al., 2019). Furthermore, the livestock industry, the primary source of animal fat, is related to greenhouse gas emissions and environmental pollution (Willett, et al., 2019). Therefore, developing plant-based fat analogues has gained increasing attention. High oil-concentrated emulsion gels and HIPEs, stabilised by plant protein aggregates, exhibit semi-solid structures with high stability, which makes them suitable as fat substitutes compared to dilute emulsions with oil fraction less than 50% (Badar, et al., 2023; Patel, 2017; Zhang,

Xie, et al., 2023). Recently, Galvão, et al. (2024) utilised lentil proteins to form HIPEs at an oil fraction of 0.75, substituting pork back fat content in Bologna sausages without compromising stability and sensory attributes. Du, et al. (2024) formed peanut protein microgel prepared by the combination of heat treatment (90 °C for 30 min), transglutaminase (2 U/g), and HPH (100 MPa) and applied them to stabilize concentrated emulsion gels at an oil fraction of 50% as fat analogues. They also found that the overall stability as well as the rheological properties of emulsion gels stabilised by microgels were remarkably increased than untreated proteins, making them become more fat-like because of greater rheological properties (Du, et al., 2024). In a recent study, PPI protein aggregates were formed through limited Alcalase hydrolysis followed by moderate heating (85 °C, 10 min). These aggregates were regarded as the fat replacement in fat-free dairy cream cheese. The results showed that incorporating PPI aggregates reduced the viscoelasticity and increased the moisture content of the fat-free cream cheese (Austin, et al., 2024).

2.6 Future work recommendations

In our view, several focuses of research arising current findings could be explored in the future:

2.6.1 Developing sustainable and high-throughput manufacturing process for plant protein aggregates

Scaling up the production of plant protein aggregates presents significant challenges. Current methods, including HPP and US, are often constrained to laboratory settings due to equipment limitations and high energy demands. In addition, processes like prolonged high-temperature heating are energy-intensive and costly, limiting their industrial applications. Developing robust, energy-efficient, and scalable manufacturing equipment and process is crucial to overcoming these barriers. Combining modification strategies may create synergistic effects, enhancing the technofunctional properties of aggregates while reducing production intensity. For example, enzymatically hydrolysed pea proteins require milder heating to form aggregates compared to untreated proteins (Austin, et al., 2024), making enzymatic hydrolysis coupled with scalable techniques like extrusion a promising approach for large-scale production. Furthermore, integrating technoeconomic analysis (TEA) and

life cycle assessment (LCA) into future research and can offer very valuable insights into the feasibility and sustainability of industrial-scale plant protein aggregate production (Priyadarshini, et al., 2022).

2.6.2 Fabrication of hybrid and functional plant protein aggregates

Most studies to date have focused on using single plant proteins to create plant protein aggregates and evaluate their properties. However, future research could explore hybrid protein aggregates that combine multiple plant proteins, plant proteins with animal proteins, or aggregates of varied microstructures and sizes. These combinations hold potential to enhance the technofunctional properties, nutritional, and digestive qualities of the aggregates. For example, cereal proteins, high in methionine and cysteine but low in lysine, could be combined with leguminous proteins, high in lysine but low in methionine and cysteine, to achieve higher digestion and nutritional quality (Herreman, et al., 2020). Similarly, hybrid aggregates with animal proteins, such as dairy proteins known for superior solubility, could address the inferior functionalities of plant proteins (Chuang, et al., 2021). Furthermore, incorporating polysaccharides, especially dietary fibers, into plant protein aggregates could improve hydration, solubility, and gastrointestinal health (Tungland & Meyer, 2002), opening new opportunities for functional and versatile applications.

2.6.3 Investigating the effect of drying on plant protein aggregates properties

Understanding the impact of manufacturing on plant protein aggregate powders is critical for their industrial applications. While most studies are more interested in the formation and characterisation of plant protein aggregates in solution, protein ingredients in the food industry are typically used in powdered form due to advantages like lower handling and transportation cost, extended shelf life, and improved stability (Fitzpatrick & Ahrné, 2005). Therefore, it is essential to examine how different drying methods such as spray-drying and freeze-drying, influence on the reconstitution and physicochemical properties of plant protein aggregates, ensuring their functionality is retained for diverse applications.

2.6.4 Harnessing Artificial intelligence (AI) for optimisation fabrication parameters of plant protein aggregates

Fabricating plant protein aggregates often requires intricate processes and precise control of various parameters, including temperature, concentration, and stirring speed. These processes typically involve a trial-and-error approach, making them labour-intensive and time-consuming. The integration of artificial intelligence (AI) as well as machine learning (ML) algorithms can significantly streamline this optimisation process. By analysing vast datasets, ML can identify optimal processing parameters to maximize yield and improve the technofunctional properties of plant protein aggregates. Moreover, ML algorithms can predict the structure-function relationship of plant protein aggregates, providing insights into how specific processing conditions influence protein functionality. Combining ML with experimental validation offers a powerful approach to deepen our understanding of the process-structure-function relationships in plant protein aggregates. This synergy between computational tools and experimental data can accelerate the development of tailored protein aggregates with enhanced properties, fostering their applications in food formulations.

2.6.5 Understanding the mechanism of plant protein aggregation using *in situ* structural characterisation

While significant efforts have been made in formulating and characterising plant protein aggregates, the mechanisms and pathways underlying their aggregation remain unclear. Employing *in situ* techniques, such as spectroscopy (e.g., CD, FTIR) and scattering methods (e.g., SAXS, SANS), to monitor aggregation in real-time could provide valuable insights into protein aggregation kinetics and pathways. This understanding could enable the fine-tuning of processing parameters to achieve desirable microstructures and technofunctional properties. In addition, the complex composition of plant protein concentrates/isolates poses a challenge, as the roles of individual proteins such as globulin and albumin and the inclusion of non-protein constituents (e.g., lipids, polysaccharides) in aggregation are not well understood. In the future, more research is needed to unravel these contributions for more effectively utilisation of plant protein aggregates.

2.6.6 Evaluation sensorial, nutritional, and digestion properties of plant protein aggregates

Sensory, tribological, and nutritional properties of plant protein aggregates are important for their effective applications in food products but remain underexplored. Investigating sensory attributes including mouthfeel of food products containing these aggregates is essential for ensuring consumer acceptance (Viejo, et al., 2024). Additionally, understanding their tribological behaviour during consumption can provide valuable insights into texture and lubrication properties. Nutritional studies are also essential to assess the health benefits, digestibility, and metabolic impacts of plant protein aggregates, advancing their potential as technofunctional ingredients in sustainable and nutritious food systems (Zhou, et al., 2023).

2.6.7 Developing versatile applications of plant protein aggregates

Beyond food applications, plant protein aggregates hold potential for use in cosmetics, pharmaceuticals, and packaging industries because of their excellent technofunctional properties, biodegradability, and biocompatibility (Liu, Li, et al., 2023). On the other hand, the relevant research in these areas remines limited. Future studies could explore their role in developing functional hydrogels, films, and microcarriers for delivery drug and bioactive compounds, thus broadening their application scope. Additionally, comprehensive safety and toxicity evaluations, particularly for fibrillar aggregates, in both *in vivo* and *in vitro* settings, should be prioritised to ensure their viability for non-food uses such as biomedical and tissue engineering (Li, Zhou, Peydayesh, et al., 2023).

2.7 Conclusions

As the demand for plant-based foods grows, the development of versatile and highly functional plant protein aggregates offers a promising solution for (partially) replacing animal sourced protein content in various food and non-food products. This review highlights various physical, chemical, or biological methods, such as high hydrostatic pressure processing, ultrasonication, and enzymatic treatments, used to induce plant protein aggregation, enhancing their technofunctional properties like emulsification, gelation, and foaming. Advanced analytical techniques including spectroscopy, scattering, and microscopy for characterizing these aggregates are crucial to understand their physiochemical properties and reveal their potential to improve products stability,

texture, and organoleptic properties, although a combination of characterisation methods is often necessary for comprehensive analysis. Modified aggregates outperform native proteins, enabling their applications in diverse food and non-food applications, including beverages, dairy and meat analogues, as well as biodegradable packaging. Future research efforts should focus on scaling up production sustainably, integrating advanced experimental characterisation techniques, and leveraging computational tools such as machine learning to optimize process and formulation, ensuring plant protein aggregates plays important roles in meeting the evolving demands for high quality, nutritious, and environmentally friendly food and non-food products.

MASSEY UNIVERSITY
TE KUNENGA KI PŪREHUROA
UNIVERSITY OF NEW ZEALAND

GRADUATE RESEARCH SCHOOL

STATEMENT OF CONTRIBUTION DOCTORATE WITH PUBLICATIONS/MANUSCRIPTS

We, the student and the student's main supervisor, certify that all co-authors have consented to their work being included in the thesis and they have accepted the student's contribution as indicated below in the Statement of Originality.

Student name:	Yinxuan Hu
Name and title of main supervisor:	Professor Aiqian Ye
In which chapter is the manuscript/published work?	Chapter 3

Describe the contribution that the student and members of the supervisory team have made to the manuscript/published work:[1]

Yinxuan Hu: Methodology, Investigation, Data curation, Formal analysis, Writing-original draft.
Lirong Cheng: Conceptualization, Supervision, Investigation, Writing-review & editing.
Sung Je Lee: Supervision, Writing-review & editing.
Zhi Yang: Conceptualization, Supervision, Project administration, Writing-review & editing

Please select one of the following three options:

(●) The manuscript/published work is published or in press

Please provide the full reference of the research output:

Hu, Y., Cheng, L., Lee, S. J., & Yang, Z. (2023). Formation and characterisation of concentrated emulsion gels stabilised by faba bean protein isolate and its applications for 3D food printing. Colloids and Surfaces A: Physicochemical and Engineering Aspects, 671, 131622. https://doi.org/10.1016/j.colsurfa.2023.131622

( ) The manuscript is currently under review for publication

Please provide the name of the journal:

( ) It is intended that the manuscript will be published, but it has not yet been submitted to a journal

Student's signature:	Yinxuan Hu Digitally signed by Yinxuan Hu Date: 2025.01.21 20:00:26 +13'00'	Main supervisor's signature:	Aiqian Ye Digitally signed by Aiqian Ye DN: cn=Aiqian Ye, c=NZ, o=Massey University, ou=Riddet Institute, email=A.M.YE@massey.ac.nz Reason: I am approving this document Date: 2025.01.22 10:04:39 +13'00'

This form should be placed at the beginning of each relevant thesis chapter.

[1] Refer to the Massey University Publishing and Authorship guidelines (OneMassey for staff, Stream for students) and/ or Contributor Roles Taxonomy (CRediT) guidelines for guidance.

Chapter 3 Formation and characterisation of concentrated emulsion gels stabilised by faba bean protein isolate and its applications for 3D food printing[2]

Abstract

Concentrated emulsions were prepared at a fixed oil concentration (50 wt%) using faba bean protein isolates (FPI) as an emulsifier and texturizer. Effects of FPI concentration (1, 3 and 5 wt %; at pH7), pH (pH 3, 5, 7, and 9; 3 wt %) and addition of salts (200 mM NaCl and 40 mM $CaCl_2$; at 3 wt % FPI and pH 7) on the emulsion formation were studied. The oil droplet size and microstructural characteristics were examined by static light scattering and confocal laser scanning microscopy (CLSM), and the viscoelastic behaviours of emulsions were characterised by oscillatory rheology. At all different FPI concentrations, the emulsions formed viscoelastic gels with different gel strengths and stability due to network formation and interactions between jammed oil droplets and protein aggregates. The oil droplet size, rheological properties, and 3D printability of emulsions were not significantly changed by the presence of salts. The storage modulus G' (1 Hz) values were higher at higher FPI concentrations, and higher pH values (i.e., pH 7 and 9) as the droplet size was smaller and the droplet packing was more compact, resulting in a better 3D printing performance. Furthermore, the heat treatment (90 °C for 30 min) remarkedly improved gel strength and the 3D printability because of protein denaturation and oil droplet aggregation. This finding demonstrated that the emulsion gel formed with FPI was tuneable for food 3D printing. Most of samples displayed high printing precision with great self-supporting capability, which may find potential applications in creating specialised diet.

Keywords: Emulsion gel; Faba bean protein isolate; 3D Printing; Viscoelasticity; Microstructures

[2] This chapter has been published as Hu, Y., Cheng, L., Lee, S. J., & Yang, Z. (2023). Formation and characterisation of concentrated emulsion gels stabilised by faba bean protein isolate and its applications for 3D food printing. *Colloids and Surfaces A: Physicochemical and Engineering Aspects*, *671*, 131622

Graphic abstract

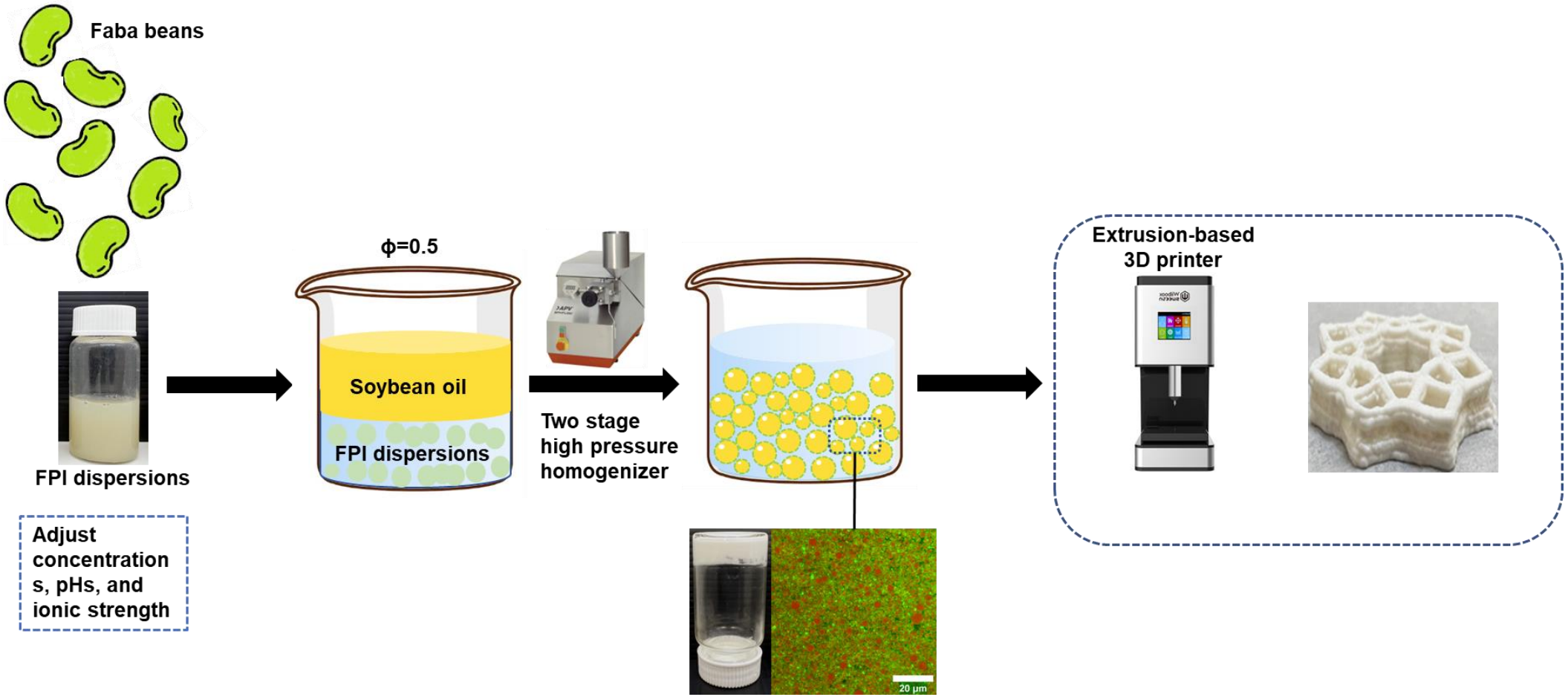

3.1 Introduction

Extrusion-based 3D food printing is an additive manufacturing method for fabricating layer-by-layer solid geometries from edible materials via digital models (Zhao, et al., 2021). Aside from creating complex structures, food 3D printing can also be used to formulate customised nutritional food formulations for consumers with different needs and preferences (Zhao, et al., 2021). For example, 3D-printed foods can enhance children's curiosity towards vegetable-based foods by building fancy food shapes, providing more appealing foods for the elderly with swallowing difficulties, and creating controllable delivery systems for medication and nutrients (Godoi, et al., 2018). However, extrusion printing requires food inks to have shear-thinning behaviour and ideal mechanical properties (e.g., $G' > 1000$ Pa) (Li, Fan, et al., 2021; Suriboot, et al., 2021). The printable food inks should flow easily through a nozzle tip and develop well-defined geometries (Shahbazi, et al., 2021).

Recently, food emulsion gels have been widely used in food 3D printing to create fat replacements (Paciulli, et al., 2020), customised diets (Lu, et al., 2019), and encapsulation of functional components (Lu, et al., 2019). Gels are soft solid-like materials with a three-dimensional network structure (Eivazzadeh-Keihan, et al., 2019; Zhang, Taheri-Ledari, et al., 2023) and emulsion gels are composite structures consisting of oil droplets within a gel matrix (Cen, et al., 2023; Cen, et al., 2022). Due to the emulsion gel's unique structure and mechanical properties, it has recently attracted considerable attention due to its potential applications as printable 3D food inks (Li, Fan, et al., 2021). However, most of emulsion gels used for food 3D printing are high internal phase emulsions (HIPEs) with a high oil content (e.g. $\phi > 0.74$) (Li, Xu, et al., 2020), which is not healthy. In addition, most of them showed weak self-supporting behaviour after 3D printing (Jiang, Zheng, et al., 2019).

Food proteins particularly from animal origins such as gelatine (Kim, Yong, et al., 2020) and whey protein isolates (WPI) (Zhao, et al., 2022) have been extensively used for fabrication of emulsion gels. Nowadays, a strategy has been taken to reduce animal protein production's ecological footprint by increasing the intake of plant proteins in the human diet (Alavi, Chen, Wang, et al., 2021). Faba bean (*Vicia faba*) is a promising alternative protein source because of its rich protein content (ranging from 27%-34%)

and widely grown around the world (Karataş, et al., 2017). Faba bean protein isolate (FPI) is an underutilised functional protein source with many technofunctional properties, such as water and fat binding, foaming, and gelation capacities (Boye, et al., 2010). It has been reported that FPI showed better emulsifying properties compared to other plant proteins such as pea protein isolates (Burger & Zhang, 2019; Karaca, et al., 2011; Liu, Pei, et al., 2022) and lentil proteins (Gumus, et al., 2017b). Therefore, it is expected that FPI could be suitable for fabrication of vegetarian emulsion gels, which may find potential applications as salad dressings, plant-based mayonnaise and 3D printing inks for creating customised diets. For example, Dille, et al. (2022) prepared emulsion gels using mixtures of faba bean protein concentrate (FPC) and λ-carrageenan with incorporations of 20% and 30% oil. The gelation is induced by acidification with glucono-δ-lactone (GDL). Recently, emulsion gels have also been prepared from whole faba bean flour using lactic acid bacterial fermentation or GDL acidification as gelation methods. However, starch removal is required to improve mechanical strength and water holding capability of emulsion gels (Jiang, Wang, et al., 2020). However, to the best of our knowledge, there is no information on preparation of emulsion gels solely stabilised by FPI and apply them in food 3D printing (Enfield, et al., 2022; Zhang, Pandya, et al., 2022). Thus, the novelty of this work lies in the preparation of 'clean-labelled' plant-based emulsion gels solely using FPI as both emulsifiers and texturizers and explore their potential applications in food 3D printing.

In addition, previous studies showed that protein concentrations (Zhang, Cheng, et al., 2021), pH (Felix, et al., 2019), and presence of salts (Wang, et al., 2010) could significantly affect the formation and characteristics of plant protein stabilised emulsion gels. For example, sufficient proteins are required to stabilise oil-water interfaces, which leads to emulsions with smaller oil droplet size with a high stability. pH values and salt (NaCl and $CaCl_2$) additions have substantial influences on particle sizes, solubilities, and electrostatic interactions of protein particles, which in turn affect the emulsification and gelation capabilities of FPI and the formation of emulsion gels. Therefore, the main objective of this work is to investigate the effects of FPI concentrations (1, 3, and 5% w/w), different salt additions (200 mM NaCl and 40 mM $CaCl_2$), and pH levels (pH 3, 5, 7 and 9) on formation physicochemical properties, microstructural characteristics, and 3D printing performances of FPI stabilised

emulsion gels containing 50% oil. Also, the impact of heat treatment (90 ºC for 30 min) on characteristics and 3D printing of FPI stabilised emulsion gels was explored as the heat treatment is commonly used in food processing as a pasteurisation method. This study provides a new route to fabricate FPI stabilised concentrated emulsion gels and insight into important factors and conditions to be considered for the formation of stable concentrated emulsion gels with desired mechanical properties for 3D food printing.

3.2 Materials and methods

3.2.1 Materials

The faba bean protein isolate (FPI) was purchased from NZ Protein Inc. (Auckland, New Zealand). According to the manufacturer's specification, the FPI contains ~85% w/w protein, ~5.4% w/w fat, less than ~1% w/w sugar and dietary fibre. Chemicals used in this study, including sodium dodecyl sulphate (SDS), NaCl, $CaCl_2$, petroleum ether, Fast Green, Nile Red, acetic acid, low viscosity mineral oil (M5904), HCl, NaOH, and sodium azide were purchased from Sigma-Aldrich (St. Louis, MO, USA). All chemicals are of analytical grade, and Milli-Q water (Millipore, USA) was used throughout sample preparations. Soybean oil was purchased from a local supermarket (Pak'in save, Albany, Auckland, New Zealand). The 4 × Laemmli sample buffer, β-mercaptoethanol, 10×Tris/Glycine/SDS running buffer, and Coomassie Brilliant Blue R-250 staining solution were purchased from Bio-Rad (Hercules, CA, USA).

3.2.2 Preparation of FPI dispersions

A stock solution of 10 wt % FPI was prepared by dispersing the FPI powder in Milli-Q water containing 0.04 wt % sodium azide as an anti-microbial agent, followed by magnetically stirring (300 rpm) at ~20 °C for 24 h to ensure complete hydration. The pH was adjusted to 7.0 using 1 M NaOH, followed by stirring (500 rpm) for 6 h. Then, the stock FPI solution was stored at 4 °C until use within a week. Different FPI dispersions with different concentrations of FPI (1, 3 and 5 wt %) were prepared by diluting the FPI stock solution in Milli-Q water. The pH of FPI dispersion (3 wt %) was adjusted to different pHs (pH 3, 5, and 9) by 1 M NaOH or 1 M HCl followed by stirring (500 rpm) for 6 h. The pH values were adjusted every 2 hours until stable during stirring.

The FPI dispersion (3 wt % at pH 7) was also mixed with salt by adding 200 mM NaCl or 40 mM $CaCl_2$. The mixture was stirred by a magnetic stirrer at 20 °C.

3.2.3 Characterisations of FPI dispersions

3.2.3.1 SDS-PAGE

SDS-PAGE (sodium dodecyl sulphate-polyacrylamide gel electrophoresis) was used to characterise the protein profiles based on their molecular weight under reducing and non-reducing conditions (Bühler, et al., 2020; Laemmli, 1970; Yang, de Campo, et al., 2022). For SDS-PAGE under reducing conditions, 0.15 wt% FPI solution (25 μL) was mixed with 1.25 μL of reducing agent (β-mercaptoethanol) at room temperature (~20 °C). Then, the sample was boiled for 10 min followed by cooling prior to loading into the Mini-protein TGX precast gel (Bio-Rad, USA) with 15% resolving gel and 4% stacking gel. A PowerPac Basic (Bio-Rad, USA) was used to perform the electrophoresis at a constant voltage of 130 V in a running buffer (10 × Tris/Glycine/SDS running buffer) (Bio-Rad, USA). After electrophoresis, the gels were stained with Coomassie Brilliant Blue R-250 staining solution (Bio-Rad, USA) for 3 h followed by detaining with 10% isopropanol/glacial acetic acid solution overnight via a shaker (OM6, RATEK, Australia). For protein band identification, a mixture of protein standards with different molecular weights (Precision Plus Protein Dual Xtra Standards) (Catalog # 161–0377, Bio-Rad, USA) with a MW range of 10–250 kDa was also used. For non-reducing SDS-PAGE, β-mercaptoethanol was replaced by Milli-Q while the other procedures remained the same.

3.2.3.2 ζ-potential of FPI dispersions

The zeta (ζ)-potential of FPI solution with different pHs and salt addtions was determined at a protein concentration of 0.1% w/w using dynamic laser scattering (DLS) by a Malvern Zetasizer Nano ZS (Malvern Instruments Ltd, Worcestershire, UK). A refractive index of 1.45 and absorption of 0.001 were applied, respectively (Vogelsang-O'Dwyer, et al., 2020). The analysis was determined in triplicate.

3.2.3.3 Oil-water interfacial tension

The interfacial tension of oil droplets in FPI (0.1 wt%) dispersions was determined by a Theta Flex Plus optical tensiometer (Biolin Scientific Instruments, Sweden) using the

pendant drop method (Zhang, Cheng, et al., 2021). The 0.1 wt% FPI dispersions were prepared by diluting 3 wt% FPI dispersion at different pHs and salt concentrations with MQ water with different pHs and salt solutions. An FPI solution (25 μL) was generated at the stainless-steel syringe tip and immersed in soy oil. The change of interfacial tension with time was monitored up to 5000 s and calculated automatically by One Attention software (Biolin Scientific Instruments, Sweden).

3.2.3.4 Protein solubility

The solubility of FPI in MQ water with different pHs and salt concentrations was determined according to Luo, Cheng, et al. (2022) with slight modifications. Specifically, the FPI dispersions were centrifuged at 2500 × *g* for 15 min at room temperature (~20 °C) by a benchtop centrifuge (Thermofisher 3000, MO, USA). Then, the soluble protein content in the supernatant was determined using a Bradford Protein Assay Kit (Bio-Rad, USA) using gamma-globulin as the standard and expressed as the concentration of soluble protein in FPI dispersions. A UV-Vis spectrophotometer (Shimadzu 2000, Kyoto, Japan) was used to determine the absorbance of protein solutions at 595 nm. The solubility (%) was calculated using the following equation:

$$\text{Solubility (\%)} = \frac{\text{Protein content in the supernatant (mg/mL)}}{\text{Total protein content before centrifuge (mg/mL)}} \times 100\% \quad (3.1)$$

3.2.4 Preparation of emulsions

For the preparation of emulsions, all FPI dispersions were mixed with 50% (v/v) soybean oil and then homogenised by a high shear mixer (T10 basic ULTRA-TURRAX®, IKA Corp., Staufen, Germany) with a 10 mm probe (S10N-10G, IKA, Germany) at 14,000 rpm for 1 min to obtain coarse emulsions. The coarse emulsions were then further homogenised two times via a two-stage high-pressure homogeniser (HPH) (APV 2000, SPX Flow Technology GmbH, Germany) at the pressure of 12 MPa (1^{st} stage)/2 MPa (2^{nd} stage) for the first pass, and 30 MPa (1^{st} stage)/5 MPa (2^{nd} stage) for the second pass. The stock salt solution was added after the first pass of HPH to ensure the uniform dissolution of salts. Then, the emulsions were stored at room temperature (~20 °C) for further tests, which were completed within three days.

3.2.5 Characterisation of emulsions

3.2.5.1 Oil droplet size

The mean particle size and particle size distribution (PSD) of emulsion oil droplets were measured using a static laser light diffraction technique (Mastersizer 2000, Malvern Instruments Ltd, Worcestershire, UK) which measures a size range of 0.01–3000 μm in diameter. The refractive indices used for soybean oil and the dispersant (water) were 1.47 and 1.33, respectively (da Silva, et al., 2021). The emulsions were mixed with 1% SDS solution at a weight ratio of ~1:15 and incubated overnight at room temperature (~20 °C) before the particle size measurements in order to displace the protein particles from the oil-water interface and break the oil droplet flocs (Péron, et al., 2007). The mean particle diameter for single oil droplets was represented as the Sauter mean diameter D [3,2].

3.2.5.2 Flowability of FPI-stabilised emulsions

To visually examine the flowability of FPI-stabilised emulsions, the glass vials containing samples were inverted and left on the bench at room temperature (~20 °C) before the photographs were taken.

3.2.5.3 Confocal laser scanning microscopy (CLSM)

Confocal laser scanning microscopy (Leica DM 6000B, Germany) was used to observe the microstructure of FPI-stabilised emulsions prepared at various conditions. Fast Green (1% w/v) and Nile Red were used to stain protein and oil phases with a ratio of 500:1 (v/v) and 5000:1 (v/w), respectively. For thermally treated emulsion gels, the emulsions were transferred onto the glass slides sealed with a glass coverslip by nail polish to avoid evaporation. Then, the samples were incubated in an oven (Thermofisher, USA) at 90 °C for 30 min. Fast green and Nile red were excited at laser wavelengths of 633 nm and 561 nm, respectively. All the images were processed with Image J software (NIH, MD, USA).

3.2.5.4 Small and large oscillatory deformation rheology

Rheological properties of different emulsion gels were characterised by a stress-controlled rheometer (Physica MCR 301, Anton Paar, Austria) using a parallel plate geometry (40 mm in diameter, 1 mm gap). Aliquots of emulsion samples were

transferred onto the bottom plate with a wood spatula. The sample was then carefully trimmed before adding low viscosity mineral oil around the edge of the sample to prevent evaporation. The rheological measurements were conducted in the following protocol, and the storage modulus G' and loss modulus G'' were recorded during the tests (Zhang, Pandya, et al., 2022). Firstly, a time sweep measurement was conducted at 1% strain and 1 Hz for 1 h to rebody the emulsion gel network after loading the samples onto the bottom plate of the rheometer. Then, a frequency sweep test was conducted at 1% strain while the frequency was varied from 0.01 to 100 Hz. Finally, the large deformation rheological behaviour of the emulsions was determined by a strain sweep test at a strain amplitude from 0.01% to 1000 % and at 1 Hz. For thermally treated samples, a temperature sweep test was conducted by heating the samples from 20 °C to 90 °C at 2 °C/min, maintaining at 90 °C for 30 min, and cooling down to 20 °C at 2 °C/min. The samples were equilibrated at 20 °C for 15 min before conducting small and large deformation rheological tests at 20 °C as mentioned above. All rheological measurements were conducted in duplicate.

3.2.6 3D Printing

3D printing of emulsion gels was performed on a Wiiboox Sweetin chocolate syringe extrusion type printer (Wiiboox, China) using a metal nozzle with a diameter of 0.84 mm. For each sample, emulsion gel (~10 g) was put into the syringe and set into the 3D printer. Printing parameters used were as follows: printing speed 25 mm s^{-1}, printing temperature 20 °C, and the layer height of sample 0.5 mm.

3.2.7 Statistical analysis

All the experiments were conducted at least in duplicate, and the results are reported as mean ± standard deviation (SD). All data were analysed using Minitab statistical software (Minitab 19 Statistical Software, USA). The one-way analysis of variance (ANOVA) was applied to analyse the data. The difference between sample mean values was evaluated via a Tukey's test at a significance level of $P < 0.05$.

3.3 Results and discussion

3.3.1 SDS-PAGE of FPI dispersions

The protein profile of FPI was characterised by both non-reducing and reducing SDS-PAGE as shown in **Fig. 3.1**. Under non-reducing conditions, an intense and smeared protein band was found in the loading well at the top of the stacking gel, suggesting the presence of large protein complex having a molecular weight larger than 250 kDa (Kaspchak, et al., 2017). In addition, there were three major protein bands visible at ~73 kDa, ~59 kDa, and ~51 kDa, which could be assigned to convicilin, legumin (11 S), and vicilin (7 S), respectively (Vogelsang-O'Dwyer, et al., 2020). Under reducing conditions, the large protein complex band at the top of the gel vanished, together with the appearance of two new intense bands at ~ 37 kDa and ~ 20 kDa. These two bands could be α-legumin and β-legumin, which are cross-linked to form legumin via a disulfide (S-S) bond (Langton, et al., 2020). In general, FPI protein profiles observed under both non-reducing and reducing conditions were consistent with previous SDS-PAGE studies of faba bean proteins (Nivala, et al., 2017; Vogelsang-O'Dwyer, et al., 2020). The major protein bands are legumin-type globulins (11S) and vicilin-type globulins (7S) (around 70-78% w/w) followed by albumins (2S) (10-20% w/w) (Singhal, et al., 2016; Zhang, Liu, et al., 2022).

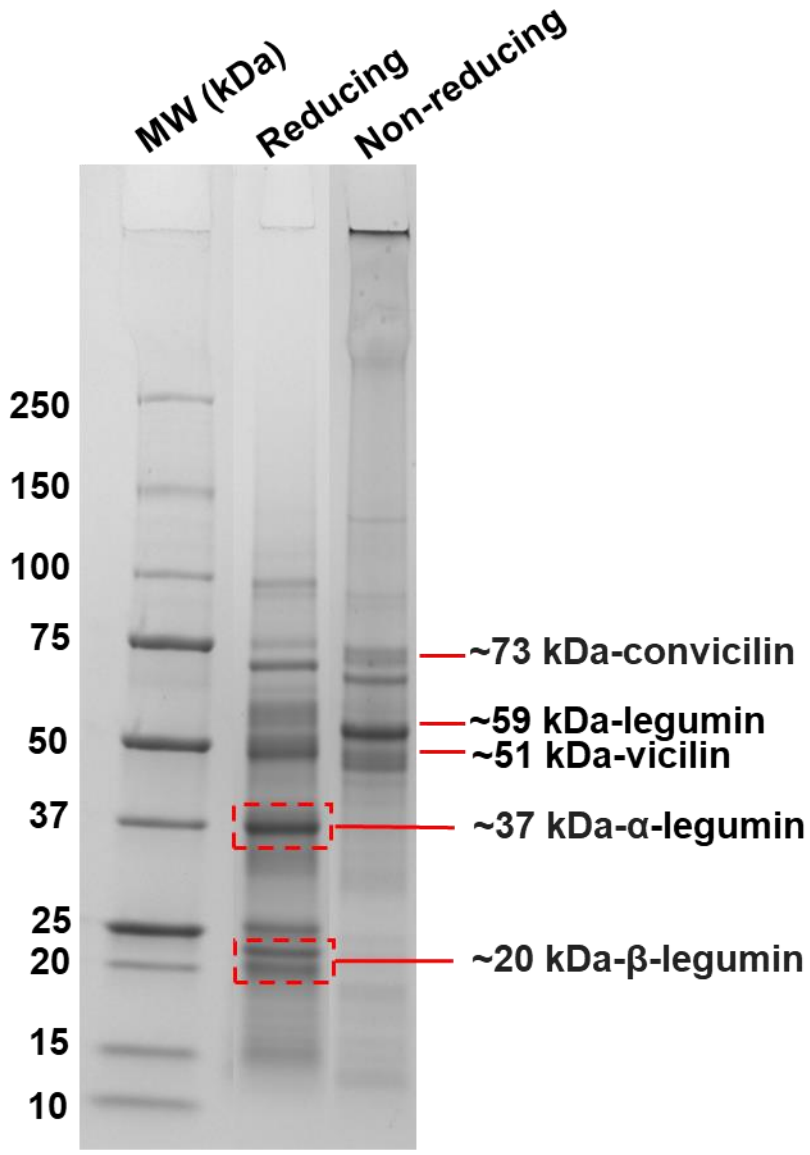

Fig. 3.1 SDS-PAGE profiles of the faba bean protein isolates (FPI) under non-reducing and reducing conditions.

3.3.2 Protein solubility and Zeta potential

Physicochemical properties of proteins such as electrical net charge (ζ-potential), solubility, and interfacial tension are critical in determining the diffusion and adsorption of protein molecules at the oil-water interface as an emulsifier (Otegui, et al., 1997; Zhang, Liu, et al., 2022). The solubility and ζ-potential of FPI as a function of pH and salt addition are plotted in **Fig. 3.2**. It can be estimated that at ~pH 4.5, the net charge was zero (**Fig. 3.2A**). The isoelectric point of pH 4.5 for FPI agrees with previous studies (Otegui, et al., 1997; Vogelsang-O'Dwyer, et al., 2020). The lowest solubility among all FPI samples was observed at pH 5 (**Fig. 3.2B**), which can be explained by its relatively low electrostatic repulsion as indicated by the smallest absolute ζ-potential values. Also, as shown in **Fig. 3.2B**, the addition of NaCl (200 mM) and $CaCl_2$ (40 mM) decreased the solubility of FPI, which can be attributed to the charge screening effect of salt as evidenced by their low ζ-potential values. The addition of salts could thus reduce the electrostatic repulsion and promote the attraction and aggregation of FPI molecules. Similar behaviours have been reported in previous studies of other plant proteins added with NaCl and $CaCl_2$, including soybean proteins (Campbell, et al., 1992), pea proteins (Amagliani, et al., 2022), and quinoa proteins (Yang, de Campo, et al., 2022). In addition, the FPI added with $CaCl_2$ has significantly lower solubility (~6.7%) than the FPI added with NaCl (~12.8%). This could be due to the fact that compared to monovalent salt, the divalent salts are more efficient in inducing protein aggregation by screening charging of protein molecules and promoting the protein cross-linking via salt bridges (Yang, de Campo, et al., 2022).

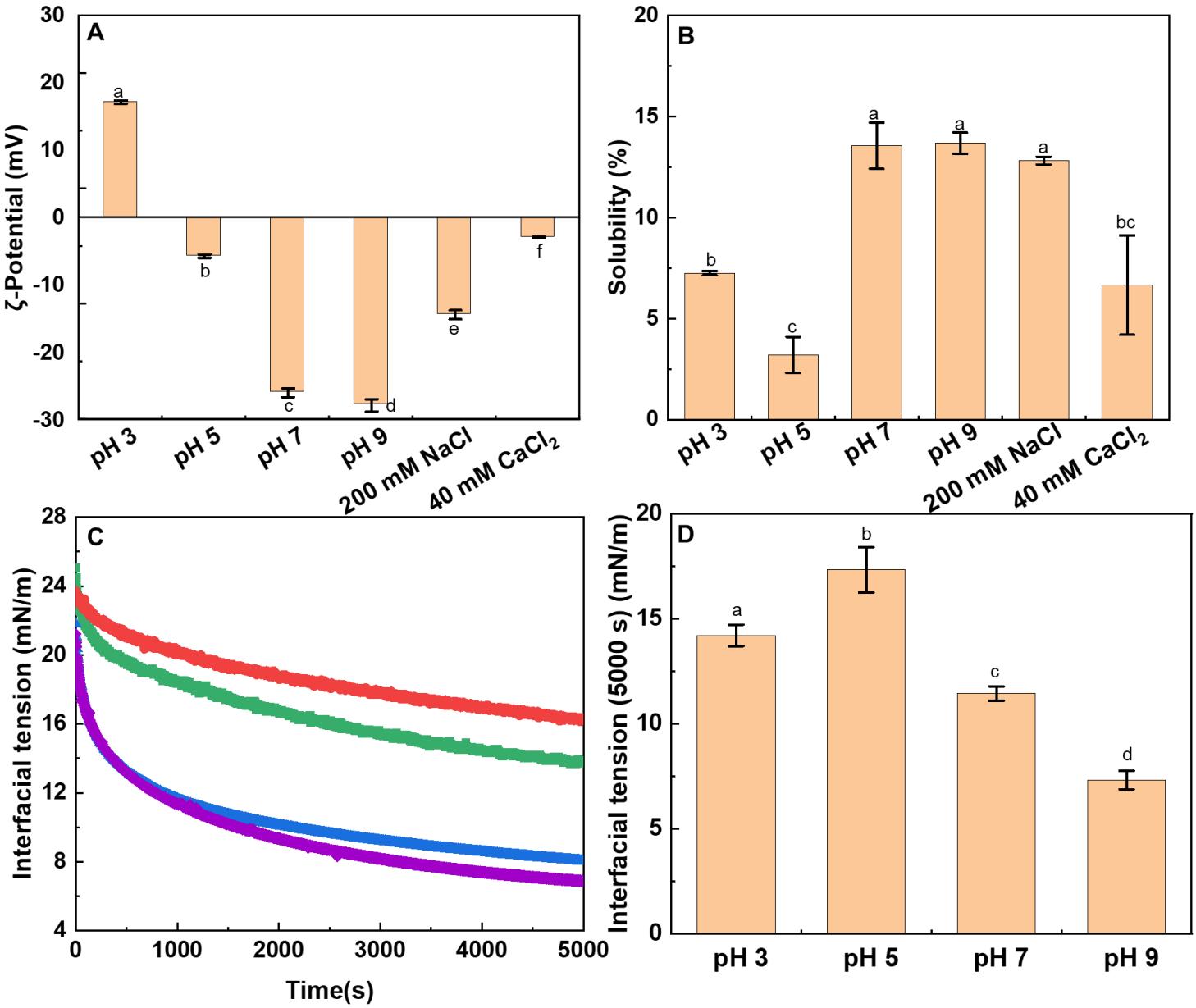

Fig. 3.2 (A) ζ potential of FPI dispersions at different pH values (3-9) and in the presence of 200 mM NaCl and 40 mM $CaCl_2$ at pH 7, (B) solubility of 3 wt% FPI dispersions at different pH values (3-9) and in the presence of 200 mM NaCl or 40 mM $CaCl_2$) at pH 7. (C) Time dependence of oil-water interfacial tension of FPI dispersions at different pH values (3-9) at 20 °C ((■)-pH 3, (●)-pH 5, (▲)-pH 7, (◆)-pH 9). (D) Final interfacial tension values at 5000 s for all emulsion samples. Different letters above the columns indicate significant difference ($P < 0.05$).

3.3.3 Oil-water interfacial tension

The interfacial tension (IFT) of FPI (3 wt%) at various pHs (3, 5, 7, and 9) as well as FPI with added salts (200mM NaCl and 40 mM $CaCl_2$) at pH 7 was determined as a function of time by the tensiometer. The interfacial tension of various FPI dispersions as a function of time are shown in **Fig. 3.2C**. For all FPI samples, the interfacial tension of the protein solutions firstly decreased significantly with time until reaching an equilibrium at ~5000 s. This is a typical characteristic of proteins indicating a stable conformation of protein has been reached after migrating from aqueous phase to adsorb and adopt at the oil-water interface (Tang, 2020a). The equilibrated IFT values at 5000 s of all the samples are shown in **Fig. 3.2D**. The equilibrated IFT value decreased from ~14.2 mN/m to ~6.9 mN/m when the pH values increased from pH 3 to pH 9, while the final IFT value was the highest (~16.3 mN/m) at pH 5. This indicates that the FPI close to the isoelectric point has the weakest interfacial activity, which could be due to its large aggregate size and minimum solubility. The similar observation has been made in pea protein isolates (PPI) (Burger & Zhang, 2019).

In addition, it shows that the equilibrated IFT values of FPI were higher at acidic pH than neutral and alkaline pHs. This finding is in line with Keivaninahr, et al. (2021), who reported that the IFT value of faba bean protein was higher at pH 2 (~15 mN/m) than pH 7 (~8 mN/m). Similar finding has been found in a IFT study of soybean protein isolate (SPI), where a higher IFT was found at pH 3 (~14 mN/m) compared to pH 7 (~11 mN/m) (Chang, et al., 2015). In general, it can be observed that protein carrying a higher charge (or with a higher absolute zeta-potential values) is more effective to reduce the interfacial tension and vice versa. A negative correlation between interfacial tension and surface charges have been also observed in previous studies of other plant proteins including SPI, pea protein isolate (PPI), lentil protein isolate (LPI) and canola protein isolate (CPI) at pH 3, 5 and 7 [45].

3.3.4 Microstructural characteristics of emulsion gels

3.3.4.1 The effect of FPI concentrations

The microstructure and flowability of emulsion gels at various protein concentrations (1, 3, and 5 wt%) before and after heat treatment (90 °C for 30 min) were characterised by using the confocal laser scanning microscopy (CLSM), as shown in **Fig. 3.3**.

In CLSM micrographs, the protein phase appears green, while the oil droplets appear red. In all samples, FPI seemed to cover and stabilise the oil droplets. As the FPI concentration increased, the oil droplets of emulsion were smaller with more compact and compressed packing, and the formation of protein aggregates became more obvious. This could lead to stronger gels observed at emulsions stabilised by 3% and 5% FPI as revealed by the tube (Tang & Ghosh, 2021) inversion test **(Fig. 3.3B and 3.3C inset),** where the samples stuck to the bottom of vials and didn't move once inverted. However, 1 wt% FPI stabilised emulsion gel was weak, which flowed to the bottom of the vial after inversion. Similar findings were also reported in previous studies of other plant protein (e.g., quinoa and pea proteins) stabilised emulsions. For example, Zhang, Cheng, et al. (2021) found that the oil droplet size of quinoa protein stabilised emulsion markedly decreased when the quinoa protein concentration increased from 1 to 5 wt %. This could be due to the fact that a higher protein concentration could stabilise a larger interfacial area, leading to smaller oil droplet size and their tighter packing behaviour (Tang & Ghosh, 2021).

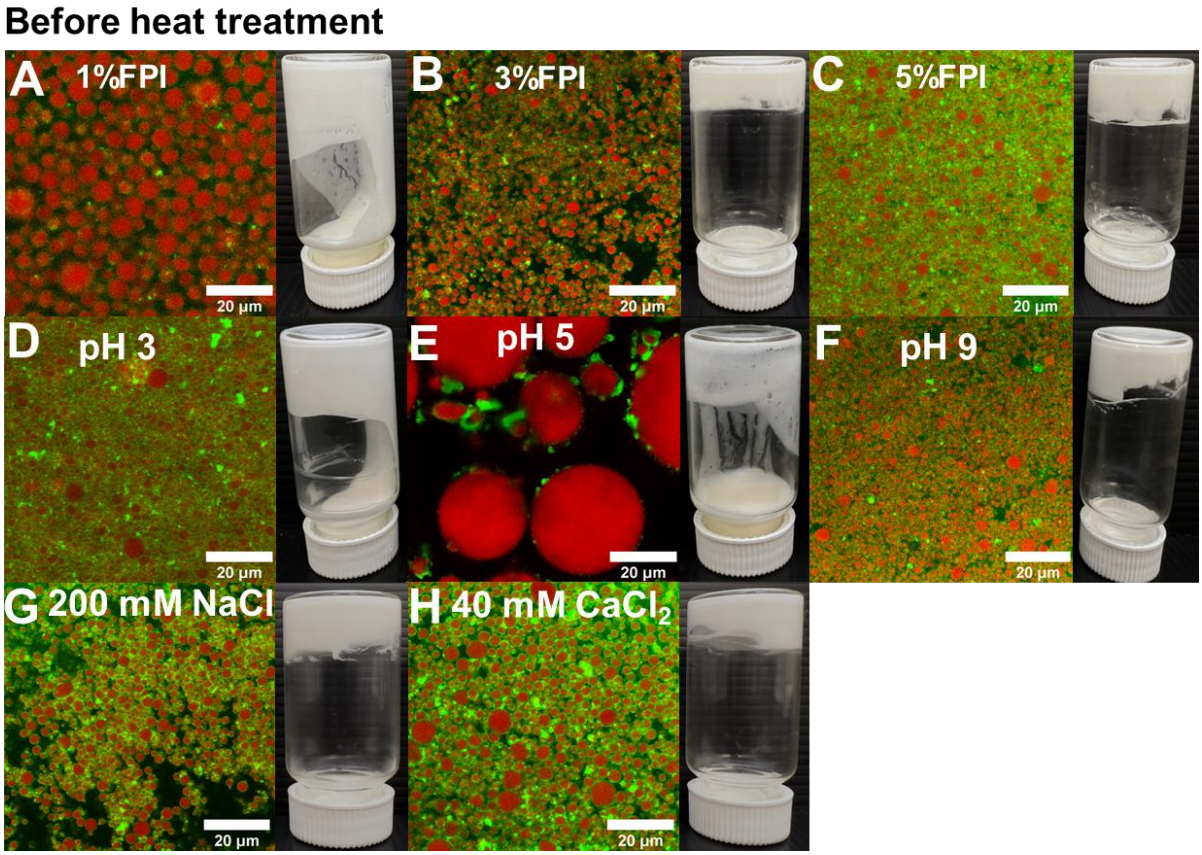

Fig. 3.3 Confocal micrographs and visual appearance of the emulsion samples before heat treatment. (A, B, and C) emulsions stabilised by 1, 3, and 5 wt% of FPI at pH 7. (D, E, and F) emulsions stabilised by 3 wt% of FPI at pH 3, pH 5, and pH 9. (G and F) emulsions stabilised by 3 wt% of FPI at pH 7 in the presence of 200 mM NaCl or 40 mM $CaCl_2$.

3.3.4.2 The effects of pH

The confocal micrographs and visual appearance of emulsion gels that were prepared from a fixed FPI dispersion (3 wt%) at different levels of pH 3, 5, 7 and 9 before and after heat treatment are shown in **Fig. 3.3**. The emulsion stabilised by FPI at pH 3 and 5 showed a lower self-supporting gel strength and visual gel fluidity. In particular, the large oil droplet and protein aggregates can be observed at pH 5 **(Fig. 3.3E).** This could be attributed to the extensive protein aggregation at the pH close to the isoelectric point (pI~4.5) (Zhu, Chen, et al., 2018), thus leading to inferior emulsification capability as revealed by a high IFT value (**Fig. 3.2D**). At pH 7 and 9, semi-solid self-supporting emulsion gels were formed as the emulsions remained at the bottom of the vials when inverted (**Fig. 3.3B and 3.3F insets**). This could be due to the formation of a strong three-dimensional network structure of oil droplets (**Fig. 3.3B and 3.3F**), preventing the movement of the oil droplets and providing elastic-like properties (Zhu, Chen, et al., 2018). This could be due to higher solubilities, large surface charges, lower IFT values, and better emulsification capabilities of FPI particles/molecules at the pHs away from the pI (pH 7 and pH 9).

3.3.4.3 The effects of salts

The visual appearance and CLSM micrographs of 3 wt% FPI stabilised emulsions with and without adding salts (NaCl and $CaCl_2$) are shown in **Fig. 3.3 G-H**. All emulsion samples formed strong self-supporting emulsion gels, regardless the addition of salts. After adding salts, particularly 40 mM $CaCl_2$, prominent protein aggregation and large oil droplet size can be observed. This could be due to charge screening effect of salts which promoted protein attraction and diminished repulsion. Similar observations have been made in other plant proteins such as quinoa protein isolates in the presence of NaCl (20-200 mM) and $CaCl_2$ (20-50 mM) (Yang, de Campo, et al., 2022).

3.3.4.4 The effects of heat treatment

Heat treatments have been extensively used in food processing to ensure food safety, therefore, the heat stability of FPI emulsions is important for their food applications. As shown in the CLSM images and via visual observations (**Fig. 3.4**), the oil droplet size and flowability of samples were not significantly changed before and after heat treatment, except for pH 5 (**Fig. 3.4E**), indicating the structural stability of emulsions

against coalescence and creaming (Zhang, Cheng, et al., 2021). After heating, the interfacial layer became thicker in all heated FPI emulsion gels and the appearance of large protein aggregates between the oil droplets was observed particularly at pH 5 and in the presence of $CaCl_2$. This could be due to the unfolding, denaturation, and aggregation of FPI at a temperature beyond its denaturation temperature (~77–85 °C) (Jiang, et al., 2016; Kimura, et al., 2008). This heat induced FPI aggregates may either adsorb at the O/W interface to make the interfacial layer thicker or be present in the aqueous phase as active fillers in between the oil droplets. This could result in a more compacted arrangement of oil droplets, thus providing a solid self-supporting structure of the emulsion gels (Li, Fan, et al., 2021; Xu, et al., 2018). The alteration in microstructures may lead to changes in rheological properties of FPI emulsion gels, which will be discussed in **Section 3.3.8**.

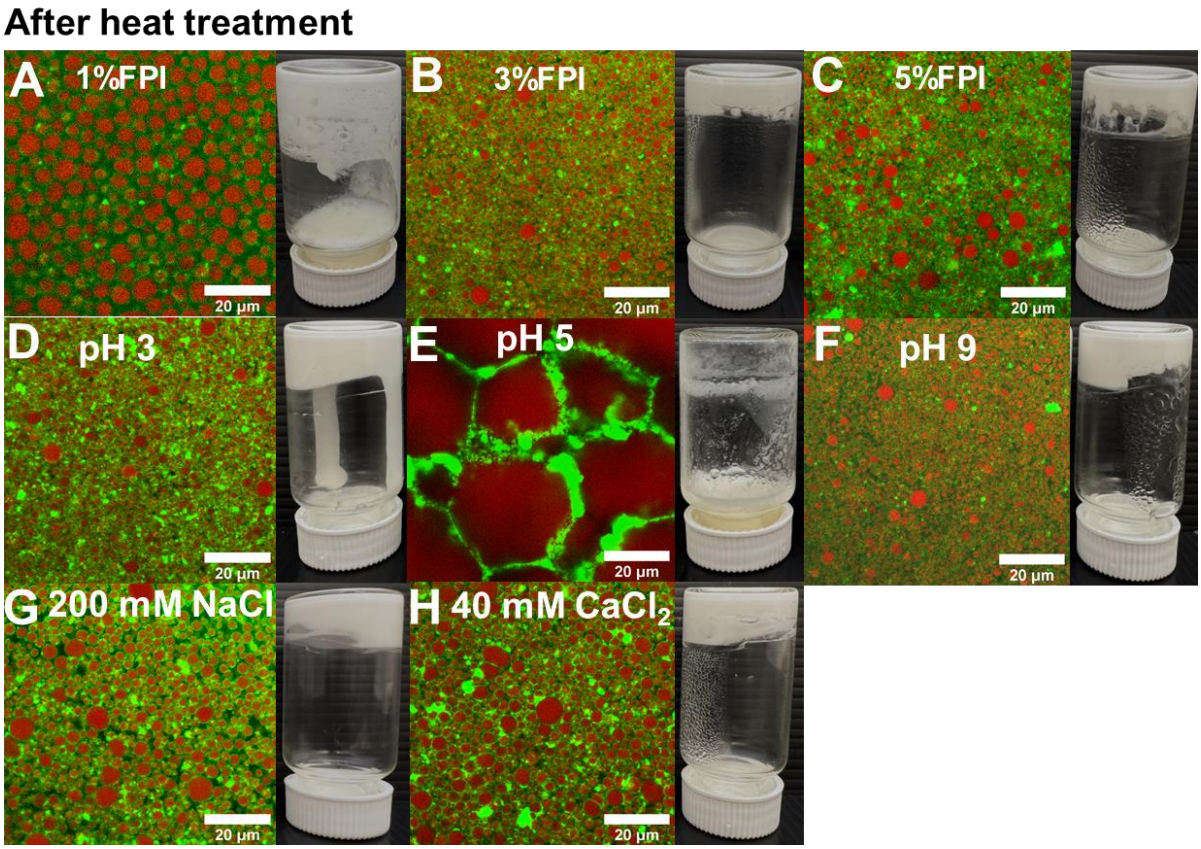

Fig. 3.4 Confocal micrographs and visual appearance of the emulsion samples after heat treatment. (A, B, and C) emulsions stabilised by 1, 3, and 5 wt% of FPI at pH 7. (D, E, and F) emulsions stabilised by 3 wt% of FPI at pH 3, pH 5, and pH 9. (G and F) emulsions stabilised by 3 wt% of FPI at pH 7 in the presence of 200 mM NaCl or 40 mM $CaCl_2$.

3.3.5 Oil droplet sizes and distribution of emulsion gels

The effects of FPI concentration on the oil droplet size distributions is shown in **Fig. 3.5A and 3.5D**. The emulsion stabilised by 1 wt% FPI displayed a bimodal distribution with a major peak at ~8 μm and a minor peak at ~1 μm. With increasing FPI concentration to 5 wt%, the peaks shifted toward smaller sizes to ~ 1 μm and ~ 0.2 μm. The surface mean diameter D [3,2] was plotted as a function of FPI concentration as shown in **Fig. 3.5D**, indicating the oil droplet size reduction induced by the increase in FPI concentration. It can be observed that the D [3,2] decreased from ~3.8 μm to ~1.6 μm when the FPI concentration was increased from 1 wt% to 5 wt%. This finding was consistent with the CLSM observation **(Fig. 3.5 A-C)** as discussed above. Previous studies suggested that an increase in protein concentration could enhance the adsorption and surface coverage ability of FPI on oil droplets, thus contributing to stabilising larger interfacial surface areas with limited extent of coalescence (Sun & Gunasekaran, 2009). Similar findings have been reported in previous studies on other plant proteins stabilised O/W emulsions. For examples, Xiao, Gonzalez, et al. (2016) utilised karifin particles from sorghum to prepare O/W emulsion and indicated that the oil droplet size considerably decreased from ~125 μm to ~40 μm when the concentration of kafirin particles increased from 0.25 wt% to 2 wt%.

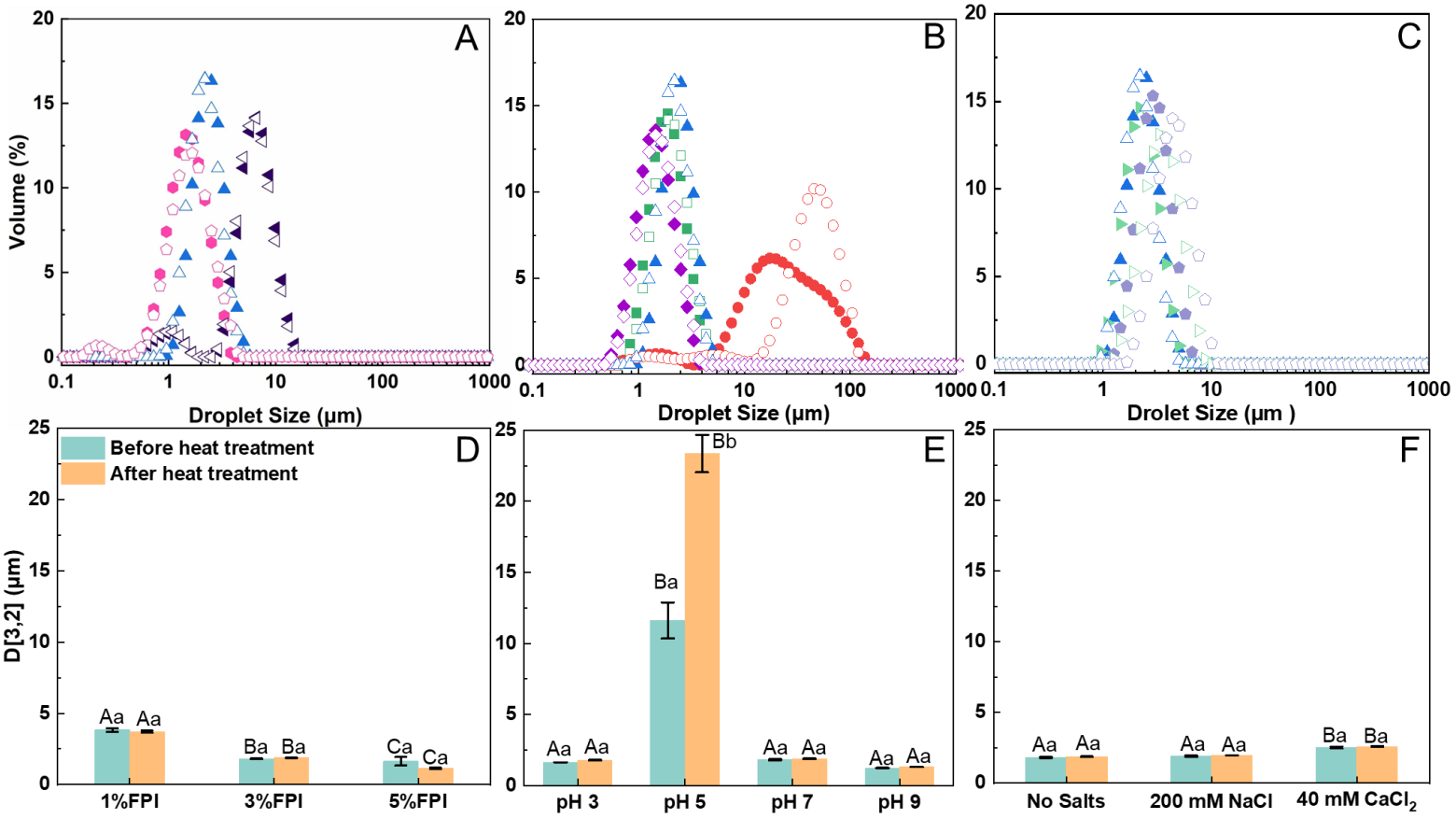

Fig. 3.5 (A, B, and C) Oil droplet size distribution of FPI stabilised emulsion gel before (open symbols) and after heat treatment (solid symbols), where (◀)-1 wt% FPI, (▲)-3 wt% FPI, (⬢)-5 wt% FPI, (■)-pH 3, (●)- pH 5, (◆)-pH 9, (▶)- 200 mM NaCl, (⬟)-40 mM $CaCl_2$. (D, E, and F) Sauter mean diameter of oil droplets for all FPI stabilised emulsions. Different capital letters above the columns denote significant differences ($P < 0.05$) in emulsions stabilised by FPI at different concentrations, different pHs or adding with salts. The different lowercase letters denote significant differences ($P < 0.05$) in emulsions before and after heat treatment.

The effects of pH of FPI on the oil droplet size distributions and D [3,2] of emulsions are shown in **Fig. 3.5B and 3.5E**, respectively. In general, the oil droplets stabilised by FPI at pH 5 were remarkedly larger (~12 μm) than those at pH 3, 7 and 9, which had comparable oil droplet sizes (~2-2.5 μm). This can be attributed to extensive protein-protein aggregation caused by the reduced electrostatic repulsions near the isoelectric point (pI~4.5) of FPI, so the FPI adsorption layer was ineffective to prevent the aggregation of droplets, and the emulsion stability was remarkably decreased (Karaca, et al., 2011; Zhu, Chen, et al., 2018). The minimum effectiveness of FPI as emulsifiers close to the pI was confirmed with the IFT result, and similar behaviour has been reported in previous studies on O/W emulsions stabilised by pea proteins (Gharsallaoui, et al., 2009), tomato seed protein isolates (Sarkar, et al., 2016), and soybean proteins (Zhang, Lei, et al., 2021). It has been suggested that proteins with higher stabilities and large surface charges could migrate to the oil-water interface faster to lower interfacial tension and provide charge repulsions once absorbed onto the interface, thereby resulting in smaller oil droplet sizes (Zhang, Lei, et al., 2021; Zhu, Chen, et al., 2018).

Salts are usually added to the food emulsions to tune their structural and machinal properties as well as for micronutrient fortification (e.g. $CaCl_2$). The influence of salt addition (NaCl and $CaCl_2$) on the oil droplet size of FPI stabilised emulsion gels was measured at pH 7 and 3 wt% FPI (**Fig. 3.5C**). The results showed that the NaCl addition (200 mM) did not induce significant changes in oil droplet size. However, the addition of 40 mM $CaCl_2$ led to a slight increase in oil droplets (from ~1.8 μm to ~2.5 μm). Similar findings were reported in previous studies of SPI stabilised emulsion gels in the presence of 40 mM $CaCl_2$ (Zhang, Zhang, et al., 2022). In general, the results indicated that divalent salts, such as $CaCl_2$, had large impact on FPI-stabilised emulsion than monovalent salts such as NaCl, which is in agreement with a previous study of tomato seed protein isolate-stabilised emulsions containing NaCl and $CaCl_2$ (Sarkar, et al., 2016). Although the effect of salts on oil droplet size of emulsions depends on the salt type, pH and concentration, it is generally believed that divalent salts have a stronger effect than the monovalent salts (Chang, et al., 2015; Xiao, Gonzalez, et al., 2016). This could be due to the strong charge screening and salt bridging effect of $CaCl_2$ than that of NaCl, leading to ion-induced droplet aggregation (Sarkar, et al., 2016; Yang, de Campo, et al., 2022).

In line with confocal imaging, the heat treatment did not induce significant changes in the oil droplet size of FPI stabilised emulsions, except at pH 5, indicating a good heat stability. However, the oil droplet size D [3,2] at pH 5 nearly doubled from ~ 12 μm to ~ 24 μm after the heat treatment at 90 °C for 30 min, which was in agreement with the CLSM observations (**Fig. 3.3E and Fig. 3.4E**). As the oil droplet size was determined after gently mixing with 1wt% SDS to dissociate the flocculated droplets, the increase in D [3,2] of FPI stabilised emulsion at pH 5 suggests this was possibly due to droplet coalescence rather than aggregation and flocculation (Zhang, Lei, et al., 2021). It has been suggested that electrostatic repulsive forces between protein films/particles adsorbed onto the oil droplets are important in stabilizing emulsions against coalescence and flocculation (McClements, 2004b). Therefore, it can be concluded that the emulsion had the lowest thermal stability at pH 5 where the repulsions were minimum.

3.3.6 Small deformation rheological properties of FPI stabilised emulsion gels

Rheological properties of emulsions are strongly related to their stabilities (White, et al., 2008) and 3D printability (Cheng, Fu, et al., 2022). The viscoelastic response of all FPI stabilised emulsion gels as a function of frequency is shown in **Fig.3.6**. For all samples, G' and G'' were parallel to each other and only slightly changed with frequency. In addition, G' values were almost 10 times higher than G''. This suggests that all samples presented a prevailing elastic behaviour that can be considered as gels (Banerjee & Bhattacharya, 2012). The predominantly elastic gel behaviour has been attributed to extensive flocculation process due to interactions among the emulsifiers (i.e., FPI particles/molecules) located at the oil-water interface of adjacent droplets and dense packing of oil droplets (Kornet, et al., 2022; Liu & Tang, 2011). Similar findings have been observed in concentrated emulsions stabilised by other plant proteins, such as canola protein-stabilised emulsions (oil fraction ϕ=0.5) (Tang & Ghosh, 2021), and dairy proteins, such as whey protein isolate (WPI)-stabilised emulsions (ϕ=0.3-0.6) (Liu, Zhang, et al., 2019).

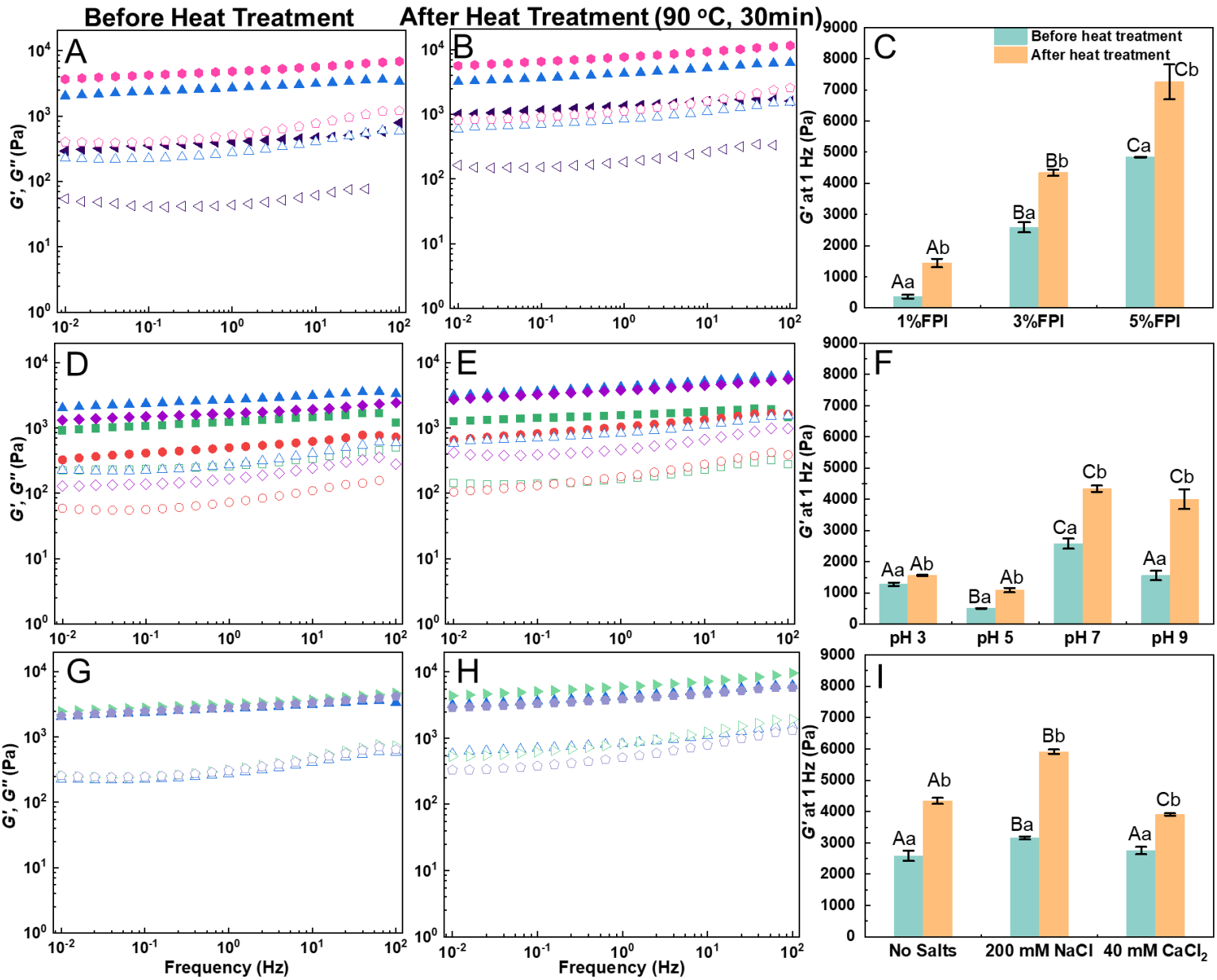

Fig. 3.6 (A and B) The G' (solid symbols) and G'' (empty symbols) as a function of frequency for FPI stablisted emulsion gel systems before (A, D, and G) and after (B, E, and H) heat treatment, where (◀)-1 wt% FPI, (▲)-3 wt% FPI, (⬢)-5 wt% FPI, (■)-pH 3, (●)- pH 5, (◆)-pH 9, (▶)-200 mM NaCl, (⬟)-40 mM $CaCl_2$. (C, F, and I) G' (1 Hz) for FPI stabilised emulsions before and after the heat treatment. Different capital letters above the columns denote significant differences ($P < 0.05$) in emulsions stabilised by FPI at different concentrations, different pHs or adding with salts. The different lowercase letters denote significant differences ($P < 0.05$) in emulsions before and after the heat treatment.

To compare the gel strength among all the samples, the G' at 1 Hz is plotted in **Fig. 3.6C, F, and I.** It is evident that increasing the concentration of FPI led to a greater gel strength of emulsion gels. To be specific, G' (1 Hz) increased from ~365 Pa to ~4840 Pa when the concentration of FPI was increased from 1 wt% to 5 wt%. Similar results have been reported in previous studies on plant-stabilised emulsions, including quinoa and kafirin proteins (Xiao, Gonzalez, et al., 2016; Zhang, Cheng, et al., 2021). For example, in quinoa protein stabilised emulsions, the G' increased from ~100 Pa to ~580 Pa when the concentration of QPI increased from 1 wt% to 5 wt%. As shown in Fig. 3, the oil droplets with smaller size and more compact packing at higher concentrations of FPI may result in a greater gel strength (Tang & Ghosh, 2021).

The impact of pH value on the rheological properties of the FPI stabilised emulsions was also measured as shown in **Fig. 3.6F** which summarised the G' at 1 Hz for different pH values. Emulsions prepared by FPI at pH 7 exhibited the highest G' value (~2800 Pa) followed by at pH 9 (~1500 Pa), pH 3 (~1100 Pa), and pH 5 (~500 Pa). The weakest gel strength at pH 5 could be attributed to the large size and loose packing of oil droplets as revealed by the CLSM observations. Interestingly, although the emulsions prepared by FPI at pH 3, 7 and 9 exhibited a similar droplet size distribution (**Fig. 3.5B and 3.5E**), their rheological properties varied. It has been previously suggested that in a highly structured emulsion system, oil droplet size distribution is not the only structural parameter influencing rheology of emulsions. Other factors such as interdroplets interactions and protein aggregates in aqueous phase may also play key roles (Franco, et al., 2000; Zhang, Cheng, et al., 2021; Zhu, Chen, et al., 2018).

As shown in **Fig. 3.6I**, adding 200 mM NaCl increased the gel strength of 3 wt% FPI (pH 7) stabilised emulsions compared to the sample in the absence of salt. This could be due to enhanced interdroplets interactions due to charge screening effect and/or protein aggregation at the oil-water interface. Similar findings have been reported in karifin stabilised emulsions added with 10-50 mM NaCl (Xiao, Gonzalez, et al., 2016). However, an increase in gel strength was not observed when the emulsion gel was added with 40 mM $CaCl_2$ which could be attributed to large oil droplet sizes and excessive protein aggregation at high ionic strength, which can be observed in the CLSM micrographs (**Fig. 3E**) (Yang, de Campo, et al., 2022; Zhang, Zhang, et al., 2022).

It is evident that the heat treatment significantly enhanced the gel strength of all FPI-stabilised emulsions (**Fig. 3.6B, 3.6C, and 3.6E**). This was in line with the microstructural characteristics of emulsions as revealed by CLSM **(Fig. 3.3-3.4)**. The heat treatment induced extensive aggregation of proteins located on surfaces of oil droplets, leading to more compact and denser packing of oil droplets. In addition, and excess proteins in the aqueous phase may also aggregated and act as active fillers in improving the gel strength (Li, Fan, et al., 2021; Xu, et al., 2018). Similar findings have been reported in previous studies on heat treatment of emulsions stabilised by canola protein isolates (Tang & Ghosh, 2021) and quinoa protein isolates (Zhang, Cheng, et al., 2021).

3.3.7 Large deformation rheological properties FPI stabilised emulsion gels

Large deformation rheological behaviour and structural breakdown characteristics of emulsions can be determined by the *strain-sweep* measurements and the results are shown in **Fig. 3.7**. For all the samples, at small strain amplitude within the linear viscoelastic region (LVR), G' and G'' were found to be independent of strain amplitude. In addition, G' was greater than G'' within the LVR, indicating a gel-like network structure with a predominant elastic behaviour (Zou, et al., 2018). When the strain amplitude was beyond the LVR, the G' values of all samples were dropped remarkably, suggesting the onset of structural disintegration. In some samples such as emulsions stabilised by 1, 3 and 5 wt% FPI before and after the heat treatment, the G'' values of samples increased and reached local maximum values then decreased sharply with the strain increase, indicating the type *III* nonlinear behaviour (weak strain overshoot) (Hyun, et al., 2002). The overshoot of G'' has been also observed in previous rheological studies of concentrated emulsions stabilised by QPI (Zhang, Cheng, et al., 2021) and CPI (Tang & Ghosh, 2021). This could be due to energy dissipation induced by the structural rearrangement under large deformations, but the underlying mechanism is still elusive that needs further studies (Mason, et al., 1995). When the strain amplitude was further increased, G'' decreased much faster than G' until crossover occurs at the breaking stress σ_b where $G'=G''$. Beyond the σ_b, G'' was greater than G', which signifies a transition from viscoelastic solid-like behaviour to viscoelastic liquid behaviour due to structural breakdown (Shahbazi, et al., 2020).

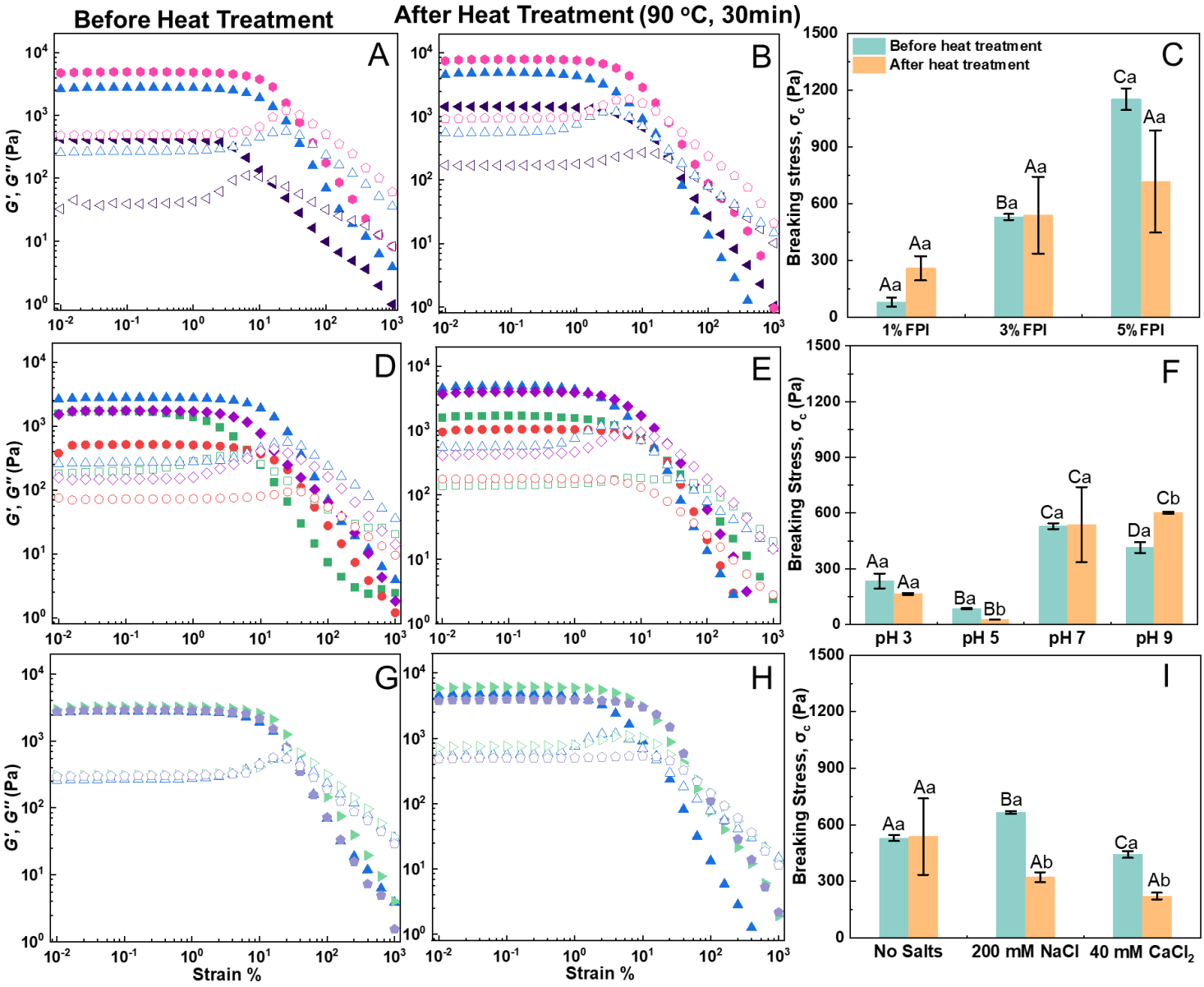

Fig. 3.7 The G' (solid symbols) and G'' (empty symbols) as a function of strain amplitude for FPI stabilised emulsions before (A, D, and C) and after (B, E, and F) heat treatment. Symbols are the same as in Fig. 3.6. (C, F, and I) breaking stress of all emulsion gels. Different capital letters above the columns denote significant differences ($P < 0.05$) in emulsions stabilised by FPI at different concentrations, different pHs or adding with salts. The different lowercase letters denote significant differences ($P < 0.05$) between the emulsions before and after the heat treatment.

To better compare the large deformation rheological behaviours of all samples, the breaking stress (σ_b of all samples are shown in **Fig. 3.7C, 3.7F and 3.7I**). When the FPI concentration increased from 1wt% to 5 wt%, the σ_b showed a substantial increase from ~80 Pa to 1150 Pa, indicating stronger gels were formed at high FPI concentrations. The effect of pH and salt addition on the σ_b also showed a similar trend as G' (1 Hz) as revealed by small deformation rheological studies, indicating the agreement between small and large deformation rheological behaviours.

However, as shown in **Fig. 3.7C, 3.7F and 3.7I**, the emulsions after heat treatment did not show similar trends in σ_b as compared to G' (1 Hz). Depending on samples, the σ_b values were either not significantly changed (e.g., 3wt% FPI stabilised emulsions at pH 3, 5 and 7) or increased (e.g., 1wt% FPI stabilised emulsion at pH 7)/decreased (e.g., 3wt% FPI stabilised emulsion at pH 7 added with 200 mM NaCl) as compared to samples without the heat treatment. As the large deformation rheological properties of concentrated emulsions are complex and affected by various factors such as interdroplets interactions, motions and rearrangement, further studies are needed to explore in more details (Derkach, 2009; Tadros, 1994).

3.3.8 3D printing of FPI stabilised emulsion gels

Rheological results indicated that several FPI-stabilised emulsion gels had great mechanical strength, which are critical for 3D printing. To compare the effects of FPI concentration, pH, salt addition, and heat treatment on the printing performance of FPI stabilised emulsions, the emulsion inks were printed into an octagon-shape geometry as shown in Fig. 9. Increasing FPI concentrations greatly improved the printing performance, and the object printed from 3 and 5 wt% FPI stabilised emulsions exhibited sharp boundaries, self-supported structures, even surface quality, and high printing precision (e.g., layers can be clearly observed in high resolutions). In contrast, FPI emulsions stabilised by 1 wt% FPI cannot be 3D printed due to their weak gel strength. 3D printing performance of FPI emulsions were also substantially affected by the pH of FPI. As shown in **Fig. 3.8**, emulsions stabilised by FPI at pH 3 and pH 5 showed distinct fluidity and structural collapse after 3D printing, while the printed objects from FPI stabilised emulsions at pH 7 and pH 9 showed excellent dimensional

stability and precision. Addition of 200 mM NaCl and 40 mM $CaCl_2$ to the FPI stabilised emulsion inks did not significantly affect the 3D printing performance, and well defined and self-supported structures were maintained.

Heat treatment can improve the 3D printability of some emulsion samples to some extent (e.g. emulsions stabilised by FPI at pH 3), but it still could not form a complete and well-defined structure. Overall, the 3D printing performances of FPI stabilised emulsions were strongly correlated with their rheological properties, which have also been reported in previous 3D extrusion printing studies of emulsion gels stabilised by pea protein-pectin-EGCG complex (Feng, et al., 2022) and whey protein isolates (Liu, Zhang, et al., 2019). It is generally believed that high gel strength (e.g., $G' > 2000$ Pa) and large LVR regimes are critical for supporting previous deposited layers and maintaining the dimensional stabilities. The greater G' values also typically led to better 3D printing performances with enhancement of printing precision and resolution of deposited layers (Liu, Zhang, et al., 2018; Zhang, Pandya, et al., 2021). In addition, all the emulsion samples demonstrated a shear thinning behaviour as revealed by the large deformation rheology, which are important for their easy and smooth extrusions from a small diameter printing nozzle (Li, Xu, et al., 2020).

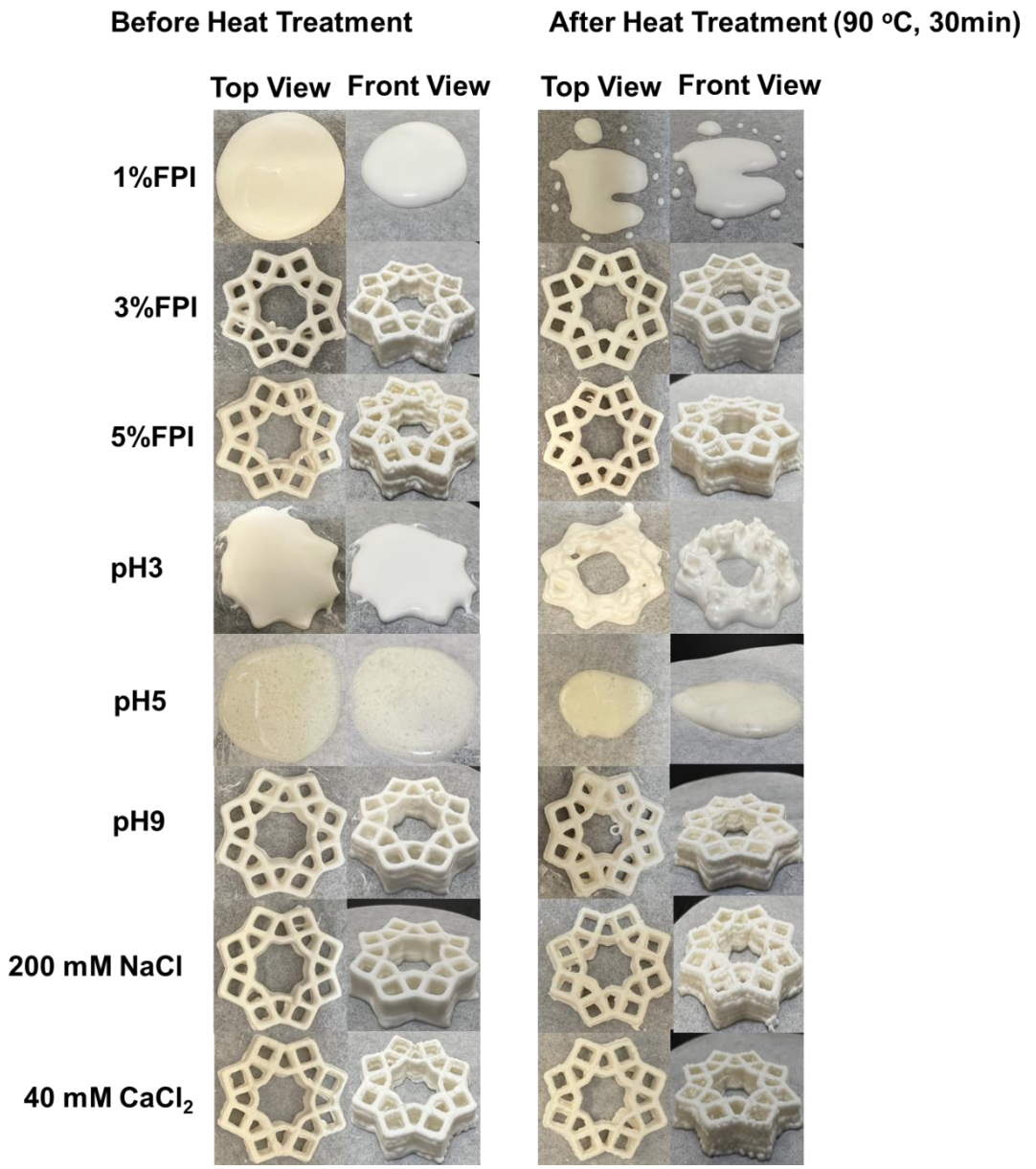

Fig. 3.8 The visual appearance of 5 mm height geometrics shape printed by emulsion gels stabilised by different FPI formulations before and after heat treatment. The images were taken after storage at 20 °C for 1 h.

3.4 Conclusions

In conclusion, this study demonstrated that faba bean protein isolate (FPI) was effective in stabilising concentrated O/W emulsions (ϕ=0.5) prepared by high pressure homogenisation. All FPI stabilised emulsions exhibited as viscoelastic gels due to interdroplets aggregation and network formation. The rheological properties and microstructural characteristics of emulsions could be tuned by changing FPI concentration and pH and adding salts (NaCl and $CaCl_2$). As the FPI concentration increased, the storage modulus G' increased. This could be explained by a decrease in oil droplet size, thus tending to form a more closely packed and flocculated emulsion network. It was shown that the FPI demonstrated the worst emulsification capability at pH values close to the isoelectric point (pH 5), as reflected by the high IFT plateau value, large oil droplet size, and weak mechanical strength. The characteristics of emulsions affected by salt addition depended on the salt type. The G' of emulsions slightly increased while the droplet size did not change in the presence of 200 mM NaCl. In contrast, the G' of emulsions remained nearly unchanged, and the droplet size slightly increased after adding 40 mM $CaCl_2$. This could be due to different charge screening effects between monovalent and divalent salts. For all emulsions, the heat treatment (90 °C, 30 min) could substantially improve the mechanical stiffness without markedly affecting the oil droplet size except for the emulsions stabilised by FPI at pH 5. Heat treatment could induce FPI denaturation and aggregation, leading to a thickened interfacial layer and stronger interactions among FPI at the oil-water interface and between non-absorbed FPI in the continuous phase. Finally, the 3D printability of FPI stabilised emulsions was evaluated, which was found to be strongly correlated with their small and large deformation rheological properties. All emulsion samples demonstrated desirable printing performance except the emulsions stabilised by 1 wt% FPI (pH 7) and 3 wt% FPI (pH 5), which showed weak gel strength. Overall, this study demonstrated a potential of using food-grade concentrated emulsion stabilised by FPI as a new material for 3D printing, broadening the applications of plant proteins in the 3D printing. Further work can be performed to explore the applications of 3D printed emulsions for encapsulation and delivery of nutraceuticals and flavours.

3.5 Acknowledgements

The author Yinxuan Hu thanks the Massey University, New Zealand for a doctoral student scholarship. We would like to acknowledge the technical support of Ms. Lan Luo for helping with SDS-PAGE.

MASSEY UNIVERSITY
TE KUNENGA KI PŪREHUROA
UNIVERSITY OF NEW ZEALAND

GRADUATE RESEARCH SCHOOL

STATEMENT OF CONTRIBUTION
DOCTORATE WITH PUBLICATIONS/MANUSCRIPTS

We, the student and the student's main supervisor, certify that all co-authors have consented to their work being included in the thesis and they have accepted the student's contribution as indicated below in the Statement of Originality.

Student name:	Yinxuan Hu
Name and title of main supervisor:	Professor Aiqian Ye
In which chapter is the manuscript/published work?	Chapter 4

Describe the contribution that the student and members of the supervisory team have made to the manuscript/published work:[1]

Yinxuan Hu: Methodology, Investigation, Data curation, Formal analysis, Writing-original draft.
Lirong Cheng: Conceptualisation, Supervision, Investigation, Writing-review & editing.
Elliot Paul Gilbert: Investigation, Data curation, Formal analysis. Trevor Loo: Investigation, Data curation, Formal analysis, Writing-review & editing. Sung Je Lee: Supervision, Writing-review & editing. John Harrison: Investigation, Methodology, Writing-review & editing.
Zhi Yang: Conceptualisation, Investigation, Methodology Supervision, Project administration, Writing-review & editing

Please select one of the following three options:

- (●) The manuscript/published work is published or in press

  Please provide the full reference of the research output:

  Hu, Y., Cheng, L., Gilbert, E. P., Loo, T. S., Lee, S. J., Harrison, J., & Yang, Z. (2024). Fibrillisation of faba bean protein isolate by thermosonication for process efficacy: Microstructural characteristics, assembly behaviour, and physicochemical properties. Food Hydrocolloids, 154, 110127. https://doi.org/10.1016/j.foodhyd.2024.11012

- ( ) The manuscript is currently under review for publication

  Please provide the name of the journal:

- ( ) It is intended that the manuscript will be published, but it has not yet been submitted to a journal

Student's signature:	Yinxuan Hu Digitally signed by Yinxuan Hu Date: 2025.01.21 20:02:35 +13'00'	Main supervisor's signature:	Aiqian Ye Digitally signed by Aiqian Ye DN: cn=Aiqian Ye, o=NZ, ou=Massey University, ou=Riddet Institute, email=A.M.YE@massey.ac.nz Reason: I am approving this document Date: 2025.01.22 10:05:10 +13'00'

This form should be placed at the beginning of each relevant thesis chapter.

[1] Refer to the Massey University Publishing and Authorship guidelines (OneMassey for staff, Stream for students) and/ or Contributor Roles Taxonomy (CRediT) guidelines for guidance.

Chapter 4 Fibrillisation of faba bean protein isolate by thermosonication for process efficacy: microstructural characteristics, assembly behaviour, and physicochemical properties[3]

Abstract

The effect of thermosonication (TS) (90 °C, 10-30 min) on the fibrillisation of faba bean protein isolate (FPI) was studied. The self-assembly behaviour, microstructural characteristics and techno-functional (gelation and emulsification) properties of FPI fibrils obtained from TS treatment were compared with those obtained from conventional prolonged heating (CH) at 90 °C up to 8 h. Compared to CH treatment, TS treatment was shown to significantly accelerate the formation of FPI fibrils with prominent β-sheet structures as revealed by Thioflavin T (ThT) fluorescence, Fourier-transform infrared spectroscopy (FTIR) and circular dichroism (CD). The characteristics of fibril building blocks were analysed by sodium dodecyl sulfate-polyacrylamide gel electrophoresis (SDS-PAGE) and liquid chromatography linked to tandem mass spectrometry (LC-MS/MS) to obtain the differences between TS and CH induced fibrillisation of FPI. Transmission electron microscopy (TEM) and small-angle neutron scattering (SANS) showed that 4 h CH and 10 min TS treatments resulted in the fibrils with similar radius (from 5-10 nm). Furthermore, SANS indicated that TS treatment induced the formation of an entangled FPI fibrillar network, which could lead to the observed viscoelastic properties of FPI at a high concentration (10 wt%). Finally, high internal phase O/W emulsions (HIPE, ϕ=0.75) stabilised by 30 min TS induced FPI fibrils (3 wt%) demonstrated a stronger gel strength and smaller oil droplet size compared to those prepared with untreated FPI, suggesting a superior emulsification capability of FPI fibrils. This finding demonstrates that TS treatment is a promising and efficient method for fibrillisation of plant proteins with the resultant fibrils generating excellent gelation and emulsification properties.

Keywords: Thermosonication; Self-assembly fibrils; Faba bean protein isolates; Small angle neutron scattering; High internal phase emulsions; Microstructures

[3] This chapter has been published as Hu, Y., Cheng, L., Gilbert, E. P., Loo, T. S., Lee, S. J., Harrison, J., & Yang, Z. (2024). Fibrillisation of faba bean protein isolate by thermosonication for process efficacy: Microstructural characteristics, assembly behaviour, and physicochemical properties. *Food Hydrocolloids*, *154*, 110127.

Graphic abstract

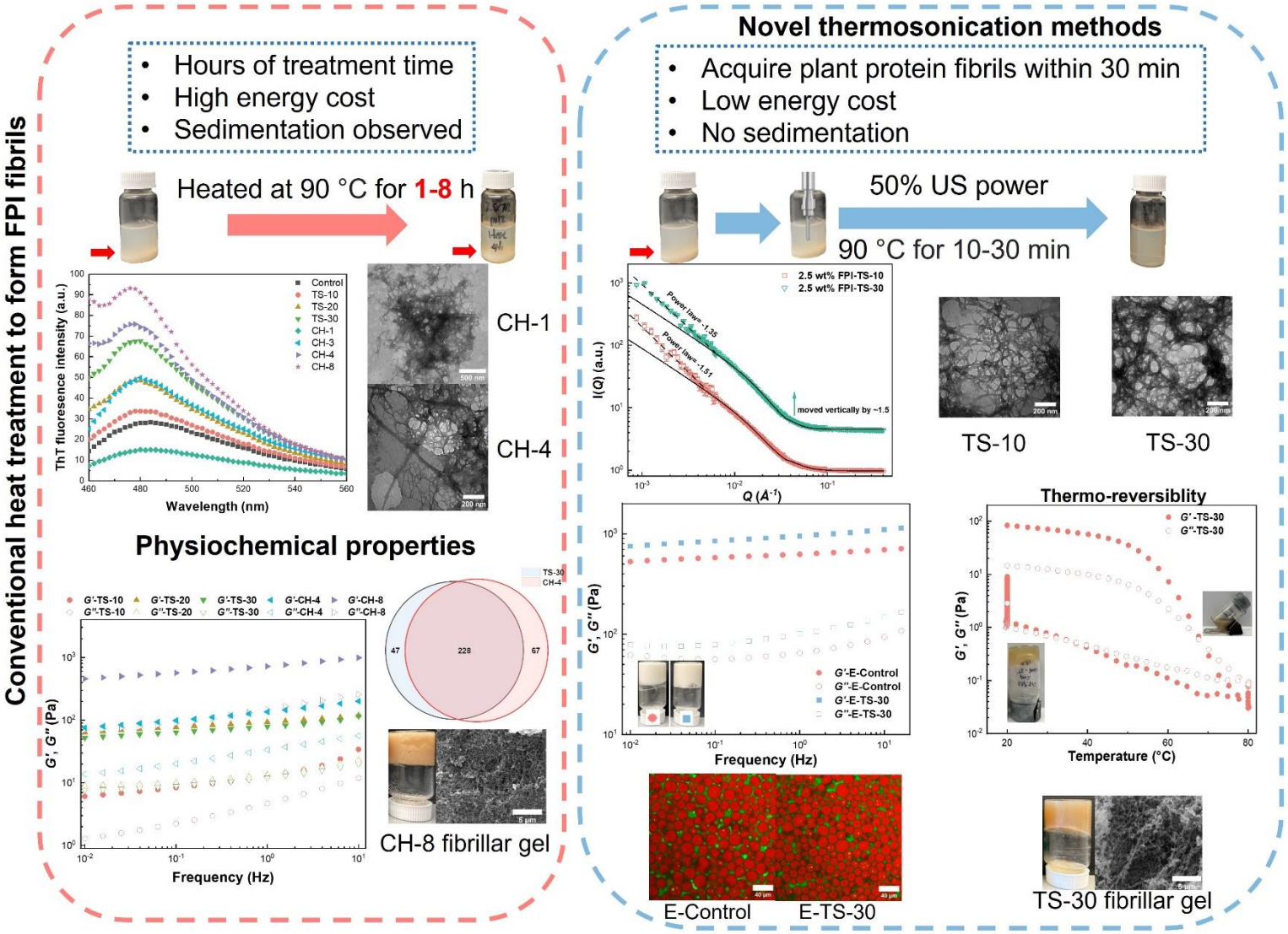

4.1 Introduction

Proteins form a variety of ordered or disordered structures including fibrils, branched structures, flexible strands, or random aggregates after denaturation (Bolder, et al., 2006). Among these structures, amyloid-like fibrils enriched in β-sheets have attracted extensive attentions due to their unique structural and physicochemical properties (Meng, et al., 2022; Ye, et al., 2019). Due to their high aspect ratio with exposure of functional groups exposed on the surface upon fibrillisation, protein fibrils demonstrate enhanced gelation behaviour (Chen, et al., 2020), improved emulsification capacity (Gao, et al., 2017), and superior mechanical properties (Xu, et al., 2022) compared to native proteins. Therefore, fibrillisation has been regarded as an efficient and promising method for improving protein techno-functionalities (Meng, et al., 2022).

To date, fibrillisation has been achieved for a wide range of food proteins, including whey protein isolate (Yang, Jiao, et al., 2022), egg white proteins (Alavi, et al., 2020), soybean protein isolate (Wang, et al., 2020), and hemp protein concentrate (Kutzli, et al., 2023). Recently, fibrillisation of plant proteins has been increasingly studied in order to improve their inferior functional properties such as low solubility and poor emulsification capability (Nasrabadi, et al., 2021). Until now, the commonly used method to induce food protein fibrillisation is a prolonged heat treatment (i.e. 12-96 h) at high temperatures (e.g. 80-90 °C) and pH 2, which are energy-intensive and time-consuming. In addition, sample pretreatments including centrifugation, membrane filtration, and/or pre-solubilisation of proteins in strong denaturants such as guanidine chloride (GuHCI) have been used in previous studies of fibril formations from plant proteins from different sources including mung bean, lupin, oat, rapeseed proteins (Herneke, et al., 2021), legume proteins (Li, Wang, Zhang, et al., 2021), rice glutelin (Li, Wang, Geng, et al., 2021), and potato proteins (Josefsson, et al., 2019). These pretreatments were generally conducted to unfold the compact structures of plant proteins and overcome their low water solubility, thereby improving the fibrillisation efficiency and conversion rate (Liu, Yang, et al., 2023). However, most treatments are cumbersome, and some may potentially leave residual chemicals in the formed protein fibrils. Therefore, in recent years, various novel and emerging physical treatment strategies such as microwave heating (Zhang, Liang, et al., 2020), hydrothermal treatment at high pressure (Yang, Jiao, et al., 2022), and radio frequency heating (Wang,

Xie, et al., 2023) have been explored in the formation of protein fibrils.

As a green and emerging food processing technology, ultrasonication (US) has been extensively used to modify plant proteins from cereals and legumes (e.g. quinoa and faba bean proteins) (Luo, Yang, et al., 2022; Rahman, et al., 2022; Wen, et al., 2019). The high shear forces, micro-jetting, and shockwaves generated by the US cavitation can disrupt large protein aggregates and improve the solubility of plant proteins (Gharibzahedi & Smith, 2020). However, most previous studies on the US treatment of plant proteins were conducted at a low temperature (e.g. ice-water bath) to prevent protein denaturation. Besides being used as a pretreatment method, US can be directly used for the formation of protein fibrils from recombinant hisactophilin (Stathopulos, et al., 2004), myoglobin (Stathopulos, et al., 2004), and β_2-microglobulin (Ohhashi, et al., 2005). It has been suggested that the strong agitation and the destabilisation of proteins at the air-liquid interface of the cavities formed during US could accelerate spontaneous nucleation of monomeric protein thus promoting the formation of protein fibrils (Ohhashi, et al., 2005; Stathopulos, et al., 2004; Yagi, et al., 2013). However, studies on the formation of plant protein fibrils using US treatment are still very limited. Recently, Kamada, et al. (2021) employed US combined with heat treatment (referred to thermosonication (TS)) (70 W, 40% amplitude, 90 °C, 30 min) to treat 10 wt% soybean protein isolate (SPI) in 30% v/v acetic acid solution and found that the SPI fibrils self-assembly occurred after cooling. The film forming capability of SPI fibrils was subsequently studied for packaging applications. They believed that the acetic acid solvent is essential for SPI fibril formation, due to its enhanced solvation of hydrophobic amino acid residues under aqueous-compatible conditions (Kamada, et al., 2021; Mason, et al., 2014). This study indicated that TS treatment under specific solvent conditions has the potential to induce fibrillisation of plant proteins. However, the systematic comparison of TS and conventional heat (CH) treatments on the formation of plant protein fibrils and its influence on technofunctional properties (e.g. gelation and emulsification), which are important for their application, have not been reported. Despite there are some recent studies on plant protein fibrils, most of them used prolonged conventional heating to induce fibrillisation (Herneke, et al., 2021; Li, Zhou, Peydayesh, et al., 2023). The systematic study of TS treatment on the formation of plant protein fibrils and its influence on technofunctional properties (e.g. gelation and

emulsification), which are important for their application, have not been reported.

Therefore, in the present study, faba bean protein (FPI) fibrils were prepared by either TS or CH treatment. FPI was selected as a model plant protein as it is commercially available and naturally rich in all nine essential amino acids (Dhull, et al., 2022). The impact of different treatments on the building blocks, morphology, assembly behaviour, and microstructural characteristics of FPI fibrils was investigated. The effects of fibrillisation on viscosity, viscoelasticity, and thermo-reversible gelation characteristics were also studied. Finally, O/W high internal phase emulsions (HIPEs) (soybean oil volume fraction ϕ=0.75) stabilised by 3 wt% TS-induced FPI fibrils were prepared. Furthermore, rheological properties and microstructural characteristics of HIPEs were studied. This study provides valuable insights into the influence of TS treatment on the formation of amyloid-like fibrils and their structural characteristics and inform their technofunctional properties.

4.2 Materials and methods

4.2.1 Materials

The FPI was purchased from NZ Protein Inc. (Auckland, New Zealand). Based on the product specification from the manufacturer, it contains ~85 wt% protein, ~5.4 wt% fat, and ~1 wt% carbohydrate and dietary fibre, respectively. Soybean protein isolate (SPI) and pea protein isolate (PPI) containing ~85 wt% protein was obtained from Yantai T. Full Biotech company (Shandong, China). Chemicals used in this study including sodium dodecyl sulphate (SDS), NaCl, Fast Green, Nile Red, acetic acid, thioflavin T (ThT), low viscosity mineral oil (M5904), sodium cacodylate, glutaraldehyde, HCl, NaOH, sodium azide, ammonium bicarbonate, urea, thiourea, dithiothreitol (DTT), iodoacetamide (IDA), trypsin, formic acid, trifluoroacetic acid, acetonitrile, acetonitrile (MeCN), and Bradford protein assay kit were all analytical grade and purchased from Sigma-Aldrich (St. Louis, MO, USA). β-mercaptoethanol, 10×Tris/Glycine/SDS running buffer, and Coomassie Brilliant Blue R-250 staining solution were purchased from Bio-Rad (Hercules, CA, USA). Milli-Q water (Millipore, USA) was used throughout sample preparations.

4.2.2 Preparation of plant protein dispersions

A stock solution of 10 wt% FPI was prepared by dispersing the FPI powder in Milli-Q water containing 0.02 wt% sodium azide to prevent microbial growth, followed by magnetically stirring (~300 rpm) at ~20 °C for 24 h for complete hydration. The pH was adjusted to 2.0 using 1 M HCl, followed by stirring (~300 rpm) for another ~24 h, and the pH was regularly checked and adjusted until stable. Afterwards, the stock FPI solution was stored at 4 °C until further use within a week. FPI dispersions of different concentrations (2.5 wt% and 3.0 wt%) were prepared by diluting the 10 wt% FPI stock solution with Milli-Q water at pH 2. SPI and PPI dispersions were also prepared according to the same procedure as FPI.

4.2.3 Formation of FPI amyloid fibrils by thermosonication (TS)

To investigate the formation of fibrils from plant-based protein sources, FPI dispersions (10 g each, 2.5-10 wt%, pH 2) were transferred to 20 mL glass vials and sonicated for 10 min (TS-10), 20 min (TS-20), and 30 min (TS-30) (50% amplitude, pulse durations of on-time 30 s and off-time 30 s) in a 90 °C water bath, respectively using a 20 kHz ultrasonicator equipped with a 6 mm horn with a dial power of 950 W (JY92-IIN, Ningbo Scientz Biotechnology Co., ltd, China) (Kamada, et al., 2021). The actual sonication power was determined as 14.4 W using the calorimetric method by determining the temperature increase of sonicated water (10 g) with time (Contamine, et al., 1995; Luo, Yang, et al., 2022). SPI and PPI fibrils were formed by the same methods as FPI (TS-30). All samples were accurately weighed before and after TS and topped up with Milli-Q water (pH 2) to compensate for water evaporation. All FPI samples were prepared in duplicate and left at 20 °C for 24 h to allow FPI fibrils and gels formation (Hu, et al., 2019). For comparison, the conventional heat treatment without ultrasonication was also employed to form fibrils by heating the dispersions of plant proteins in an air oven (Thermo Fisher Scientific Inc., USA) at 90 °C for 1 h (CH-1), 3 h (CH-3), 4 h (CH-4), and 8 h (CH-8). FPI dispersions (2.5-10 wt%, pH 2) without any treatment are defined as controls in this study.

4.2.4 Characterisation of FPI fibrils

4.2.4.1 Thioflavin T (ThT) fluorescence spectroscopy

Thioflavin T (ThT) fluorescence assay was conducted using a fluorescence

spectrophotometer (RF-6000, Shimadzu, Kyoto, Japan) to detect β-sheet structure according to Nilsson (2004) and Herneke, et al. (2021) with slight modifications. Briefly, ThT solution (2 mM) was prepared in Milli-Q water and filtered with a 0.22 μm syringe filter (Thermo Fisher Scientific, USA). FPI fibril samples were diluted to 0.01 wt% with Milli-Q water (pH 2). An aliquot of FPI fibril dispersion (2 mL) was subsequently mixed with 2 μL of ThT solution and incubated at room temperature (~20 °C) for 10 min in the dark. Fluorescence intensity was measured at an excitation wavelength λ_{ex} of 440 nm and an emission wavelength λ_{em} from 460 to 560 nm. ThT working solution added with 2 mL Milli-Q water (pH 2) was measured as a background.

4.2.4.2 Measurement of FPI fibrils conversion

Fibril conversion was assessed following the method outlined by Akkermans, et al. (2007) and Zhou, et al. (2024) with minor modifications. Briefly, diluted FPI fibril samples (5 mg/mL) were allowed to sediment on the bench overnight, then the supernatants were collected, and protein concentrations of the supernatant was determined using a Bradford protein assay kit (Sigma-Aldrich, St. Louis, MO, USA). Thereafter, the supernatant (1 mL) was passed through 2 mL centrifugal membrane filter (100 kDa MWCO, Merck Millipore Ltd, Ireland) under consecutive centrifugations at 4000 *g* for 15 min at 20 °C in order to remove small peptides and nonfibrillar proteins. The retentates were washed with Milli-Q water (pH 2) 2-3 times until no protein was detected in the filtrated solution. Then, the filtrate was collected, and the protein concentration was determined by a Bradford protein assay kit (Sigma-Aldrich, St. Louis, MO, USA). The conversion rate of FPI fibrils was calculated using equation (4.1):

$$C = \frac{S - F}{P} \times 100\ \% \tag{4.1}$$

where C is the conversion rate of FPI fibrils (%), S (g) is the protein content in the supernatant of FPI dispersion after sedimentation, F (g) is the protein content in the filtrate obtained from centrifugal filtration, and P (g) is the initial protein content (g) in the solution.

4.2.4.3 Negative staining transmission electron microscopy (TEM)

The morphology and microstructure of FPI fibrils were observed using negative staining TEM according to Ji, et al. (2021). The protein dispersions containing 2.5 wt% protein was firstly diluted to 0.05 wt% by Milli-Q water (pH 2), and then 20 μL of sample solution was transferred onto a copper TEM grid coated with formvar and then stained with uranyl acetate (2%) for 3 min. Afterwards, the excess stain was washed with 20 μL Milli-Q water for another 3 min. Finally, the excess liquid was drained off from the copper grid by a filter paper. The microstructure of FPI fibrils was observed by a Philips electron microscope (NL-5600 MD, Philips, Eindhoven, The Netherlands) at an acceleration voltage of 60 kV.

4.2.4.4 Small-angle neutron scattering (SANS)

SANS experiments were performed on the QUOKKA instrument at ANSTO, Sydney, Australia, covering a Q-range from 0.003 to 0.4 $Å^{-1}$ (Gilbert, et al., 2006; Wood, et al., 2018; Yang, de Campo, et al., 2022). The samples were prepared following the same procedure as described in **Sections 4.2.2** and **4.2.3**. Approximately 1 mL samples were loaded into demountable SANS sample cells with the 1 mm path length by disposable syringes. Gel samples were first melted at 90 °C for 30 min in an oven before transferring to the SANS sample cells and then equilibrated at room temperature (~20 °C) for at least 5 h before SANS measurements to allow gel network formation. A multi-position tumbler was used to prevent sample sedimentation for liquid samples (e.g. 2.5 wt% and 5 wt% TS-30 samples). All SANS measurements were conducted at room temperature (~20 °C) for ~3 h for each measurement. Instrumental configurations were: (i) source-to-sample distance (SSD) = sample-to-detector distance (SDD) = 20 m, (ii) SSD = SDD = 8 m and (iii) SSD = 4 m and SDD = 1.3 m with 300 mm detector offset, using a λ of 5 Å with 10% resolution. There was an additional focussing optics configuration (iv) with the same SSD and SDD as (i) which was used to access lower Q_{min} with λ of 8.1 Å with 10% resolution. A sample aperture with a diameter of 12.5 mm was used for all configurations. Source aperture of 50 mm was used for (i), (ii) and (iii) and 30 mm for (iv). The data were reduced following a standard procedure (Kline, 2006) using the Igor Pro software (Wavemetrics, USA).

SANS data analysis:

SANS data were analysed using a Modelling II tool in the Irena SAS package embedded in Igor Pro 8.0 software (Wavemetrics, USA). In the low Q range (Q < 0.005 Å^{-1}), SANS data were analysed using the power law model shown in eq (4.2).

$$\mathrm{I}(Q) = aQ^{-n} \tag{4.2}$$

where *a* represents scale factor, and *n* is the power law exponent. In the mid to high Q regime (0.005< Q <0.4 Å^{-1}), data were modelled using an isotropically distributed cylindrical form factor (P(Q)) with radius following a log-normal distribution, as described in eq (4.3) (Guinier, et al., 1955).

$$p(Q) = \frac{Scale}{V_{cyl}} \int_0^{\pi/2} f^2(Q,\alpha) sin\alpha d\alpha$$

$$f(Q,\alpha) = 2(\rho_{cly} - \rho_{solv}) V_{cyl} j_0(QH\ cos\alpha) \frac{J_1(Qr\ sin\alpha)}{(Qr\ sin\alpha)}$$

$$j_0(x) = \frac{sin(x)}{x} \tag{4.3}$$

where V_{cyl} represents the volume of the cylinder. $J_1(x)$ is first order Bessel function, and α is the angle between cylinder axis and the scattering vector. H is the half length of the cylinder. ρ_{cyl} and ρ_{solv} are the neutron scattering length densities (SLDs) of the cylindrical scattering object and the surrounding solvent. During the modelling, the length of fibrils was fixed to 20000 Å and the SLD of FPI fibrils and solvent (H_2O) were 1.9 ×10^{-6} Å^{-2} and -0.56 ×10^{-6} Å^{-2}, respectively (Zhang, et al., 2012).. A log-normal radius distribution of cylinder radius D (R) can be expressed:

$$D(R) = \frac{\varphi}{\sqrt{2\pi\sigma}} \left(\frac{1}{2R'}\right) exp \left\{ \frac{-\left(ln\left[\frac{R'}{R'_{med}}\right]\right)^2}{2\sigma} \right\} \tag{4.4}$$

$$R' = R - R_{min} \tag{4.5}$$

$$R'_{med} = R_{med} - R_{min} \tag{4.6}$$

$$\sigma = ln\left(\frac{R_{med} - R_{min}}{R_{mode} - R_{min}}\right) \tag{4.7}$$

Where φ is the volume fraction, R_{min} is the minimum radius, R'_{med} is the modified median radius and σ is the standard deviation.

4.2.5 Secondary protein structure of FPI fibrils

4.2.5.1 Far UV-Circular dichroism (CD) spectroscopy

Conformational changes of FPI secondary structures upon fibrillisations were investigated with CD spectroscopy using a Chirascan spectrometer (Applied Photophysics, UK). Samples were diluted with Milli-Q water (pH 2) to a concentration of 0.5 wt%. To remove some peptides, some samples were also purified by the same procedure as described in 2.3.1 using a 50-mL 10 kDa centrifugal filter (Merck Millipore Ltd, Ireland). The retentates were washed with Milli Q water (pH 2) three times followed by centrifugation and all the supernatants and retentates were collected. Samples (~80 μL) were subsequently transferred into a quartz cell (Hellma, Germany) with a 0.1 mm path length. Spectra were obtained at 20 °C in a wavelength range of 180–260 nm, with 1 nm steps and at 0.5 s per point, and then were averaged from 10 measurements.

4.2.5.2 Attenuated total reflectance Fourier-transform infrared (ATR-FTIR) analysis

FTIR spectra of FPI samples were acquired using a diamond ATR-FTIR spectrometer (ALPHA II, Bruker, Germany) over a wavelength range from 4000 to 400 cm^{-1} with 4 cm^{-1} resolution by averaging over 32 scans, as based on previous studies (Kutzli, et al., 2023; Luo, Yang, et al., 2022). Sample solution (5 μL) was pipetted on top of the ATR diamond and left to dry for 15 min at room temperature (~20 °C) before measurement.

4.2.6 Sodium dodecyl sulphate–polyacrylamide gel electrophoresis (SDS-PAGE)

SDS-PAGE under reducing conditions was used to characterise the protein profiles after different treatments based on their molecular weight (Laemmli, 1970). Diluted 0.15 wt% FPI solution (10 μL) was mixed with 10 μL of sample buffer at room temperature (~20 °C). The sample buffer consisted of 13% (v/v) 0.5 M Tris–HCl buffer, 10% (v/v) glycerol, 2% (w/v) SDS, 0.04% (w/v) bromophenol blue and β-mercaptoethanol (19:1, v/v). The sample was subsequently boiled for 10 min followed by cooling. Samples (15 μL) were then loaded onto a previously prepared SDS gel (Mini-PROTEAN II system). The gel was prepared at 16% (w/v) acrylamide concentration for the resolving gel and at 4.0% (w/v) acrylamide concentration for the stacking gel. The electrophoresis was performed using a PowerPac Basic (Bio-Rad, USA) at a constant voltage of 130 V in a

running buffer (10 × Tris/Glycine/SDS running buffer) for ~1 h (Bio-Rad, USA). Afterwards, the gels were stained with Coomassie Brilliant Blue R-250 staining solution (Bio-Rad, USA) for 45 min. After destaining with 10% isopropanol/glacial acetic acid solution overnight on a shaker (OM6, RATEK, Australia), the gel was scanned by a molecular imager GelDoc XR system (Bio-Rad Laboratories, Hercules, USA). A mixture of protein standards with a molecular weight range of 2–250 kDa (Precision Plus Protein Dual Xtra Prestained Standards, Catalog #1610377, Bio-Rad, USA) was used to identify protein bands.

4.2.7 Liquid chromatography linked to tandem mass spectrometry (LC-MS/MS)

LC-MS/MS was used to identify the differences in peptide released between US and CH treatments on the formation of FPI fibrils according to the methods from Visser, et al. (2023) with slight modifications. Firstly, FPI fibril dispersions were diluted to 1 wt% with Milli-Q water (pH 2) and filtered (4000 × *g*, 15 min, 20 °C) using centrifugal filter units (2 mL) with a MWCO of 100 kDa (Merck Millipore Ltd, Ireland) to remove small peptides hydrolysates (Yang, Jiao, et al., 2022). The retentate was washed with Milli-Q water (pH 2) and centrifuged three times until the absorbance of filtrate at 280 nm dropped close to 0 according to Chatani, et al. (2009). Retentate fibrils were lyophilised for 4 days with a Labconco freeze dryer (FreeZone 6 Liter Console, Labconco, USA). Lyophilised fibrils were then solubilised in 0.3 mL of 1 M ammonium bicarbonate buffer containing 6 M urea/2 M thiourea in a sonicator bath (Elma®, model EP30H) at room temperature for 10 min until completely solubilised. The solubilised proteins were centrifuged (17,000 g, 20 °C, 15 min) and 30 µl of the supernatant were transferred to clean centrifuge tubes (Protein LoBind 0.5 mL tubes, cat. # EP0030108094, Eppendorf). The samples were reduced by 10 mM dithiothreitol (DTT) (50 °C, 1 h), followed by alkylation with 15 mM iodoacetamide (IDA) in the dark at 20 °C for 30 min. Excess IDA were neutralised by adding 10 mM DTT and incubated in the dark at 20 °C for 30 min. MS grade water (Optima™ LC/MS Grade, cat. #FSBW6-4, Fisher Chemical™) was added to the reaction mixture to dilute the urea to 0.6 M for trypsin digestion. Trypsin (1 µg) (SOLu-Trypsin, cat. # EMS0004, Sigma) was added to each sample and incubated at 37 °C for 16 h. Another portion (0.5 µg) of trypsin was added to each sample after incubation and continued to incubate for another 5 h. The digestions were stopped by adding formic acid to a final concentration (1%). Samples were then

centrifuged (17,000 g, 4°C) for 15 min and filtered through a 0.45 µm filter (Millex syringe filter, PES, 13 mm, cat. # SLHPX13NK, Millipore) before transferring to HPLC vials for LC-MS/MS analysis.

The liquid chromatography (LC) system (Dionex UltiMate™ 3000 Binary RSLCnano LC system, Thermo Fisher Scientific) equipped with a 50 mm reverse phase analytical column (PepMap™100, C18, 2 µm particle size, 75 µm inner diameter, 50 cm length, Thermo Fisher Scientific) and an in-line RP-HPLC trap for desalting (PepMap™100 C18, 3 µm particle size, 75 µm inner diameter, 2 cm length, Thermo Fisher Scientific) was used in this study. The trap loading buffers were trifluoroacetic acid (TFA) (0.1 %) and acetonitrile (MeCN) (2 %) in MS-grade water with the flow rate of 15 µL/min. LC buffer A (0.1 % formic acid (FA) and 2 % MeCN) and B (0.1 % FA and 98 % MeCN) were used to efficiently separate and elute the tryptic peptides in a gradient of 3–30% B over 60 min at a flow rate of 300 nL/min. The LC system was coupled to a Q-Exactive™ Plus mass spectrometer (ThermoFisher Scientific) equipped with a higher-energy collision-induced dissociation (HCD) collision cell, an Orbitrap mass analyser and a Nano Flex ion source. MS1 scans were acquired with a resolution setting of 70,000 FWHM and fragment ion spectra produced via HCD were acquired with a normalised collision energy of 28% and a resolution setting of 17,500 FWHM. For data-dependent acquisition of HCD spectra, the top 10 most intense peptide ions within a mass range of 375–1650 *m/z* were fragmented to obtain their sequence information for identification. Exclusion conditions were optimised according to observed chromatographic peak width (~15 s).

Proteome Discoverer software (version 2.4.1.15, Thermo Fisher Scientific, USA) was used for data visualisation. The following search parameters were used for identification: Trypsin/P, precursor mass tolerance 10 ppm, fragment mass tolerance 0.02 Da, up to two missed cleavages were allowed, minimum peptide length of six amino acids, oxidation (M), deamination (N/Q), protein N-terminal acetylation, met-loss, and met-loss with acetylation were set as variable modifications and carbamidomethyl (C) as fixed modification. The minimal number of unique peptides for each protein identified was set to two and the false discovery rate was set at 1 % or

less. Data were searched against the UniProt database (taxonomy: *Vicia faba* on 18-08-2023).

4.2.8 Characterisation of FPI fibrillar gels

4.2.8.1 Flowability of FPI fibrillar gels

To visually examine the flowability of FPI fibrillar gels, after samples preparation for 24 h at room temperature (~20 °C), the glass vials were inverted, and photographs were taken to observe the flowability.

4.2.8.2 Small and large oscillatory deformation rheology

Rheological properties of FPI fibrillar gels formed by different treatment methods were characterised by a stress-controlled rheometer (Physica MCR 301, Anton Paar, Austria) equipped with a parallel plate geometry (40 mm in diameter, 1 mm gap). Samples were transferred onto the bottom plate with a wooden spatula, and then carefully trimmed around the edge of the sample before covering with low viscosity mineral oil (Sigma-Aldrich, USA) to prevent evaporation. Rheological measurements were conducted according to the following protocol. Firstly, a time sweep measurement was conducted at a fixed strain (1%) and frequency (1 Hz) for 2 h to monitor fibrillar gels after sample loading. A frequency sweep test was then conducted at 1% strain while the frequency was varied from 0.01 to 100 Hz to probe the viscoelasticity of the gel network. Finally, a strain sweep test was performed at a constant frequency of 1 Hz while the strain amplitude was varied from 0.01 to 1000%. The storage modulus G' and loss modulus G'' were recorded throughout the tests (Hu, et al., 2023). To determine the thermoreversibility of TS-30 gel, a temperature sweep with a heating and cooling rate of 2 °C/min at a fixed strain 1% and a constant frequency of 1 Hz was conducted from 20 °C to 80 °C and held at 80 °C for 10 min and subsequently from 80 °C to 20 °C to obtain the gelation temperature and melting temperature, respectively.

4.2.8.3 Viscosity determinations

The viscosity was measured by the same rheometer and geometry used in the oscillatory deformation test. The measurement was performed by applying a shear rate sweep from 0.1 to 1000 s^{-1} followed by a reverse sweep from 1000 to 0.1 s^{-1}. The extent of the protein aggregation can be determined by the area (S) of the hysteresis delimited by the

up and down curves, calculated by Origin Pro software (version 2020, Origin Lab, MA, USA) (Luo, et al., 2021). All measurements were performed in duplicate at 20 °C.

4.2.8.4 Scanning electron microscopy (SEM)

The methods for SEM sample preparation and images were based on Goeden-Wood, et al. (2003) with modifications. Gels were firstly cut into small pieces using a spatula and were then fixed in 0.1 M sodium cacodylate phosphate buffer containing 2.5% glutaraldehyde overnight at 4 °C. Fixed gels were washed three times with 0.1 M sodium cacodylate phosphate buffer. After washing, gels were dehydrated in a series of aqueous ethanol solutions (30%, 50%, 70%, 80%, 90%, and 100% ethanol, v/v). Dehydrated gels were frozen by liquid nitrogen and then freeze-dried for 48 h. Finally, gels were cut to approximately 1 mm × 1 mm in size and placed in a sample holder. The samples were coated with gold for 240 s at 12 mA at a temperature of ~ 20 °C. Images were taken by a scanning electron microscope (Philips XL 30S FEG, Eindhoven, The Netherlands) at 5 kV.

4.2.9 Formation and characterisation of high internal phase emulsions (HIPEs)

4.2.9.1 Interfacial tension measurements

The interfacial tension of oil droplets in FPI fibrils (0.1 wt%) was conducted through a Theta Flex Plus optical tensiometer (Biolin Scientific Instruments, Sweden) with the pendant drop method (Hu, et al., 2023). An FPI fibril solution (25 μL) was generated at the stainless-steel syringe tip and immersed in soy oil, and interfacial tension changes with time were monitored up to 6000 s and calculated automatically by One Attention software (Biolin Scientific Instruments, Sweden).

4.2.9.2 Preparation of HIPEs

HIPEs were prepared by homogenising TS-30 FPI fibril solution (3%, w/w) with soybean oil at oil-phase volume fractions (ϕ) of 0.75 (v/v) using a high shear mixer (T10 basic ULTRA-TURRAX®, IKA Corp., Staufen, Germany) with a 10 mm probe (S10N-10 G, IKA, Germany) at a speed of 14, 500 rpm for 2 min. After homogenising, a semi-solid HIPE was formed. HIPE prepared by the same procedure with 3% FPI (w/w) solution without any treatment was used as a control.

4.2.9.3 Oil droplet size

The mean particle size and particle size distribution (PSD) of oil droplets in HIPEs were measured by a static laser light diffraction technique (Mastersizer 2000, Malvern Instruments Ltd, Worcestershire, UK) according to Hu, et al. (2023). The refractive indices used for soybean oil and the dispersant (Milli-Q waster) were 1.47 and 1.33, respectively (da Silva, et al., 2021). The Sauter mean diameter (D [3,2]) was used to represent mean particle diameter for oil droplets.

4.2.9.4 Confocal laser scanning microscopy (CLSM) of HIPEs

For CLSM sample preparations, Fast Green (1% w/v) and Nile Red were used to stain protein and oil phases with a ratio of 500:1 (v/v) and 5000:1 (v/w), respectively (Hu, et al., 2023). Once HIPEs were made, aliquots of samples were added into a glass slide with a cavity covered with a coverslip and sealed by nail polish to prevent water evaporation. The HIPE samples were observed with a confocal laser scanning microscope (Leica DM 6000B, Germany) equipped with an oil immersed 100× objective lens at laser wavelengths of 633 nm for Fast green and 561 nm for Nile red. All images were processed using Image J software (NIH, MD, USA).

4.2.9.5 Rheological measurements of HIPEs

Rheological measurements were conducted according to the same methods as described in **Section 4.2.8.2**. All data were collected at 20 °C. Storage modulus (G') and loss modulus (G'') were recorded during the frequency sweep (0.01 to 100 Hz, 1% strain) and strain amplitude tests (0.1 to 1000%, 1 Hz).

4.2.10 Statistical analysis

All the experiments were conducted at least in duplicate, and the results are reported as mean ± standard deviation (SD). All data were analysed using Minitab statistical software (Minitab 19 Statistical Software, USA). The one-way analysis of variance (ANOVA) was applied to analyse the data. The difference between sample mean values was evaluated via a Tukey's test at a significance level of $P < 0.05$.

4.3. Results and discussion

4.3.1 Visual appearance, ThT fluorescence, and microstructures of FPI fibrils

4.3.1.1 Visual appearances of FPI dispersions and gels

The appearances of FPI fibril solutions (2.5 wt%) and gels (10 wt%) prepared from different treatments are shown in **Fig. 4.1A**. For 2.5wt% FPI, control and CH treated samples are highly turbid and protein sedimentation at the bottom of glass vials was clearly observed (indicated by red arrows in (**Fig. 4.1A**). This was due to the low water solubility of plant protein and heat induced protein aggregation (Alavi, Chen, & Emam-Djomeh, 2021; Alavi, Chen, Wang, et al., 2021). After the TS treatment for 10-30 min, FPI dispersions became translucent indicating a significant improvement in solubility. Similar observations have been made in previous studies of mung bean protein isolate dispersion (10 wt%) (Zhong & Xiong, 2020) and SPI dispersions (10 wt%) after TS treatment (5-30 min and 30-90 °C) (Kamada, et al., 2021). It was reported that ultrasound could help the infiltration of the protein with water so that the solubility can be improved (Frydenberg, et al., 2016). Fibrillar gels can be observed in TS-20 and CH-4 samples (10%, w/w), and the TS-induced gels were more transparent than CH-induced gels (**Fig. 4.1A**). These results also showed that the CH treatment required longer time (>3 h) to induce self-supporting gels than the TS treatment, which only needs 20 min (**Fig. 4.1A**). Rheological properties and microstructural characteristics of FPI gels induced by different treatments are discussed in **Section 4.3.4**.

4.3.1.2 Thioflavin T (ThT) fluorescence assay

The ThT fluorescent dyes can specifically bind to the β-sheet structures in protein fibrils, so ThT fluorescence has been widely used to detect protein fibril formation by measuring the increase of fluorescence intensity (Biancalana & Koide, 2010; Wang, Xie, et al., 2023). The ThT fluorescence spectra of FPI sample before and after various CH or TS treatments are shown in **Fig. 4.1B**. The results shows that the TS or CH treatment (except for CH-1) resulted in a significant increase in ThT fluorescence compared to control, indicating the formation of β-sheet rich fibrillar structures (Xu, Wang, et al., 2023). The peak fluorescence intensity at 480 nm of all samples is plotted in **Fig. 4.1C**. For both TS and CH treated samples, an increase in treatment time led to an increase in fluorescence intensity at 480 nm, demonstrating a time-dependent fibrillisation kinetics. Even after 10 min TS, FPI proteins showed a significantly higher

ThT intensity than the control groups, and the maximum intensity increased with the increasing TS time from~35 at TS10 to ~69 at TS30 (**Fig. 4.1C**). A similar trend was also found in the CH samples, which showed that heating for longer time led to greater ThT intensity, increasing from ~16 (CH-1) to ~92 (CH-8). Notably, TS-20 sample had a comparable ThT intensity at 480 nm (~50) compared to CH-3 samples (~51), indicating a similar extent of fibrillisation (Yang, Jiao, et al., 2022). The similar increase of ThT fluorescence intensity with heat treatment time during fibrillisation has been also reported in other proteins, such as WPI, SPI, and PPI (Biancalana & Koide, 2010; Wang, Xie, et al., 2023; Zhang & Dee, 2023). The results also indicated that the TS treatment accelerated formation of FPI fibril formation compared to the CH treatment. The lowest ThT fluorescence intensity observed in the CH-1 sample could be attributed to the protein aggregation making less surface area available for ThT binding (Jo, et al., 2020; Josefsson, et al., 2019).

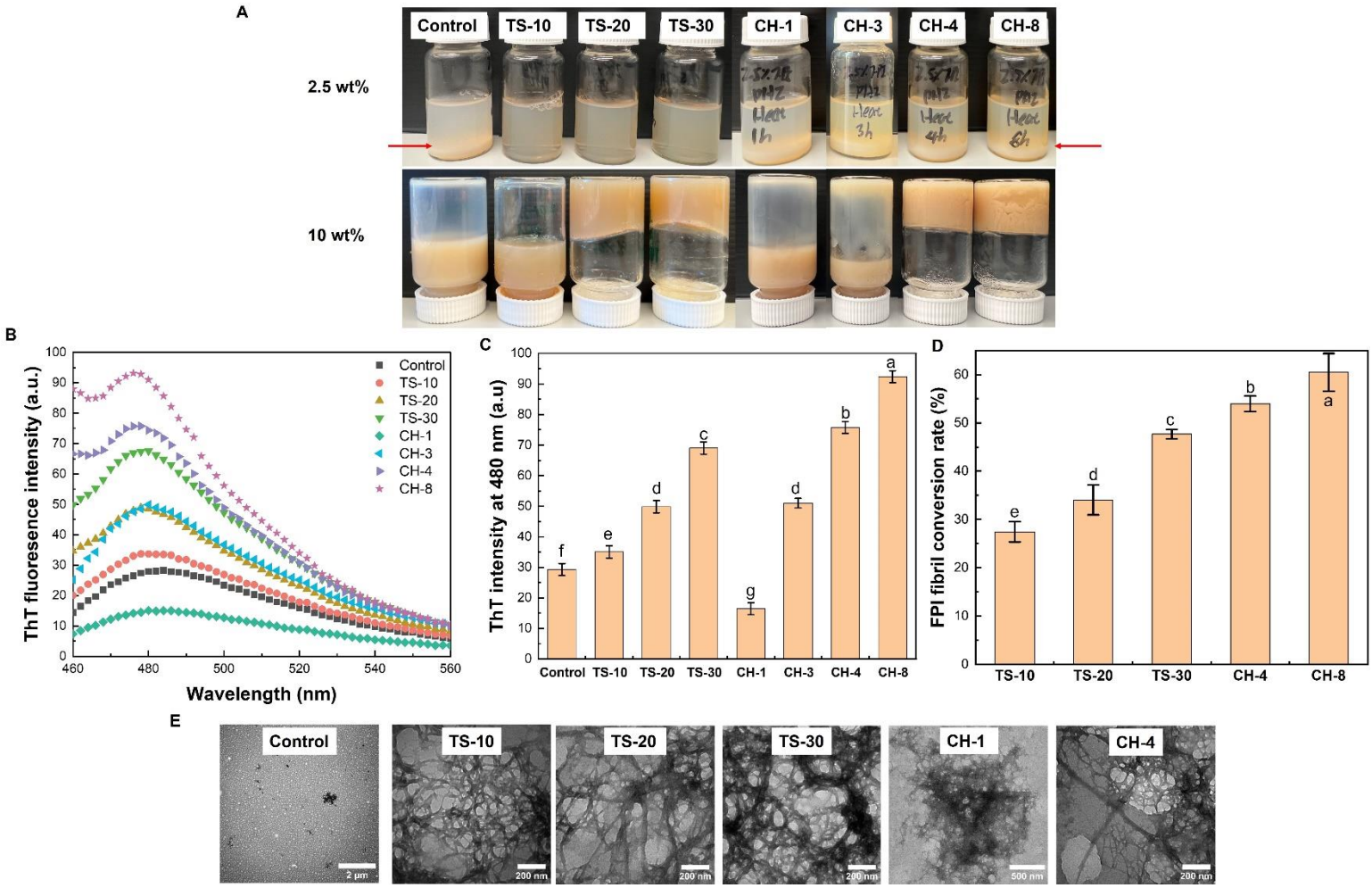

Fig. 4.1 (A) Visual appearance of 2.5 wt% and 10 wt% faba bean protein isolate (FPI) samples after thermosonication (TS) and conventional heat treatment (CH) for different time at pH 2. (B) ThT fluorescence spectrum of FPI dispersions before and after TS (10, 20, and 30 min) or CH (1, 4, and 8 h) treatment at pH 2. (C) ThT fluorescence intensity at 480 nm at pH 2 as function of different treatment and time. (D) FPI fibril conversation rate (%) as function of different treatment and time. (E) TEM images of FPI fibrils (2.5 wt %) formed after TS (10, 20, and 30 min) and CH (1 and 4 h) at pH 2. All samples were extensively diluted to ~0.05wt% prior to TEM observations. Different letters above the columns indicate significant difference ($P < 0.05$).

4.3.1.3 Analysis of fibril conversion rate

The relative conversion rate of the FPI fibrils after different treatments and time is shown in **Fig.4.1D**. Among all the samples, the maximum FPI fibril conversion was found at CH-8 (~60%), followed by CH-4 (~53%) and TS-30 (~47%). In either TS or CH treated FPI samples, the extent of fibril conversion rate increased with an increase in treatment time. Similar trend can also be found in Yu, et al. (2024) and Sun, et al. (2021), who reported that longer treatment time at acidic heating resulted in a greater protein fibril conversion rate. Furthermore, it is worth noting that only a limited portion of FPI were involved in fibrillation induced by either TS or CH treatment, and other proteins may exist as peptides or amorphous protein aggregates (Cao & Mezzenga, 2019; Zhang & Dee, 2023). In addition, the FPI fibril conversion rate results generally agree well with the ThT fluorescence findings (**Fig. 4.1C**). Similar findings have been reported in previous studies on other food protein fibrillisations, such as SPI fibrils (Yu, et al., 2024) and WPI fibrils (Bolder, et al., 2007).

4.3.1.4 Morphology of FPI fibrils as revealed by TEM

TEM images of FPI samples before and after TS or CH treatment are displayed in **Fig. 4.1D.** In the control FPI sample, the presence of submicron particle aggregates was observed. However, after only 10 min of TS treatment, long, straight, and interconnected FPI fibrils with a diameter of approximately 5-12 nm are clearly visible. Similar fibril morphologies have been observed in a previous TEM study of soy protein isolate fibrils included by the TS treatment (90 °C, 30 min) (Kamada, et al., 2021). With increasing TS treatment time to 20 and 30 min, a larger number of fibrils with a more compact and more entangled fibril network can be observed. This finding agrees well with ThT fluorescence results that longer TS treatment induced an increase in the amount of β-sheet in the protein fibrils (**Fig. 4.1C**). In addition, TS treatment (90 °C for 30 min at pH 2) is also effective in fibrillisation of other plant proteins such as SPI and PPI (**Fig. S4.1**). For the CH-treated sample, the morphology of FPI fibrils underwent significant changes during the CH treatment. There was only large amorphous protein aggregate with short fibrils formed at a shorter acidic heating time (e.g. 1 hour in CH-1 sample). This was also consistent with its low ThT fluorescence (**Fig. 4.1C**). After the acidic heating for a longer time (CH-4), the formation of fibrils with a well spanned

network was observed. The morphologies of FPI fibrils induced by TS or CH treatment as shown in **Fig. 4.1D** agree well with previous studies of fibrils derived from plant proteins including faba bean protein (Herneke, et al., 2021), hemp proteins (Kutzli, et al., 2023) and rice bran proteins (Zhang & Huang, 2014). In summary, compared to traditional fibrillisation approaches such as prolonged heating, TS treatment under acidic conditions (pH 2) could significantly accelerate the fibrillisation of plant proteins (**Fig. 4.1D and Fig. S4.1**). This is likely due to the reduction of the high free-energy barrier by ultrasound, which is the most limiting factor to form protein fibrils (So, et al., 2011). Although the mechanism of TS induced protein fibrillisation has received limited attention in the literature, US has been proved to regulate protein fibrillisation through the transient cavitation (Nakajima, et al., 2017) and the increased surface hydrophobicity of proteins (Hu & Li, 2021).

4.3.2 Small-angle neutron scattering (SANS) analysis

The TEM images shown in **Fig. 4.1D** only provide a local view of fibril microstructures and may involve in artefacts problems during sample preparation (Chen, Goode, et al., 2016; Verkade, 2012). To obtain more statistically representative structural information, SANS was applied to probe the microstructures of TS-induced FPI fibrils at various concentrations and treatment times (**Fig. 4.2**). The SANS profile was fitted with a dilute rigid cylinder model (equation (4.2)) and the structural parameters obtained from fitting are listed in **Table 4.1**. It should be noted that the fibril length L is too large to be determined by the SANS setup used in the current study, therefore only the radius of the fibrils was determined. The radius of 2.5wt% FPI fibrils slightly increased from ~4.3 nm to ~5.5 nm when the TS treatment time increased from 10 min to 30 min. This result agrees well with the TEM observation that longer treatment led to thicker bundle formation from stacking of fibrils (**Fig. 4.1D**). It has been reported that once the monofibrils created initially, they arrange themselves in close proximity to each other to form thicker and more expansive fibril bundles (Aggeli, et al., 2001; Mihara, et al., 2005; Rubinov, et al., 2012). However, the radius of fibrils kept nearly constant ~5.3-5.5 nm for different concentrations of FPI, indicating FPI concentration has limited impact on the radius of fibrils formed by TS-30 treatment. Generally, the fibril radius calculated from SANS analysis matched the average single fibril radius observed by TEM and also previous studies of FPI fibrils induced by conventional heating (e.g.

AFM height: 2.7-5.3 nm) (Herneke, et al., 2021; Herneke, Lendel, et al., 2023). In the low Q regime ($0.0008 < Q$ ($Å^{-1}$) < 0.005), the scattering intensity follows a power law decay $I(Q) \sim Q^{-n}$. The expected power law exponent n for long cylindrical fibrils is n=1. However, all FPI fibrils had power law exponent (n) derived from 1 in the low Q region. For example, n=1.47 (TS-10) and 1.35 (TS-30) for 2.5wt% FPI fibrils and n=1.36 for 5 and 10 wt% FPI fibrils formed by TS-30 treatment. This could be attributed to the attractive fibril-fibril interactions and entanglements (Stanley, et al., 2011) that have been observed in a previous SAXS study of α-synuclein fibrils (Pogostin, et al., 2019) and a SANS study of amyloid β peptide fibrils (Lattanzi, et al., 2021). This finding also agrees well with the TEM observations of extensive fibril-fibril interaction and entanglements in TS induced FPI fibril samples (**Fig. 4.1D**).

Table 4.1 SANS model fit structural parameters of faba bean protein isolate (FPI) fibrils and fibrillar gels formed at different FPI concentrations (2.5 and 10 wt%) and thermosonication time (10 and 30 min).

Samples	Power law exponent, n	Mean radius (nm)	Standard deviation, σ
	$Q < 0.005$ Å^{-1}	$0.005 < Q < 0.4$ Å^{-1}	
2.5 wt% FPI-TS-10	1.47 (0.03) *	4.3 (0.1)	0.56 (0.02)
2.5 wt% FPI-TS-30	1.35 (0.03)	5.5 (0.1)	0.38 (0.03)
5 wt% FPI-TS-30	1.36 (0.02)	5.3 (0.2)	0.39 (0.02)
10 wt% FPI-TS-30	1.36 (0.03)	5.4 (0.2)	0.37 (0.03)

*Numbers in parentheses represent σ error bars (or 68.3% confidence levels)

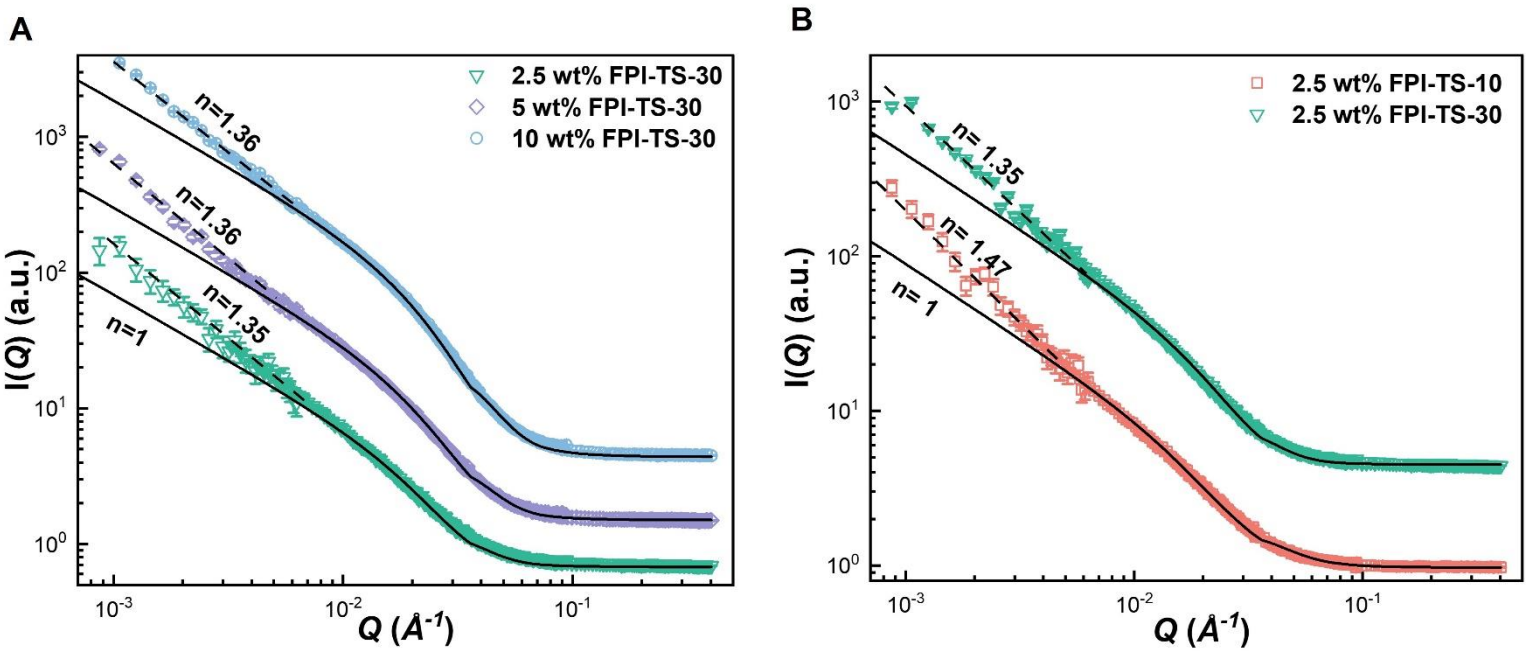

Fig. 4.2 Small-angle neutron scattering (SANS) profiles of (A) Faba bean protein isolate (FPI) fibrils induced by thermosonication (TS) treatment for 30 min at pH 2 at various FPI concentrations (2.5, 5, and10 wt%). (B) FPI fibrils (2.5wt%) induced by TS for 10 min and 30 min. Scattering profiles in (B) were arbitrarily vertically shifted for clarity. The solid black lines are the ling-cylinder form factor fits to the scattering data (eq (4.2)). Deviations observed between the experimental scattering data and the extrapolated fit around $Q < 0.005$ Å^{-1} are attributed to fibril-fibril interactions.

4.3.3 Secondary protein structure of FPI fibrils revealed by CD and FTIR

The secondary protein structure changes of FPI upon fibrillisation can be determined by far-UV circular dichroism (CD) and FTIR. **Fig. 4.3A and B** show the CD spectra in the far-UV region (190–260 nm) of FPI before and after TS and CH treatment for various times. The spectrum of untreated FPI (Control) showed a negative peak around 205 nm with a small shoulder peak located ~220 nm. This suggests that secondary structure of native FPI is dominated by random coil and α-helix with a small portion of β-sheet (Greenfield, 2006). This agrees well with a previous CD study of FPI (Husband, et al., 1994). It can be seen that the peak shifted only slightly from 205 nm to ~ 208 nm in the CH-1 sample, indicating limited conformational changes of FPI after 1 h conventional heating. However, with increasing treatment time to 4 h in CH samples, the negative peak of FPI at ~205 nm shifted to ~216 nm accompanied with a significant increase in magnitude as well, indicating the formation of β-sheet structure (Greenfield, 2006; Kutzli, et al., 2023). Similar findings were found in all TS treated samples with prominent negative peaks appearing around ~218-220 nm, which demonstrated that the TS treatment even for a shorter time (10-30 min) is highly efficient in promoting secondary protein structural changes in FPI. This finding is in line with the results of ThT fluorescence as shown in **Fig. 4.1C**. Formation of β-sheet structures has been widely reported in a broad range of proteins during fibrillisation by using different methods such as β-lactoglobulin fibrils induced by microwave treatment (Hettiarachchi, et al., 2012), WPI treated by hydrothermal treatment (Yang, Jiao, et al., 2022), and hemp proteins treated by conventional heat treatment (Kutzli, et al., 2023), suggesting that amyloid fibrils are typically rich in β-sheet structures.

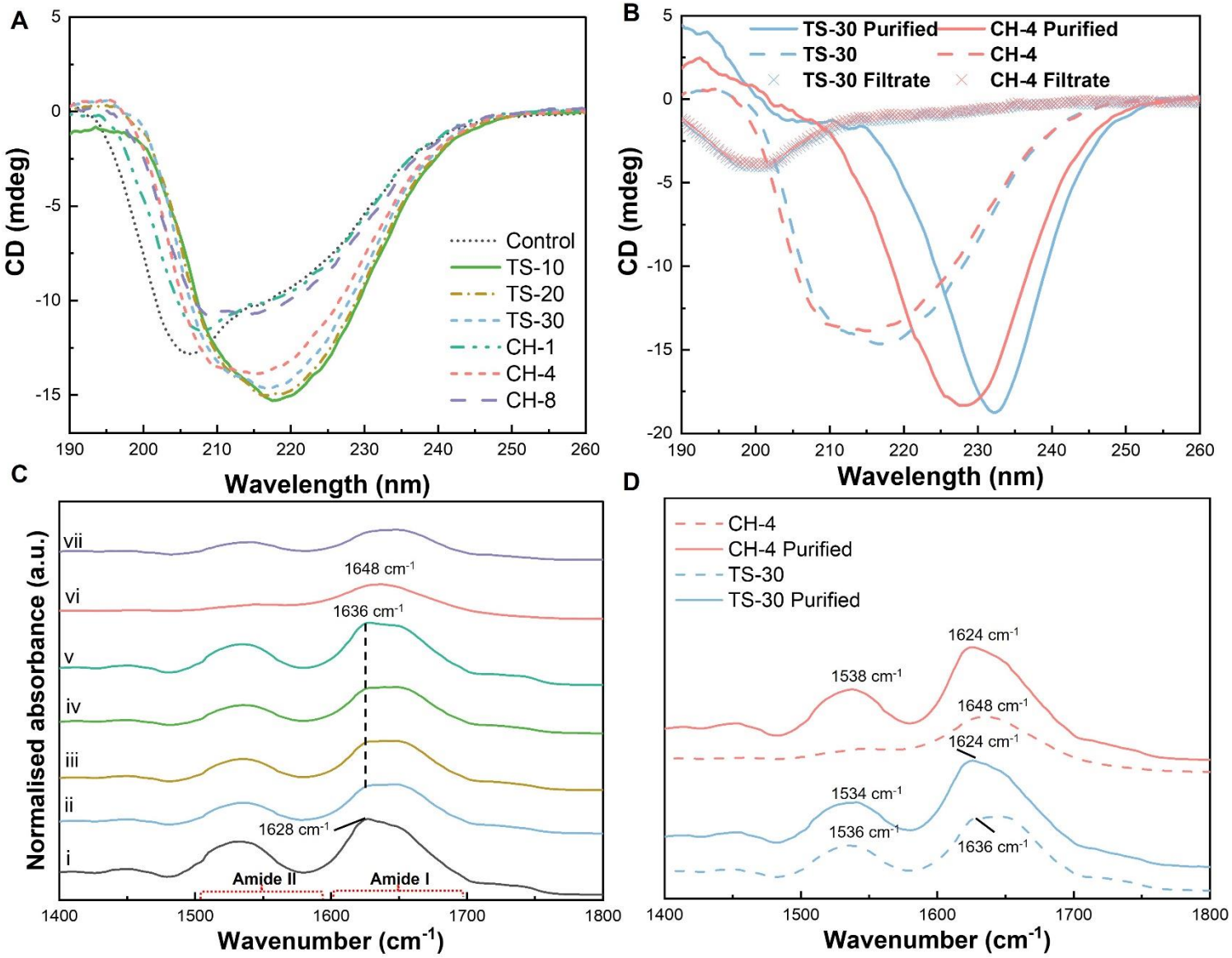

Fig. 4.3 Secondary structural characterisations of faba bean protein isolate (FPI) before and after thermosonication (TS) (10, 20, and 30 min) and conventional heat treatment (CH) (1-8 h) at pH 2. (A) far ultraviolet (UV) circular dichroism (CD) spectra; (B) CD spectra of purified fibrils (retentates) and filtrates of selected samples (TS-30 and CH-4). (C) Amide I and II regions of the FTIR spectra ((i) Control, (ii) TS-10, (iii) TS-20, (iv) TS-30, (v) CH-1, (vi) CH-4, and (vii) CH-8). (D) amide I and II regions of the FTIR spectra of purified fibrils (retentates) and filtrates of selected samples (TS-30 and CH-4).

It is worth noting that in the sample obtained from prolonged heating (e.g. CH-8), the negative peak was centred ~215 nm with a decrease in magnitude compared to CH-4 sample. This could be due to the fact that both amyloid fibrils and released peptides contribute to the final CD signal (Josefsson, et al., 2019; Kutzli, et al., 2023), thus making the interpretation the complex CD spectrum more difficult. This becomes more prominent in CH-8 sample as more hydrolysed peptides are released as identified by SDS-PAGE (**Fig. 4.4**). The similar issue has been reported in a previous study of hemp protein fibrils (Kutzli, et al., 2023). Therefore, selected samples (TS-30 and CH-4) were further studied after purification and removing hydrolysed peptides (**Fig. 3B**). The filtrate fractions of both samples containing a large proportion of hydrolysed peptides that did not participate in fibril formation showed characteristics of a random coil structure with the minimum ~195 nm (**Fig. 4.3B**) (Greenfield, 2006). In terms of the purified fractions (retentates), a significant shift of this minimum from ~195 nm to ~228 nm to ~232 nm was observed. Further, the peak became narrow compared with unpurified samples (**Fig. 4.3B**). Similar results have been reported in previous CD studies of potato protein fibrils and hemp protein fibrils (Josefsson, et al., 2019; Kutzli, et al., 2023).

Complementary to CD, FTIR was also used to study protein secondary structures of FPI fibrils induced by different treatment. **Fig. 4.3C** shows the FTIR spectra of untreated and CH/TS treated FPI samples in amide I and II regions. According to Arrondo, et al. (1993), the amide I IR band (1600–1700 cm^{-1}) provides information on the C=O and C–N stretching vibrations, and the amide II region (1470–1570 cm^{-1}) contains in-plane stretching vibrations of the C–N and C–C groups as well as the N–H bending. The FPI control sample shows a prominent peak ~1628 cm^{-1} in amide I and ~1543 cm^{-1} in amide II. Similar IR spectral features can be observed in previous FTIR studies of FPI (de la Rosa-Millán, et al., 2018; Martínez-Velasco, et al., 2018). After TS or CH treatment, the peak in amide I area was shifted to a higher wavenumber (~1636 cm^{-1} for TS-10, 20, 30 and CH-1 and 1648 cm^{-1} for CH-4 and 8), but the peaks in the amide II band region did not show a significant change for all samples (~1543 cm^{-1}). Previous FTIR studies demonstrated that the protein fibrillisation typically resulted in a shift of the amide I bands towards lower wavenumbers at ~1615-1630 cm^{-1}, due to a transition of protein secondary structure from random coil to β-sheet

(Arrondo, et al., 1993; Zhou, et al., 2022). However, the opposite observation was made here which could be attributed to the extensive overlapping of other component bands of random coils (~1645 cm^{-1}), α-helices (~1654 cm^{-1}), and β-turns (~1681 cm^{-1}) in the amide I region (Hong, et al., 2011; Kutzli, et al., 2023). Similar observations have been found in the CD spectra (**Fig. 4.3A**) along with the previous FTIR studies of fibrils made from hemp proteins (Kutzli, et al., 2023). Therefore, to better resolve the protein secondary structural changes from FTIR spectra, TS-30 and CH-4 samples were purified to remove hydrolysed peptides (**Fig. 4.3D**). Compared to the unpurified samples, the amide I peak of the purified amyloid fibrils shifted from ~1636 cm^{-1} (TS-30) and ~1648 cm^{-1} (CH-4) towards much lower wavenumbers of ~1624 cm^{-1}, representing significant changes in protein secondary structure from random coil to β-sheets, in line with the CD results. A similar finding have been reported in the FTIR study of SPI fibrils upon self-assembly after TS treatment (90 °C, 30 min) in 30%v/v acetic acid solution (Kamada, et al., 2021).

4.3.4 Characterisation of FPI fibrils

4.3.4.1 SDS-PAGE

SDS-PAGE was conducted to investigate the protein hydrolysis in FPI induced by different treatments (i.e., TS and CH) (**Fig. 4.4**). The control FPI sample exhibited numerous major protein bands at approximately ~75 kDa (convicilin), ~50 kDa (7S vicilin), ~ 37 kDa (α-legumin), and ~ 20 kDa (β-legumin), representing the typical protein profiles of FPI (Hu, et al., 2023; Vogelsang-O'Dwyer, et al., 2020). Except for the control sample, all protein bands (>20 kDa) were gradually degraded to lower molecular weight (<20 kDa). As a consequence, the bands corresponding to peptides less than 10 kDa showed significantly increased intensity from TS-20, TS-30, CH-4, and CH-8 samples, indicating the partial hydrolysis of FPI after TS and CH at pH 2. Such hydrolysis has been widely reported during protein fibrillisation, such as WPI (Yang, Jiao, et al., 2022) and PPI (Yi, et al., 2022). In both FPI samples treated with TS and CH, the density of protein bands corresponding to convicilin, vicilin, α-legumin, and β-legumin decreased with an increase in the treatment time, similar to the hydrothermal method-induced WPI fibrils at pH 2 where longer hydrothermal time led to greater hydrolysis (Yang, Jiao, et al., 2022). The extent of protein band degradation was comparable between the TS-30 and CH-4 samples, indicating similar efficiencies

in FPI hydrolysis (**Fig. 4.4**). Conversely, the CH-8 sample showed the greatest protein degradation, suggesting that prolonged heating contributed to a much higher protein hydrolysis level. These results indicated that the TS treatment was efficient in the hydrolysis of FPI proteins to peptides or polypeptides, which is a critical prerequisite for fibril formations, indicating the hydrolysed peptides acting as building blocks for the protein fibrils (Yang, Jiao, et al., 2022). In summary, the SDS-PAGE and the conversion rate results above indicate that the process of protein hydrolysis is extensively important in the formation of protein amyloid fibrils (Yu, et al., 2024).

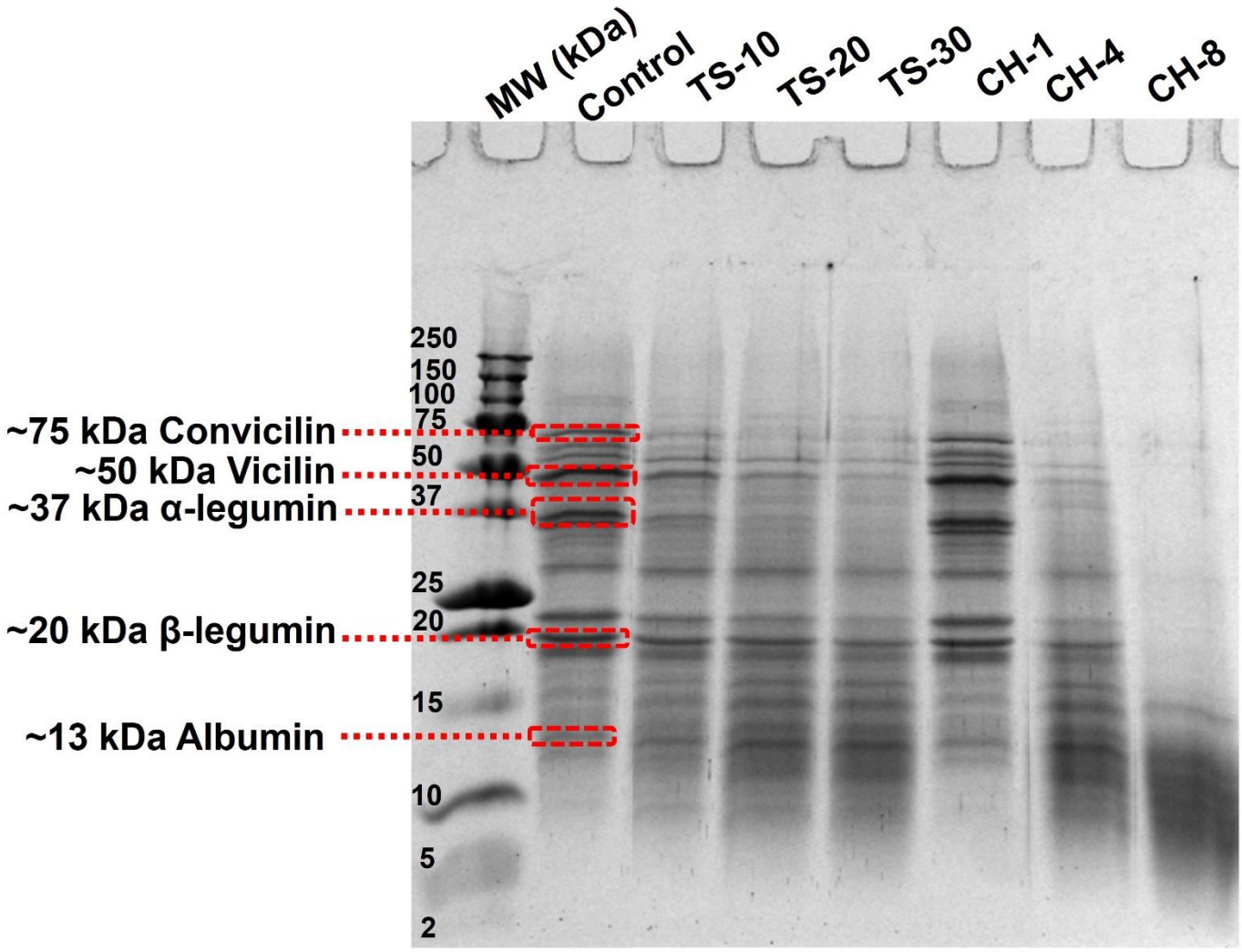

Fig. 4.4 SDS-PAGE profiles of the faba bean protein isolates (FPI) at pH 2 before and after thermosonication (TS) (10, 20, and 30 min) or conventional heat treatment (CH) (90 °C, 1 h, 4 h, and 8 h) under reducing conditions.

4.3.4.2 LC-MS/MS analysis

Identification of the peptide building blocks in FPI fibrils

For further identification of the building blocks (peptides) of FPI fibrils, TS-30 and CH-4 samples were selected for characterisation by LC-MS/MS. As shown in **Fig. 4.5A**, a large number of peptides were identified from both samples by mass spectrometry separated by high- performance liquid chromatography (LC). Comparing the data with the Uniprot protein database (https://www.uniprot.org/), there were 275 peptides, and 295 peptides identified in TS-30 and CH-4 fibril samples, respectively (**Table. S4.1**). The Venn diagram (**Figure 4.5B**) displays the overlap in peptide sequences of FPI fibrils prepared by TS-30 and CH-4 treatment. Despite 228 building block peptides induced by TS-30 and CH-4 treatments were identified to be in common, some unique peptides were still be detected in different treatments (**Figure 4.5B**). For example, there were 47 and 67 unique peptides identified in the TS-30 and CH-4 samples, respectively. As revealed by SDS-PAGE (**Fig. 4.4**), legumin and vicilin were the two major proteins in FPI, therefore, peptides derived from hydrolysis of these two proteins by TS and CH treatment were also compared in **Fig. 4.5B**. There was a total of 52 (TS-30) and 54 (CH-4) peptides derived from legumin, where 41 peptides were the same, and 11 peptides were only identified in TS-30. As for vicilin, there are 71 and 74 peptides found in TS-30 and CH-4 samples, respectively with 60 identical peptides found between the two treatments. In addition, TS-30 and CH-4 samples had 11 and 14 unique peptides, respectively. Distinctive building block peptides of protein fibrils formed by different treatment methods have also been reported in previous studies. For example, Yang, Jiao, et al. (2022) reported that there were 102 and 48 unique peptides identified in WPI fibrils formed by conventional heating (90 °C for 10 h, pH 2) and using a hydrothermal method (110 °C for 4 h, pH 2), respectively. Combined with SDS-PAGE results, it can be clearly seen that the hydrolysis of proteins to small peptides are critical prerequisite steps for subsequent assembly and fibril formation induced by both CH and TS treatment (Meng, et al., 2022). The high efficiency of TS induced FPI fibrillisation could be partially attributed to the rapid hydrolysis of proteins under ultrasonication at elevated temperatures (Yang, Jiao, et al., 2022).

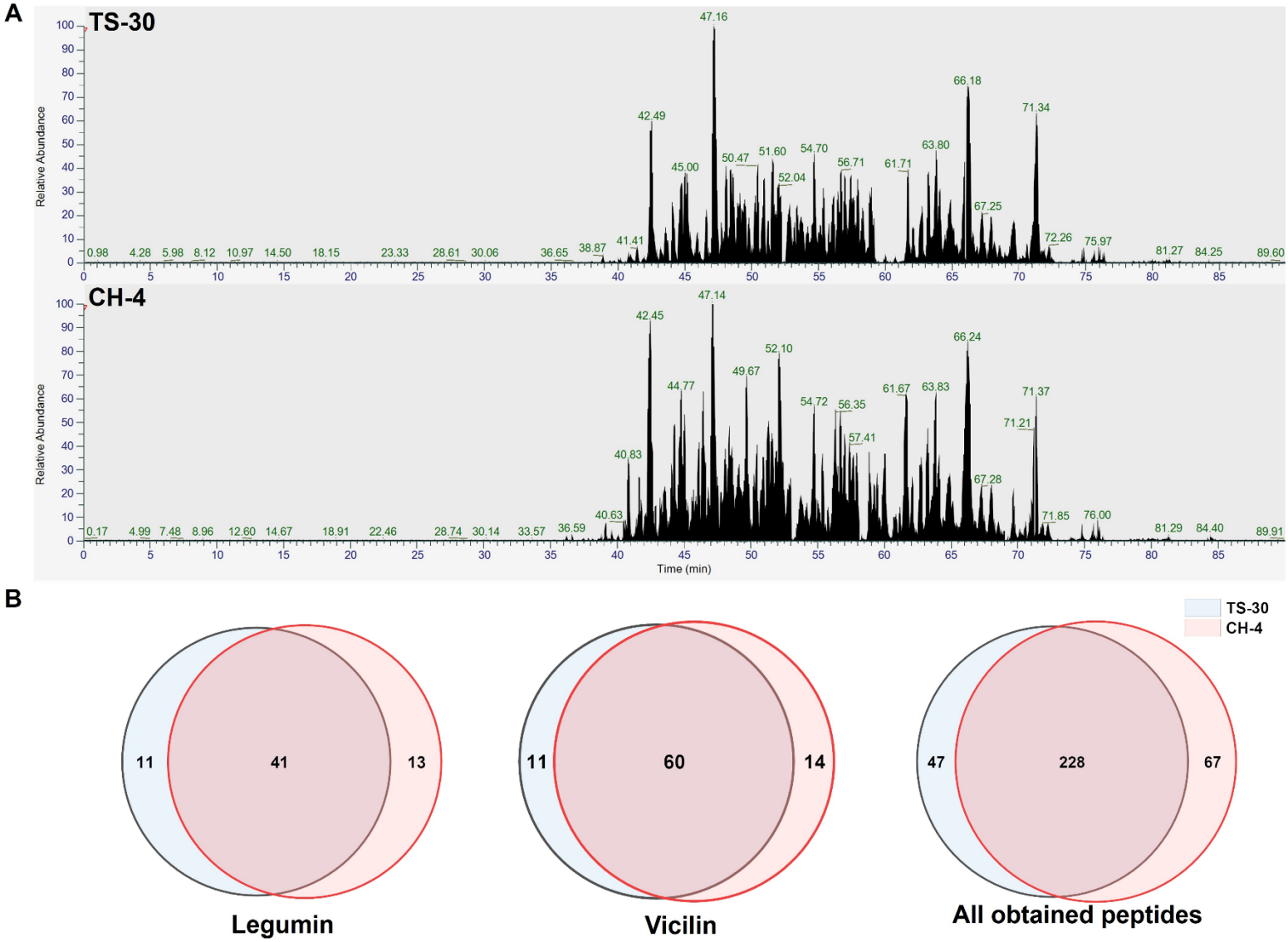

Fig. 4.5 (A) Basepeak peaks of faba bean protein isolates (FPI) fibirils induced by thermosonication for 30 min (TS-30) and conventional heat treatment for 4 h (CH-4). (B) Venn diagram of peptide sequences derived from legumin, vicilin, and all FPI fibrils after hydrolysis under TS-30 and CH-4 treatment. The numbers represent the number of peptides in the corresponding circle.

WALTZ and TANGO analysis of FPI fibrils

To further understand the assembly behaviour of peptide building blocks to fibrils, WALTZ (Maurer-Stroh, et al., 2010) was utilised to compute polypeptide sequences with amyloidogenic potentials and compared with the potential amyloidogenic regions in two major proteins of FPI, namely legumin and vicilin. In recent years, several algorithms such as WALTZ and TANGO have been widely used for identification of amyloid-forming sequences in proteins (Li, Zhou, Wu, et al., 2023; Maurer-Stroh, et al., 2010). **Table 4.2** shows the amyloidogenic regions in legumin and vicilin identified by WALTZ compared to detected peptide sequences of fibrils formed by TS-30 and CH-4 treatment. For legumin (**Table. 4.2A**), both TS and CH treatments could generate peptides that match with predicted amyloidogenic core regions of fibrils including LAQTFNTE and NSLLYVIR. For examples, TS-30 and CH-4 treatments generated 3 and 8 peptides respectively that contained the predicted sequence LAQTFNTE. In terms of vicilin, WALTZ predicted 7 peptides amyloidogenic potential regions (**Table. 4.2B**). After matching with the detected sequences (**Table. S4.1**), TS-30 treatment and CH-4 treatment generated 11 and 10 peptides, respectively containing 4 predicted sequences NLQNYRLLEYK, ADFILVVLSG, KFFEI, and QDLNIFVNYVEIN (**Table. 4.2B**).

To further examine the amyloid fibril formation propensity of detected peptides, another algorithm, TANGO, was used to calculate their β-sheet aggregation propensity at 25 °C with peptide concentration 0.01 wt%, pH 2 and ionic strength 100 mM (Cheng, et al., 2024; Fernandez-Escamilla, et al., 2004). The list of all peptides of FPI fibrils formed by TS-30 or CH-4 treatments and their *AGG* scores is shown in Table S2. Peptides were considered to have high β-sheet propensity if assigned *AGG* scores ≥ 1 computed by TANGO (Cerda-Costa, et al., 2007). As shown in **Table. S4.1**, in the common 228 peptides generated from TS-30 and CH-4, 166 peptides which had *AGG* scores of ≥ 1. In addition, there were 29 out of 47 and 44 out of 67 peptides with *AGG* scores of ≥ 1 in the unique peptides of FPI fibrils formed by TS-30 and CH-4 treatments, respectively. In general, TANGO calculations demonstrated that peptides with a high β-aggregate forming propensity could participate in the formation of amyloid fibrils.

Table 4.2 Comparison of amyloidogenic core regions from legumin (A) and vicilin (B) in faba bean protein isolates (FPI) predicted by the algorithm WALTZ with the LC-MS/MS detected peptide sequence in FPI fibrils formed by conventional heating treatment (4 h) or thermosonication (30 min).

A

Legumin				
Hypothesised sequences	**Measured sequence (TS-30)**	**Measured sequence (CH-4)**	**Location**	**Molecular mass (Da)**
PYWTYN	-	-	-	-
LAQTFNTE	-	FSSEFLAQTFNTEEDTAKR	91-109	2221.04
	GFSSEFLAQTFNTEEDTAKR	GFSSEFLAQTFNTEEDTAKR	90-109	2278.06
	-	GGQHQQEEESEEQKDGNSVLSGFSSEFLAQTFNTEEDTAK	69-108	4414.94
	-	GGQHQQEEESEEQKDGNSVLSGFSSEFLAQTFNTEEDTAKR	69-109	4574.05
	RGGQHQQEEESEEQKDGNSVLSGFSSEFLAQTFNTEEDTAK	RGGQHQQEEESEEQKDGNSVLSGFSSEFLAQTFNTEEDTAK	68-108	4574.05
GLRIINP	-	-	-	-
NSLLYVIRG	INANSLLYVIRGEGR	INANSLLYVIRGEGR	220-234	1675.91
	-	LYRNGIYAPHWNINANSLLYVIRGEGR	208-234	3159.66
	NGIYAPHWNINANSLLYVIRGEGR	NGIYAPHWNINANSLLYVIRGEGR	211-230	2328.22

B

Vicilin				
Hypothesised sequences	**Measured sequence (TS-30)**	**Measured sequence (CH-4)**	**Location**	**Molecular mass (Da)**
NLQNYRLLEYK	LLENLQNYRLLEYK	LLENLQNYRLLEYK	66-79	1809.97
	SKLLENLQNYRLLEYK	-	-	-
ADFILVVLSG	ADFILVVLSGK	ADFILVVLSGK	93-103	1161.69
	-	DADFILVVLSGK	92-103	1276.71
	SKPHTIFLPQQTDADFILVVLSGK	SKPHTIFLPQQTDADFILVVLSGK	80-103	2654.46
	TDADFILVVLSGK	TDADFILVVLSGK	91-103	1377.76
	TIFLPQQTDADFILVVLSGK	TIFLPQQTDADFILVVLSGK	84-103	2205.22
	PQQTDADFILVVLSGK	-	88-103	1730.93
VIVKIS	-	-	-	-
KFFEI	-	FGKFFEITPK	267-276	1213.66
	SREPIYSNKFGKFFEITPK	SREPIYSNKFGKFFEITPK	258-276	2288.21
QDLNIFVNYVEIN	NPQLQDLNIFVNYVEINEGSLLLPHYNSR	NPQLQDLNIFVNYVEINEGSLLLPHYNSR	278-306	3399.73
	RNPQLQDLNIFVNYVEIN	-	277-294	2189.13
	RNPQLQDLNIFVNYVEINEGSLLLPHYNSR	RNPQLQDLNIFVNYVEINEGSLLLPHYNSR	277-303	3555.83
QVQNYK	-	-	-	-
NQRYFL	-	-	-	-

4.3.5 Characterisation of FPI fibrillar gels

4.3.5.1 Small and large deformation rheological properties of FPI fibrillar gels

Small deformation rheological properties

Gelation and rheological behaviour are among the most critical properties of self-assembled protein fibrils. Understanding the rheological properties of fibrillar gels enables insights to be gained on the relationship between fibril microstructure and their associated macroscopic mechanical properties (Xu, Wang, et al., 2023). The viscoelastic properties of FPI fibrillar gels as a function of frequency are shown in **Fig. 4.6A**. For all the samples, G' and G'' were parallel to each other and only slightly varied with frequency, indicating a prevailing elastic behaviour with a solid-like behaviour in all samples (Banerjee & Bhattacharya, 2012; Wei & Huang, 2020). These results agree well with the observation that self-supporting 10 wt% FPI hydrogels were formed by both TS and CH treatment for 4 h and 8 h (**Fig. 4.1A**). Fibrillar gel formation at pH 2 after prolonged heating has been also found in soy protein at 50 g/L after heating from 12 h to 48 h (Xu, Wang, et al., 2023) and lentil protein at 8 wt% after heating from 4 h to 16 h (Jo, et al., 2020), for examples. This could be due to the formation of a denser and entangled fibril network at pH 2 (Peng, et al., 2018).

To better compare the gel strength, the G' at 1 Hz of all the samples was plotted in **Fig. 4.6C**. The CH samples showed greater G' (1 Hz) values compared to the TS samples, indicating that the prolonged CH treatment (4 h and 8 h) was more effective in the formation of the fibrillar gel network with a stronger gel strength, and longer time heating resulting in a stronger gel strength. For instance, G' (1 Hz) increased from ~161 Pa to ~713 Pa when the heat treatment time was increased from 4 h to 8 h. Similar observations have been made in lentil proteins at pH 2 with increasing heating time from 1-16 h. It has been suggested that protein molecules could undergo greater unfolding, interactions, and entanglement under longer heating time, thereby forming a stronger gel network (Jo, et al., 2020). However, the G' (1 Hz) of the TS-induced fibrillar gel (**Fig. 4.6A and 4.6C**) was lower after 30 min TS (~56 Pa) treatment than TS-20 (~88 Pa), which could be due to a break-down of long FPI fibrils induced by prolonged TS treatment, resulting in a weakened fibril-fibril entanglement and network (Nakajima, et al., 2021; Pathak, et al., 2022). Further, fibrils and other non-fibrillar

components including unconverted peptides, soluble and insoluble protein aggregates may co-exist in FPI fibril samples induced by either TS or CH treatment. Depending on their concentrations and assembly state or interactions, their contributions to gel network formation can be different (Meng, et al., 2022; Yang, de Campo, et al., 2022). This may also lead to different gel strength observed in different treatment and time.

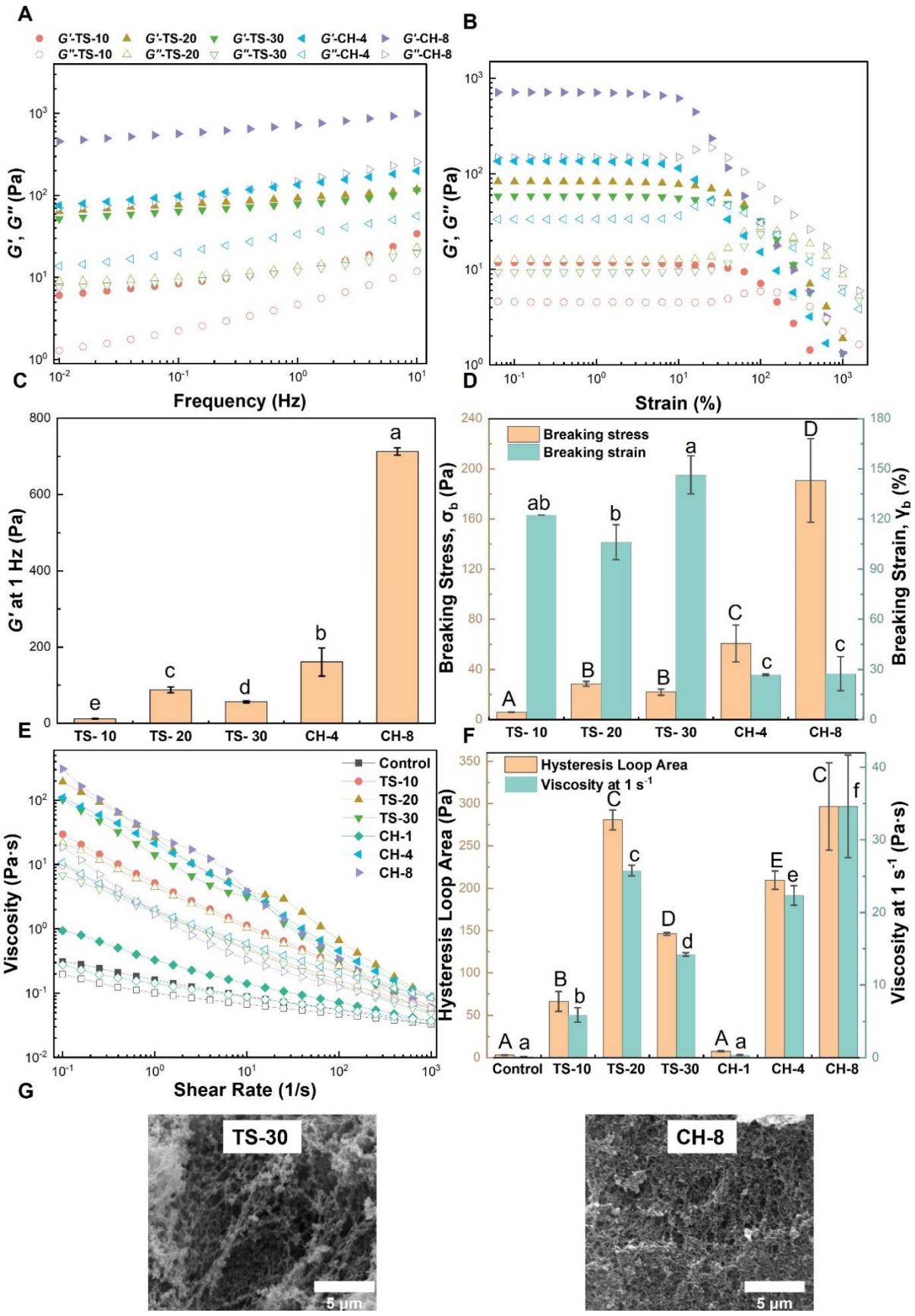

Fig. 4.6 (A) Storage modulus G' (solid symbols) and loss modulus G'' (empty symbols) as a function of frequency (A) and strain amplitude (B) for faba bean protein isolate

(FPI) fibrillar gels induced by different treatment. (C) Gel strength G' (1 Hz) (C) and breaking strain (γ_b) and breaking stress (σ_b) (D) for FPI fibrillar gels induced by different treatments. (E) Viscosity as a function of shear rate for FPI fibrils induced by different treatments. Solid and open symbols represent the "up" and "down" measurements, respectively. (F) Thixotropic hysteresis loop area of thermosonciation (TS) and conventional heat treatment (CH) treated FPI fibrils obtained from the "up" and "down" viscosity measurements. (G) SEM images of seleced FPI fibrillar gels (TS-30 and CH-8). In (C, D, and F) different superscript letters above the column denote significant differences ($P < 0.05$).

Large deformation rheological properties

Large deformation rheological behaviour and structural breakdown characteristics of FPI fibrillar gels were measured by the *strain-sweep* test as shown in **Fig. 4.6B**. All samples demonstrated a quantitatively similar strain dependent behaviour. When the strain amplitude is small, i.e. within the linear viscoelastic region (LVR), both G' and G'' were nearly constant with the increase in strain amplitude. This is a typical characteristic of linear viscoelastic behaviour. In addition, G' was greater than G'' within the LVR, indicating a solid-like structure with a prevailing elastic behaviour as confirmed by the *frequency sweep* measurements and visual appearance (**Fig. 4.1A**) (Munialo, et al., 2014). When the strain amplitude was beyond the LVR, the G' values of all fibrillar gel samples dropped remarkably due to structural disintegration (Yang, de Campo, et al., 2022). On the other hand, for the G'', it firstly increased and reached a maximum before decreasing remarkedly with the strain increase, indicating a typical type III nonlinear rheological (weak strain overshoot) behaviour (Hyun, et al., 2002). This could be caused by an increase in flow or energy dissipation induced by structural rearrangement such as disentanglement of the fibril network (Nechyporchuk, et al., 2016; Zhang, Cheng, et al., 2021). Similar results were reported in previous large deformation rheological studies on other fibrillar gel systems such as cellulose nanofibril hydrogels (Krüger, et al., 2020) and β-hairpin peptide hydrogels (Micklitsch, et al., 2015). With a further increase in strain amplitude, a crossover of G' and G'' occurred and the corresponding strain and stress at the crossover point ($G' = G''$) were defined as breaking strain and breaking stress, respectively. Beyond this point, G'' is dominant over G', suggesting flow of samples due to significant structural disintegration (Yang, et al., 2016). To further compare large deformation rheological behaviour among different gel samples, the breaking stress (σ_b) and breaking strain (γ_b) of all the samples are shown in **Fig. 4.6D**. For CH induced fibrillar gels, the σ_b increased with an increase in treatment time, but σ_b firstly increased when TS treatment time increased from 10 to 20 min and then slightly reduced in the TS-30 sample, following a similar trend to G' at 1 Hz (**Fig. 4.6C**). For example, CH-8 exhibited the greatest value of σ_b (~191 Pa) among all samples, while TS-20 had the largest σ_b (~28 Pa) among TS induced FPI fibrillar gel samples.

As shown in **Fig. 4.6D**, fibrillar gels induced by TS treatments had much larger γ_b values than their CH counterparts) For example, the γ_b values of TS fibrillar gels were in the range of ~120-150%, while the γ_b values of CH fibrillar gels were much smaller at ~30%. This indicated that the TS fibrillar gels could withstand a significant larger shear deformation before breaking down. It has been suggested that rheological properties of fibrillar gels are closely related to their microstructural characteristics including contour length, flexibility, and aspect ratio of the individual fibrils as well as fibril-fibril entanglement and interactions (Cen, et al., 2022; Rodriguez, et al., 2016; Xu, Wang, et al., 2023). These results therefore suggest that different treatments (CH and TS) could result in FPI fibrillar gels with distinct structural characteristics.

4.3.5.2 Viscosity of FPI fibrillar gels

Flow curves of the control, CH- and TS-treated 10wt% FPI dispersions at different treatment times are shown in **Figure 4.6E**. All samples displayed shear-thinning behaviour in which the viscosity decreases as the shear rate increases. Compared to the control, CH and TS treated FPI samples showed a significant increase in viscosities and stronger shear thinning behaviour, which could be due to formation of a denser network induced by entanglements of the fibrils (Kuijk, et al., 2013; Peng, et al., 2018). To better compare viscosities among different samples, values at 1 s^{-1} are plotted as shown in **Fig. 4.6F**. It can be observed that the control and CH-1 samples had a significantly lower viscosity compared to other TS and CH samples, which was in line with the visual observation in **Fig. 4.1A**. Specifically, TS-20 had the greatest viscosity (~25.8 Pa·s) among TS samples, and viscosity significantly increased (from ~0.4 to ~34.6 Pa·s) for CH samples with heating time increasing from 1 h to 8 h. Similar shear-thinning behaviour of plant protein fibrillar gels had also been observed in soybean protein fibrils (Ji, et al., 2021) and rice bean protein fibrils (Zhang & Huang, 2014).

The “up” and “down” viscosity sweep measurements are shown in **Fig. 4.6E.** For all samples, the viscosity was lower upon decreasing the shear rate compared to the viscosity when the shear rate was increased. The presence of a hysteresis loop suggests that FPI fibrillar gels were thixotropic with a time-dependent flow behaviour (Peng, et al., 2018). The hysteresis loop area between the up and down curves was calculated to investigate the extent of thixotropy, where the larger area corresponded to stronger

thixotropic behaviour and larger protein fibrillar aggregates (Armelin, et al., 2006; Luo, et al., 2021). The hysteresis loop areas calculated from all FPI samples are presented in **Fig. 4.6F**. The change of hysteresis loop area among samples was in line with the viscosities at 1 s^{-1} (**Fig. 4.6F**). The CH-8 sample had a largest hysteresis loop area (~297 Pa) followed by the TS-20 sample (~281Pa). This hysteresis behaviour was also observed for WPI fibrils (Peng, et al., 2018) and wood cellulose microfibrils (De Kort, et al., 2016).

4.3.5.3 Microstructural network characteristics of FPI fibrillar gels by SEM

The microstructures of selected FPI fibrillar gels induced by different methods (TS-30 and CH-8) were observed by SEM (**Fig. 4.6G**). For both samples, it can be clearly seen that fine-stranded fibrils are entangled and crosslinked, leading to the formation of network structure with thin connective walls composed of flexible fibrillar aggregates. Similar SEM morphologies of fibrillar gels have been reported for lentil proteins and pea proteins (Jo, et al., 2020; Zhu, Huang, et al., 2022). Furthermore, CH-8 samples exhibited a more compact and much denser fibrillar protein network structure than the TS-30 sample. This might explain the greater gel strength and larger extent of thixotropic behaviour in CH-8 gels. This is because the hysteresis area is related to the energy required to disrupt the internal structures within the gels, so it is expected that FPI fibrillar gels with large and compact aggregates required higher energy to destroy the internal structure contributing to a greater hysteresis (Dankar, et al., 2018; Luo, et al., 2021). In contrast, uneven, less compact protein network structures with large porosity was observed in TS-30 fibrillar gel, leading to their weaker gel strength as discussed above.

4.3.5.4 Thermo-reversible gelation of FPI fibrillar gels

A study on rheological response of hydrogels to environmental factors such as temperature is important for their application and also to help understand the underlying gelation mechanism (De Kort, et al., 2016; Yang, Yang, et al., 2018). Therefore, the rheological properties of TS-30 fibrillar gel as a function of temperature were studied. **Fig. 4.7 and Fig. S4.2** show G' and G'' of TS-30 fibrillar gel as a function of temperature and time, respectively. As the temperature increased from 20 to ~60 °C, G' and G'' gradually decreased but G' was still larger than G'', indicating the sample was still in

the solid state. When the temperature was further increased from 60 to 80 °C, both G' and G'' decreased considerably and G' decreased much faster than G''; this resulted in a crossover of G' and G'' at ~68.5 °C. This temperature can be defined as the melting temperature and beyond this temperature G'' was larger than G', suggesting a gel to solution transition had occurred and the sample was flowable (**Fig. 4.7 inset**). Upon cooling, both G' and G'' increased progressively with G' increasing faster than G''. Therefore, at a certain temperature (~34.3 °C), $G' = G''$ was reached and below this temperature G' was larger than G'' suggesting the liquid like sample solidified again to form self-supporting hydrogel (**Fig. 4.7 inset**). The FPI solution was re-gelled during cooling, and a gradual increase in G' was observed when temperature was maintained at 20 °C for 2 h, indicating that the gel network was formed during the cooling process. Based on this result, it can be inferred that hydrogen bonding is critical in the formation of the fibrillar gel network where hydrogen bonding is reinforced at a low temperature while being diminished at a high temperature (Cen, et al., 2023; Damodaran, 2008; Yang, de Campo, et al., 2022). To the best of our knowledge, reports on thermally reversible gels derived from plant proteins are scant. Recently, Zhu, Huang, et al. (2022) developed thermally reversible pea protein gels, however, pea proteins need to be extracted by using an ammonium sulfate precipitation method. Our study suggests that the thermally reversible FPI gel can be simply made using TS treatment, and the gel may have the potential to substitute gelatine in vegan products.

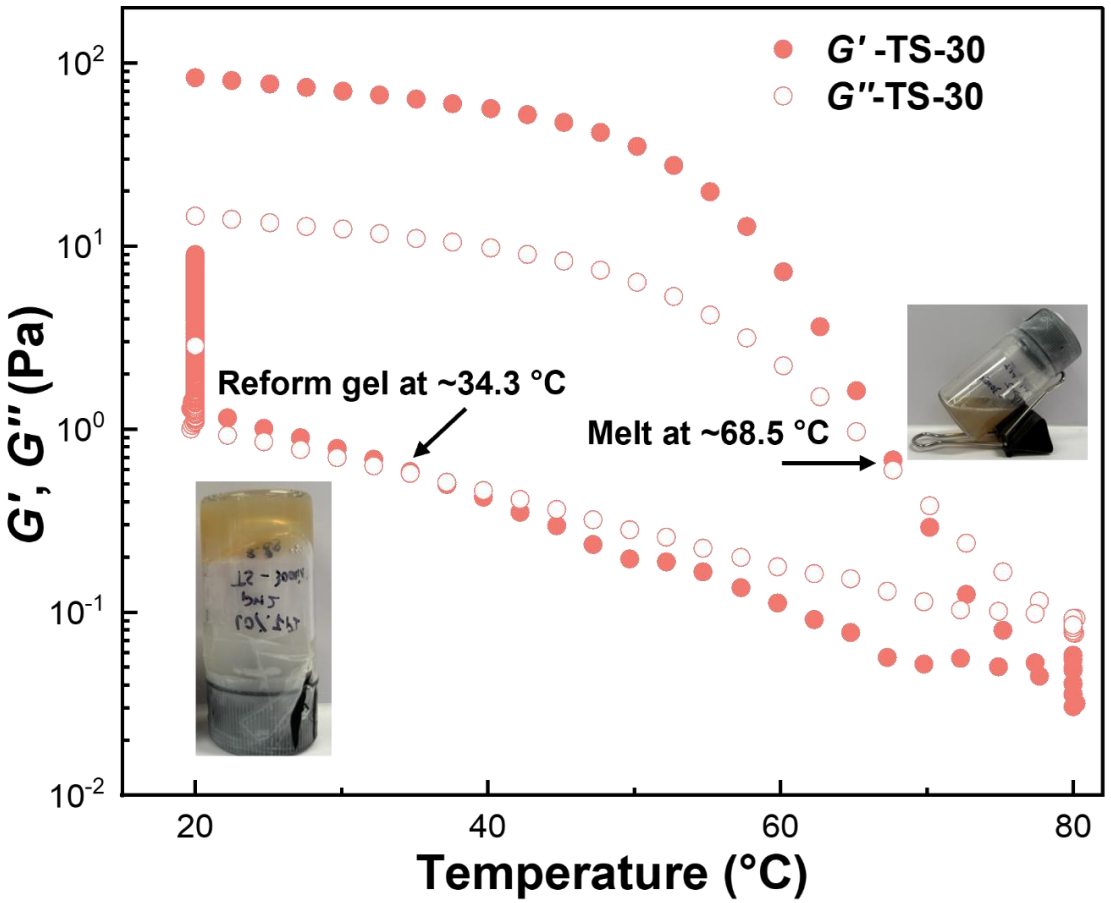

Fig. 4.7 Storage modulus *G′* (solid symbols) and loss modulus *G″* (empty symbols) as a function of temperature for faba bean protein isolate (FPI) sample treated by thermosonciation for 30 min (TS-30) during a rheological temperature sweep measurement (*inset*: visual appreance of samples during sol-gel and gel-sol transitions).

4.3.6 Physicochemical properties and microstructural characteristics of HIPEs made from FPI fibrils

4.3.6.1 Oil-water interfacial tension

The interfacial tension (IFT) of FPI dispersions before and after TS-30 treatment at pH 2 as a function of time is shown in **Fig. 4.8A**. The interfacial tension of both samples initially decreased remarkably with time and tended to reach an equilibrium at ~5000 s, which is a typical behaviour of proteins suggesting that proteins have adopted their stable conformations after migrating from the aqueous phase to the oil-water interface (Tang, 2020b). The IFT values at 5000 s are shown in **Fig. 4.8A inset** and were ~15.8 mN/m (control) and to ~14.0 mN/m for the TS-30 sample. This finding indicated that TS-30 FPI fibrils are more surface active and capable of reducing the oil-water interfacial tension, in line with previous outcomes of SPI fibrils (Ansarifar, et al., 2019). This may be due to the high aspect ratio of protein fibrils and/or the presence of surface-active peptides resulting from protein hydrolysis (Xu, Ma, et al., 2023).

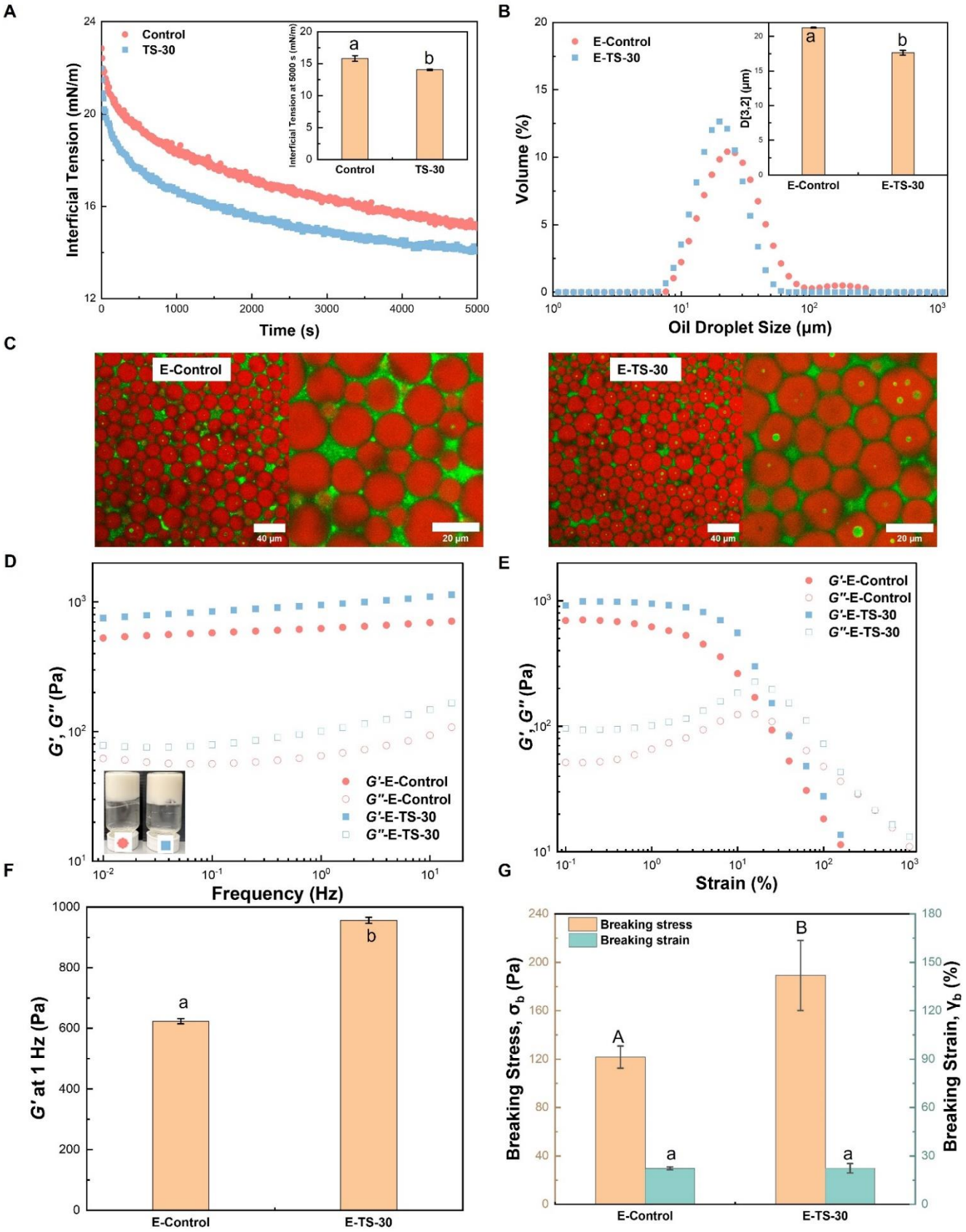

Fig. 4.8 (A) Oil-water interfacial tension of faba bean protein isolate (FPI) before and after 30 min thermosonication treatment (TS-30), and final interfacial tension values at

5000 s (*inset*). (B) Oil droplet size distribution of HIPEs stabilised by 3wt% native FPI solution and FPI fibrils (TS-30). Insets are Sauter mean diameter D [3,2] of oil droplets. (C) Confocal micrographs of HIPEs stabilised by 3wt% native FPI solution and FPI fibrils (TS-30). Scale bar is 40 μm. Insets areassociated zoom-in images with scale bar of 20 μm. (D) The frequency dependence of G' (solid symbols) and G'' (empty symbols) for HIPEs stabilised by native FPI and FPI fibrils (TS-30). Insets are visual appearance of HIPEs. (E) The strain amplitude dependence of G' (solid symbols) and G'' (emptysymbols) for HIPEs stabilised by native FPI and FPI fibrils (TS-30). (F) Gel strength G' (1 Hz) and breaking strain (γ_b) and breaking stress (σ_b) for HIPEs stabilised by native FPI and FPI fibrils (TS-30). In (A, B, F, and G) different superscript letters above the column, denote significant differences ($P < 0.05$). E-control and E-TS-30 indicate the HIPEs stabilised by native FPI and FPI fibrils (TS-30), respectively.

4.3.6.2 Oil droplet sizes distributions of HIPEs

The droplet size distributions of HIPEs (ϕ = 0.75) stabilised by native FPI dispersion (E-control) or TS-30 FPI fibrils (3wt%, pH 2) (E-TS-30) are shown in **Fig. 4.8B**. The droplet size distributions of E-Control and E-TS-30 were different, where E-Control had a prominent peak at ~30 μm, but E-TS-30 had a much smaller size with a prominent peak around 20 μm. Furthermore, the D [3,2] of E-TS-30 (~17.6 μm) was much smaller than that of E-control (~21.2 μm) (**Fig. 4.8B, inset**). This finding was in agreement with the interfacial tension results (**Fig. 4.8A**), that the superior emulsification capability of TS-30 FPI fibrils could stabilise larger surface areas leading to smaller oil droplet size. Similar findings were reported in previous studies (e.g., β-lactoglobulin and lentil protein isolate) (Gao, et al., 2017; Wynnychuk, et al., 2021). For example, Wynnychuk, et al. (2021) studied the O/W emulsions (ϕ =0.5) stabilised by 1.5 wt% lentil protein fibrils induced by conventional heat treatment under pH 2 at 90 °C for 2 h. The results showed that the oil droplet size (D_{90}) of emulsions stabilised by fibrils was smaller (~35 μm) compared to emulsions stabilised by unheated proteins (~45 μm).

4.3.6.3 Microstructure of HIPEs as influenced by FPI structures

CLSM was employed to examine the microstructural characteristics of the HIPEs stabilised by 3 wt% FPI and TS-30 FPI fibrils at pH 2, and the micrographs are shown in **Fig. 4.8C**. Oil droplets stained by Nile Red are shown in red while the protein stained by Fast Green is shown in green. For both emulsion samples, oil droplets were closely packed, and compressed, demonstrating a typical structural characteristic of HIPEs (Zhang, Cheng, et al., 2021; Zhang, Zuo, et al., 2021). Additionally, it can be observed that the oil droplet size decreased when the emulsions are stabilised by TS-30 fibrils compared to native FPI proteins, which was in line with oil droplet size distribution results (**Fig. 4.8B**). Moreover, in the E-TS-30 sample, oil droplets were more compact and more densely packed, showing polyhedron type shapes. Similar microstructural characteristics were also observed in pea protein fibril (2 wt%, formed by heating at 85°C, 20 h at pH 2) stabilised HIPEs with oil fractions of 80% (Wu, et al., 2022).

4.3.6.4 Rheological properties of HIPEs

The G' and G'' of the HIPEs stabilised by control or TS-30 fibrils as a function of frequency are showed in **Fig. 4.8D**. For both emulsion samples, G' and G'' were nearly

independent of frequency with G' being greater more than ten times greater G'', indicating strong gel and solid-like characteristics dominated by elasticity (Hu, et al., 2023). This agrees well with the visual appearance (**Fig. 4.8D inset**) that both FPI stabilised emulsions formed strong and self-supporting gels that can adhere to the bottom of the vial after inversion. The solid and gel-like characteristics of HIPEs have been widely reported in HIPEs stabilised by plant proteins such as quinoa protein isolate (Zhang, Cheng, et al., 2021) and pea protein isolate (Wu, et al., 2022). This has been attributed to the densely packed oil droplets as observed by CLSM (**Fig. 4.8C and 4.8D**). In addition, the TS-30 FPI fibril stabilised HIPEs demonstrated a stronger gel network than native FPI (control) stabilised HIPEs. Specifically, the E-TS-30 sample had a greater G' (1 Hz) (~950 Pa) than E-control (~ 600 Pa). The more compact and tightly arranged oil droplets of smaller size with a possible protein fibril network in the aqueous phase could lead to stronger resistance of oil droplets against movement, thus resulting in a greater mechanical strength of HIPE stabilised by TS-30 FPI fibrils of E-TS-30 (Wei, et al., 2019). Similar observations have been made in O/W HIPEs (ϕ =0.8) stabilised by WPI and WPI fibrils. It has been reported that WPI fibrils stabilised HIPEs had a greater G' and hardness than WPI stabilised HIPEs (Yang, Jiao, et al., 2022). In addition, the presence of non-fibrillar components such as unconverted peptides and soluble protein aggregates may also play important roles in stabilising HIPEs and contributing to a stronger gel strength (Gao, et al., 2017; Mantovani, et al., 2018).

Large deformation rheological behaviour and structural breakdown characteristics of emulsions are shown in **Fig. 4.8E and G**. Within the LVR, G' was greater than G'' and both HIPEs were independent of the applied strain amplitude. As the strain amplitude was beyond the LVR, G' and G'' decreased significantly indicating the structure of HPIEs started to breakdown. Also, a clear overshoot of G'' was observed when the strain was close to the crossover point (i.e., type III nonlinear behaviour) (Hyun, et al., 2002). This behaviour has been reported on HIPEs stabilised by quinoa protein isolate (Zhang, Cheng, et al., 2021), which was attributed to energy dissipation caused by structural rearrangement under large strain deformation (Masalova, et al., 2011; Mason, et al., 1995; Zhang, Cheng, et al., 2021). With a further increase in strain amplitude, the inter-oil droplet interactions were destroyed, leading to the occurrence of G' and G'' crossover. The corresponding strain and stress at the crossover point were defined as breaking

strain and breaking stress, respectively as shown in **Fig. 4.8G**. It was found that the breaking stress of E-TS-30 was significantly greater (~180 Pa) than that of E-Control (~120 Pa), which agrees well with the small oscillatory deformation results. However, the breaking strain is similar for both samples (~35%). Beyond the crossover point, G'' became higher than G', implying that the gel structure was significantly destroyed and started to flow.

4.4 Conclusions

This study systematically compared two methods including thermosonication (TS) and conventional heating (CH) on the fibrillisation of faba bean protein isolates (FPI) at pH 2. The results demonstrated that although both methods could successfully form amyloid fibrils with a high aspect ratio and dominated by β-sheet secondary structures, TS could significantly accelerate the fibril formation. This could be due to the high solubility and more extensive degradation of FPI when exposed to ultrasonication at elevated temperatures, thus promoting fibril self-assembly during cooling. The building blocks of FPI fibrils were characterised by LC-MS/MS and there were 47 and 67 unique peptides identified from TS-30 and CH-4 treatment, respectively. A few peptide sequences such as GFSSEFLAQTFNTEEDTAKR from legumin and ADFILVVLSGK from vicilin were identified as amyloidogenic core regions for fibril formations according to WALTZ. Formation of amyloid-like fibrils was also evidenced by an increase in ThT fluorescence intensity, a higher content of β-sheet secondary structure, and fibrous nanoscale morphology within an entangled network as revealed by TEM and SANS. Increases in viscosity and the formation of a viscoelastic network were observed in 10wt% FPI fibril solutions, indicating their potential applications in tuning rheological properties of food. Finally, the TS-induced FPI fibrils were used to stabilise HIPEs (ϕ = 0.75), and the HIPEs formed by TS-30 had microstructural features with smaller oil droplet size, greater mechanical strength, and more compact od oil droplets than HIPEs formed by untreated proteins. This study showed the TS treatment was effective in the preparing of plant protein fibrils. The resultant formed fibrils provide a range of potential applications including as gelling and emulsifying agents.

4.5 Acknowledgements

The author Yinxuan Hu thanks the Massey University, New Zealand for a doctoral

student scholarship. We also thank the Manawatu Microscopy and Imaging Centre at Massey University, Palmerston North for technical support.

4.6 Supplementary information

Table. S4.1 TANGO predicted β-sheet aggregation propensity of all detected peptide sequences derived from faba bean protein isolate fibrils induced by thermosonication (30 min) (TS-30) and conventional heat treatment (4 h) (CH-4).

TS-30	*AGG* score*	CH-4	*AGG* score
AADLLVEFFEK	255.28	AADLLVEFFEK	255.28
NIENYGLAVLEIKANAFLSPHHYDSEAILFNIK	262.77	NIENYGLAVLEIKANAFLSPHHYDSEAILFNIK	262.77
NIENYGLAVLEIK	113.33	NIENYGLAVLEIK	113.33
NGIYAPHWNINANSLLYVIRGEGR	427.77	NGIYAPHWNINANSLLYVIRGEGR	427.77
NGIYAPHWNINANSLLYVIR	479.64	NGIYAPHWNINANSLLYVIR	479.64
NAMFVPHYNLNANSVLYALKGR	138.01	NAMFVPHYNLNANSVLYALKGR	138.01
NILEASFNTDYKEIEK	1.01	NILEASFNTDYKEIEK	1.01
NAMFVPHYNLNANSVLYALK	252.69	NAMFVPHYNLNANSVLYALK	252.69
NAMFVPHYNLNANSILYALKGR	132.32	NAMFVPHYNLNANSILYALKGR	132.32
NAMFVPHYNLNANSILYALK	245.67	NAMFVPHYNLNANSILYALK	245.67
MIPTKPMVVETFAEYPPLGR	31.70	MIPTKPMVVETFAEYPPLGR	31.70
NILEASFNTDYKEIEKVLLEEHGK	1.01	NILEASFNTDYKEIEKVLLEEHGK	1.01
NILEASFNTKYETIEK	1.00	NILEASFNTKYETIEK	1.00
RGGQHQQEEDGNSVLSGFSSEFLAQTFNTEEDTAKR	10.17	RGGQHQQEEDGNSVLSGFSSEFLAQTFNTEEDTAKR	10.17
RGGQHQQEEDGNSVLSGFSSEFLAQTFNTEEDTAK	10.17	RGGQHQQEEDGNSVLSGFSSEFLAQTFNTEEDTAK	10.17
RFYLAGNQEQEFLR	2.98	RFYLAGNQEQEFLR	2.98
RDFLEDALNVNRHIVDR	0.00	RDFLEDALNVNRHIVDR	0.00
QWIGGEVIQALAYDVPIPGYQTK	59.49	QWIGGEVIQALAYDVPIPGYQTK	59.49
QLLNILGVIYR	657.09	QLLNILGVIYR	657.09
QLLNIFGIVYR	707.93	QLLNIFGIVYR	707.93
QAYYLSMEFLQGR	34.30	QAYYLSMEFLQGR	34.30
NPQLQDLNIFVNYVEINEGSLLLPHYNSR	540.22	NPQLQDLNIFVNYVEINEGSLLLPHYNSR	540.22
NNNPAFSNQFGTLFEVGPSLEK	27.16	NNNPAFSNQFGTLFEVGPSLEK	27.16

TS-30	*AGG* score*	CH-4	*AGG* score
NNLLILCFEVNAQR	551.60	NNLLILCFEVNAQR	551.60
NLRLSAEYVLLYR	420.90	NLRLSAEYVLLYR	420.90
NILEASLNTKYETIEK	0.00	NILEASLNTKYETIEK	0.00
RGGQHQQEEESEEQKDGNSVLSGFSSEFLAQTFNTEEDTAK	10.15	RGGQHQQEEESEEQKDGNSVLSGFSSEFLAQTFNTEEDTAK	10.15
LYRNGIYAPHWNINANSLLYVIR	479.64	LYRNGIYAPHWNINANSLLYVIR	479.64
LLIAAFHLPPSSGSAPVNLEPFFESGGR	140.83	LLIAAFHLPPSSGSAPVNLEPFFESGGR	140.83
LLKNIENYGLAVLEIK	113.14	LLKNIENYGLAVLEIK	113.14
IIFELFADVTPR	173.21	IIFELFADVTPR	173.21
ILENVELPAEFADILVK	61.05	ILENVELPAEFADILVK	61.05
LLENLQNYR	0.00	LLENLQNYR	0.00
IKTVTSLDLPVLR	0.00	IKTVTSLDLPVLR	0.00
LLIAAFHLPPSSGSAPVNLEPFFESGGRRPESVLSTFSSK	164.29	LLIAAFHLPPSSGSAPVNLEPFFESGGRRPESVLSTFSSK	164.29
LKQQYTLCSASLQDIIAR	0.00	LKQQYTLCSASLQDIIAR	0.00
LKPGMVFVVPAGHPYVNIASKK	128.67	LKPGMVFVVPAGHPYVNIASKK	128.67
YPIEHGIVSNWDDMEKIWHHTFYNELR	0.00	YPIEHGIVSNWDDMEKIWHHTFYNELR	0.00
LKPGMVFVVPAGHPYVNIASK	128.72	LKPGMVFVVPAGHPYVNIASK	128.72
IGFSATTGAEYATHEVLSWTFLSELTGPSN	339.06	IGFSATTGAEYATHEVLSWTFLSELTGPSN	339.06
LFYIGGNPEAEFPETQEQHQQRHSSPIGR	1.49	LFYIGGNPEAEFPETQEQHQQRHSSPIGR	1.49
LKQQYFLCSASLQDIISR	16.13	LKQQYFLCSASLQDIISR	16.13
LIPSAALGDSKVFYLK	0.00	LIPSAALGDSKVFYLK	0.00
LLQKFDQHSKLLENLQNYR	0.00	LLQKFDQHSKLLENLQNYR	0.00
IITQWIGTEDWILNTEK	11.29	IITQWIGTEDWILNTEK	11.29
ITNFYTNFQVDEIGR	8.11	ITNFYTNFQVDEIGR	8.11
ITKDGQEEVAEDWLEMGNPWEIVR	0.00	ITKDGQEEVAEDWLEMGNPWEIVR	0.00
ISTVNSLTLPILR	0.00	ISTVNSLTLPILR	0.00
LSPGDVLVIPAGYPVAIK	15.32	LSPGDVLVIPAGYPVAIK	15.32
LSAEYVLLYR	415.34	LSAEYVLLYR	415.34
LRLNIGSSSSPDIYNPQAGR	0.00	LRLNIGSSSSPDIYNPQAGR	0.00
LPAGTIGYLVNRDDEEDLR	63.17	LPAGTIGYLVNRDDEEDLR	63.17

TS-30	*AGG* score*	CH-4	*AGG* score
LNIGSSSSPDIYNPQAGR	0.00	LNIGSSSSPDIYNPQAGR	0.00
IVNSQGNPVFDDKVR	0.00	IVNSQGNPVFDDKVR	0.00
RGGQQQQEEESEEQNEGKSVLSGFSAEFLGHSLNTK	2.31	RGGQQQQEEESEEQNEGKSVLSGFSAEFLGHSLNTK	2.31
RGTIGSIAPLAIGLVVGANVLAGGPFDGACMNPAR	700.90	RGTIGSIAPLAIGLVVGANVLAGGPFDGACMNPAR	700.90
VHINIVVIGHVDSGK	387.16	VHINIVVIGHVDSGK	387.16
VFYLGGNPEVEFPETQEEQQERHQQKHSLPVGR	0.76	VFYLGGNPEVEFPETQEEQQERHQQKHSLPVGR	0.76
VFYLGGNPEVEFPETQEEQQER	0.76	VFYLGGNPEVEFPETQEEQQER	0.76
VFYLGGNLLEAEFPETQEQHPQR	2.34	VFYLGGNLLEAEFPETQEQHPQR	2.34
VETGVVKPGMLVTFAPTGLTTEVK	149.17	VETGVVKPGMLVTFAPTGLTTEVK	149.17
VHINIVVIGHVDSGKSTTTGHLIYK	386.99	VHINIVVIGHVDSGKSTTTGHLIYK	386.99
VESEAGLTETWNPNHPELQCAGVSLIRR	0.00	VESEAGLTETWNPNHPELQCAGVSLIRR	0.00
VESEAGLTETWNPNHPELQCAGVSLIR	7.83	VESEAGLTETWNPNHPELQCAGVSLIR	7.83
VAVQMNDTHPTLCIPELMR	0.00	VAVQMNDTHPTLCIPELMR	0.00
TVTSLDLPVLR	0.00	TVTSLDLPVLR	0.00
VESQAGLTETWNPNHPELQCAGVSLIR	7.83	VESQAGLTETWNPNHPELQCAGVSLIR	7.83
VLDLVIPVNRPGEPQSFLLSGNQNQPSILSGFSK	5.25	VLDLVIPVNRPGEPQSFLLSGNQNQPSILSGFSK	5.25
VIFVPDYNVSVAEMLIPASELSQHISTAGMEASGTSNMK	3.64	VIFVPDYNVSVAEMLIPASELSQHISTAGMEASGTSNMK	3.64
YHAEFTPLFSPEKFELPQAFIATAQSVR	60.75	YHAEFTPLFSPEKFELPQAFIATAQSVR	60.75
YFLAGEEDNVISQIHKPVKELAFPGSAQEVDTLLENQK	2.29	YFLAGEEDNVISQIHKPVKELAFPGSAQEVDTLLENQK	2.29
YFLAGEEDNVISQIHKPVK	1.08	YFLAGEEDNVISQIHKPVK	1.08
YEEIVKEVSSYLKK	0.00	YEEIVKEVSSYLKK	0.00
VYGLNEIQAGELVEFASGVK	9.06	VYGLNEIQAGELVEFASGVK	9.06
VVDLAISVNRPGKVESFNLYGNKNQYLR	17.10	VVDLAISVNRPGKVESFNLYGNKNQYLR	17.10
VVDLAISVNRPGKVESFNLYGNK	17.08	VVDLAISVNRPGKVESFNLYGNK	17.08
VTAAVESEELTVEER	0.00	VTAAVESEELTVEER	0.00
VSEDDKLIEYDALLLDR	4.95	VSEDDKLIEYDALLLDR	4.95

TS-30	*AGG* score*	CH-4	*AGG* score
VPPLANPLAEKPDEIASNISYHAQYTPHFSPFK	0.00	VPPLANPLAEKPDEIASNISYHAQYTPHFSPFK	0.00
VPAGTPTYLVNRDENEKLLIAAFHLPPSSGSAPVNLEPFFESGGR	302.57	VPAGTPTYLVNRDENEKLLIAAFHLPPSSGSAPVNLEPFFESGGR	302.57
VLLEEQDKESQQSIGQR	0.00	VLLEEQDKESQQSIGQR	0.00
TVLIMELINNVAK	414.65	TVLIMELINNVAK	414.65
TVAYTNHTVLPEALEKWSMDLMEK	0.00	TVAYTNHTVLPEALEKWSMDLMEK	0.00
TTGIVLDSGDGVSHTVPIYEGYALPHAILR	13.02	TTGIVLDSGDGVSHTVPIYEGYALPHAILR	13.02
SLSDRFTYVAFK	331.06	SLSDRFTYVAFK	331.06
SKPHTIFLPQQTDADFILVVLSGK	590.67	SKPHTIFLPQQTDADFILVVLSGK	590.67
SGVFGSYNYDELIGSLEGNEGFGR	2.09	SGVFGSYNYDELIGSLEGNEGFGR	2.09
SGIVTVIKDALIPSGTVI	318.11	SGIVTVIKDALIPSGTVI	318.11
SFSHMLNLANLAEEVQIAHR	0.00	SFSHMLNLANLAEEVQIAHR	0.00
SDQDNPFVFESNRFQTLFENENGHIR	3.73	SDQDNPFVFESNRFQTLFENENGHIR	3.73
SCISEGAIIEDTLLMGADYYETDADRR	1.53	SCISEGAIIEDTLLMGADYYETDADRR	1.53
RTIDPNGLHLPSYSPSPQLIYIIQGK	484.60	RTIDPNGLHLPSYSPSPQLIYIIQGK	484.60
RTIDPNGLHLPSYSPSPQLIFIIQGK	499.73	RTIDPNGLHLPSYSPSPQLIFIIQGK	499.73
RSLWPFGGTFKGPFNIR	0.00	RSLWPFGGTFKGPFNIR	0.00
RSLWPFGGTFK	0.00	RSLWPFGGTFK	0.00
RPESVLSTFSSKVLQAALK	25.17	RPESVLSTFSSKVLQAALK	25.17
RPESVLSTFSSK	23.65	RPESVLSTFSSK	23.65
RNPQLQDLNIFVNYVEINEGSLLLPHYNSR	540.17	RNPQLQDLNIFVNYVEINEGSLLLPHYNSR	540.17
RHPEYAVSVLLR	452.26	RHPEYAVSVLLR	452.26
SLWPFGGTFK	0.00	SLWPFGGTFK	0.00
LFYIGGNPEAEFPETQEQHQQR	1.49	LFYIGGNPEAEFPETQEQHQQR	1.49
SLWPFGGTFKGPFNIR	0.00	SLWPFGGTFKGPFNIR	0.00
SNNPFKFLVPPR	0.00	SNNPFKFLVPPR	0.00
TIDPNGLHLPSYSPSPQLIYIIQGK	484.60	TIDPNGLHLPSYSPSPQLIYIIQGK	484.60
TIDPNGLHLPSYSPSPQLIFIIQGK	499.73	TIDPNGLHLPSYSPSPQLIFIIQGK	499.73

TS-30	*AGG* score*	CH-4	*AGG* score
TLADYNIQKESTLHLVLR	0.00	TLADYNIQKESTLHLVLR	0.00
TGYSVSPDSMFDIQVK	0.00	TGYSVSPDSMFDIQVK	0.00
TDWLDGKHVVFGQVVDGLNVVR	100.58	TDWLDGKHVVFGQVVDGLNVVR	100.58
TDKWVTNLDLLTGLR	13.34	TDKWVTNLDLLTGLR	13.34
TAMWFWMTPQANKPSSHDVITGR	166.68	TAMWFWMTPQANKPSSHDVITGR	166.68
SVLSGFSAEFLGHSLNTKEDTAKR	5.69	SVLSGFSAEFLGHSLNTKEDTAKR	5.69
SVLSGFSAEFLGHSLNTKEDTAK	5.68	SVLSGFSAEFLGHSLNTKEDTAK	5.68
SVLSGFSAEFLGHSLNTK	5.68	SVLSGFSAEFLGHSLNTK	5.68
SVLGIILGGGAGTR	473.26	SVLGIILGGGAGTR	473.26
STSSESEPFNLR	0.00	STSSESEPFNLR	0.00
SNYNFEKPFLYLAR	151.12	SNYNFEKPFLYLAR	151.12
SNKFLTLFENENGHIR	225.57	SNKFLTLFENENGHIR	225.57
LFSIDWYR	11.49	LFSIDWYR	11.49
LFHDKESLHPLLEFLR	10.37	LFHDKESLHPLLEFLR	10.37
ELAFDLAAQKVDK	4.74	ELAFDLAAQKVDK	4.74
EHALLAFTLGVK	403.67	EHALLAFTLGVK	403.67
EGQEEVAEDWLEKFSPWEIVR	0.00	EGQEEVAEDWLEKFSPWEIVR	0.00
DSTLIMQLLR	68.19	DSTLIMQLLR	68.19
DILSTIKQELLQSLK	7.74	DILSTIKQELLQSLK	7.74
ELAFDLAAQKVDKIFER	4.75	ELAFDLAAQKVDKIFER	4.75
DKFPGANDFGSEVIPGATELGMR	0.00	DKFPGANDFGSEVIPGATELGMR	0.00
DGQEEVAEDWLEMGNPWEIVR	0.00	DGQEEVAEDWLEMGNPWEIVR	0.00
DFLEDALNVNRHIVDR	0.00	DFLEDALNVNRHIVDR	0.00
DENEKLLIAAFHLPPSSGSAPVNLEPFFESGGRRPESVLSTFSSK	326.71	DENEKLLIAAFHLPPSSGSAPVNLEPFFESGGRRPESVLSTFSSK	326.71
DENEKLLIAAFHLPPSSGSAPVNLEPFFESGGR	303.29	DENEKLLIAAFHLPPSSGSAPVNLEPFFESGGR	303.29
DDEEDLRVLDLVIPVNRPGEPQSFLLSGNQNQPSILSGFSK	17.27	DDEEDLRVLDLVIPVNRPGEPQSFLLSGNQNQPSILSGFSK	17.27
ELAFPGSAQEVDTLLENQK	1.21	ELAFPGSAQEVDTLLENQK	1.21
EIWNIEPVKLE	0.00	EIWNIEPVKLE	0.00
GDTIKLPAGTIGYLVNR	74.98	GDTIKLPAGTIGYLVNR	74.98

TS-30	*AGG* score*	CH-4	*AGG* score
FTAATLEHGMHPPISPKPEWR	0.00	FTAATLEHGMHPPISPKPEWR	0.00
FSKGDVIAIPPGIPYWTYNYGDEPLVAISLLDTSNTLNQLDSTPR	488.62	FSKGDVIAIPPGIPYWTYNYGDEPLVAISLLDTSNTLNQLDSTPR	488.62
FRPDQPNLIFQGGGYTTKEKLTLTK	0.95	FRPDQPNLIFQGGGYTTKEKLTLTK	0.95
FRPDQPNLIFQGGGYTTK	0.95	FRPDQPNLIFQGGGYTTK	0.95
FNLEEGDLIRVPAGTPTYLVNRDENEK	0.83	FNLEEGDLIRVPAGTPTYLVNRDENEK	0.83
FLTLFENENGHIR	2.15	FLTLFENENGHIR	2.15
FITDVGATVNHDPEIGDLLK	1.99	FITDVGATVNHDPEIGDLLK	1.99
EVAAFAQFGSDLDAATQALLNR	52.86	EVAAFAQFGSDLDAATQALLNR	52.86
ERTGYSVSPDSMFDIQVK	0.00	ERTGYSVSPDSMFDIQVK	0.00
EMPYIASMGIYVVSK	607.49	EMPYIASMGIYVVSK	607.49
FNLEEGDLIRVPAGTPTYLVNR	2.32	FNLEEGDLIRVPAGTPTYLVNR	2.32
GDTIKLPAGTIGYLVNRDDEEDLR	64.30	GDTIKLPAGTIGYLVNRDDEEDLR	64.30
CQLDSINALEPDHRVESEAGLTETWNPNHPELQCAGVSLIR	7.83	CQLDSINALEPDHRVESEAGLTETWNPNHPELQCAGVSLIR	7.83
ALLNAIGNLELTGPYAEALSQLSYKLEDVAHQEPDAALGNGGLGR	4.03	ALLNAIGNLELTGPYAEALSQLSYKLEDVAHQEPDAALGNGGLGR	4.03
ALLNAIGNLELTGPYAEALSQLSYK	4.03	ALLNAIGNLELTGPYAEALSQLSYK	4.03
AIADGSLLDFLR	16.04	AIADGSLLDFLR	16.04
AKPHTIFLPQHIEADLILTVLSGK	547.10	AKPHTIFLPQHIEADLILTVLSGK	547.10
AKPHTIFLPQHIDADLILVVFSGK	590.97	AKPHTIFLPQHIDADLILVVFSGK	590.97
AKLSPGDVLVIPAGYPVAIK	15.32	AKLSPGDVLVIPAGYPVAIK	15.32
AILTVLLPNDR	335.30	AILTVLLPNDR	335.30
AGSISTANSLTLPILR	0.00	AGSISTANSLTLPILR	0.00
AFSKNILEASLNTKYETIEK	0.00	AFSKNILEASLNTKYETIEK	0.00
ADLYNPRAGSISTANSLTLPILR	0.00	ADLYNPRAGSISTANSLTLPILR	0.00
ADLYNPR	0.00	ADLYNPR	0.00
AAVSHVQQVFR	0.00	AAVSHVQQVFR	0.00
CAGHGFYTYDAFIAAAR	223.37	CAGHGFYTYDAFIAAAR	223.37

TS-30	*AGG* score*	CH-4	*AGG* score
AILTVLLPNDRNSFSLER	334.67	AILTVLLPNDRNSFSLER	334.67
ATPAEVLANVFGLRHSEVAQIK	157.17	ATPAEVLANVFGLRHSEVAQIK	157.17
ATPAEVLANVFGLR	202.35	ATPAEVLANVFGLR	202.35
ATPADVLANAFGLR	17.71	ATPADVLANAFGLR	17.71
ASDAFVELADASGYALAVMPSAK	73.27	ASDAFVELADASGYALAVMPSAK	73.27
ANAFLSPHHYDSEAILFNIK	185.07	ANAFLSPHHYDSEAILFNIK	185.07
AIVVLVVNEGQGNLELVGFKNEQQEQSLKEDEQQER	595.09	AIVVLVVNEGQGNLELVGFKNEQQEQSLKEDEQQER	595.09
AINENLINNPDLVSTNPTISFK	0.00	AINENLINNPDLVSTNPTISFK	0.00
AIVVLLVNEGKGNLELVGIQNEQQEQQER	598.07	AIVVLLVNEGKGNLELVGIQNEQQEQQER	598.07
ALVVHELEDDLGKGGHELSLSTGNAGGR	0.00	ALVVHELEDDLGKGGHELSLSTGNAGGR	0.00
AIVIVTVNEGKGDFELVGQRNENQQGLR	587.79	AIVIVTVNEGKGDFELVGQRNENQQGLR	587.79
AIVIVTVNEGKGDFELVGQR	587.80	AIVIVTVNEGKGDFELVGQR	587.80
AIVIVTVNEGK	587.84	AIVIVTVNEGK	587.84
ALTNAIGNLNIQDAYADALR	0.00	ALTNAIGNLNIQDAYADALR	0.00
AIVVLLVNEGK	592.31	AIVVLLVNEGK	592.31
GDVIAIPPGIPYWTYNYGDEPLVAISLLDTSNTLNQLDSTPR	488.65	GDVIAIPPGIPYWTYNYGDEPLVAISLLDTSNTLNQLDSTPR	488.65
FRKGDIIAIPSGIPYWTYNNGDEPLVAISLLDTSNIANQLDSTPR	479.42	FRKGDIIAIPSGIPYWTYNNGDEPLVAISLLDTSNIANQLDSTPR	479.42
GFFEVTHDISHLTCADFLR	11.33	GFFEVTHDISHLTCADFLR	11.33
KYPQLQDLDIFISSVEIK	192.62	KYPQLQDLDIFISSVEIK	192.62
KNNLLILCFEVNAQR	590.49	KNNLLILCFEVNAQR	590.49
KNAMFVPHYNLNANSVLYALK	252.69	KNAMFVPHYNLNANSVLYALK	252.69
KNAMFVPHYNLNANSILYALK	245.66	KNAMFVPHYNLNANSILYALK	245.66
KGVSSELEPFNLR	0.00	KGVSSELEPFNLR	0.00
KGQLVVVPQNFVVAQQAGNEEAFEYVVFK	560.04	KGQLVVVPQNFVVAQQAGNEEAFEYVVFK	560.04

TS-30	*AGG* score*	CH-4	*AGG* score
KGQLVVVPQNFVVAEQAGEEEGLEYLVFKTNDR	147.35	KGQLVVVPQNFVVAEQAGEEEEGLEYLVFKTNDR	147.35
KGQLVVVPQNFVVAEQAGEEEGLEYLVFK	247.56	KGQLVVVPQNFVVAEQAGEEEEGLEYLVFK	247.56
KGDIIAIPSGIPYWTYNNGDEPLVAISLLDTSNIANQLDSTPR	479.45	KGDIIAIPSGIPYWTYNNGDEPLVAISLLDTSNIANQLDSTPR	479.45
HVVFGQVVDGLNVVR	188.07	HVVFGQVVDGLNVVR	188.07
KYPQLQDLDIFVSFSEISEGALLLPHYNSR	381.47	KYPQLQDLDIFVSFSEISEGALLLPHYNSR	381.47
HVEIIEMIDEELIR	19.09	HVEIIEMIDEELIR	19.09
LAEQAERYEEMVEFMEK	0.93	LAEQAERYEEMVEFMEK	0.93
LAGTSSVINDLPLDVVAATFNLERNEAR	262.27	LAGTSSVINDLPLDVVAATFNLERNEAR	262.27
IFERKEELFFPYDEER	0.00	IFERKEELFFPYDEER	0.00
LFEITPEKKYPQLQDLDIFVSFSEISEGALLLPHYNSR	381.71	LFEITPEKKYPQLQDLDIFVSFSEISEGALLLPHYNSR	381.71
LFEITPEKKYPQLQDLDIFISSVEIK	192.59	LFEITPEKKYPQLQDLDIFISSVEIK	192.59
LFEITPEK	0.00	LFEITPEK	0.00
LDNINALEPDHRVESEAGLTETWNPNHPELR	0.00	LDNINALEPDHRVESEAGLTETWNPNHPELR	0.00
LDETLTANRNEILALLSR	209.51	LDETLTANRNEILALLSR	209.51
LDALEPDNRIESEGGLIETWNPNNRQFR	6.77	LDALEPDNRIESEGGLIETWNPNNRQFR	6.77
LDALEPDNRIESEGGLIETWNPNNR	6.81	LDALEPDNRIESEGGLIETWNPNNR	6.81
LASCFLDSLATLNYPAWGYGLR	3.52	LASCFLDSLATLNYPAWGYGLR	3.52
LAGTSSVINDMPVDVVAATFNLERNEAR	285.22	LAGTSSVINDMPVDVVAATFNLERNEAR	285.22
LAGTSSVINDMPVDVVAATFNLER	288.31	LAGTSSVINDMPVDVVAATFNLER	288.31
LAGTSSVINDLPLDVVAATFNLER	265.36	LAGTSSVINDLPLDVVAATFNLER	265.36
HWVGGEDIKAVAHDVPIPGYK	0.00	HWVGGEDIKAVAHDVPIPGYK	0.00
GQLVVVPQNFVVAEQAGEEEGLEYLVFK	241.17	GQLVVVPQNFVVAEQAGEEEGLEYLVFK	241.17
GFSKNILEASFNTKYETIEK	0.00	GFSKNILEASFNTKYETIEK	0.00
GGQHQQEEDGNSVLSGFSSEFLAQTFNTEEDTAK	10.17	GGQHQQEEDGNSVLSGFSSEFLAQTFNTEEDTAK	10.17
GGQHQQEEDGNSVLSGFSSEFLAQTFNTEEDTAKR	10.17	GGQHQQEEDGNSVLSGFSSEFLAQTFNTEEDTAKR	10.17
GKGIIGLVAEDQTERFNLEEGD	170.63	GKGIIGLVAEDQTERFNLE	170.6

TS-30	*AGG* score*	CH-4	*AGG* score
LIR		EGDLIR	3
GKGILQHHQVIAEFEEIPEENR	5.73	GKGILQHHQVIAEFEEIPEENR	5.73
GIIGLVAEDQTERFNLEEGDLIR	276.75	GIIGLVAEDQTERFNLEEGDLIR	276.75
GIIGLVAEDQTERFNLEEGDLIRVPAGTPTYLVNR	278.84	GIIGLVAEDQTERFNLEEGDLIRVPAGTPTYLVNR	278.84
GILQHHQVIAEFEEIPEENRQK	5.72	GILQHHQVIAEFEEIPEENRQK	5.72
GQLVVVPQNFVVAQQAGNEEAFEYVVFK	553.67	GQLVVVPQNFVVAQQAGNEEAFEYVVFK	553.67
GRYEEIVKEVSSYLK	0.61	GRYEEIVKEVSSYLK	0.61
YPQLQDLDIFISSVEIK	192.64	YPQLQDLDIFISSVEIK	192.64
GVIGLTLPGCPQTYQEPR	13.17	GVIGLTLPGCPQTYQEPR	13.17
GVIGLTLPGCPETYEEPR	13.18	GVIGLTLPGCPETYEEPR	13.18
GVLGLAVPGCPETYEEPR	11.12	GVLGLAVPGCPETYEEPR	11.12
YLLELIR	22.45	YLLELIR	22.45
IAKEDVLSLAPK	0.00	IAKEDVLSLAPK	0.00
FFEITPK	0.00	FFEITPK	0.00
ELETVLDEQQK	2.33	ELETVLDEQQK	2.33
HKVETELSNICIDVMR	7.50	HKVETELSNICIDVMR	7.50
NKYEETKELLLQVATHK	31.99	NKYEETKELLLQVATHK	31.99
EIKFEFPAMDTL	0.00	EIKFEFPAMDTL	0.00
LGVASAYLALKPSEVALR	33.28	LGVASAYLALKPSEVALR	33.28
NILEASFNTK	1.01	NFTLNFGPQHPAAHGVLR	7.32
QQYTLCSASLQDIIAR	0.00	QAFDEAIAELDTLGEESYKDSTLIMQLLR	79.97
QAFDEAISELDTLNEESYKDSTLIMQLLR	79.84	NSPIDFELGGGQVIK	0.00
MHASFIRPGGVAQDLPLGLCR	0.00	NRFQVNDVLVFK	93.43
IVIGLFGDAVPK	199.95	LYRNGIYAPHWNINANSLLYVIRGEGR	427.74
LSEEEIGGLKELFK	0.00	LLENLQNYRLLEYK	0.00
LSAEHGSLRKNAMFVPHYNLNANSVLYALK	252.71	IKTVTSVDLPVLR	0.00
IRENIAQPAR	0.00	ILILNKFHEK	0.00
LQDDLGTKFHLLVR	0.00	IINEPTAAALAYGLDK	17.00
LNQCRLDNINALEPDHRVESEAGLTETWNPNHPELR	0.00	IINEPTAAALAYGLDKK	16.81
IITQWIGTEDWILNTEKLAELR	10.92	IVNSQGNAVFDNKVR	0.00
VFYLGGNLLEAEFPETQEQHPQRHSSPIGR	2.34	LTEVLKQPQYAPLPIEK	0.00
VESEAGLTETWNPNHPELR	0.00	MLDADITDSVIGEGCVIK	1.75
VIDEHLIPSAAAGESTVFYYK	268.82	LIQQWNETYLHFHKVDPK	0.00

TS-30	*AGG* score*	CH-4	*AGG* score
YEEIVKEVSSYLK	0.61	VFYLGGNPEVEFPETQEEQQERHQQK	0.76
VVPLFEKLDDLEAAPAALAR	0.00	VCENIPIVLCGNKVDVK	5.16
SVEKGWGLELGELAR	0.00	VAVTGLTVAEHFR	31.17
EACKWSPELAAACEVWK	7.92	VAVQLNDTHPTLSIPELMR	0.00
DFLEDAFNVNRHIVDR	0.00	VGVEFDKAGAIVVNEYSR	50.83
DGQTREHALLAFTLGVK	456.57	YPIEHGIVSNWDDMEK	0.00
IFKIAKEDVLSLAPK	0.00	YETIEKVLLEEQDKESQQSIGQR	0.00
EITLGFVDLLR	300.84	TSPSSFAPDTTSIVSSIK	11.99
EQSQQNECQLERLDALEPDNRIESEGGLIETWNPNNR	6.80	SLPSKFEPINLR	0.00
ATSESETLYCVYVAIGQK	776.64	RTIDPNGLHFPSFSPSPQLIFIIQGK	499.73
AGIQEVHFLPFNPTDKR	0.00	SCISEGAIIEDTLLMGADYYETEADKR	1.53
ACADDFDLFLFNDGQLESASVLHSR	285.55	TGYSVSPDSMFDIQVKR	0.00
AGRISTVNSLTLPILR	0.00	SNKFLTLFQNK	233.39
AIPWIFAWTQTR	386.75	SVEMHHEALTEALPGDNVGFNVK	2.25
ALTVPQNYAVAAK	9.37	EAFPGDVFYLHSR	19.15
KYEPTIGVEVHPLDFFTNCGK	3.52	DRFLFCAEAIYK	67.69
HVVFGQVVDGLNVVRDIEK	177.09	DNLTLWTSDMQDDGADEIKEAAPK	9.71
HVVFGHVIEGLDVVK	1.15	DFLEDALNVNR	0.00
LDNINALEPDHRVESEAGLTETWNPNHPELRCAGVSLIR	4.46	DFLEDAFNVNR	0.00
LAQYVLQVTGENIDPDSLFDIQVK	78.72	EITLGFVDLLRDDYIEKDR	231.07
GHVNPAVTFGALIGGR	286.94	EMPFIASMGIYVISK	782.51
GILQHHQVIAEFEEIPEENR	5.73	FRKGDIIAIPSGIPYWTYNDGDEPLVAVSLLDTSNIANQLDSTPR	486.61
GTIGSIAPLAIGLVVGANVLAGGPFDGACMNPAR	700.91	FRGVNDRNAAEALNGLELYIER	5.89
GWDEGVLGMQLGEVAR	0.00	FRCPEVLFQPSMIGMEAAGIHETTYNSIMK	0.00
GDFELVGQR	0.00	FQLQQAYYATAESVR	6.09
GKGIIGLVAEDQTER	170.95	FLDILQDLHGEDLKDSVQEVYELSAEYER	0.00
ATPADVLANAFGLRQRQVTELK	12.89	FGKFFEITPK	0.00
VKGGLSIITPPER	1.08	FDTRSDLFENLQNYR	0.00

TS-30	*AGG* score*	CH-4	*AGG* score
GWNEEVLTLTIEADAETASPNKPVERMIAAAYEIGATRPGDR	344.43	AILTVLSPNDRNSYNLER	309.50
GIRPAINVGISVSR	7.80	AFGPALVGWR	7.84
SGIVTIIKDALIPSGTVL	311.24	AILTVLSPNDRNSYNLERGDTIK	309.25
SFSHMLNLANLAEEVQIAHRR	0.00	ALMDQMAVIATEEYR	75.10
DFLEDALNVNRHIVDRLQGR	0.00	ASSNLNLVGFGINAENNQR	51.97
-	-	ARVAVTGLTVAEHFR	74.60
-	-	CQLDSINALEPDHRVESQAGLTETWNPNHPELQCAGVSLIR	7.83
-	-	ANAFLSPHHYDSEAILFNIKGK	93.35
-	-	LAEQAERYEEMVSFMQK	3.94
-	-	KGDIIAIPSGIPYWTYNDGDEPLVAVSLLDTSNIANQLDSTPR	486.64
-	-	FSPWEIVR	0.00
-	-	LASCFLDSMATLNLPAWGYGLR	1.68
-	-	GGQHQQEEESEEQKDGNSVLSGFSSEFLAQTFNTEEDTAK	10.16
-	-	GGQHQQEEESEEQKDGNSVLSGFSSEFLAQTFNTEEDTAKR	10.16
-	-	GLSWKDAWNITQR	0.00
-	-	GPILLEDYHLVEK	0.00
-	-	GDIIAIPSGIPYWTYNNGDEPLVAISLLDTSNIANQLDSTPR	478.26
-	-	FYLAGNQEQEFLR	0.00
-	-	FTYVAFK	89.96
-	-	GVLGLAVPGCPETYEEPRSQSR	11.10
-	-	GVIGLTLPGCPETYEEPRSSQSR	13.16
-	-	HAGDLGNIVANAEGVAEATIVDNQIPLTGPNSVVGR	12.15
-	-	GGGPTHLAILSQPPDTIHGSLR	5.04
-	-	IFSVDVNFHPLNETVSLIAMAILNPK	758.75
-	-	ATPADVLANAFGLRQR	13.05

***AGG calculation conditions:** 0.01 wt% peptide concentration with ionic strength of 100 mM (pH 2, 25 °C). 29/47 (TS-30) and 44/67 (CH-4) peptides had *AGG* scores of ≥

1.

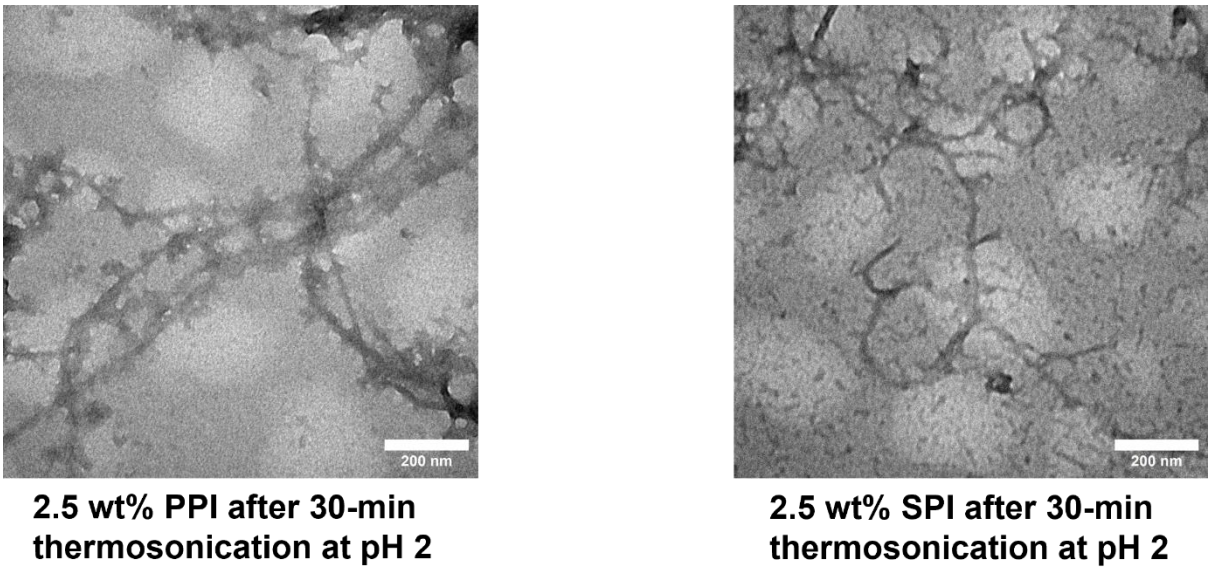

Fig. S4.1 TEM images of pea protein isolate and soybean protein isolate fibrils formed after 30-min thermosonication at pH 2.

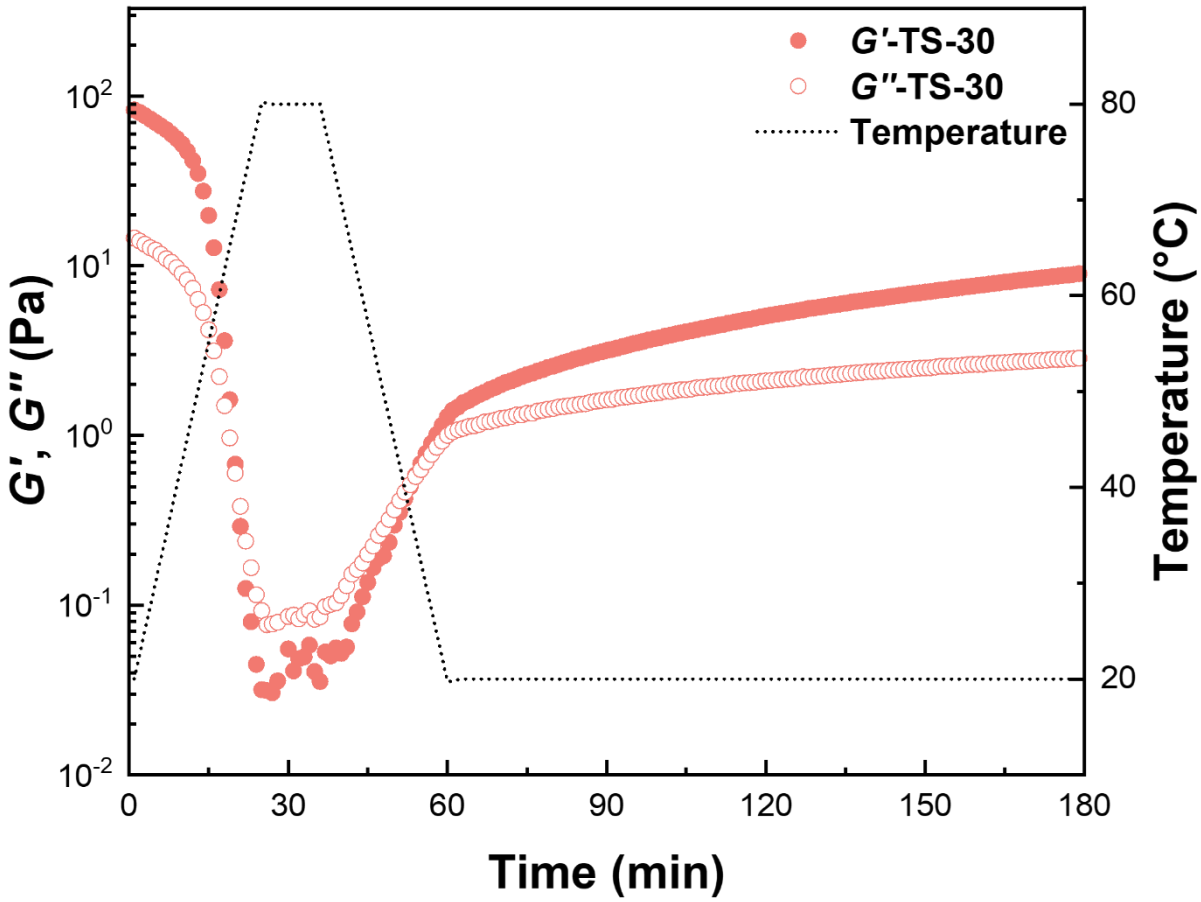

Fig. S4.2 Thermo-reversible rheological response TS-30 FPI dispersion at pH 2 (10%, w/w) as a function of time.

MASSEY UNIVERSITY
TE KUNENGA KI PŪREHUROA
UNIVERSITY OF NEW ZEALAND

GRADUATE RESEARCH SCHOOL

STATEMENT OF CONTRIBUTION
DOCTORATE WITH PUBLICATIONS/MANUSCRIPTS

We, the student and the student's main supervisor, certify that all co-authors have consented to their work being included in the thesis and they have accepted the student's contribution as indicated below in the Statement of Originality.

Student name:	Yinxuan Hu
Name and title of main supervisor:	Professor Aiqian Ye
In which chapter is the manuscript/published work?	Chapter 5

Describe the contribution that the student and members of the supervisory team have made to the manuscript/published work:[1]

Yinxuan Hu: Methodology, Investigation, Data curation, Formal analysis, Writing-original draft.
Lirong Cheng: Conceptualization, Supervision, Investigation, Writing-review & editing.
Elliot Paul Gilbert: Investigation, Data curation, Formal analysis.
Sung Je Lee: Supervision, Writing-review & editing.
Zhi Yang: Conceptualization, Investigation, Methodology Supervision, Project administration, Writing-review & editing.

Please select one of the following three options:

(●) The manuscript/published work is published or in press

Please provide the full reference of the research output:

Hu, Y., Cheng, L., Gilbert, E. P., Lee, S. J., & Yang, Z. (2024). Impact of thermosonication at neutral pH on the structural characteristics of faba bean protein isolate dispersions and their physicochemical and techno-functional properties. Food Hydrocolloids, 154, 110140. https://doi.org/10.1016/j.foodhyd.2024.110140

( ) The manuscript is currently under review for publication

Please provide the name of the journal:

( ) It is intended that the manuscript will be published, but it has not yet been submitted to a journal

Student's signature:	Yinxuan Hu Digitally signed by Yinxuan Hu Date: 2025.01.21 20:03:39 +13'00'	Main supervisor's signature:	Aiqian Ye Digitally signed by Aiqian Ye DN: cn=Aiqian Ye, o=NZ, ou=Massey University, ou=Riddet Institute, email=A.M.YE@massey.ac.nz Reason: I am approving this document Date: 2025.01.22 10:05:40 +13'00'

This form should be placed at the beginning of each relevant thesis chapter.

[1] Refer to the Massey University Publishing and Authorship guidelines (OneMassey for staff, Stream for students) and/ or Contributor Roles Taxonomy (CRediT) guidelines for guidance.

Chapter 5 Impact of thermosonication at neutral pH on the structural characteristics of faba bean protein isolate dispersions and their physicochemical and techno-functional properties[4]

Abstract

The effect of thermosonication (TS) (90 °C, 10-30 min) on faba bean protein isolate (FPI) at pH 7 was investigated. The microstructural and techno-functional properties of TS-treated FPI were compared with native FPI or FPI treated with conventional prolonged heating (CH, up to 8 h) at 90 °C. TS treatment effectively converted FPI to amorphous aggregates containing predominant β-sheet secondary structures, as determined by Thioflavin T (ThT) fluorescence and circular dichroism (CD). According to sodium dodecyl sulfate-polyacrylamide gel electrophoresis (SDS-PAGE), these amorphous aggregates could be formed by disulfide bonds. Additionally, TS treatment is efficient in disrupting large protein aggregates of FPI, thus improving their solubility. Both TS and CH treatments induced formation of viscoelastic FPI hydrogels, and whose gel strength depends on the type and time of treatment. Hydrogels formation is likely to arise from the entanglement and interaction of protein aggregates as revealed by small angle neutron scattering (SANS) and scanning electron microscopy (SEM). TS-treated FPI was also used to prepare O/W emulsions and whose structural and physical properties were compared with those stabilised by untreated FPI. At all oil volume fractions (ϕ=0.2, 0.5, and 0.7) and FPI concentrations (1, 3, and 5 wt %), emulsions stabilised by TS-treated FPI exhibited smaller oil droplet size, greater mechanical strength and superior stability compared to those stabilised by untreated FPI. The study suggests that TS treatment is promising in improving techno-functional properties of FPI; further studies are needed to exploit TS-treated plant proteins as a novel food ingredient in food product development.

Keywords: Thermosonication; Faba bean protein isolates; Viscoelasticity; O/W emulsions; Microstructure

[4] This chapter has been published as Hu, Y., Cheng, L., Gilbert, E. P., Lee, S. J., & Yang, Z. (2024). Impact of thermosonication at neutral pH on the structural characteristics of faba bean protein isolate dispersions and their physicochemical and techno-functional properties. *Food Hydrocolloids*, *154*, 110140.

Graphic abstract

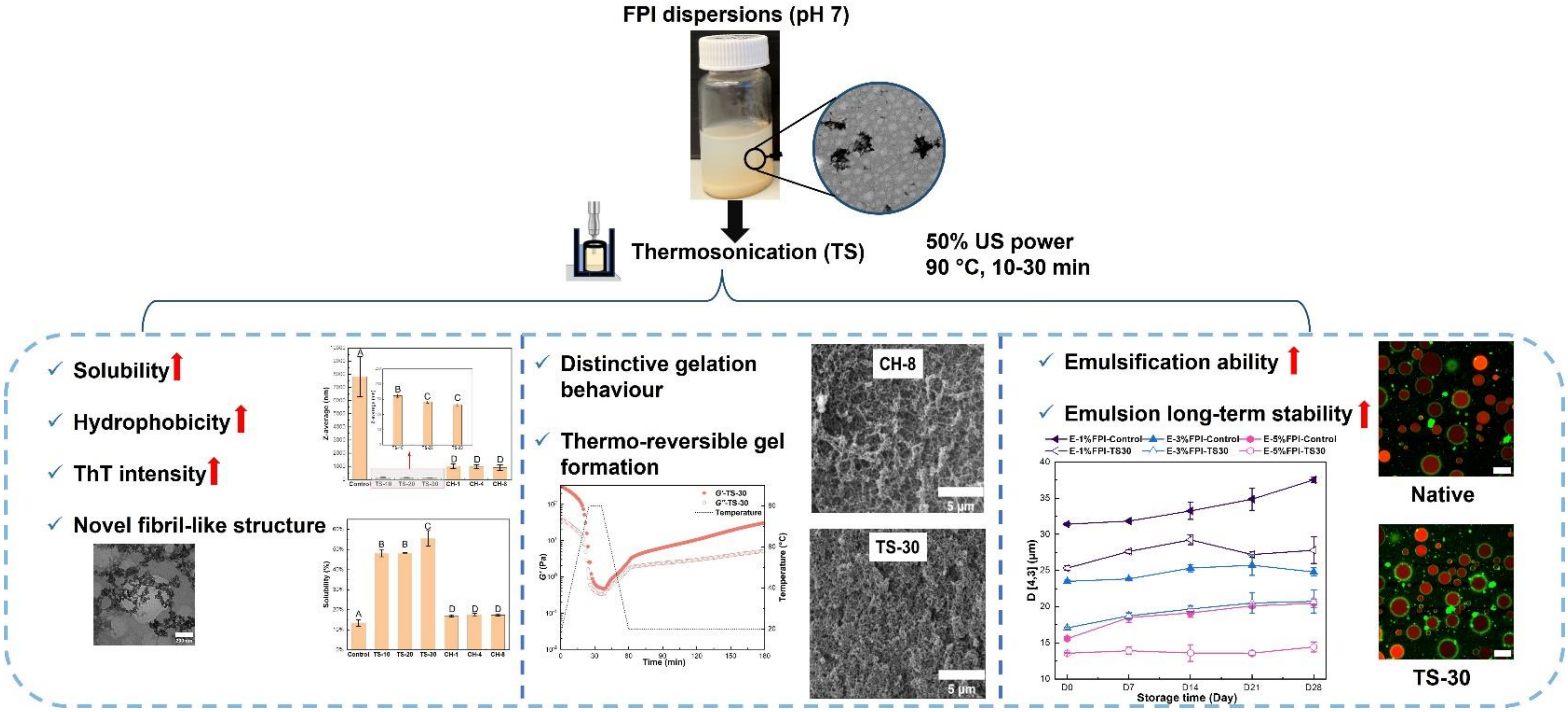

5.1 Introduction

Owing to its high protein content (27-36 w/w%), low allergenicity and high nutritive value, faba bean (*Vicia faba*) is one of the most popular plant foods (Augustin & Cole, 2022). It has recently attracted attention as a sustainable plant protein in the food industry (Augustin & Cole, 2022; Samaei, et al., 2020). However, like other plant protein ingredients, faba bean protein isolate (FPI) generally exhibits poor techno-functional characteristics, such as low solubility and unfavourable emulsifying capability in comparison with animal proteins (Schwenke, 2001; Tamang, et al., 2021). Therefore, various modification strategies including physical methods (e.g. ultrasonication (McCarthy, et al., 2016), heat treatment (Yang, de Campo, et al., 2022), and high hydrostatic pressure (Luo, Yang, et al., 2022), chemical methods (e.g. pH shifting (Jiang, et al., 2018), and biochemical methods (e.g. enzymatic hydrolysis) (Wang, Cheng, et al., 2022) have been recently applied to enhance the properties of plant protein ingredients. Compared to chemical and biochemical methods, physical processing exhibits unique advantages such as the ease of operation and avoidance of the use of chemicals.

Conventional heat treatment (CH) has been extensively employed for protein modifications. Typically, the plant protein dispersions are heated above their denaturation temperature (e.g. 75-95 °C) at different pHs and/or times to allow extensive protein unfolding, denaturation, and aggregation, resulting in alterations in their techno-functional characteristics such as gelation and emulsification capabilities (Du, et al., 2023; Zhu, et al., 2023). For example, Jo, et al. (2020) reported that the prolonged heat treatment (90 °C, up to 16 h) could significantly improve the gelation properties and alter the microstructural characteristics of lentil proteins. However, prolonged heating is not feasible nor sustainable for applications in food industry. CH treatment has been also used to inactivate bacteria in faba bean proteins, improve its nutritional value and sensory properties, making it safer and more acceptable for consumers (Hu, et al., 2023; Karolkowski, et al., 2022).

Ultrasonication (US) is another popular physical processing methods that has been employed to modify physicochemical and techno-functional properties of plant protein ingredients such as FPI (Martínez-Velasco, et al., 2018) and quinoa protein isolates

(QPI) (Luo, Yang, et al., 2022). During the US treatment, high shear forces and cavitation can induce microbubbles formed in the liquid to collapse, releasing high energy locally to breakdown large protein aggregates and improve their solubility (Taha, et al., 2018; Zhang, Luo, et al., 2021). However, US treatment alone is insufficient in alteration of plant protein structures for enhanced techno-functional properties (Zhong & Xiong, 2020); US has therefore been recently combined with other treatments including heat treatment (Zhong & Xiong, 2020) and pH-shifting (Yildiz, et al., 2017) to achieve more efficient modification of plant proteins.

Thermosonication (TS) that combines sonication and heat treatment has been demonstrated as an effective method to modify protein conformation through the combined effects of thermal energy input and ultrasound induced cavitation (Chen, Ettelaie, et al., 2019; Zhong & Xiong, 2020). Recently, Zhong and Xiong (2020) applied TS to 10 wt % mung bean protein isolates (MPI) at pH 7 at 30-70 °C for different times (5-30 min) and found that TS considerably enhanced the solubility and heat stability of MPI dispersions accompanied by alteration of protein secondary structures and conformations. In another study, Chen, Ettelaie, et al. (2019) found that TS treatment (72 °C, 10 min) could improve the efficiency of Alcalase hydrolysis of peanut protein isolates due to the generation of fibril like protein aggregates with a high aspect ratio. Furthermore, TS has been applied as a sufficient method to inactivate microorganisms in beverages to prolong their shelf-life without damaging bioactive substances or nutrients (Guimarães, et al., 2018; Monteiro, et al., 2018).

Despite TS treatment has been employed to modify plant protein dispersions, most of previous studies focused on the simple physicochemical properties such as particle size and solubility. There is scant information on protein secondary and tertiary structures, morphology, and techno-functional characteristics as affected by the TS treatment, which are imperative to elucidate process-structure-function relationship of FPI dispersions under different processing conditions. In addition, detailed comparisons of the TS treatment with conventional heating in modifications of FPI dispersions have not been conducted yet. Therefore, the present study aimed to systematically examine and compare the effect of TS and conventional heating treatment with different time (10-30 min) on protein profiles, secondary and tertiary structures, microstructural

characteristics, and techno-functional properties (e.g. gelation and emulsification property) of FPI dispersions. In particular, small angle neutron scattering (SANS) was employed to reveal hierarchical structures of FPI as affected by various processing conditions in dispersion and gel states covering multiple length scales in order to gain better understanding of different nanostructure formations induced by various processing methods. This study could provide important insights on applying TS treatment to modify FPI dispersions that targets their specific requirements as texturing and emulsifying agent.

5.2 Materials and methods

5.2.1 Materials

The FPI used was acquired from NZ Protein Inc. (Auckland, New Zealand) and as stated in ingredient specifications, contains 85 wt % protein, 5.4 wt % fat, and 1 wt % carbohydrate and dietary fibre. Chemicals used in this study, such as sodium dodecyl sulphate (SDS), Fast Green, Nile Red, acetic acid, thioflavin T (ThT), low viscosity mineral oil (M5904), HCl, and sodium azide, were of analytical grade and purchased from Sigma-Aldrich (St. Louis, MO, USA). Coomassie Brilliant Blue R-250 staining solution, β-mercaptoethanol, and 10×Tris/Glycine/SDS running buffer were purchased from Bio-Rad (Hercules, CA, USA). All samples were prepared using Milli-Q water (Millipore, USA).

5.2.2 Preparation of FPI dispersions

For preparation of 10 wt% FPI stock solution, FPI powder was dispersed in 0.02 wt% sodium azide solution at 20 °C using magnetic stirring (300 rpm) for 24 h for full hydration. For pH adjustment to pH 7, aliquots of 1 M HCl was pipetted to the stock solution under stirring for 24 h, while the pH value was regularly monitored until stable. FPI dispersions at 2.5, 3, and 5 wt % were made by mixing the 10 wt% FPI solution (10 wt %) with 0.02 wt% sodium azide (pH 7) solution.

5.2.3 Thermosonication of FPI dispersions

FPI dispersions (10 g each, 2.5, 3, 5, and 10 wt %, pH 7) prepared as described in **Section 5.2.2** were thermosonicated for 10 min (TS-10), 20 min (TS-20), and 30 min (TS-30) (50% power amplitude, pulse durations of on-time 30 s and off-time 30 s) by a

20 kHz ultrasonicator (6 mm horn) with a dial power 950 W (JY92-IIN, Ningbo Scientz Biotechnology Co., ltd, China) in a 20 mL glass vials at 90 °C in a jacket bottle (100 mL, Shanghai Leigu Instrument Ltd, China) connected with a temperature-controlled water bath (Thermofisher, USA). To compensate for water evaporation during the TS treatment, samples were supplemented with Milli-Q water (pH 7) to the original weight. All samples were prepared in duplicate and kept at 20 °C for 24 h before characterisation. Conventional heat treatment was conducted according to Wynnychuk, et al. (2021) with slight modifications. FPI dispersions were heated at 90 °C for 1 h (CH-1), 4 h (CH-4), and 8 h (CH-8) in an air oven (Thermofisher, USA). The control samples in this study were defined as the FPI dispersions without any treatment.

5.2.4 Physico-chemical characterisations of FPI dispersions

5.2.4.1 Sodium dodecyl sulphate–polyacrylamide gel electrophoresis (SDS-PAGE)

Reducing and non-reducing SDS-PAGE was performed according to Laemmli (1970) and our previous study (Hu, et al., 2023).

5.2.4.2 Determination of FPI particle size

A ZetaSizer Nano ZS (Malvern instruments, UK) was utilised to measure particle size of control and treated FPI dispersions (2.5 wt %) at 20 °C. The laser scattering angle is 173° and wavelength is 633 nm. The FPI dispersion was diluted one hundred times in Milli-Q water before measurements, using the refractive index and viscosity of dispersant (water) of 1.33 and 0.89 mPa s, respectively (Luo, Yang, et al., 2022). Triplicate measurements were performed for each sample and results are represented as z-average size.

5.2.4.3 Determination of FPI solubility

The solubility of FPI at 2.5 wt % after various treatments was determined following the method of Hu, et al. (2023) with small modifications. A centrifuge (Thermofisher 3000, MO, USA) was used to centrifuge the FPI dispersions at 3000 × g for 15 min at ~20 °C and supernatant was collected. After that, soluble protein content was quantified from the supernatant using the Bradford Protein Assay Kit (Sigma-Aldrich, St. Louis, MO, USA) by determining the protein absorbance at 595 nm by a UV-Vis spectrophotometer

(Shimadzu 3000, Kyoto, Japan). The solubility (%) was calculated according to the equation (5.1).

$$\text{Solubility (\%)} = \frac{\text{Protein content in the supernatant (mg/mL)}}{\text{Total protein content before centrifuge (mg/mL)}} \times 100\% \quad (5.1)$$

5.2.4.4 Thioflavin T (ThT) fluorescence spectroscopy

Thioflavin T (ThT) fluorescence assays were conducted to detect secondary structural changes in FPI dispersions using a fluorescence spectrophotometer (RF-6000, Shimadzu, Kyoto, Japan) with an excitation wavelength λex of 440 nm and an emission wavelength λem of 460-560 nm (Herneke, et al., 2021). Specifically, ThT solution (2 mM) was passed through a syringe filter (0.22 μm, ThermoFisher Scientific, USA). The FPI dispersions were first diluted to 0.01 wt% using Milli-Q water (pH 7), followed by mixing with 2 μL ThT solution and kept in the dark for 10 min ~20 °C. The background solution was prepared by adding 2 μL ThT to 2 mL Milli-Q water (pH 7).

5.2.4.5 Negative staining transmission electron microscopy (TEM)

The microstructures of various treated FPI were observed by negative staining TEM according to Cheng, Ye, et al. (2022). The FPI dispersions (2.5 wt %) were diluted 50 times with Milli-Q water (pH 7). Afterwards, the diluted sample solution (20 μL) was transferred onto a formvar-coated copper TEM grid and stained with uranyl acetate (2%) for 3 min. Excess stain was subsequently rinsed with 20 μL Milli-Q water for 3 min. Finally, a filter paper was used to drain excess liquid from the copper grid. Micrographs were acquired by an electron microscope (NL-5600 MD, Philips, Eindhoven, The Netherlands) at an acceleration voltage of 60 kV.

5.2.4.6 Circular dichroism (CD) spectroscopy

Secondary structure of various untreated and treated FPI dispersions were probed by a Chirascan CD spectrometer (Applied Photophysics, UK) according to Dave, et al. (2013). The FPI dispersions were diluted with Milli-Q water (pH 7) to 0.5 wt%. For a far ultraviolet (FUV) CD study, samples (~80 μL) were loaded to a quartz cell (a path length of 0.1 mm) (Hellma, Germany). FUV CD spectra were collected at 1 nm intervals for 0.5 s per point in a wavelength range of 180 nm to 260 nm at ~20 °C. The values of

the FUV spectra were averaged from 10 measurements. The near-UV spectrum (NUV, wavelength 250–350 nm) were recorded at ~20 °C after transferring ~2 mL samples into a 10 mm Quartz Suprasil cell (#100-QX, Hellma, Germany) for a total scan time of 40 s.

5.2.4.7 Determination of surface hydrophobicity

The surface hydrophobicity (H_0) of various FPI samples (2.5 wt %) was measured by fluorescence spectrophotometry using 8-anilino-1-naphthalene sulphonate (ANS) as a fluorescence probe Luo, Cheng, et al. (2022). FPI dispersions (2.5 wt %) were diluted separately to concentrations of 62.5, 125, 250, and 500 μg/mL using 10 mM Tris-HCl buffer (pH 7). ANS solution (8.0 mM, 50 μL) was then added to each FPI solution (3 mL) and kept in the dark for 20 min at ~20 °C. A Shimadzu RF-6000 fluorescence spectrometer (Shimadzu, Kyoto, Japan) was employed to determine the fluorescence at 470 nm (emission) and 390 nm (excitation) with a 5 nm slit length. Fluorescence intensities after subtracting background (FPI samples without ANS) were plotted against FPI concentrations, and H0 was represented as an original slope determined from linear regression analysis (Kato & Nakai, 1980).

5.2.4.8 Small-angle neutron scattering (SANS)

The QUOKKA instrument at ANSTO in Sydney, Australia, with a Q-range of 0.003-0.4 Å−1 was used for the SANS experiments (scattering wave vector $Q = (4\pi/\lambda)\sin(\theta)$, and λ is the neutron wavelength (Å) and 2θ is the scattering angle)(Gilbert, et al., 2006; Wood, et al., 2018; Yang, de Campo, et al., 2022). Samples were prepared according to the same procedures as depicted in **Sections 5.2.2** and **5.2.3**. Liquid samples were pipetted into demountable SANS samples cells (thickness: 1 mm). Gel samples thermally melted in an oven at 90 °C for 30 min, then transferred to SANS sample cells and incubated at ~20 °C for at least 5 h prior to SANS measurements to allow for gel network formation. Liquid samples (such as the 2.5 wt % and 10 wt % control samples and the CH-1 sample were transferred into quartz cuvettes (path length: 1 mm) and placed into a tumbler to avoid sample sedimentation, such as the 2.5 wt % and 10 wt % control samples and the CH-1 sample. SANS measurement of each sample lasts for approximately 3 h at 20 °C. SANS data were reduced using procedures developed in ANSTO (Kline, 2006) with algorithms embedded in commercial Igor Pro software

(Wavemetrics, USA).

SANS data analysis

The correlation length model (Hammouda, et al., 2004) was used to fit the SANS scattering profiles (equation 5.2):

$$I(Q) = \frac{A}{Q^n} + \frac{C}{1 + (Q\xi)^m} \quad (5.2)$$

Where n is the power law exponent of the power law scattering in the low Q region originating from protein aggregates. The ξ is the correlation length (particle size) of protein particles and m is the power law exponent of the power law scattering in the high Q region. A and C are scale constants for the first and second term, respectively. The SasView software (version 5.0.5, http://www.sasview.org/) was used for the modelling implementation.

5.2.5 Characterisation of FPI gels

5.2.5.1 Flowability of FPI gels

The flowability of FPI gels was examined by inverting glass bottles containing differently treated FPI dispersions (10 wt %) after storage at ~20 °C for 24 h. Afterwards, photos were taken to observe the flowability of the gels.

5.2.5.2 Determination of rheological properties of FPI gels

Rheological characteristics of various FPI gels were assessed by a Paar Physica rheometer (Anton Paar, MCR 301, Austria). A plate-plate geometry (diameter: 40 mm) with a gap of 1 mm was used throughout the test. The FPI gels were loaded onto the bottom plate of the rheometer using a plastic spatula and carefully trimmed around the edge of the sample if necessary. To avoid evaporation, samples were covered with mineral oil. The rheological tests were performed in accordance with the following protocol. First, to structurally recover the FPI gel after loading, a time lapse measurement at strain 1% and frequency 1 Hz was conducted over 120 min. A frequency sweep test (frequency: 0.01-100 Hz) was then performed at 1% strain to investigate the viscoelasticity of the gel network. Finally, as strain sweep test was conducted with the strain amplitude varying from 0.01 to 1000 % at a constant

frequency of 1 Hz. Storage modulus (G') and loss modulus (G'') were determined throughout the test at 20 ° C (Hu, et al., 2023). The thermoreversibility of TS-30 gel was assessed by recording G′ and G″ at a fixed frequency 1 Hz and strain 1% during a temperature sweep test, in which the temperature was ramped from 20 °C to 80 °C at 2 °C/min and then hold at 80 °C for 10 min before being decreased from 80 °C to 20 °C at the same rate.

5.2.5.3 Viscosity measurements

Viscosity was determined following the same protocol as depicted in **Section 5.2.5.2**. Viscosity measurements were performed by applying a shear rate sweep from 0.1 to 1000 s^{-1} and a reverse sweep from 1000 to 0.1 s^{-1}. The degree of protein aggregation was measured by the area (S) of the hysteresis defined by the shear rate incline and decline curves, which was calculated with Origin Pro software (v. 2020, Origin Lab, MA, USA) (Luo, et al., 2021). Duplicate measurements were made for each sample at 20 °C.

5.2.5.4 Scanning electron microscopy (SEM) observations of FPI gels

SEM sample preparation and imaging were performed according to Goeden-Wood, et al. (2003) with slight modifications. FPI gels were cut into small pieces using a spatula and fixed overnight (~4 °C) in 0.1 M sodium cacodylate phosphate buffer containing 2.5% glutaraldehyde. After fixation, the gels were rinsed three times with 0.1 M sodium cacodylate phosphate buffer. Subsequently, the gels were dehydrated in aqueous ethanol solutions with increased ethanol concentrations (30, 50, 70, 80, 90, and 100% ethanol, v/v). Finally, the dried FPI gels obtained from lyophilisation were cut to ~1 mm × 1 mm in size. The gel samples were coated with gold for 240 s at 12 mA at ~20 °C. SEM images were acquired at 5 kV using a scanning electron microscope (Philips XL 30S FEG, Eindhoven, The Netherlands).

5.2.6 Formation and characterisation of FPI stabilised emulsions

5.2.6.1 Interfacial tension measurements

A Theta Flex Plus optical tensiometer (Biolin Scientific Instruments, Sweden) built on the pendant drop principle was used to monitor interfacial tension at O/W interface up to 6000 s (Hu, et al., 2023). A drop of selected FPI samples after treatments (25 μL)

was formed at the tip of a stainless-steel syringe needle and immersed in soybean oil. The data was processed using One Attention software (Biolin Scientific Instruments, Sweden).

5.2.6.2 Preparation of emulsions

FPI-stabilised emulsions were made by homogenising different concentrations of control and TS-30 FPI solutions (1, 3, and 5 wt %) with soybean oil at various oil-phase volume fractions (ϕ=0.2-0.7, v/v). An Ultra-Turrax rotor stator mixer (T10 basic, IKA Corp., Staufen, Germany) equipped with a 10 mm probe (S10N-10 G, IKA, Germany) was used to homogenise the oil-water mixture at 20,000 rpm for 2 min. Emulsions prepared from FPI dispersions without any treatment were used as controls.

5.2.6.3 Determination of oil droplet sizes

A Mastersizer instrument (Malvern Instruments Ltd, Worcestershire, UK) was employed to determine the average particle size distribution (PSD) of oil droplets as described by Hu, et al. (2023). The refractive indices used for soybean oil and dispersant (Milli-Q water) were 1.47 and 1.33, respectively (da Silva, et al., 2021). Sauter mean diameter (D [3,2]) was used to indicate the mean size of oil droplets (in diameter), and changes in droplet size were also monitored over 28 days at 20 °C.

5.2.6.4 Rheological measurements of emulsions

Rheological tests were conducted following the same methodology as depicted in **Section 5.2.5.2**. Data were collected at 20 °C, and G' and G'' were recorded throughout a frequency sweep (ranging from 0.01 to 100 Hz at 1% strain) and strain sweep test (ranging from 0.1 to 1000% at 1 Hz frequency). Viscosity determinations were also conducted at a shear rate increased from 0.1 to 1000 s^{-1} and then declined from 1000 to 0.1 s^{-1} at 20 °C.

5.2.6.5 Microstructures of emulsions

The emulsions were imaged by a light microscope (BX53, Olympus, Japan) equipped with a ×40 objective lens. After gently inverting the emulsion samples 3–5 times, the emulsions were transferred on a microscope slide and covered. Observations were performed in triplicate, and representative images are shown. To visualise the interfacial

structures at the oil-water interface, confocal laser scanning microscopy (CLSM) was applied to selected samples. Fast Green (1% w/v, ratio to emulsion 1:500 (v/v)) and Nile Red (ratio to emulsion 1:5000 (v/w)) was utilised to stain protein and oil phases of emulsions, respectively (Hu, et al., 2023). Afterwards, aliquots of the emulsion samples were loaded on a glass slide with a cavity. The edges of slides were then carefully enclosed with nail polish to minimise water evaporation. A confocal laser scanning microscope (Leica DM 6000B, Germany) equipped with an oil immersed 100× objective lens was utilised to observe emulsions at laser wavelengths of 633 nm (Fast green) and 561 nm (Nile red). Optical light and CSLM micrographs were analysed by using Image J software (NIH, MD, USA).

5.2.6.6 Creaming index

Emulsion stability was assessed visually according to Wynnychuk, et al. (2021), including observation of the occurrence of phase separation or coalescence in emulsions. The creaming index was calculated from Equation (5.3).

$$Creaming\ index = \left(\frac{H_s}{H_0}\right) \times 100\% \tag{5.3}$$

where H_s is the height of serum measured, and H_0 is the height of the emulsion. Therefore, a smaller creaming index indicates emulsions with a higher creaming stability.

5.2.7 Statistical analysis

At least duplicate measurements for conducted for each characterisation, and the results are shown as average with standard deviation (SD). The statistical analysis was conducted using Minitab statistical software (version 19, USA), and a one-way analysis of variance (ANOVA) was employed to assess mean differences with a significance level of $P < 0.05$ according to Tukey's test.

5.3 Results and discussion

5.3.1 FPI protein profiles by SDS-PAGE

SDS-PAGE was performed to reveal modifications in FPI protein profiles as affected by TS or CH treatments (**Fig. 5.1)**. In non-reducing SDS-PAGE (**Fig. 5.1**), a profound and smeared protein band were identified in the loading wells for all the samples,

suggesting the existence of large protein complexes with molecular mases greater than 250 kDa (Kaspchak, et al., 2017). Additionally, the native FPI (control) exhibits a complicated protein profile consisting of two dominant protein bands locating at ~70 kDa and ~50 kDa, which are assigned as convicilin and vicilin, respectively (Vogelsang-O'Dwyer, et al., 2020). Some small proteins at ~37 kDa and ~20 kDa are assigned to α-legumin and *β*-legumin, respectively (Langton, et al., 2020). This protein profile of native FPI is consistent with previous studies (Hu, et al., 2023; Nivala, et al., 2017; Vogelsang-O'Dwyer, et al., 2020).

Application of TS or CH treatment significantly reduced the densities of protein bands (40-70 kDa, 30-37 kDa, and 15-20 kDa) compared to untreated FPI. (**Fig. 5.1A**). Similar results were found in heat-treated FPI (70 °C, 30 min) at pH 7 (Alavi, Chen, Wang, et al., 2021) and TS-treated mung bean protein (70 °C, 30 min) at pH 7 (Zhong & Xiong, 2020). Moreover, with increasing treatment time in either CH or TS treatment, the fading of protein bands in particular at 40-70 kDa became more significant, indicating that more severe treatment at longer times induces more extensive intermolecular bond formation (Luo, et al., 2021; Zhong & Xiong, 2020). For example, it can be observed that the CH-8 sample (conventional heating for 8 h) exhibited the lowest density for all protein bands. Previous studies suggested that the effect of CH and TS processing on the degree of protein aggregation is highly dependent on the treatment temperature and time (Speroni, et al., 2009).

Under reducing conditions, the large protein aggregates observed in the loading wells disappeared (**Fig. 5.1B**), indicating that they were mainly stabilised by disulfide bond. In addition, all FPI dispersions show similar protein profiles, which is consistent with a previous TS study on mung bean proteins (Zhong & Xiong, 2020). Additionally, for all samples, densities of protein bands at ~37 kDa (α-legumin) and ~20 kDa (β-legumin) became much denser under reducing conditions, suggesting that these two legume subunits were associated via disulfide bonds (Hu, et al., 2023). In CH-8 FPI sample, a decrease in densities of all protein bands (< 150 kDa) was seen, which could be due to production of protein aggregates with a low solubility (Luo, Yang, et al., 2022).

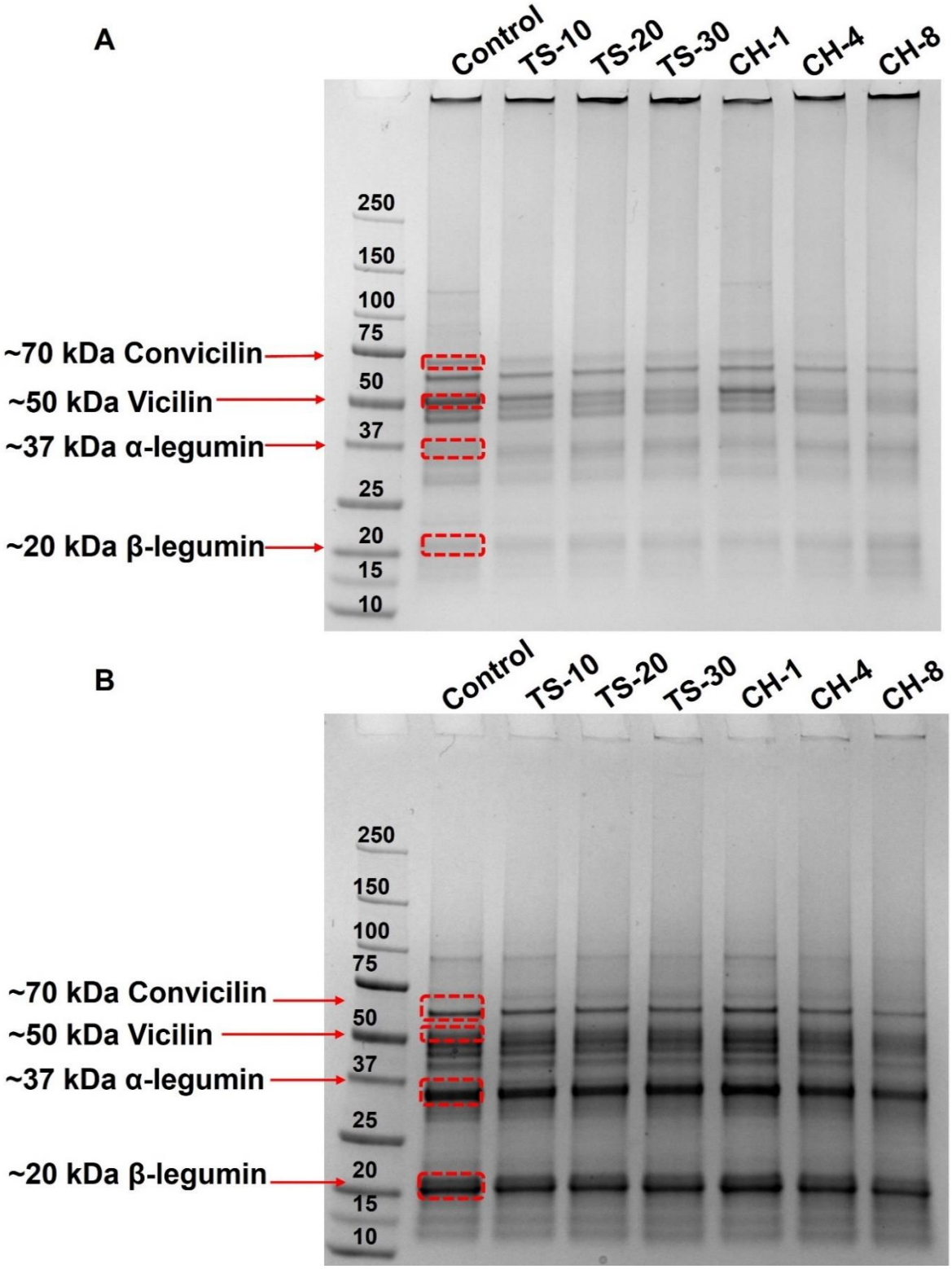

Fig. 5.1 SDS-PAGE patterns of faba bean protein isolates (FPI) dispersions at pH 7 before and after thermosonication (TS) (10, 20, and 30 min) or conventional heat treatment (CH) (90 ºC, 1 h, 4 h, and 8 h) under non-reducing (A) and reducing (B) conditions.

5.3.2 Effect of CH and TS treatments on physicochemical peroperties of FPI dispersions

5.3.2.1 Visual appearance

The appearance of the FPI dispersions (2.5 wt %) and gels (10 wt %) after TS and CH is shown in **Fig. 5.2A**. For 2.5 wt % FPI, the control and CH-treated samples showed significant turbidity, and protein sedimentation was observed at the bottom of glass vials, as indicated by the red arrow (**Fig. 5.2A**). This could be due to the low solubility of FPI and protein aggregation after CH (Alavi, Chen, & Emam-Djomeh, 2021; Alavi, Chen, Wang, et al., 2021). After TS treatment (10-30 min), the FPI dispersions became translucent. Furthermore, at a high protein concentration (10wt%), all TS and CS treatments induced formation of self-supporting gels (**Fig. 5.2A**). The rheological and microstructural properties of FPI gels induced by different treatments were further investigated in **Section 5.3.6**.

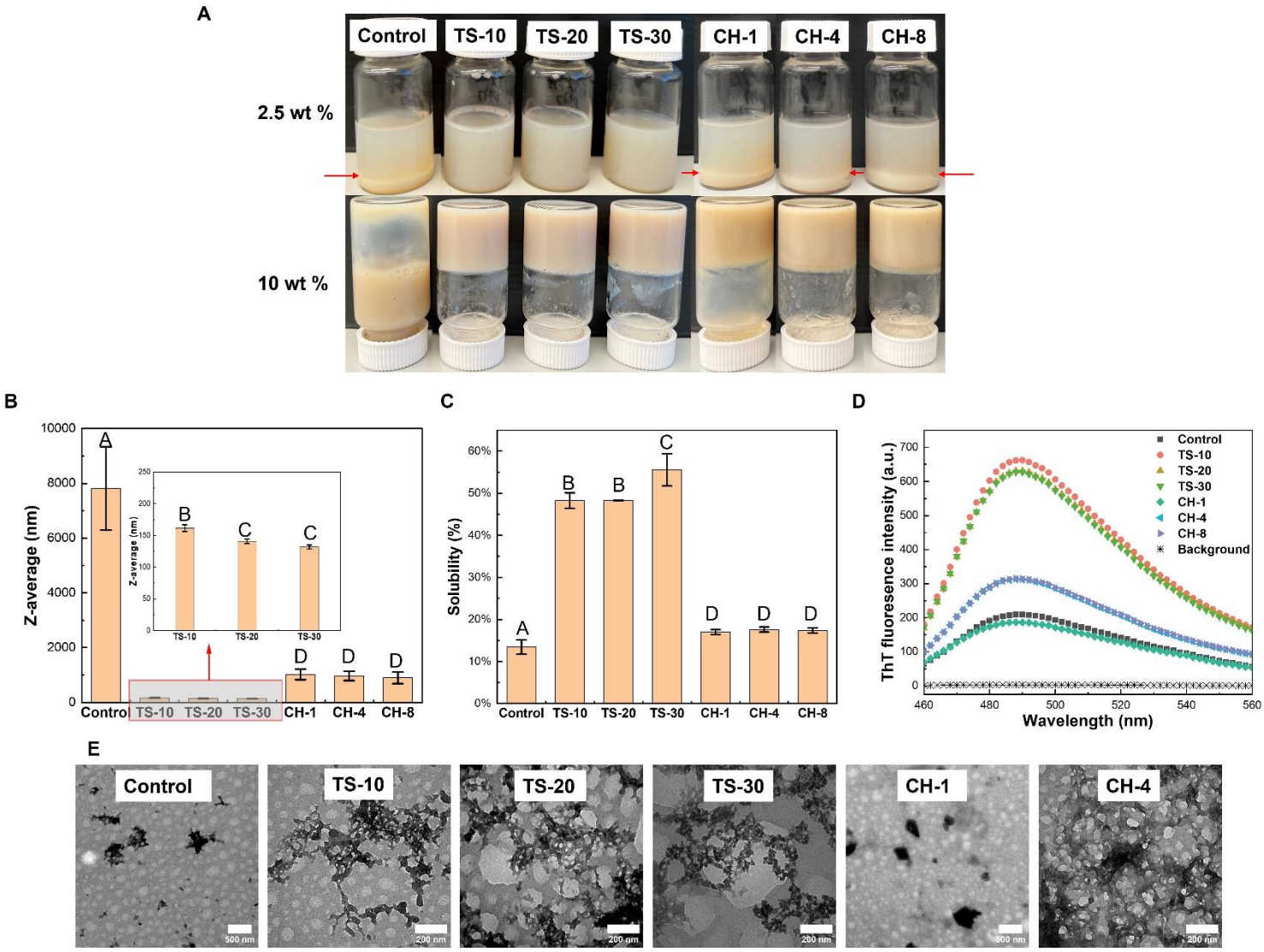

Fig. 5.2 (A) Visual appearance of 2.5 wt% and 10 wt% faba bean protein isolate (FPI) samples before and after thermosonication (TS) or conventional heat treatment (CH) for different times at pH 7. (B) Particle size (z-average) of control and TS- or CH-treated FPI dispersions at pH 7. (C) Solubility of control and TS- or CH-treated FPI dispersions at pH 7. (D) ThT fluorescence spectra of various FPI samples before and after TS (10, 20, and 30 min) or CH treatments (1, 4, and 8 h) at pH 7. (E) TEM images of FPI dispersions before and after TS (10, 20, and 30 min) and CH (1 and 4 h) at pH 7. Different letters above the columns indicate significant differences ($P < 0.05$).

5.3.2.2 Particles sizes and solubilities of FPI affected by TS and CH

The particle size and solubility of control, CH- and TS- treated FPI dispersions (2.5 wt %) at pH 7 are demonstrated in **Fig. 5.2B and C**. The control sample exhibits the largest particle size (~7800 nm) and the lowest solubility (~13.43%) among all samples. Previous studies showed that most native and untreated plant proteins have the largest particle size and lowest solubility, such as quinoa protein isolates (QPI) before sonication (Luo, Yang, et al., 2022) and soy protein isolate (SPI) before pH shifting (Fang, et al., 2021). This could be typically caused by protein aggregation during isoelectric point precipitation after alkaline extraction (Grossmann & McClements, 2023). TS treatment induced a significant reduction in particle size from ~7800 nm (Control) to ~140 nm (TS-30) at pH 7 (**Fig. 5.2B**). Previous studies suggested that some protein interactions, such as hydrophobic interactions and hydrogen bonds, may be destroyed by the combination of heating and sonication, resulting in smaller particle size and higher solubility (Frydenberg, et al., 2016; Zhu, et al., 2023). This was further confirmed with the solubility results showing that FPI solubility remarkably increased from ~12% (control) to ~55% (TS-30) (**Fig. 5.2C**). The improvement in FPI solubility could be associated with creation of hydrogen bonds between water and protein after TS, which improved protein solubilisation by replacing the intramolecular hydrogen bonds in protein molecules (Jiang, et al., 2017). Zhong and Xiong (2020) also reported that TS significantly improved the solubility of mung bean protein dispersions at different temperatures (e.g. 30, 50, and 70 °C) for 5-30 min and the solubility improved with an increase in treatment temperature and time.

Compared to untreated FPI (Control), CH-treated samples had reduced particle size (from ~7800 to ~1000 nm) which did not change significantly with increased CH time (**Fig. 5.2B**). Similar results were reported for heated SPI (O′ Flynn, et al., 2021) and egg white proteins (Sponton, et al., 2017), which could be due to partial protein dissociation at high temperature. In addition, compared to the native sample, the solubility of the CH-treated FPI samples increased slightly to ~17% (**Fig. 5.2C**). A similar observation has been made previously for SPI after heat treatment (90 °C, 20 min). This could be attributed to a decreased protein particle size and alterations of various non-covalent and covalent interactions under heat treatment, thereby affecting

protein conformations and their hydration capabilities (O′ Flynn, et al., 2021; Zhao, et al., 2020).

5.3.2.3 Thioflavin T (ThT) fluorescence assay

To identify the formation of FPI aggregates after various treatments, thioflavin-T (ThT) fluorescence experiments were conducted. ThT can specifically attach to the β-sheet surface, giving rise to higher fluorescence intensity (Biancalana & Koide, 2010; Stathopulos, et al., 2004). In **Fig. 5.2D**, compared to the background, all TS-treated FPI samples show a significant increase in ThT fluorescence with a peak intensity at ~480 nm, which suggests that protein aggregates containing β-sheet were formed after TS. Similar findings were reported by Chen, Ettelaie, et al. (2019), who also identified that the ThT intensity of peanut protein was significantly enhanced after a TS treatment (72 °C, 500 s) at pH 7. In addition, **Fig. 5.2D** shows a slight increase in ThT fluorescent intensity in CH-4 and CH-8 samples compared to the untreated FPI (control), indicating an increase in β-sheet structure formation after prolonged heating. A comparable result has been reported in a previous FTIR study on lentil proteins after a 16 h heat treatment at 90 °C. It has been suggested that the prolonged heating could promote protein unfolding followed by formation of protein aggregates that are rich in β-sheet secondary structures (Jo, et al., 2020). However, the lowest ThT fluorescence intensity was found in the CH-1 sample. This could be related to protein aggregation, which reduces the surface area available for ThT binding (Hu, et al., 2023; Jo, et al., 2020; Josefsson, et al., 2019).

5.3.2.4 Morphology of FPI fibrillar aggregates as revealed by TEM

TEM images of untreated and treated FPI (TS or CH) samples are shown in **Fig. 5.2E**. The untreated (control) FPI showed submicron scale particle aggregates. In comparison, after 10 min of TS treatment, an interconnected protein network with clusters of loosely packed FPI aggregates can be observed, contributing to an increase in ThT fluorescence intensity shown in **Fig. 5.2D**. As the TS time increases to 20 and 30 min, more and denser interconnected protein aggregate network can be observed. CH treatment also induced significant structural changes of FPI. At shorter heating times (e.g., CH-1), large and dense protein aggregates can be observed, consistent with the low ThT fluorescence intensity (**Fig. 5.2D**). On the other hand, the formation of interconnected

FPI aggregates was observed after heating FPI for longer heating times (CH-4). Similar microstructures have been reported in lentil protein dispersions after a prolonged heating at pH 7 (Jo, et al., 2020). Combined with the findings of SDS-PAGE and ThT fluorescence, TS treatment and prolonged heating under neutral conditions (pH 7) causes FPI to denature and aggregate by disulfide bond formation and non-covalent interactions (**Fig. 5.1**) (Jiang, et al., 2017; Luo, Yang, et al., 2022). These protein aggregates could undergo further structural rearrangement to form fibril-like FPI aggregates through the formation of β-sheet structures, which play an important role in stabilising fibrillar like structures (Chen, Ettelaie, et al., 2019; Kong & Yu, 2007).

5.3.3 Changes in protein secondary structures probed by CD spectra

Fig. 5.3A demonstrates the far-UV CD spectra of FPI treated by TS or CH. The native FPI (Control) samples exhibited a molar ellipticity positive peak at ~195 nm, and another two negative minimums at ~206 nm and ~220 nm, respectively. These peaks indicate that the secondary structure of native FPI at pH 7 is dominated by random coils, α-helices, and β-sheets (Gülseren, et al., 2007), similar to a previous study (Nivala, et al., 2021). In **Fig. 5.3A,** the peak change for the CH-treated FPI samples was not significant, and the secondary structure of the CH-treated FPI samples showed native-like shapes with a slightly strengthened peak at ~206 nm and a weakened peak at ~220 nm. The slight increase in intensities ~220 nm could indicate an increase in β-sheet structure, which agrees well with the ThT results (**Fig. 5.2D**).

Conversely, in the far-UV CD spectra of TS-treated FPI (**Fig. 5.3A**), the negative peak of native FPI at ~206 nm was red shifted to ~218-220 nm with a remarkable increase in peak intensity, indicating an increased β-sheet secondary structures after the TS treatment (Greenfield, 2006; Kutzli, et al., 2023). This finding agrees well with the ThT fluorescence results. The dominated β-sheet secondary structures have been also observed in TS-treated peanut protein isolate (Chen, Ettelaie, et al., 2019) and mung bean protein (Zhong & Xiong, 2020). Compared to ultrasonication alone, the TS treatment with combination of heat and ultrasound could generate more intensive and steady acoustic cavitation field, leading to extensive protein denaturation and unfolding (Chen, Ettelaie, et al., 2019; Villamiel & de Jong, 2000). Under certain circumstances, the unfolded protein molecules structurally rearranged to produce secondary structures

(i.e. *β*-sheets) with a higher thermodynamic stability (Kong & Yu, 2007; Lefevre & Subirade, 2000).

To determine the tertiary structure changes after CH or TS treatment, the near-UV CD spectra of native FPI (control), TS- and CH-treated FPI were also recorded (**Fig. 5.3B**). In general, the near-UV CD spectra indicated the number of aromatic amino acids of proteins and associated mobility as well as their interactions (e.g. hydrophobic bonds) (Fasman, 2013). As demonstrated in **Fig. 5.3B**, native FPI had a significant positive dichroic peak at ~270 nm, indicating the presence of accumulated tyrosine residues (Yang, et al., 1986). For the CH-1 sample, the magnitude of the positive peak at ~270 nm decreased slightly, suggesting a little impact on tertiary structure of FPI; the slight decrease in dichroic intensity could be due to protein aggregation. This is consistent with ThT fluorescence results (**Fig. 5.2D**). However, the magnitude of this peak increased substantially after 30 min of TS, suggesting the formation of a more well-defined and stable tertiary structure (Tang, et al., 2012).

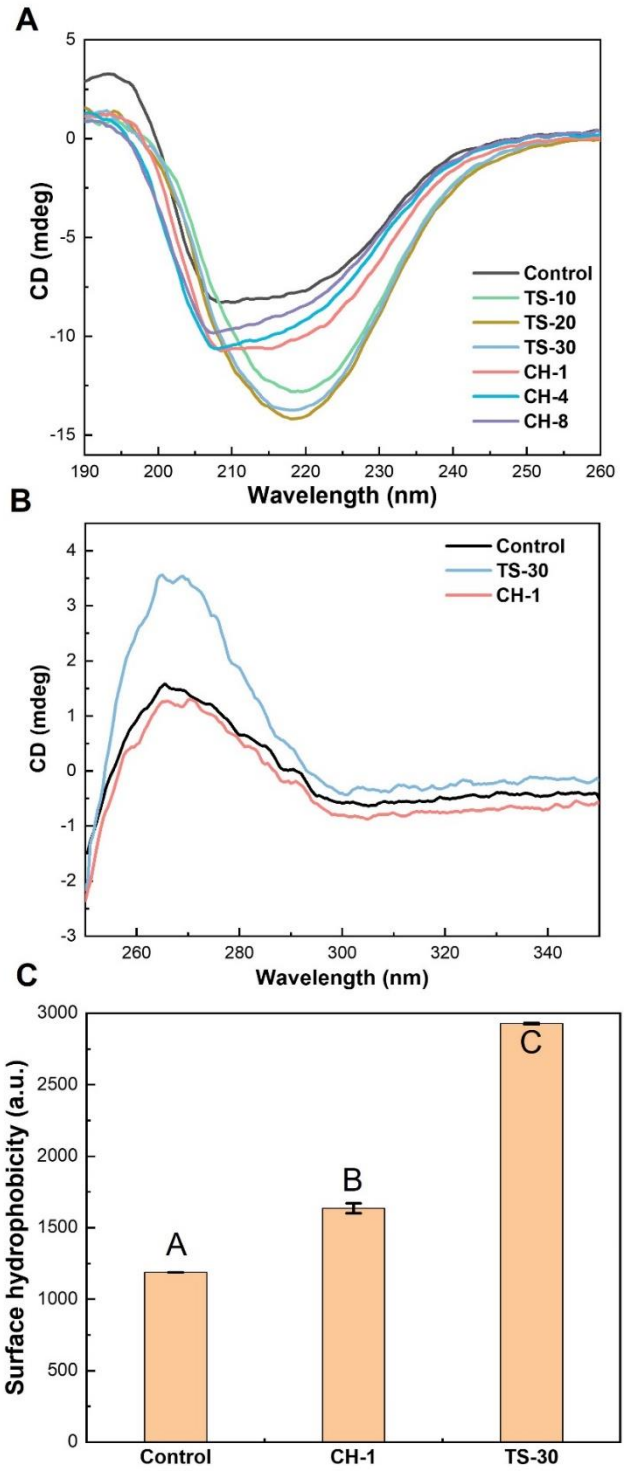

Fig. 5.3 (A) Far ultraviolet (UV) circular dichroism (CD) spectra of faba bean protein isolate (FPI) dispersions before and after thermosonication (TS) (10, 20, and 30 min) or conventional heat treatment (CH) (1-8 h) at pH 7; (B) Near-UV CD spectra of untreated and selected TS- (30 min) or CH- (1 h) treated FPI samples (TS-30 and CH-1). (C) Surface hydrophobicity of untreated and selected TS- or CH-treated FPI samples (TS-30 and CH-1).

5.3.4 Surface hydrophobicity

The surface hydrophobicity of untreated (Control), CH- and TS-treated FPI samples is shown in **Fig. 5.3C**. The surface hydrophobicity of FPI samples increased significantly after CH- or TS-treatment (from ~1187 to ~1635 after CH and ~2927 after TS). The largest increase in hydrophobicity was found in the TS-treated samples, which could be due to a significant exposure of interior hydrophobic groups caused by unfolding of protein molecules (Hernoux Villière, et al., 2013). Although there was a slight rise in surface hydrophobicity after CH treatment compared to untreated FPI, the surface hydrophobicity of CH samples was still significantly lower than TS samples (**Fig. 5.3C**), which could be attributed to the limited exposure of initially buried hydrophobic groups after heat treatment only (Voutsinas, et al., 1983; Zhao, et al., 2020). This observation was also in accordance with Guo, et al. (2015) and Wang, et al. (2014), who showed that the surface hydrophobicity of SPI slightly increased after heating at 90 °C for 30-60 min.

5.3.5 Small-angle neutron scattering (SANS) analysis

The nanostructure of various treated FPI dispersions and hydrogels were further investigated by SANS (**Fig. 5.4)**. In **Fig. 5.4A**, the scattering intensity I (Q) at low Q ($6\times10^{-4}< Q$ (Å^{-1}) $< 2\times10^{-2}$) of the TS-30 sample (2.5 wt% FPI) was greater compared to that of the native FPI (2.5 wt%), and the shape of the scattering pattern was also significantly changed after TS, indicating the microstructure of FPI was dramatically changed. The increase in the scattering intensity could be due to large nanoscale protein aggregates induced by the TS treatment. In addition, a greater scattering intensity was also observed in the higher concentration (10 wt% TS-30 and CH-1) FPI samples, which could be due to more considerable protein aggregation and gel network formation (Napieraj, et al., 2022). A correlation length model (**equation (5.2)**) was utilised to fit SANS profiles and fitting parameters are summarised in **Table 5.1**. Specifically, in the low Q region, all samples exhibited a Porod exponent (n) in a range of 2.3-2.6, which is a characteristic of mass fractal structures. The differences in the low-Q Porod exponent (n) suggest different large scale structural arrangement in FPI as affected by TS or CH treatment (Yang, et al., 2016). The Lorentz exponent, m of all the FPI samples is ~4.0, indicating a relative sharp interface between protein particles and solvent (Boukari, et al., 1997).

The largest structural difference among different FPI samples is the correlation length (ξ), representing structural inhomogeneities or nanoaggregates within protein aggregates or gel networks (Banc, et al., 2016). From **Table 5.1**, TS-30 treatment induced a substantial increase in the correlation length (ξ) compared to control and CH-1 samples. These structural inhomogeneities with a size of 120-144 Å may indicate the size of protein aggregates, confirming that the TS treatment is efficient to induce FPI protein unfolding and aggregation which agrees with the SDS-PAGE and TEM findings.

Table 5.1 SANS model fit structural parameters of faba bean protein isolate (FPI) dispersions (2.5 wt%) and gels (10 wt%) as affected by thermosonication treatment for 30 min (TS-30) or conventional heat treatment for 1 h (CH-1).

Samples	Porod exponent, n	Correlation length, ξ (Å)	Lorentzian exponent, m
2.5 wt% FPI-control	2.3 (0.1)	60 (5)	4.0 (0.1)
2.5 wt% FPI-TS-30	2.5 (0.1)	120 (2)	4.0 (0.1)
10 wt% FPI-TS-30	2.5 (0.1)	144 (3)	4.0 (0.1)
10 wt% FPI-CH-1	2.6 (0.1)	87 (3)	4.0 (0.1)

#Numbers in parentheses represent error bars.

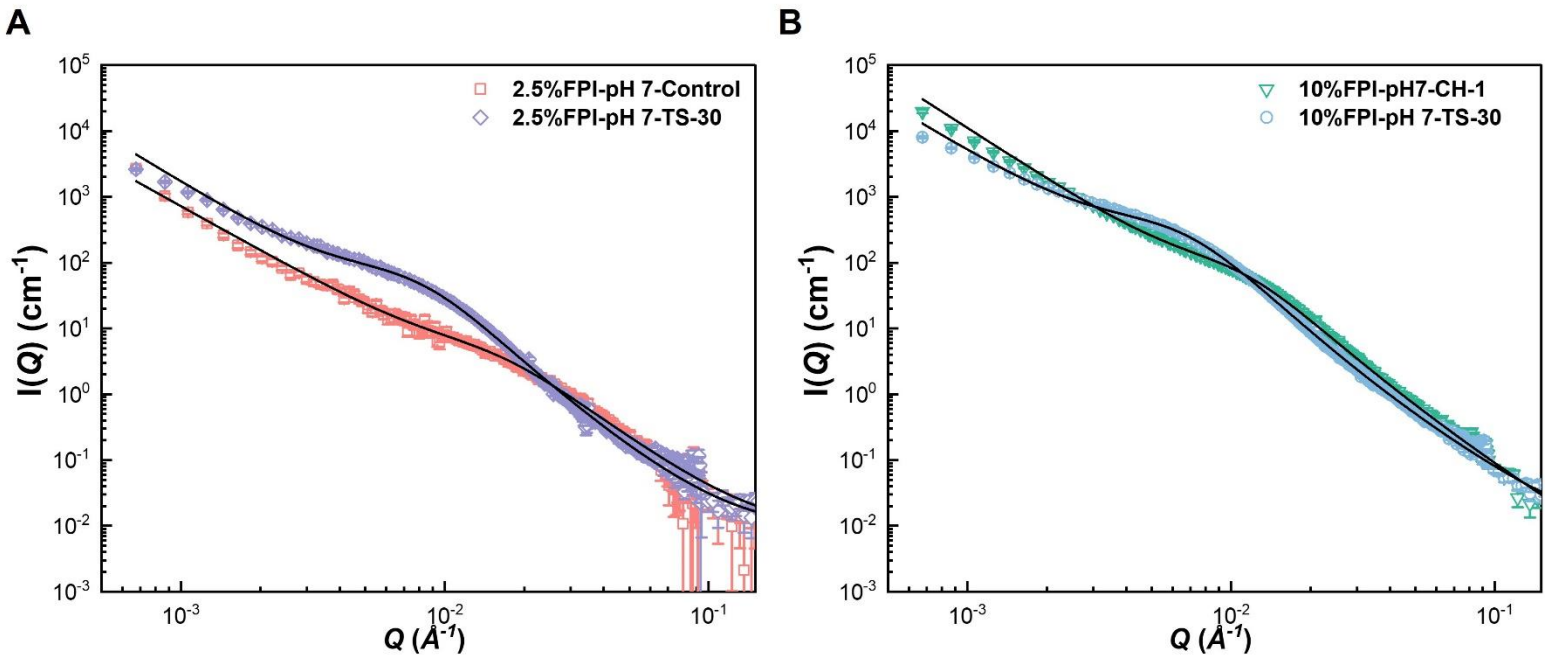

Fig. 5.4 Small-angle neutron scattering (SANS) profiles of (A) faba bean protein isolate (FPI) (2.5wt%) dispersions before and after thermosonication (TS) treatment for 30 min (TS-30) at at pH 7 (B) FPI gels (10 wt%) induced by TS treatment for 30 min (TS-30) or conventional heat treatment (CH) for 1 h (CH-1) at pH 7. The solid black lines are the correlation length model fits to the scattering data (eq (5.2)).

5.3.6 Characterisation of FPI gels

5.3.6.1 Small and large deformation rheological properties of FPI gels

Gelation and rheological behaviour are among one of the most important properties of plant proteins (Akharume, et al., 2021; Loveday, 2019). The frequency dependent viscoelastic properties of FPI gels induced by TS or CH treatments are shown in **Fig. 5.5A**. The G' and G'' of all samples were parallel to each other and only slight changes were observed with frequency. This indicates that all treated FPI samples had prevailing elastic and solid-like behaviours (Banerjee & Bhattacharya, 2012; Wei & Huang, 2020). This agrees well with the visual observation in **Fig. 5.1A**, which shows a self-supporting 10 wt % FPI hydrogel formed at pH 7 after TS treatment (10-30 min) and CH treatment (1-4 h).

To better compare gel strengths between FPI gels induced by different treatments, the G' (1 Hz) is plotted in **Fig. 5.5C** for all samples. CH-treated FPI gels showed significantly larger G' (1 Hz) values compared to TS-induced gels after prolonged heat treatment, suggesting that heat treatment (> 1 h) is more effective in facilitating formation of FPI gel network. The longer the CH time, the greater the gel strength. Specifically. G' (1 Hz) increased from ~150 Pa (CH-1) to ~1255 Pa (CH-8) with increasing CH time. Similar findings have been observed with other plant proteins. For example, a two folds increase in gel strength was found for lentil proteins after heating at 90 °C from 1 h to 16 h. The prolonged heating above the protein denaturation temperature could substantially facilitate the disintegration of protein molecules and exposure of the initially buried hydrophobic groups, thereby facilitating interactions between proteins and subsequent gel network formation (Jo, et al., 2020). TS treatment could also induce the formation of FPI gels even within a very short time (e.g. 10 min), showing its high potential as a novel gel formation method. However, the G' (1 Hz) of the TS-induced FPI gels (**Fig. 5.5A and 5.5C**) gradually decreased as the TS time increased from 10-min TS (~372 Pa) to 30-min TS (~289 Pa). This effect may have arisen from over-exposure of the molecules to acoustic cavitation by sonication, which breaks down protein chains, disrupts protein association, and impairs further aggregation (Hu, Li-Chan, et al., 2013; Khatkar, et al., 2020).

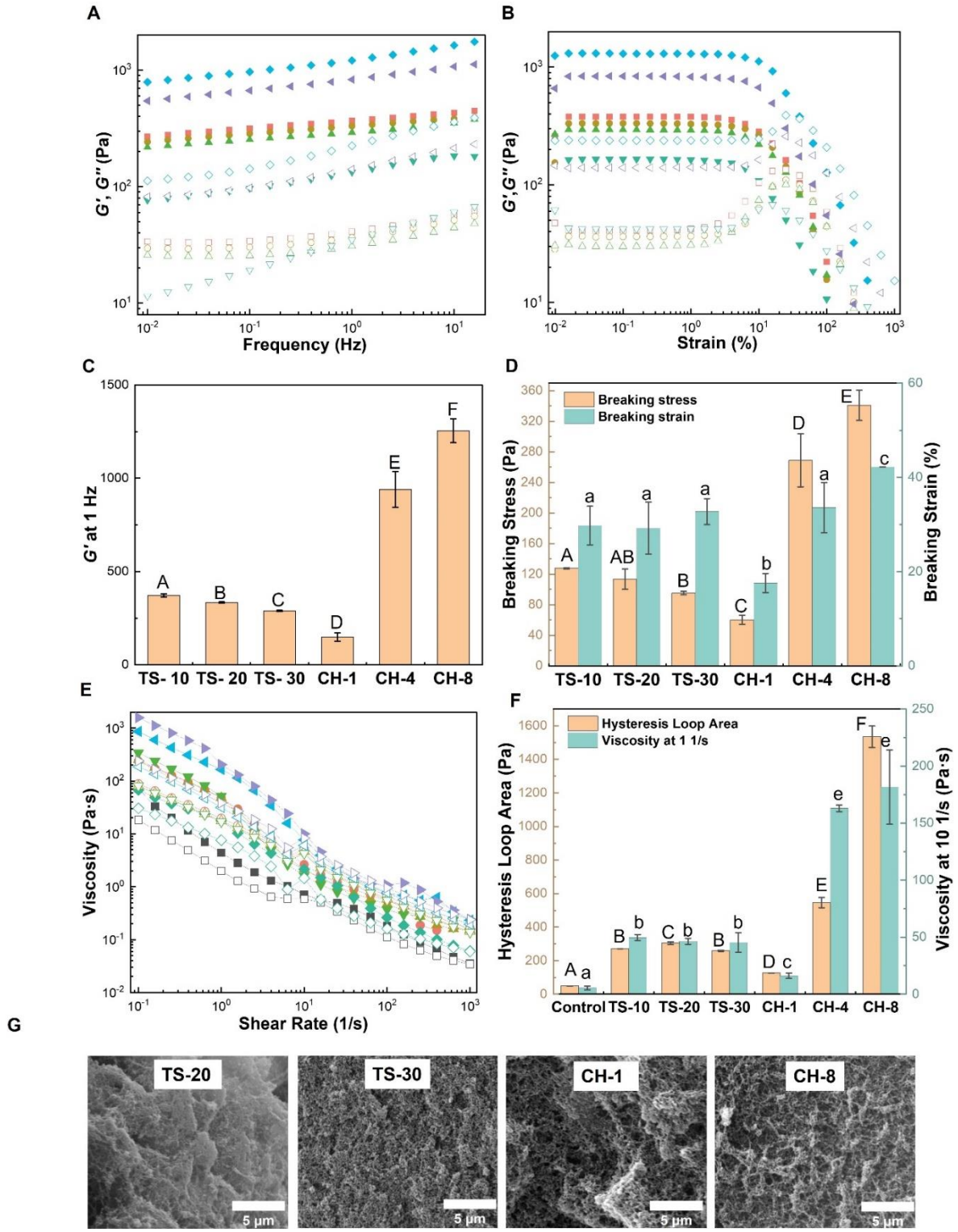

Fig. 5.5 Storage modulus (G', solid symbols) and loss modulus (G", empty symbols) as a function of frequency (A) and strain amplitude (B) for faba bean protein isolate (FPI) gels induced by thermosonication (TS) or conventional heat treatment (CH). Symbols correspond to: TS-10 (■), TS-20 (●), TS-30 (▲), CH-1(▼), CH-4 (◀), and CH-8 (◆). (C) Gel strength (G' at 1 Hz) and (D) breaking strain (γ_b) and breaking stress (σ_b) for

varoius FPI gels induced by thermosonication (TS) or conventational heating treatment (CH). (E) Viscosity as a function of shear rate for various untreated and treated FPI dispersions (10 wt%, pH 7). Solid and open symbols represent the "up" and "down" measurements, respectively. Symbols correspond to: Control (■), TS-10 (●), TS-20 (▲), TS-30 (▼), CH-1 (◆), CH-4 (◀), and CH-8 (▶). (F) Thixotropic hysteresis loop area and viscosity at 10 s-1 of TS- and CH-treated FPI dispersions (10 wt%, pH 7) obtained from the "up" and "down" viscosity measurements. (G) SEM images of selected FPI (10wt%, pH 7) gels induced by thermosonication (TS) for 20 min (TS-20) and 30 min (TS-30) or conventional heating treatment (CH) for 1 h (CH-1) and 8 h (CH-8). In (C, D, and F) different superscript letters above the column denote significant differences ($P < 0.05$).

Strain-sweep test was used to measure the strain dependent rheological behaviour and structural yield characteristic of FPI gels formed after TS or CH treatments (**Fig. 5.5B)**. Quantitatively similar strain dependent behaviours were observed in all FPI gels. At the small strain amplitude that was within the linear viscoelastic region (LVR), both G′ and G″ were constant with an increase in strain amplitude, indicating a typical characteristic of linear viscoelastic behaviour. Furthermore, within the linear viscoelastic region (LVR), the value of G′ was greater than G″, suggesting a prevailing elastic behaviour with a solid-like structure consistent with visual appearance and frequency sweep measurements (Munialo, et al., 2014). When the strain amplitude was further increased above the LVR, a sharp drop in G' was observed in all FPI gels due to structural disintegration (Yang, de Campo, et al., 2022). As for the value of G'', when the strain increased above the LVR, it initially increased to a maximum and then decreased remarkedly with further increases in strain; this can be categorised as type III nonlinear rheological (weak strain overshoot) behaviour (Hyun, et al., 2002). The overshoot of G'' could be due to structural rearrangement under large shear deformation (Hyun, et al., 2002). Similar large deformation rheological behaviour has been observed for hydrogels made from other plant proteins such as soybean protein (Xia, Siu, et al., 2021) and pea protein (Wittek, et al., 2021).

As the further increase in strain amplitude, crossover of G' and G'' was observed and the strain and stress values at that point can be identified as the breaking strain and breaking stress, respectively. After passing this point, the G'' value is higher than G', indicating the sample began to flow due to significant structural disintegration (Yang, et al., 2016). The values of breaking stress (σ_b) and breaking strain (γ_b) are shown in **Fig. 5.5D**. For CH induced FPI gels, the σ_b increased with treatment time (from ~60 to ~341 Pa), but with increasing TS treatment time, the σ_b gradually decreased following a similar trend (from ~128 to ~95 Pa) as G' at 1 Hz (**Fig. 5.5C**). However, FPI gels induced by TS treatments showed similar γ_b values with the longer treatment time (**Fig. 5.5D**). The γ_b values of TS-treated FPI gels ranged from ~29 to 33%, which were similar to the γ_b value of ~34% for CH-4 FPI gels. This indicates that TS treatment can effectively form FPI gels with similar resistance to larger shear deformation before breakdown using a shorter treatment time than CH treatment.

5.3.6.2 Viscosity of various FPI gels

The flow curves of control, CH- and TS-treated 10 wt % FPI dispersions at pH 7 are shown in **Figure 5.5E**. Shear-thinning behaviour was observed in all samples with viscosity decreasing with increasing shear rate. This has been widely reported in plant protein gels, including SPI gels (Ningtyas, Tam, et al., 2021), pea protein gels (Beck, et al., 2017), and quinoa proteins (Luo, et al., 2021). Compared to the control, CH or TS-treated FPI samples showed significantly higher viscosity, following the trend of G' at 1 Hz (**Fig. 5.5C**). The viscosity values at 10 s^{-1} are plotted in **Fig. 5.5F**, in which the control and CH-1 samples had significantly lower viscosity at 10 s^{-1} than the other treated samples; this is consistent with the visual observation in **Fig. 5.2A**. Similarly, TS samples had a similar viscosity range of ~46 to ~49 Pa·s, which was not significantly affected by TS time. For CH-treated samples, the viscosity increased dramatically when the heating time was increased from 1 h (~130 Pa·s) to 8 h (~1500 Pa·s).

Fig. 5.5E shows the "up" and "down" viscosity sweep tests. All samples had lower viscosity in "up" measurement than in "down" measurement. The consequent hysteresis loop indicates that these samples are thixotropic and suggests a time-dependent flow behaviour (Armelin, et al., 2006). The thixotropy was indicated by determination the area between the up and down curves (hysteresis) in **Fig. 5.5E** with larger areas indicating stronger thixotropic behaviour as shown in **Fig. 5.5F** (Armelin, et al., 2006; Luo, et al., 2021). Basically, the trend of hysteresis loop area among samples was consistent with the viscosity at 10 s^{-1} (**Fig. 5.5E**). Briefly, the CH-8 sample had the largest hysteresis loop area (~1535 Pa), while the TS-treated samples had a similar area ranging from ~259 to ~304 Pa. FPI gels that require higher energy to break the internal structure are expected to result in greater hysteresis. This finding is in line with the rheological behaviour and will be further discussed in the context of microstructural characteristics below.

5.3.6.3 SEM imaging of FPI gels

The microstructure of selected FPI gels induced by TS (20 and 30 min) and CH (1 and 8 h) was observed by SEM (**Fig. 5.5G**). The CH-treated samples exhibited large irregular pores with non-homogeneous spatial structure. Specifically, the CH-8 sample exhibited a cross-linked protein network structure with thicker strands compared to the

other samples, which explains its greater gel strength and larger extent of thixotropic behaviour. With prolonged heating time (4 and 8 h), FPI molecules unfolded more sufficiently so that active groups of proteins were extensively exposed, subsequently forming stronger gel networks (Jo, et al., 2020). Similar gel microstructures have been reported in a previous SEM investigation of lentil protein gels induced by prolonged heating (Jo, et al., 2020). In contrast, an uneven and less compact protein network structure a large pores and thinner strands was observed in the CH-1 FPI gel, which resulted in a weaker gel strength, as discussed above. However, TS-treated FPI gels had a more uniform microstructure with smaller porosity than CH-1 gels; the microstructure was not significantly different between TS-20 and TS-30 samples, following similar gel strength trends above. The uniform microstructure could be attributed to the production of soluble protein aggregates and β-sheet dominated protein aggregates after TS, which facilities protein-protein interactions and subsequent formation of gel network (Hu, Li-Chan, et al., 2013).

5.3.6.4 Thermo-reversible gelation behaviour of FPI gels

Investigating the rheological behaviour of hydrogels in response to various environmental parameters, such as temperature, is important for their practical application and assists in understanding their underlying gelation mechanism (De Kort, et al., 2016; Yang, Yang, et al., 2018). Herein, the temperature responsive rheological property of TS-30 FPI gel was studied, as shown in **Fig. 5.6**. When the temperature was increased from 20 to 60 °C, G' and G'' gradually decreased, and G' remained larger than G'', representing a solid-like behaviour. As the temperature increased further from 60 to 80 °C, both G' and G'' decreased significantly, with G' decreasing to a similar value as G''. This indicates a weak gel behaviour with flowability as indicated by the visual appearance shown in **Fig. 5.6C** suggesting a gel-sol transition. When the temperature was decreased, both G' and G'' increased, with G' increasing progressively faster than G''. After 75 min, G' was much greater than G'' and the liquid-like sample solidified again to form a hydrogel with a self-supporting behaviour (**Fig. 5.6 inset**). Additionally, when the temperature was held at 20 °C for 2 h, G' increased gradually with time, showing that the gel network progressively strengthened. This result suggests that critical role of hydrogen bonding in the formation of TS-induced FPI gel networks (Damodaran, 2008; Yang, de Campo, et al., 2022). Finally, this result demonstrated

thermally reversible gelation behaviour of TS-treated FPI at a neutral pH, which may find potential application as a gelatine alternative in vegan food products.

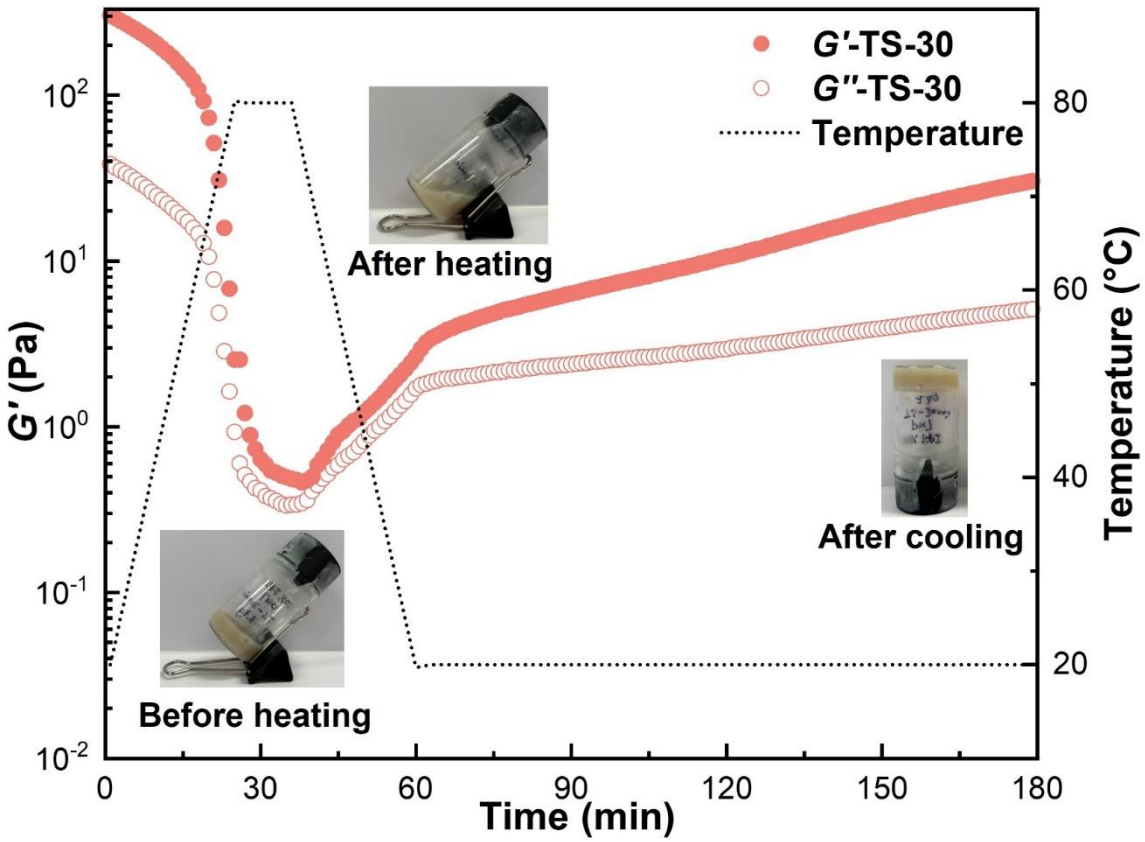

Fig. 5.6 (A) Storage modulus G' (solid symbols) and loss modulus G'' (empty symbols) as a function of time for faba bean protein isolate (FPI) dispersion (10wt%, pH 7) treated by thermosonciation for 30 min (TS-30) during a rheological temperature sweep measurement. Inset are visual appearance of samples during sol-gel and gel-sol transitions.

5.3.7 Physicochemical properties and storage stabilities of emulsions prepared from TS-treated FPI

5.3.7.1 Oil-water interfacial tension

Fig. 5.7A illustrates the dependence of interfacial tension (IFT) of FPI dispersions (pH 7) with time before and after TS-30 treatment. An initial significant decrease in the interfacial tension of both samples was observed over time (up to ~1000 s), eventually attaining a plateau at ~6000 s. This indicates that a proportion of the proteins transfer from aqueous phase to the droplet interface (Tang, 2020b). The IFT values at 6000 s are shown in **Fig. 5.7A inset** and were ~12.35 mN/m (Control) and ~11.51 mN/m (TS-30), respectively, indicating a slightly better interfacial activity of the TS-30 FPI solutions. This may be due to the dominant intermolecular β-sheet structure (Afkhami, et al., 2024; Lefèvre & Subirade, 2003) and higher surface hydrophobicity (Phoon, et al., 2014) of TS-treated FPI as revealed in **Fig. 5.3A and 5.3C**, which may play an important role in reducing the oil-water interfacial tension.

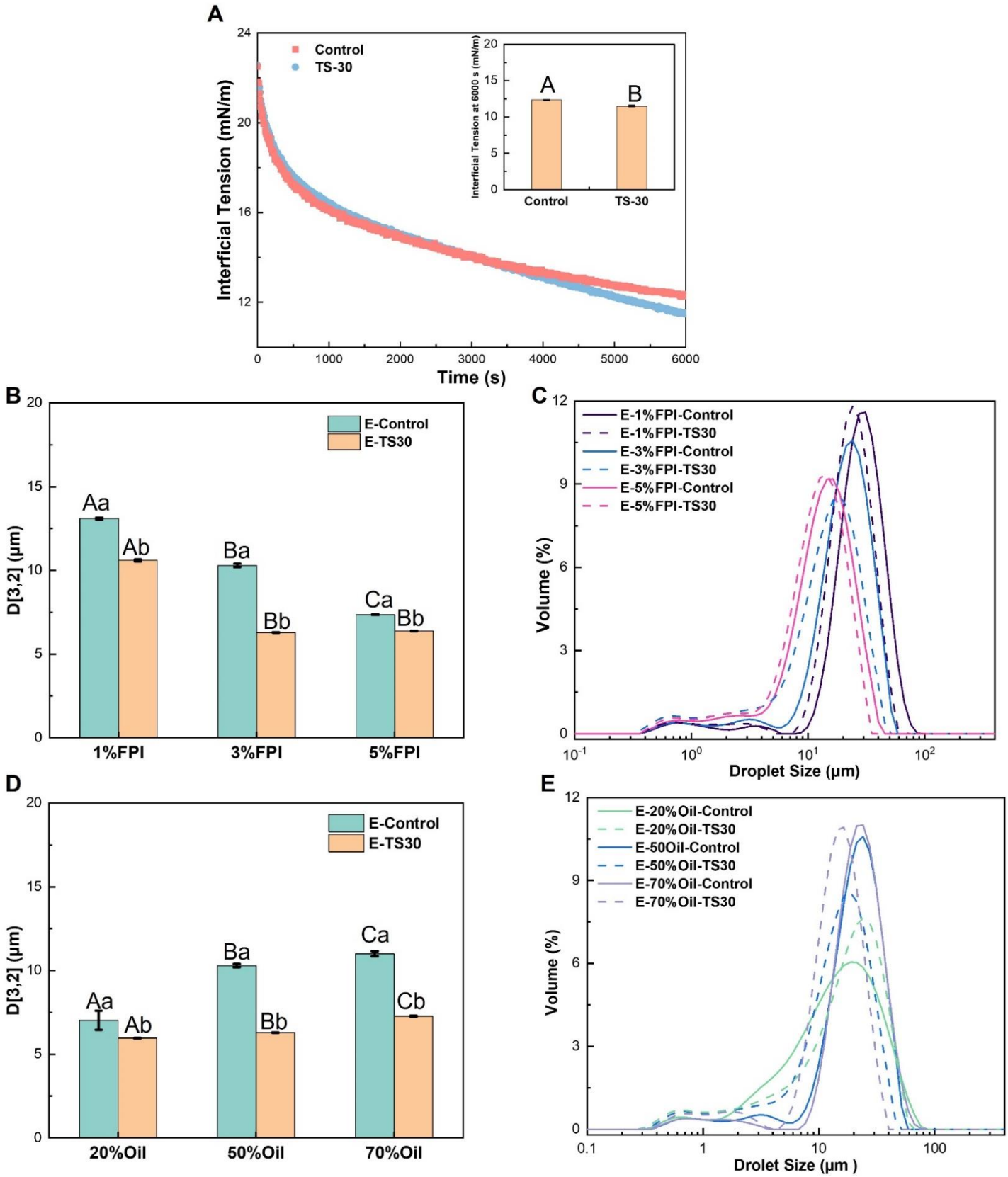

Fig. 5.7 (A) Time dependence of oil-water interfacial tension of faba bean protein isolate (FPI) before and after 30 min thermosonication treatment (TS-30), and final interfacial tension values at 6000 s (*inset*). (B) Oil droplet size distribution of emulsions

stabilised by different concentrations (1, 3, 5 wt%) of native and 30 min thermosonicated FPI (TS-30)at an oil volume fraction of 50% (v/v). (C) Sauter mean diameter D [3,2] of emulsions stabilised by different concentrations (1, 3, 5 wt%) of native and TS-30 treated FPI at oil fraction of 50% (v/v). (D) Sauter mean diameter D [3,2] of emulsion oil droplets stabilised by 3 wt% native orTS-30 treated FPI dispersions at different oil volume fractions (20, 50, and 70%, v/v). (E) Oil droplet size distribution of emulsions stabilised by 3 wt% native or TS-30 treated FPI dispersions at different oil volume fractions (20, 50, and 70%, v/v). In (A) different superscript letters above the columndenote significant differences ($P < 0.05$). In (B and D) different capital letters above the columns denote significant differences ($P < 0.05$) in emulsions stabilised by FPI at different concentrations or oil fractions. The different lowercase letters denote significant differences ($P < 0.05$) in emulsions stabilised by FPI solutions with/without TS treatment. E-Control and E-TS30 indicate emulsions stabilised by native FPI and TS-30 treated FPI, respectively.

5.3.7.2 Oil droplet size distribution within emulsions

Effect of FPI concentrations

The effect of native and TS-treated FPI dispersions on the size distribution is illustrated in **Fig. 5.7B and C**. For the native FPI stabilised emulsions, the oil droplet size (D [3,2]) declined from ~13.1 μm to ~7.4 μm as the FPI concentration increasing from 1 wt % to 5 wt % (**Fig. 5.7B)**. In **Fig. 5.7C**, the 1 wt % native FPI stabilised emulsions exhibited a trimodal distribution with a dominant peak at ~40 μm and minor peaks at ~4 μm and ~1 μm, respectively. Increasing the FPI concentration to 5 wt % induce the major peak of the emulsion shifted toward a smaller size to ~12 μm, indicating that the oil droplet size decreases with a rise in FPI concentration. At greater protein concentrations, more proteins are available to cover the newly formed oil surfaces, thus leading to smaller oil droplets (Wynnychuk, et al., 2021; Zhang, Holmes, et al., 2020). As shown in **Fig. 5.7B**, the oil droplet sizes of the emulsions stabilised by TS-treated FPI were substantially smaller than the ones stabilised by native FPI at the same protein concentration. Increasing the FPI concentration from 1 to 3 wt% led to a significant decrease in oil droplet sizes from ~10.4 to ~6.3 μm in TS-treated FPI stabilised emulsions. For TS-30 stabilised emulsion, the oil droplet size is similar at ~6.3 μm when FPI concentration increased from 3 wt% to 5 wt%, suggesting that the protein is excess at this oil volume fraction (ϕ) of 0.5. This discovery is in a good agreement with a study reported by McClements (2004b), who found that the oil droplet size is independent of emulsifier concentrations when in excess. In summary, TS-treated FPI is a more effective emulsifier than its native form.

Effect of oil volume fraction

The oil droplet size of emulsions stabilised by native or TS-treated FPI is considerably affected by the oil volume fraction ϕ at a constant protein concentration 3 wt%. When the ϕ increased from 0.2 to 0.7 in the native FPI prepared emulsions, the oil drop size (D [3,2]) increased from 7.0 to 11.0 μm (**Fig. 5.7D)**; this is in line with the peak in particle size distribution shifting to a greater value with increasing ϕ (**Fig. 5.7E).** The increase in oil droplet sizes with increasing in ϕ at constant protein concentrations agrees well with studies on emulsions stabilised by other plant proteins, such as soy protein (Liu & Tang, 2013), lentil protein (Wynnychuk, et al., 2021), and pea protein (Li, Liu, et al., 2022). The oil droplet sizes of the emulsions stabilised by TS30 were

from ~5.9 to ~7.3 μm (**Fig. 5.7D)** which were much smaller than the emulsions prepared from native FPI. However, the oil droplet size showed a opposite trend, i.e., the oil droplet size decreases slightly with increasing ϕ, and the main particle size distribution peak shifted to smaller sizes as shown in **Fig 5.7D & E**. A drop in droplet size with an increase in ϕ is typically observed when the emulsifiers are in excess. Liu and Tang (2013) reported that the oil droplet size of emulsion stabilised by SPI nanoparticles increased with increaseing ϕ from 0.2-0.6 at a low SPI concentration (2 wt%) but decreased with increasing ϕ at a high SPI concentration (6 wt%). When the emulsifier concentration is greater than the interfacial saturation concentration, more proteins were able to adsorb to the droplet surface to enhance the inter-droplet interactions thus leading to the generation of a gel-like network. A high viscosity in the gelled emulsions could impart a high shear stress under turbulent flow during homogenisation thus leading to a more efficient breakup of oil droplets and a decreased droplet size (Tcholakova, et al., 2011). The viscosity of such emulsions is further discussed in **Section 5.3.7.4**.

5.3.7.3 Microstructure of emulsions

The microstructures of emulsions were also visually observed by light microscopy and CLSM as shown in **Fig. 5.8**. Light micrographs showed that the oil droplet size substantially decreased as increasing FPI concentration in emulsions stabilised by native FPI or TS-treated FPI (**Fig. 5.8A**). Light micrographs showed that the oil droplet size substantially decreased as increasing FPI concentration in emulsions stabilised by native FPI or TS-treated FPI at a fixed oil volume fraction ϕ=0.5 (**Fig. 5.8A**). Furthermore, the oil droplets of emulsions stabilised by TS30 were substantially smaller than that of the native FPI-stabilised emulsions, consistent with the oil droplet size distribution results. As revealed by CLSM in **Fig. 5.8B**, different interfacial layer structures and aqueous phase networks were observed in the native FPI- and TS-FPI-stabilised emulsions (oil volume fraction ϕ=0.5) at different protein concentrations. In native FPI stabilised emulsions, the proteins formed a thinner interfacial layer on the droplet surfaces and some protein aggregates were observed in the aqueous phase. However, TS-30 stabilised emulsions had a thicker interfacial layer on the droplet surfaces and some localised gel-networks can be observed due to bridging between adjacent droplets, in particular in emulsions with high protein concentrations of 3 and

5 wt % TS-FPI. The droplet networking was also evident in the tube inversion test as shown in **Fig. S5.1**, where emulsions do not flow upon inverted. This could be due to the interactions and entanglements between protein aggregates in the aqueous phase and/or bridging of oil droplets, leading to the formation of a gel network structure (Bai, et al., 2018; Tang & Ghosh, 2021).

The microstructures of emulsions with different ϕ at a fixed 3 wt % FPI concentration were also investigated (**Fig. 5.8C and D**). It can be seen that the oil droplet packing became denser with increasing ϕ in the emulsion stabilised by 3 wt % native and TS-treated FPI (**Fig. 5.8C**) (Liu & Tang, 2013). The oil droplet size of emulsion stabilised by native FPI was increased with increasing oil fraction. In addition, droplet flocculation became more visible with increasing oil fraction (**Fig. 5.8D**), in particular at oil volume fraction ϕ=0.7, which gave rise to emulsion gel network formation as also observed in **Fig. S5.1**. The gel-like network with a high oil fraction has also been reported in the emulsions stabilised by other plant proteins, such as SPI (Tang & Liu, 2013), FPI (Hu, et al., 2023), and pea protein (Velez-Erazo, et al., 2020). In emulsions stabilised by TS-treated FPI, oil droplet sizes decreased with increasing ϕ (**Fig. 5.8C**), which agreed well with particle sizing results (**Fig. 5.7E**). Further, CLSM revealed that that the oil droplets stabilised by TS-treated FPI have a thicker interfacial layer and greater network formation due to protein aggregate entanglement and droplet-droplet interactions compared to the emulsions stabilised by native FPI. The microstructural differences could result in differences in mechanical properties, which will be discussed in the following sections.

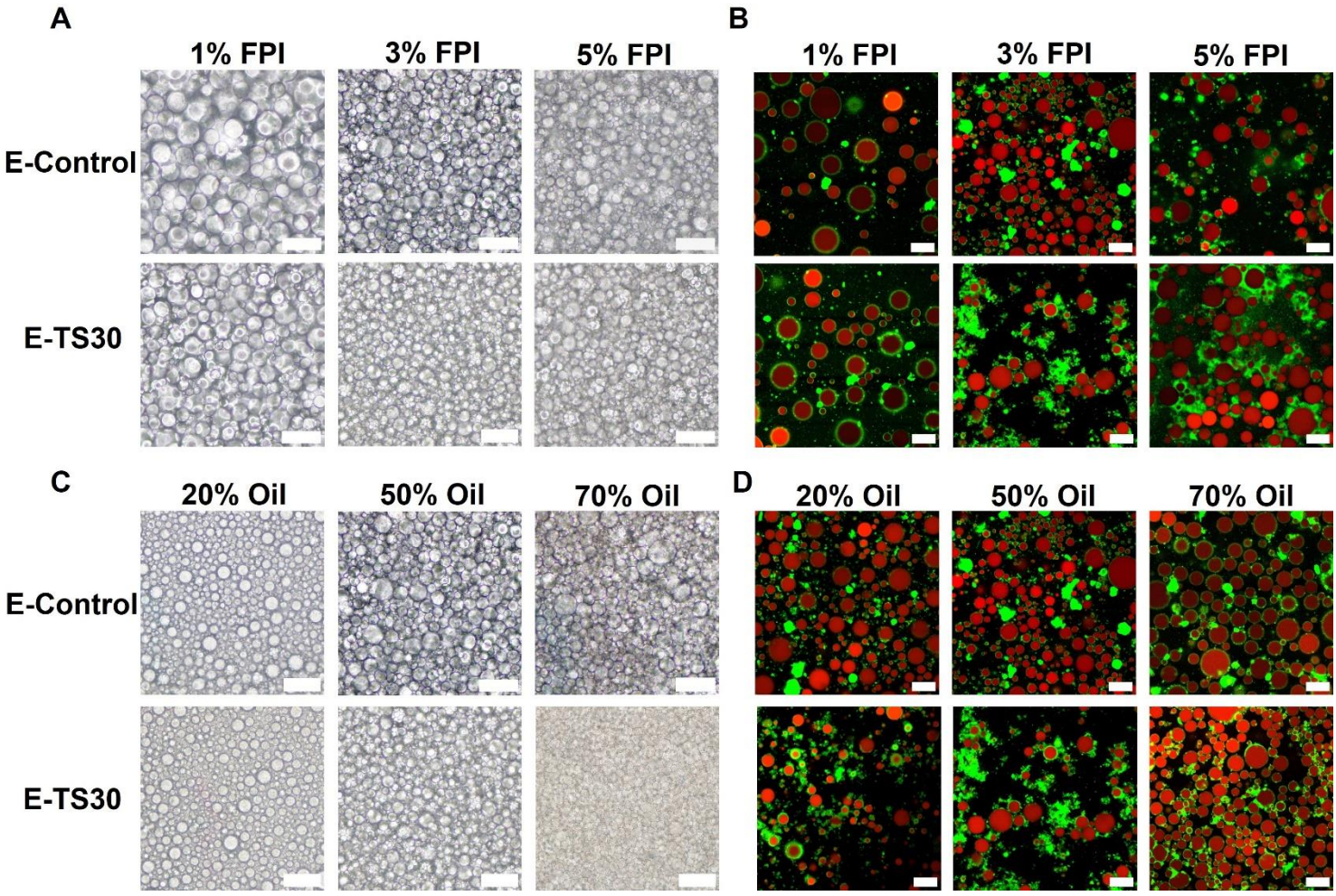

Fig. 5.8 Optical microscopic (left) and confocal laser scanning microscopic (CLSM) (right) images of (A and B) emulsions stabilised by different concentrations (1, 3, 5 wt%) of native and TS-30treated faba bean protein isolate (FPI) dispersionsat a oil volume fraction of 50% (v/v). Optical microscopic images (C) and CLSM images (D) of emulsion stabilised by 3 wt% native and TS-30 treated FPI dispersions at different oil volume fractions (20, 50, and 70%, v/v). Scale bar = 20 μm.

5.3.7.4 Rheological properties of emulsions

Small deformation rheological properties of emulsions

The viscoelastic response of emulsion systems stabilised by native or TS-treated FPI as a function of frequency is illustrated in **Fig. 5.9 A to D**. G' and G'' of all the samples were parallel to each other with a slight dependence on frequency, indicating that all samples were dominated by an elastic behaviour consistent with a gel (Banerjee & Bhattacharya, 2012). The emulsion systems stabilised by native FPI were found to be weaker, which was also confirmed by previous findings. The greater gel strength found in TS-30 FPI stabilised emulsions could be attributed to interactions and entanglements of FPI protein aggregates located on the oil-water interface of neighbouring small oil droplets, compact arrangement of oil droplets, and thick interfacial layer of FPI aggregates as revealed by CLSM (**Fig. 5.8**) (Hu, et al., 2023; Kornet, et al., 2022).

The G' (1 Hz) of all emulsions stabilised by various FPI concentrations is plotted in **Fig. 5.9E**. An increase in the FPI concentration resulted in the increased gel strength of the emulsions. Specifically, in native FPI stabilised emulsions, G' (1 Hz) increased from ~1 Pa for 1wt% FPI stabilised emulsion to ~18 Pa for 5 wt% FPI stabilised emulsion. While for TS-30 FPI stabilised emulsion, G' (1 Hz) increased dramatically from ~8 Pa (1 wt% FPI) to ~250 Pa (5 wt% FPI). This finding is consistent with reports on other plant protein (e.g. QPI) stabilised emulsions (Hu, et al., 2023; Zhang, Cheng, et al., 2021). The stronger gel found at higher FPI concentrations could be due to the smaller oil droplet size, compact interactions between adjacent oil droplets and protein network formation in the continuous phase as revealed by CLSM in **Fig. 5.8**.

The effect of oil volume faction on the gel strength G' (1 Hz) of native/TS-treated FPI stabilised emulsions is shown in **Fig. 5.8F**. Similar to **Fig. 5.9E**, emulsions prepared by TS-treated FPI exhibited significantly higher G' values ranging from ~6 Pa to ~1121 Pa with increasing oil fraction ϕ from 0.2 to 0.7 compared to native FPI (~0.53 Pa to ~662 Pa). Additionally, it can be assumed that the greater the oil fraction, the greater the gel strength. At continuously increasing oil fractions, the number of dispersed oil droplets will increase, leading to a higher packing state of the droplets (Brinkman, 1952). The number of interactions between protein particles and oil droplets also increases, thus leading to the increase in gel strength at higher oil ratios (Krieger & Dougherty, 1959).

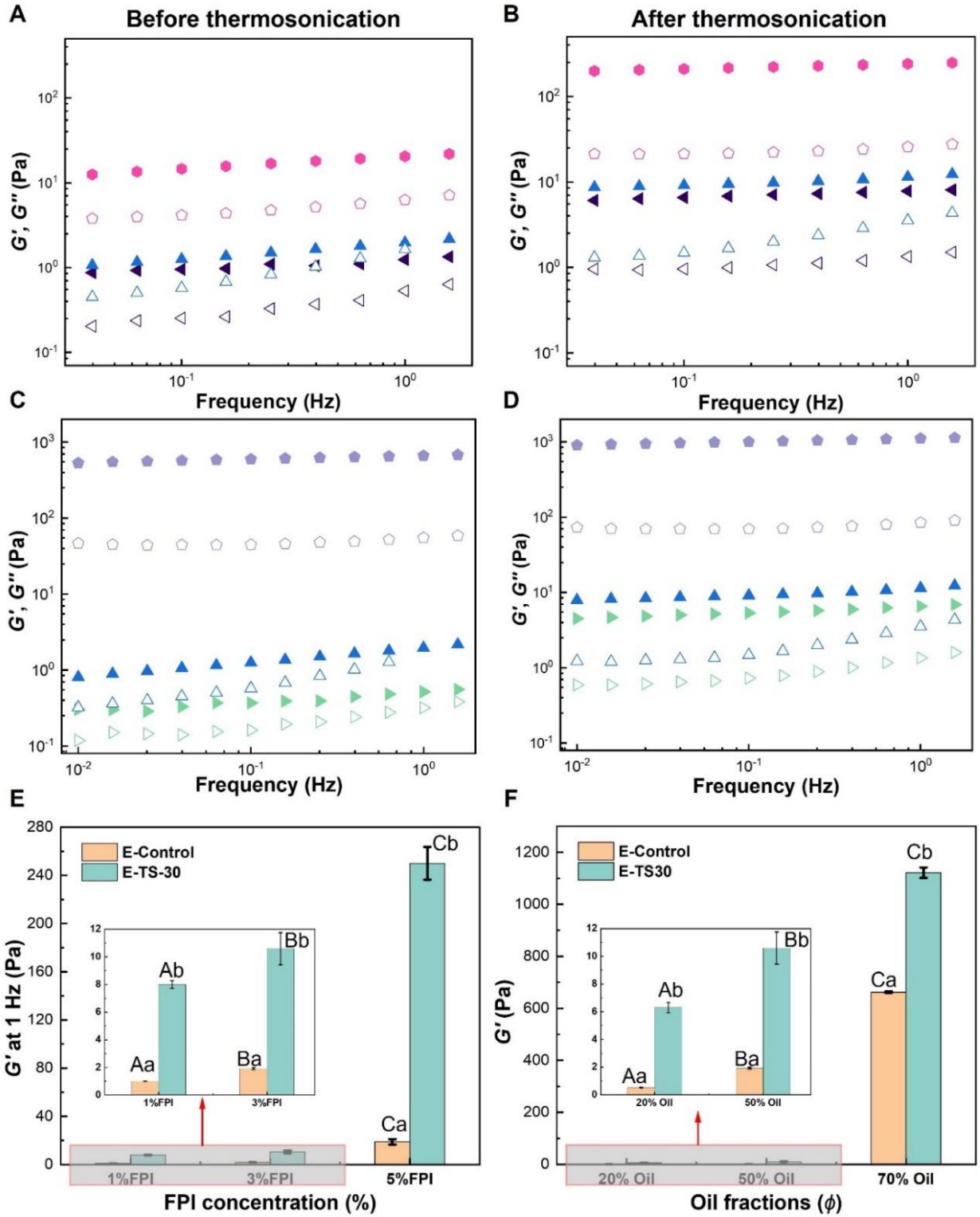

Fig. 5.9 The frequency dependence of G' (solid symbols) and G'' (empty symbols) for emulsions stabilised by faba bean protein isolate (FPI) before (A and C) and after (B and D) 30 min thermosonication treatment (TS-30). (A and B) Emulsions stabilised by different concentrations of native and TS-30 treated FPI dispersion (1, 3, 5 wt%) at an oil volume fraction of 50% (v/v). Symobls correspond to 1 wt% FPI (◀), 3 wt% FPI

(▲), and 5wt% FPI (⬢). (C and D) Emulsions stabilised by 3 wt% native and TS-30 treated FPI dispersion at different oil fractions (20, 50, and 70%, v/v). Symobls correspond to: (▶)-20% oil, (▲)-50% oil, and (⬟)-70% oil. (E and F) G' (1 Hz) of emulsions stabilised by untreated and TS-30 treated FPI. Different superscript capital letters above columns denote significant differences ($P < 0.05$) between the emulsions stabilised by different concentrations of FPI (1, 3, 5 wt%) or different oil volume fractions (20, 50, and 70%, v/v). Above the column, different lowercase superscripts denote significant differences ($P < 0.05$) between the emulsion systems prepared by FPI treated with/without TS.

Large deformation rheological properties of emulsions

The strain dependent rheological characteristics of emulsions are shown in **Fig. 5.10**. G' and G'' of all the samples were independent of strain amplitude within the LVR, with G' being larger than G'', which confirmed the gel-like network structure of all emulsion systems as shown in **Fig. 5.9** (Zou, et al., 2018). Once the strain amplitude was above the LVR, the G' values for all samples decreased substantially, indicating structural disintegration. For emulsions stabilised by TS-treated FPI, the G'' values increased with strain amplitude and reached a local maximum, which has been assigned as type III nonlinear (weak strain overshoot) behaviour (Hyun, et al., 2002). This could have resulted from structural rearrangements under large strain deformation (Masalova, et al., 2011; Mason, et al., 1995; Zhang, Cheng, et al., 2021). For most native FPI-stabilised samples, Type I (*strain thinning*) behaviour was observed (**Fig. 5.10**) as G' and G'' decreased monotonically with increasing strain (Hyun, et al., 2002; Zhang, Lu, et al., 2021). Xu, Sun, et al. (2023) attributed this Type I behaviour to the rearrangement of the emulsion microstructure with the direction of flow field.

The values of breaking stress (σ_b) are shown in **Fig. 5.10C and F**. In line with the small deformation rheology results, the σ_b values of emulsions stabilised by TS-treated FPI were significantly greater than those of native FPI stabilised emulsions. Specifically, as the untreated FPI concentration rise from 1 to 5 wt%, the σ_b slightly increased from ~0.4-~7 Pa, whereas TS-30 stabilised emulsion had a larger σ_b in the range of ~0.7-~38 Pa, indicating a stronger gel was formed. Also, σ_b increased with an increase in oil fraction, which agrees well with the small deformation rheological findings.

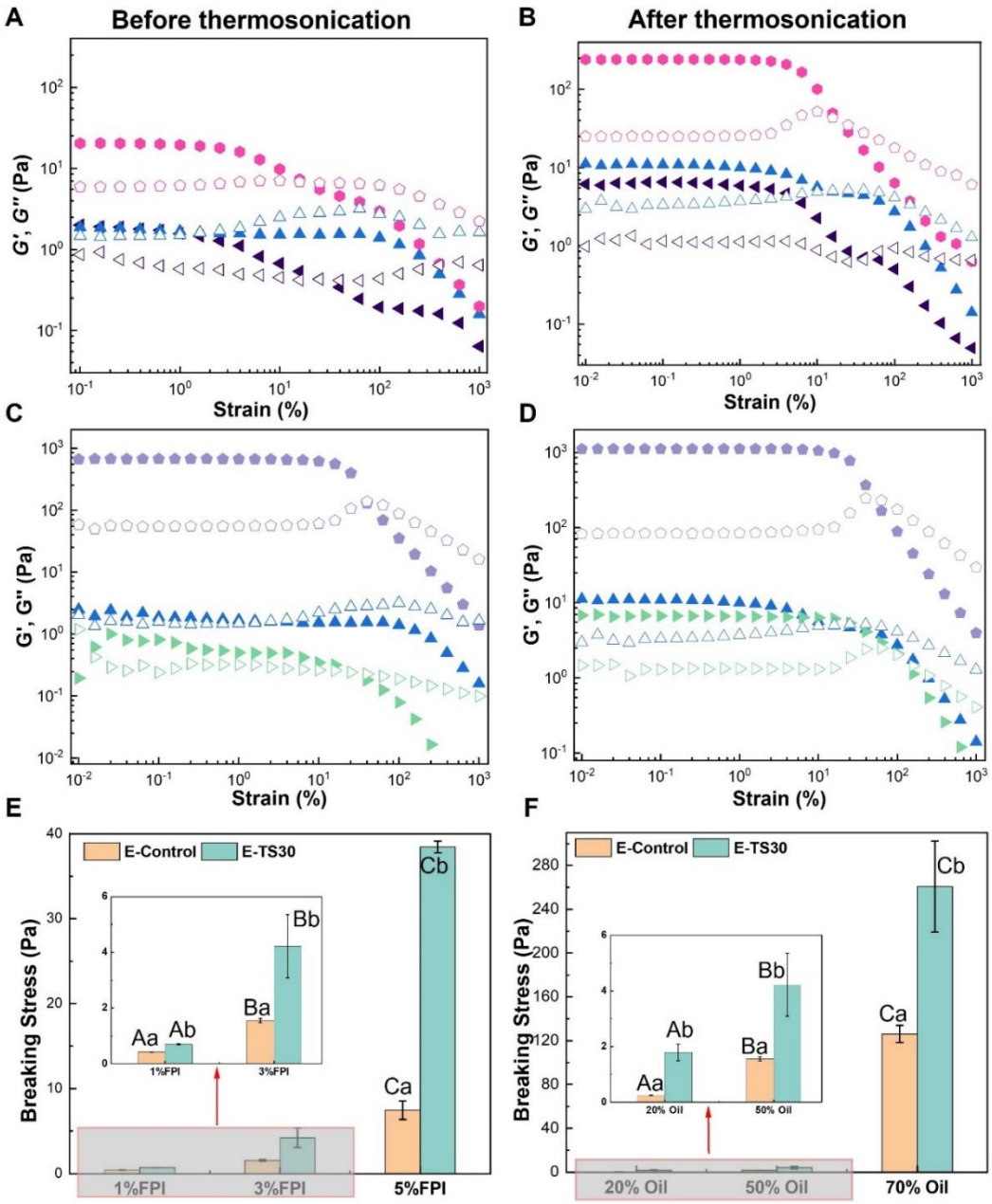

Fig. 5.10 The G′ (solid symbols) and G" (empty symbols) as a function of strain amplitude for emulsions stablised by faba bean protein isolate (FPI) before (A and C) and after (B and D) thermosonication treatment for 30 min (TS-30). (A and B) Emulsions stabilised by different concentrations of native and TS-30 treated FPI dispersion (1, 3, 5 wt%) at an oil volume fraction of 50% (v/v). Symbols correspond to 1 wt% FPI (◀), 3 wt% FPI (▲), and 5wt% FPI (⬢). (C and D) Emulsions stabilised by 3 wt% native and TS-30 treated FPI dispersion at different oil fractions (20, 50, and 70%, v/v). Symobls correspond to: (▶)-20% oil, (▲)-50% oil, and (⬟)-70% oil. (E and F) Breaking stress of all emulsion systems. Different superscript capital letters above

columns denote significant differences ($P < 0.05$) between the emulsions stabilised by different concentrations of FPI (1, 3, 5 wt%) or different oil volume fractions (20, 50, and 70%, v/v). The different lowercase letters denote significant differences ($P < 0.05$) between the emulsion systems stabilised by FPI treated with/without TS.

5.3.7.5 Long-term storage stability of emulsions

Fig. S5.1 shows photographs of emulsions stabilised by native or TS- 30-treated FPI (1, 3 and 5 wt%) containing oil volume fractions of 0.2, 0.5, and 0.7 over a storage period of 28 days at 20 °C. **Fig. S5.2** shows the creaming index and volume-weighted mean droplet diameter (D [4,3]) of the emulsions during storage. In all samples, a cream layer and high serum phase were clearly observed along with an increase in creaming index and D [4,3] of oil droplets increasing with storage time (**Fig. S5.2A and B**). In addition, as the FPI concentration increased, the creaming phenomenon and oil droplet coalescence decreased. Furthermore, emulsions containing higher oil fractions also exhibited superior stabilities, which could be due to gel network formation as revealed by rheology and CLSM observations (McClements, 2007). Finally, at all conditions, emulsions stabilised by TS-30 FPI showed greater stability compared to the emulsions stabilised by native FPI. This could be explained by the smaller oil droplet size, denser and more compact arrangement of oil droplets (especially at a high oil volume fraction), and greater mechanical strength found in emulsions stabilised by TS-30 FPI. In general, this study suggested that TS treatment is promising and efficient to enhance emulsification capability and stability of FPI for use in emulsion-based beverage and gels.

5.4 Conclusions

This study systematically studied the impacts of thermosonication (TS) on the physicochemical properties, techno-functional performances, and microstructural characteristics of FPI dispersions at pH 7 and compared with the conventional heating (CH) method. The results demonstrated that the TS treatment formed FPI protein aggregates that are rich in β-sheet secondary structures, as evidenced by ThT fluorescence, CD spectra, TEM, and SANS results. This may be due to extensive denaturation and unfolding of FPI molecules when exposed to ultrasonication at high temperatures followed by structural rearrangements and assembly. In addition, TS significantly decreased FPI particle size and increased the solubility. The formation of a thermoreversible viscoelastic gel network was identified in TS-induced 10wt% FPI dispersions, suggesting potential applications as a texturizer in vegan food products. Finally, different concentrations of TS-30 treated FPI dispersions (1, 3, and 5 wt%) were used to stabilise O/W emulsions at various oil volume fractions (ϕ = 0.2, 0.5, and 0.7).

The emulsions formed by TS-30 treated FPI exhibited smaller oil droplet size, greater mechanical strength, more compact and denser oil droplet microstructure, as well as a better storage stability than those formed by the native FPI. In summary, this study showed that the TS treatment can form FPI protein aggregates at pH 7 with distinctive gelation behaviour and improved emulsification capability. The resulting new structures of FPI offers a range of potential applications for use as a texturing and emulsifying agent in food, cosmetic, and pharmaceutical products.

Acknowledgements

The author Yinxuan Hu would like to thank Massey University, New Zealand, for providing a doctoral scholarship. We thank the Manawatu Microscopy and Imaging Centre (MMIC) at Massey University, Palmerston North for their kind support and assistance. The authors thank the support of the Australian Centre for Neutron Scattering, ANSTO in supporting the QUOKKA neutron research infrastructure used in this work via ACNS proposal P15802.

Supplementary Information

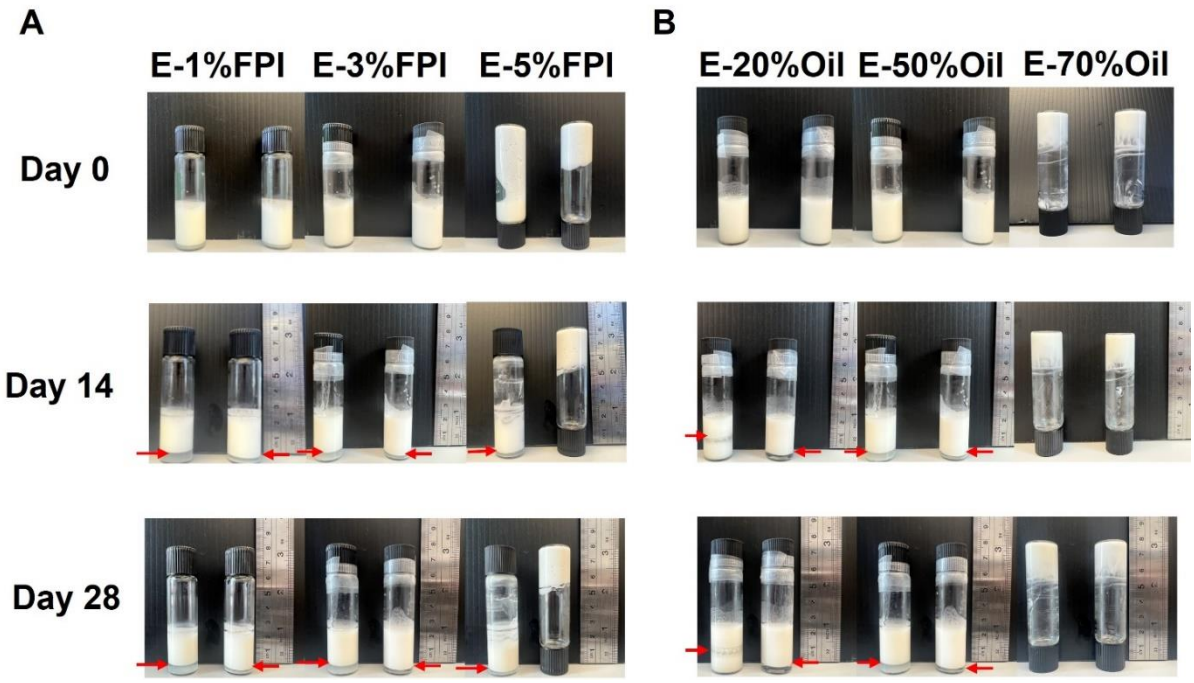

Fig. S5.1 (A) Visual observations of soy oil (O/W) emulsions stabilised by 30 min thermosoniation treated (TS-30) or native faba bean protein isolate (FPI) at 1 wt % (E-1%FPI), 3 wt % (E-3%FPI), and 5 wt % (E-5%FPI) containing a fixed oil volume fraction of 0.5 during storage at 20 °C up to 28 days; and (B) visual observations of soy oil (O/W) emulsions stabilised by 3 wt % native or TS-30 FPI at different oil volume fractions (v/v) of 0.2 (E-20% oil), 0.5 (E-50% oil), and 0.7 (E-70% oil) during storage at 20 °C up to 28 days. In all images, native FPI stabilised emulsions are on the left side and TS-30 FPI stabilised emulsion samples are on the right side.

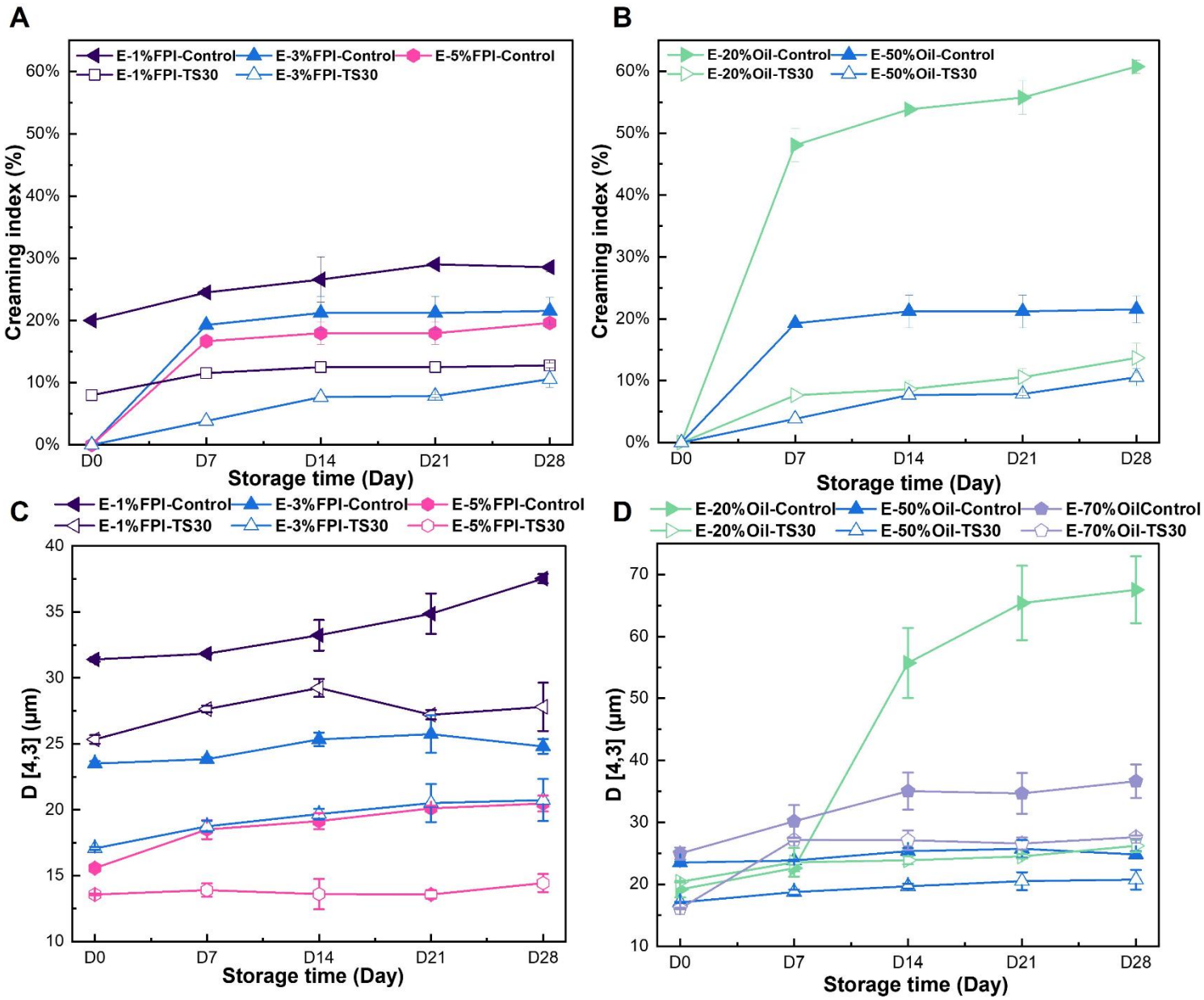

Fig. S5.2 Creaming index (A)and the volume-weighted mean diameter D [4,3] of oil droplets (C) of emulsions stabilised by 30 min thermosoniation treated (TS-30) or native faba bean protein isolate (FPI) at 1 wt % (E-1%FPI), 3 wt % (E-3%FPI), and 5 wt % (E-5%FPI) containing a fixed oil volume fraction of 0.5; and creaming index (B) and the volume mean diameter D [4,3] of oil droplets (D) of emulsions stabilised by 3 wt % native or TS-30 FPI at different oil volume fractions (v/v) of 0.2 (E-20% oil), 0.5 (E-50% oil), and 0.7 (E-70% oil) during storage at 20 °C up to 28 days.

MASSEY UNIVERSITY
TE KUNENGA KI PŪREHUROA
UNIVERSITY OF NEW ZEALAND

GRADUATE RESEARCH SCHOOL

STATEMENT OF CONTRIBUTION DOCTORATE WITH PUBLICATIONS/MANUSCRIPTS

We, the student and the student's main supervisor, certify that all co-authors have consented to their work being included in the thesis and they have accepted the student's contribution as indicated below in the Statement of Originality.

Student name:	Yinxuan Hu
Name and title of main supervisor:	Professor Aiqian Ye
In which chapter is the manuscript/published work?	Chapter 6

Describe the contribution that the student and members of the supervisory team have made to the manuscript/published work:[1]

Yinxuan Hu: Methodology, Investigation, Data curation, Formal analysis, Writing-original draft.
Lirong Cheng: Conceptualization, Supervision, Investigation, Writing-review & editing.
Zhi Yang: Conceptualization, Investigation, Methodology, Supervision, Project administration, Writing-original draft, Writing-review & editing

Please select one of the following three options:

- (●) The manuscript/published work is published or in press

  Please provide the full reference of the research output:

  Hu, Y., Cheng, L., & Yang, Z. (2025). Impact of various physical treatments on physicochemical and microstructural characteristics of vegetable oil-based whipped cream stabilised by faba bean protein isolate. Food Hydrocolloids, 163, 111084. https://doi.org/10.1016/j.foodhyd.2025.111084

- ( ) The manuscript is currently under review for publication

  Please provide the name of the journal:

- ( ) It is intended that the manuscript will be published, but it has not yet been submitted to a journal

Student's signature:	Yinxuan Hu Digitally signed by Yinxuan Hu Date: 2025.01.21 20:04:32 +13'00'	Main supervisor's signature:	Aiqian Ye Digitally signed by Aiqian Ye DN: cn=Aiqian Ye, o=NZ, ou=Massey University, ou=Riddet Institute, email=A.M.YE@massey.ac.nz Reason: I am approving this document Date: 2025.01.22 10:06:16 +13'00'

This form should be placed at the beginning of each relevant thesis chapter.

[1] Refer to the Massey University Publishing and Authorship guidelines (OneMassey for staff, Stream for students) and/ or Contributor Roles Taxonomy (CRediT) guidelines for guidance.

Chapter 6 Impact of various physical treatments on physicochemical and microstructural characteristics of vegetable oil-based whipped cream stabilised by faba bean protein isolate[5]

Abstract

In this study, faba bean protein isolate (FPI) aggregates, prepared through various treatments including conventional heating (CH), ultrasonication (US), and thermosonication (TS), were used to formulate plant-based whipped creams. The objective is to develop a clean-label and dairy-free whipped cream using vegetable oil and plant proteins. The effects of these treatments on the characteristics of FPI aggregates and the oil-in-water (O/W) emulsions made from them, both before and after whipping, were evaluated. Among the different treatments, TS was the most effective at denaturing and unfolding FPI molecules, resulting in the formation of extended, strand-like aggregates with the highest surface hydrophobicity and solubility. These strand-like aggregates, potentially formed by disulfide bonds, were confirmed through sodium dodecyl sulphate-polyacrylamide gel electrophoresis (SDS-PAGE). In contrast, untreated and CH-treated FPI samples formed large aggregates with low solubility and surface hydrophobicity. Moreover, emulsions stabilised by TS-treated FPI exhibited the smallest oil droplet size and the greatest mechanical strength, leading to superior whipping performance, with the highest overrun and lowest serum release. The strand-like aggregates formed by TS had a higher aspect ratio than the particle aggregates, facilitating better interfacial absorption, coverage, and the formation of a network structure. This enhanced the entrapment and stabilisation of air bubbles, contributing to improved whipping capability and stability. This study highlights TS-treated FPI as a promising ingredient for formulating plant-based whipped creams and aerated emulsions. Future research could explore other plant protein ingredients and improving organoleptic properties of plant-based whipped creams such as mimicking milk fat's melting behaviour.

Keywords: Faba bean protein isolates; Thermosonication; Plant-based whipped cream; O/W emulsions; Rheology; Microstructure

[5] This chapter has been published as Hu, Y., Cheng, L., & Yang, Z. (2025). Impact of various physical treatments on physicochemical and microstructural characteristics of vegetable oil-based whipped cream stabilised by faba bean protein isolate. *Food Hydrocolloids, 163*, 111084.

Graphic abstract

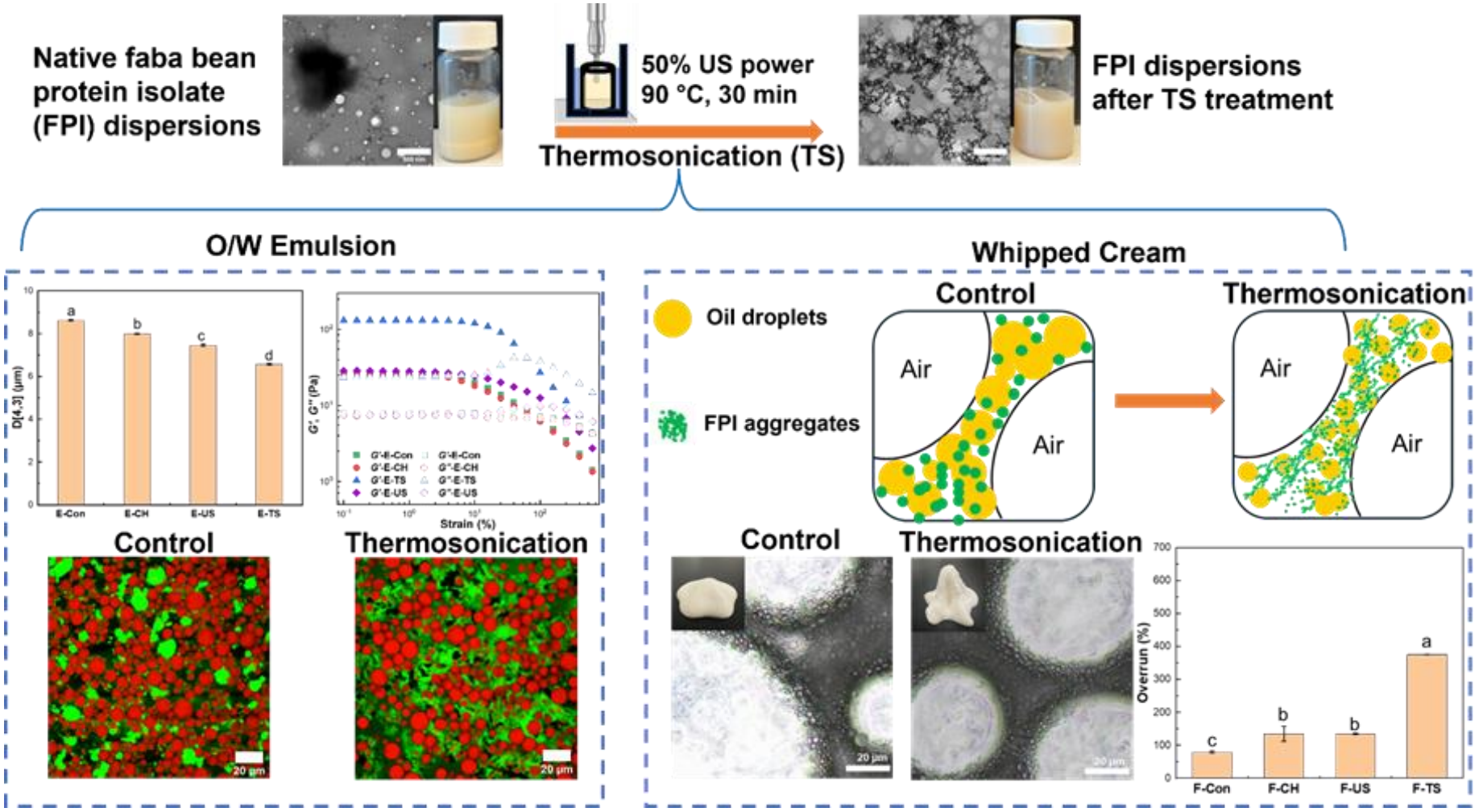

6.1 Introduction

Whipped cream, traditionally made from oil-in-water (O/W) emulsions containing 30-40% oil, such as hydrogenated vegetable oil cream and milk fat cream, is a popular food product (Fu, et al., 2020). However, it may not be suitable for vegetarians or individuals with lactose intolerance or dairy allergies (Fu, et al., 2020). In addition, many vegetable fat-based whipped creams are manufactured using hydrogenated vegetable oil, such as hydrogenated palm kernel oil (Zhang, et al., 2024), which contains trans fats and saturated fats. These components can negatively impact consumer health, increasing the risk of heart disease, cancer and type II diabetes (Islam, et al., 2019; Shin, et al., 2021). To address these concerns, there is a need to develop plant-based cream using plant proteins as surfactants and non-hydrogenated vegetable oils (Wang, Ma, et al., 2022).

In recent years, considerable efforts have been devoted to developing vegan whipping cream using plant protein ingredients such as soybean protein hydrolysates (Fu, et al., 2020), mung bean proteins (Wei, et al., 2023), faba bean proteins (Zhang, et al., 2024), and kidney bean proteins (Wu, Zhang, et al., 2023). However, in most previous studies, small molecules surfactants such as sucrose ester and monoglycerides of fatty acids were usually added to improve emulsification and whipping performance (Wu, Zhang, et al., 2023; Zhao, et al., 2013). In addition, complicated protein modifications such as fibrillation and extreme pH shifting were usually employed. The use of such additives and chemicals is not favourable for consumers, who increasingly prefer clean label products.

As one of the most widely consumed pulses in the world, faba bean (*Vicia faba*) has a high protein content ranging from 27-36 wt% (Augustin & Cole, 2022). Due to its balanced amino acids profile and high nutritional quality, faba bean protein has increasingly been used as a food ingredient in various food products, including beverages (Gumus, et al., 2017a), pasta (Rosa-Sibakov, et al., 2016), and gluten-free biscuits (Schmelter, et al., 2021). However, like many other plant protein isolates, faba bean protein isolates (FPI) usually exhibit inferior technofunctional properties, such as solubility, emulsification and foaming ability, limiting their applications in stabilisation of emulsions and foams (Schwenke, 2001; Tamang, et al., 2021). To address these

limitations, extensive efforts have been made to improve technofunctional properties of FPI using various modification strategies, including ultrasonication (Adal, 2024), heat treatment (Hu, et al., 2023), pH shifting (Zhou, et al., 2019), and transglutaminase induced microparticulation (Zhang, et al., 2024), and enzymatic hydrolysis (Nivala, et al., 2021). Among these methods, physical modifications that are not based on chemicals or enzymes stand out due to ease of operations and cost-effectiveness (Asioli, et al., 2017). However, current physical modification methods for plant proteins have several shortcomings. For instance, high hydrostatic pressure (HHP) treatment usually induces the formation of large protein aggregates, reducing solubility and limiting their use in emulsification and foaming (Avelar, et al., 2021; Luo, et al., 2021). Conventional heat treatment requires prolonged exposure of proteins at high temperatures, which lacks scalability for industrial applications (Hu, Cheng, Gilbert, Loo, et al., 2024). In addition, ultrasonication treatment alone is often inefficient to effectively modify protein structures for enhanced functionality (Zhong & Xiong, 2020).

Thermosonication (TS) is an emerging technology that effectively modifies protein conformation by harnessing the synergistic effects of heat energy and cavitation generated by ultrasonication (Chen, Ettelaie, et al., 2019; Zhong & Xiong, 2020). In our previous studies, TS treatment (90 °C, 10-30 min, pH 7) significantly enhanced the techno-functional properties (e.g. solubility and emulsification capability) of FPI. This improvement was attributed to the formation of amorphous protein aggregates with high content of β-sheet structures (Hu, Cheng, Gilbert, Lee, et al., 2024). However, the application of TS treated FPI in aerated emulsion systems such as whipped creams, has not yet been explored.

This study investigated the effects of different physical treatments namely conventional heat treatment (CH), ultrasonication (US), and thermosonication (TS) on the structural and technofunctional properties of FPI. FPI that did not undergo any treatment was used as a control. These treated and untreated FPI were solely used as surfactants to formulate emulsions and whipped cream. The quality of whipping creams was assessed by analysing oil droplet size, rheological properties, microstructures and whipped properties. Additionally, factors such as protein concentrations and oil droplet sizes in relation to whipping performances were also considered. The overall goal of this work

is to develop an efficient protein modification method for producing clean-label, plant-based whipped creams using plant-derived protein ingredients.

6.2 Materials and methods

6.2.1 Materials

The FPI used in this research was obtained from NZ Protein Inc. (Auckland, New Zealand) with a composition of 85 wt% protein, 5.4 wt% fat, and 1 wt% carbohydrate and dietary fibre. Corn syrup was purchased from Davis Food Ingredients, New Zealand. Soybean oil (Pams, New Zealand) and dairy-based full fat cream containing 2.2% protein and 36% fat (Meadow Fresh, New Zealand) were purchased from the same local supermarket (Pakn'Save, Albany, New Zealand). The chemicals used were of analytical grade and obtained from Sigma-Aldrich (St. Louis, MO, USA), including sodium dodecyl sulfate (SDS), Fast Green, Nile Red, acetic acid, HCl, and sodium azide. Xanthan gum and locust bean gum (LBG) were purchased from Hawkins Watts (Auckland New Zealand). Staining solution (Coomassie Brilliant Blue R-250), β-mercaptoethanol, and 10× Tris/Glycine/SDS running buffer were bought from Bio-Rad (Hercules, CA, USA). Milli-Q water (Millipore, USA) was used for preparing all samples.

6.2.2 Preparation of FPI dispersions

A 5wt% FPI stock solution was prepared by dispersing FPI powder into Milli-Q water containing 0.04% sodium azide under magnetic stirring at 20 °C and 300 rpm for 24 h to ensure full hydration. The pH of the dispersion was adjusted to 7 by using 1 M HCl and stirred continuously for an additional 24 h. During this time the pH values were checked and readjusted every 4 h until stabilisation was achieved. After preparation, the stock solution of FPI was stored at 4 °C and utilised within one week. FPI solutions at 1 wt% and 3 w % were prepared by diluting the 5 wt% FPI stock solution with Milli-Q water at pH 7.

6.2.3 Treatments of FPI dispersions

The thermosonication procedure was adapted from our previous work (Hu, Cheng, Gilbert, Lee, et al., 2024). FPI dispersions (200 g, 5 % wt, pH 7) prepared as described in **Section 6.2.2** underwent thermosonication for 30 min (TS) using a 20 kHz

ultrasonicator (JY92-IIN, Ningbo Scientz Biotechnology Co., Ltd, China, dial power 950 W) equipped with a 6 mm horn and 50% power amplitude. The pulse durations were set to 30 s on and 30 s off. FPI dispersions (200 mL) were thermosonicated at 90 °C for 30 min in a 200 mL reagent bottle within in a 1 L jacketed bottle (Shanghai Leigu Instrument Ltd, China) connected to a temperature-controlled water bath (Thermofisher, USA). The samples were restored to their original weight with Milli-Q water (pH 7) to compensate for water loss due to evaporation during the treatment. Each sample was prepared in duplicate and stored at 20 °C for 24 h prior to analysis. To study the effect of FPI concentration, TS treated FPI dispersions at 1wt% and 3wt% were prepared by diluting the 5wt% FPI dispersion with Milli *Q* water (pH 7) containing 0.04 wt% sodium azide. To study the effects of heat treatment and ultrasonication alone, ultrasonication (US) was conducted for samples incubated in an ice-water bath for the same duration as thermosonication, with the highest temperature measured recorded during US treatment being below 30 °C. Conventional heat treatment (CH) was performed following the method of Wynnychuk, et al. (2021) and Hu, Cheng, Gilbert, Lee, et al. (2024) with slight modifications. In this process, FPI solutions (5 wt %, pH 7) were heated in an air oven (Thermofisher, USA) at 90 °C for 1 h (CH). FPI dispersions without any treatments were used as the control samples (Con).

6.2.4 Physicochemical characterisations of FPI dispersions

6.2.4.1 Sodium dodecyl sulphate–polyacrylamide gel electrophoresis (SDS-PAGE)

SDS-PAGE analyses under both reducing and non-reducing conditions were carried out according to the method described by Laemmli (1970). A commercial precast Mini-protein TGX (Tris/Glycine) gel from Bio-Rad (USA) was used, which consisted of a 4% stacking gel and a 15% resolving gel. The electrophoresis running buffer was diluted ten times with Milli-Q water from 10× Tris/Glycine/SDS running buffer (Bio-Rad). Electrophoresis was performed at 130 V for 60 min. Subsequently, the gels were stained for 45 min using Coomassie Brilliant Blue R-250 (Bio-Rad), followed by shaking in a destaining solution that contained 10% isopropanol and 10% glacial acetic acid in Milli-Q water. The destaining solution was replaced every 2 h until the gel background was transparent, then the gel was preserved in Milli-Q water at 4 °C. Protein bands were identified by commercial protein standards that span a molecular weight range from 10

to 250 kDa (Precision Plus Protein Dual Xtra Prestained Standards, Catalog #1610377, Bio-Rad, USA). The gels were imaged using a ChemiDoc XRS system (Bio-Rad, USA).

6.2.4.2 Visual appearance of FPI dispersions

To visually examine the FPI dispersions following different treatments, glass vials containing both control and treated FPI dispersions (5 wt %) were photographed after being stored at room temperature (~20 °C) for 12 h.

6.2.4.3 Determination of FPI particle size

According to Luo, Yang, et al. (2022), the particle size (hydrodynamic diameter Z-average) of control and treated FPI dispersions (5 wt %) was measured by dynamic light scattering (DLS) using a ZetaSizer Nano ZS instrument (Malvern Instruments, UK) at 20 °C. The device was configured with a scattering angle of 173° and a wavelength of 633 nm. Prior to measurement, the FPI dispersion was diluted 150 times with Milli-*Q* water containing 0.04 wt% sodium azide (pH 7). The refractive index and viscosity settings for water were set at 1.33 and 0.89 mPa·s, respectively (Luo, Yang, et al., 2022). Each sample was determined in triplicate, with results reported as the Z-average size.

6.2.4.4 Determination of FPI dispersions solubility

The solubility of FPI dispersions (5 wt %) following different treatments was assessed based on the method of Hu, et al. (2023), with slight modifications. The FPI dispersions were centrifuged at 3000 × *g* for 15 min using a benchtop centrifuge (Thermofisher 3000, MO, USA) at room temperature (~20 °C). Following centrifugation, the soluble protein content in the supernatant was determined using a Bradford Protein Assay Kit (Sigma-Aldrich, St. Louis, MO, USA) using Gamma-globulin as standard. The absorbance of soluble protein at 595 nm was determined using a UV-Vis spectrophotometer (Shimadzu 3000, Kyoto, Japan). The solubility (%) was calculated using the Eq. (6.1):

$$\text{Solubility (\%)} = \frac{\text{Protein content in the supernatant (mg/mL)}}{\text{Total protein content before centrifuge (mg/mL)}} \times 100\% \quad (6.1)$$

6.2.4.5 Determination of surface hydrophobicity

The surface hydrophobicity of control and variously treated FPI dispersions (5 wt %) was measured by fluorescence spectrophotometry according to Luo, Cheng, et al. (2022) with slight modifications. The 8-anilino-1-naphthalene sulphonate (ANS) was used as a fluorescence probe. FPI dispersions (5 wt %) were individually diluted to concentrations of 125, 250, and 500 μg/mL using a 10 mM Tris-HCl buffer (pH 7). Subsequently, 50 μL of an 8.0 mM ANS solution was blended with the aliquots FPI solution (3 mL) and incubated in the dark for 20 min at ~20 °C. Fluorescence measurements were conducted using a fluorescence spectrophotometer (Shimadzu RF-6000, Shimadzu, Kyoto, Japan) at an emission wavelength of 470 nm (emission) and an exciting wavelength of 390 nm (excitation), with a slit width set at 5 nm. The fluorescence intensities, after the subtraction of background levels (FPI samples without ANS), were graphed against the FPI concentrations. The initial slope derived from linear regression analysis was employed as the index of surface hydrophobicity (H_0) (Kato & Nakai, 1980).

6.2.4.6 Negative staining transmission electron microscopy (TEM)

The microstructures of FPI before and after various treatments were observed using negative staining TEM according to our previous study with slight modifications (Hu, Cheng, Gilbert, Loo, et al., 2024). Various FPI dispersions (5 wt %) were first diluted to a 0.05 wt % concentration using Milli-Q water (pH 7), followed by placing 20 μL of the diluted sample onto a formvar-coated copper TEM grid. The sample was then stained with 2% uranyl acetate for 3 min. Excess stain was washed off by 20 μL Milli-Q water for an additional 3 min. After washing, excess liquid was absorbed from the grid using filter paper. The micrographs of the samples were captured by a Philips electron microscope (NL-5600 MD, Philips, Eindhoven, The Netherlands) at an acceleration voltage of 60 kV.

6.2.5 Formation and characterisation of FPI stabilised cream emulsions

6.2.5.1 Preparation of cream emulsions

The recipe of all cream emulsions consisted of 30% (v/v) soybean oil, 15 wt% corn syrup, 0.1 wt% xanthan gum, 0.05 wt% locust bean gum (LBG), and FPI after various treatments (Con, CH, US, and TS at 5wt%) or TS treated FPI at various concentrations

(1 wt%, 3 wt%, and 5 wt%). Firstly, various FPI solutions were mixed with corn syrup, xanthan gum, and LBG under magnetic stirring at 300 rpm for 3 h. Then, the oil was slowly added to the aqueous phase and oil-water mixture was homogenised using a high shear mixer (T10 basic ULTRA-TURRAX®, IKA Corp., Staufen, Germany) equipped with a 10-mm probe (S10N-10G, IKA, Germany) at 20,000 rpm for 2 min. All cream emulsions were aged in the refrigerator at 4 ℃ for 12 h before further analysis.

6.2.5.2 Determination of oil droplet sizes

The average particle size and particle size distribution (PSD) of cream emulsions were measured by a static laser light scattering method using a Mastersizer instrument (Mastersizer 3000, Malvern Instruments Ltd, Worcestershire, UK) (Hu, et al. (2023)). The refractive indices used for soybean oil and dispersant were 1.47 (Hu, Cheng, Gilbert, Lee, et al., 2024) and 1.33 (Milli-*Q* water), respectively. The emulsions were dispersed in a 1% v/v SDS solution at a weight ratio of approximately 1:20 and incubated overnight at room temperature (~20 ℃) before measuring particle size. This step was taken to displace the protein particles from the oil-water interface and breakup the oil droplets flocs (Péron, et al., 2007). The volume mean diameter (D [4, 3]) was used to represent the average diameter of oil droplets in emulsions.

6.2.5.3 Microstructures of emulsions

Confocal laser scanning microscopy (CLSM) was employed to observe the microstructure of cream emulsions. Protein was stained by Fast Green (1% w/v) and oil phases were stained by Nile Red at ratios of 500:1 (v/v) and 5000:1 (v/w), respectively (Hu, et al., 2023). After emulsion preparation, aliquots of the samples were positioned on a cavity slide covered with a coverslip and sealed with nail polish to prevent evaporation. The emulsions were observed using a confocal laser scanning microscope (Leica DM 6000B, Germany), equipped with an oil immersed 100× objective lens, using a 633 nm laser wavelength for Fast green and 561 nm laser wavelength for Nile red. Images obtained from CLSM were analysed and processed using Image J software (NIH, MD, USA).

6.2.5.4 Flow behaviour of cream emulsions

The viscosities of various cream emulsions stabilised by FPI were analysed by a stress-

controlled rheometer (DHR-3, TA instruments, USA) with a 40 mm parallel plate geometry, and the gap was set to 1 mm. The emulsions were transferred onto the bottom plate of the rheometer using a plastic spatula. Excess samples were carefully trimmed when necessary. The viscosity measurements were performed by applying a shear rate sweep from 0.1 to 1000 s^{-1}. All measurements were performed at least twice at 4 °C to be in line with the storage conditions of cream emulsion in the food industry (Wu, Zhang, et al., 2023).

6.2.5.5 Small and large oscillatory deformation rheology

The viscoelasticity properties of cream emulsions were determined by the same rheometer and geometry as described in **Section 6.2.5.3**. The rheological properties measurements were performed in accordance with the following protocol. A time sweep measurement was conducted over 120 s at a strain of 1% and a frequency of 1 Hz to structurally recover the samples at 4 °C. Afterwards, a frequency sweep was performed ranging from 0.5 to 10 Hz frequency at 0.1% strain to probe the viscoelasticity of the emulsion network. Finally, a strain sweep test was performed from 0.01 to 1000 % strain amplitude at a constant frequency (1 Hz). Storage modulus (G') and loss modulus (G'') were recorded throughout the test at 4 °C (Hu, et al., 2023).

6.2.6 Formation and characterisation of whipped creams

6.2.6.1 Preparation of whipped creams

Cream whipping was performed according to n Blankart, et al. (2021) with slight modification, using a 250 mL Gourmet Whip Dispenser (iSi, Vienna, Austria) charged with nitrous oxide (N_2O) capsules (iSi, Vienna, Austria, 7.5 g N_2O per capsule). Approximately 250 g of emulsion or dairy cream was added to the metal canister, and after securing the lid and spout, the system was equilibrated at 4 °C for 15 min in a refrigerator (Fu, et al., 2020). A single nitrous oxide capsule was then injected, and the metal canister was thoroughly shaken by hand before dispensing the whipped cream.

6.2.6.2 Visual appearance of whipped creams

The whipped cream was sprayed onto a black PVC paper board by holding the canister head at a 90° angle and pressing the lever halfway through a straight nozzle. Then The appearance of whipped cream was then photographed at room temperature (~20 °C).

6.2.6.3 Determining the cream overrun

Overrun was determined following the method of Wu, Zhang, et al. (2023) and Scurlock (1986) with slight modifications. It was performed by filling a PET container (50 mm × 50 mm × 100 mm) to a set volume (100 mL) with the whipped cream. The overrun was determined by the ratio of the wight of 100 mL cream emulsions before (W_1) and after whipping (W_2), It was calculated using the following equation (Eq. 6.2):

$$\text{Overrun (\%)} = \frac{W_1 - W_2}{W_2} \times 100\% \quad (6.2)$$

6.2.6.4 Rheological measurements of whipped cream

The viscosity and viscoelasticity measurements of whipped cream were performed following the similar procedure outlined in the **Section 6.2.5.2**. Data were collected at 20 °C. Viscosity measurements were performed at a shear rate sweep ranging from 0.1 to 1000 s^{-1} at 20 °C. Storage (G') and loss moduli (G'') were recorded throughout a frequency sweep (0.5 to 10 Hz) at a fixed strain (0.2 %). Subsequently, a strain sweep test was conducted, varying the strain amplitude varied from 0.1 to 1000% at a fixed frequency (1 Hz).

6.2.6.5 Microstructures of whipped creams

The microstructure of whipped creams was observed using an optical microscope (BX53, Olympus, Japan) equipped with a ×40 objective lens. The cream samples were gently placed on a microscope slide and covered with cover slips. Observations were performed in triplicate, and representative images selected for analysis. Optical light microscopy images were processed by Image J software (NIH, MD, USA).

6.2.6.6 Stability of whipped cream during storage

Whipped cream stability was determined according to Rezvani, et al. (2020). The whipped cream sample (~10 g) was transferred into a funnel (5 mm inner diameter × 10 mm outer diameter) at the room temperature (~20 °C) for up to 2 h. A graduated cylinder was used to collect the serum at 15, 30, 25, 60, 90, and 120 min. The weight of liquid drained under gravity was determined. Syneresis was calculated using Eq. (6.3):

$$\text{Syneresis (\%)} = \frac{\text{Weight of serum collected (g)}}{\text{Weight of initial whipped cream (g)}} \times 100\% \qquad (6.3)$$

6.2.7 Statistical analysis

All experiments were performed in duplicate or more, and results are reported as mean values with standard deviation (SD). Data analysis was carried out from Minitab statistical software (Minitab 19 Statistical Software, USA). A one-way analysis of variance (ANOVA) was conducted to identify differences, followed by Tukey's test, at a significance level of $P < 0.05$.

6.3 Results and discussion

6.3.1 FPI protein profiles revealed by SDS-PAGE

Protein profiles of FPI before and after various treatments are revealed by SDS-PAGE under both non-reducing and reducing conditions (**Fig. 6.1**). Under non-reducing conditions, native (FPI) shows two predominant protein bands with a molecular weight of ~70 kDa and ~50 kDa; corresponding to convicilin and vicilin, respectively. This finding agrees with previous studies, indicating the typical FPI protein profiles (Berrazaga, et al., 2019; Hu, et al., 2023). For all FPI samples particularly CH and TS treated ones, a profound and smeared protein band can be observed in the loading wells, which could be attributed to the large protein complexes with greater molecular mass (>250 kDa) (Kaspchak, et al., 2017). In addition, compared to native FPI, TS treatment significantly reduced densities of protein bands in the ~50 to ~70 kDa range, indicating substantial intermolecular bonds formation (Luo, et al., 2021; Zhong & Xiong, 2020), which agrees with a previous study (Hu, Cheng, Gilbert, Lee, et al., 2024).

Under reducing conditions, after adding β-mercaptoethanol to break the disulfide bonds, large protein aggregates in the loading wells disappeared. This suggests that a significant proportion of these aggregates particularly in CH and TS samples were formed through disulfide linkages (Wright & Boulter, 1974). In addition, α-legumin and β-legumin, with molecular weights of approximately 37 kDa and 20 kDa, were observed in all FPI samples. This finding aligns with a previous study showing that legumin subunits in FPI consist of α- and β-type subunits, which associate through disulfide bonds (Wright & Boulter, 1974). On the other hand, the bands of convicilin at

~70 kDa and vicilin at ~50 kDa remained unchanged under the reducing condition. Notably, all FPI dispersions displayed similar protein profiles under reducing conditions, both before and after treatments. This observation is consistent with previous studies on FPI involving TS, US, and CH treatments (Alavi, Chen, & Emam-Djomeh, 2021; Hu, Cheng, Gilbert, Lee, et al., 2024).

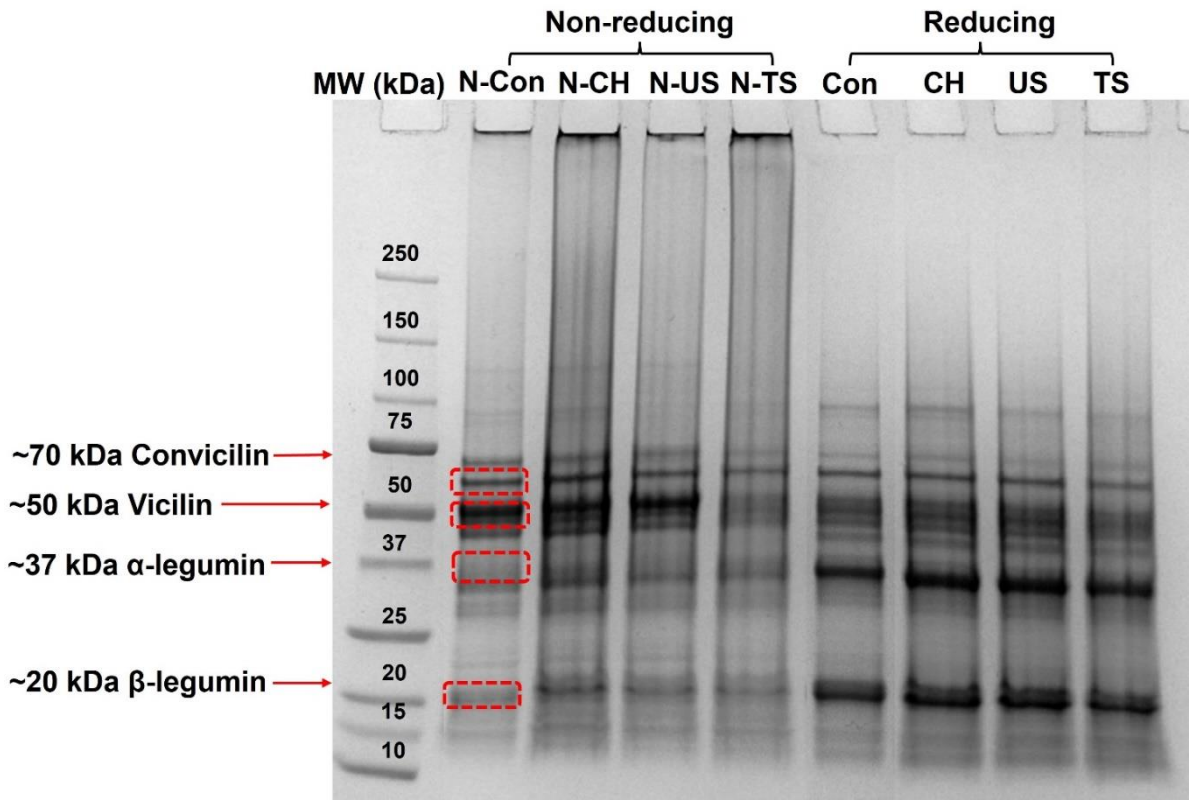

Fig. 6.1 SDS-PAGE patterns of faba bean protein isolates (FPI) dispersions at pH 7 before and after conventional heat treatment (CH), ultrasonication (US) (30 min), and thermosonication (TS) (30 min) under non-reducing and reducing conditions.

6.3.2 Effect of CH, US, and TS treatments on physicochemical properties of FPI dispersions

6.3.2.1 Visual appearance

The visual appearance of the FPI dispersions (5 wt %) after before and after various treatments is shown in **Fig. 6.2A**. It can be seen that the control and CH-treated samples had significant sedimentation at the bottom of glass vials, which was indicated by the red arrow (**Fig. 6.2A**). The presence of large protein aggregates in plant protein dispersions has been extensively reported (Luo, Cheng, et al., 2022). This aggregation is likely a result of the protein extraction process, which typically involves involving isoelectric point precipitation followed by alkaline extraction, leading to protein aggregation (Yang, et al., 2024). In addition, heat treatment could induce formation of denatured insoluble large protein aggregates due to the unfolding and aggregation of FPI when exposed to temperatures higher than its denaturation temperature (~77–85 °C) (Jiang, et al., 2016). After US and TS treatment for 30 min, the sedimentation in the FPI dispersions became undetectable. This could be because large FPI aggregates were disrupted into small particles, which then reaggregated to form soluble aggregates (Ryan & Foegeding, 2015; Zhong & Xiong, 2020).

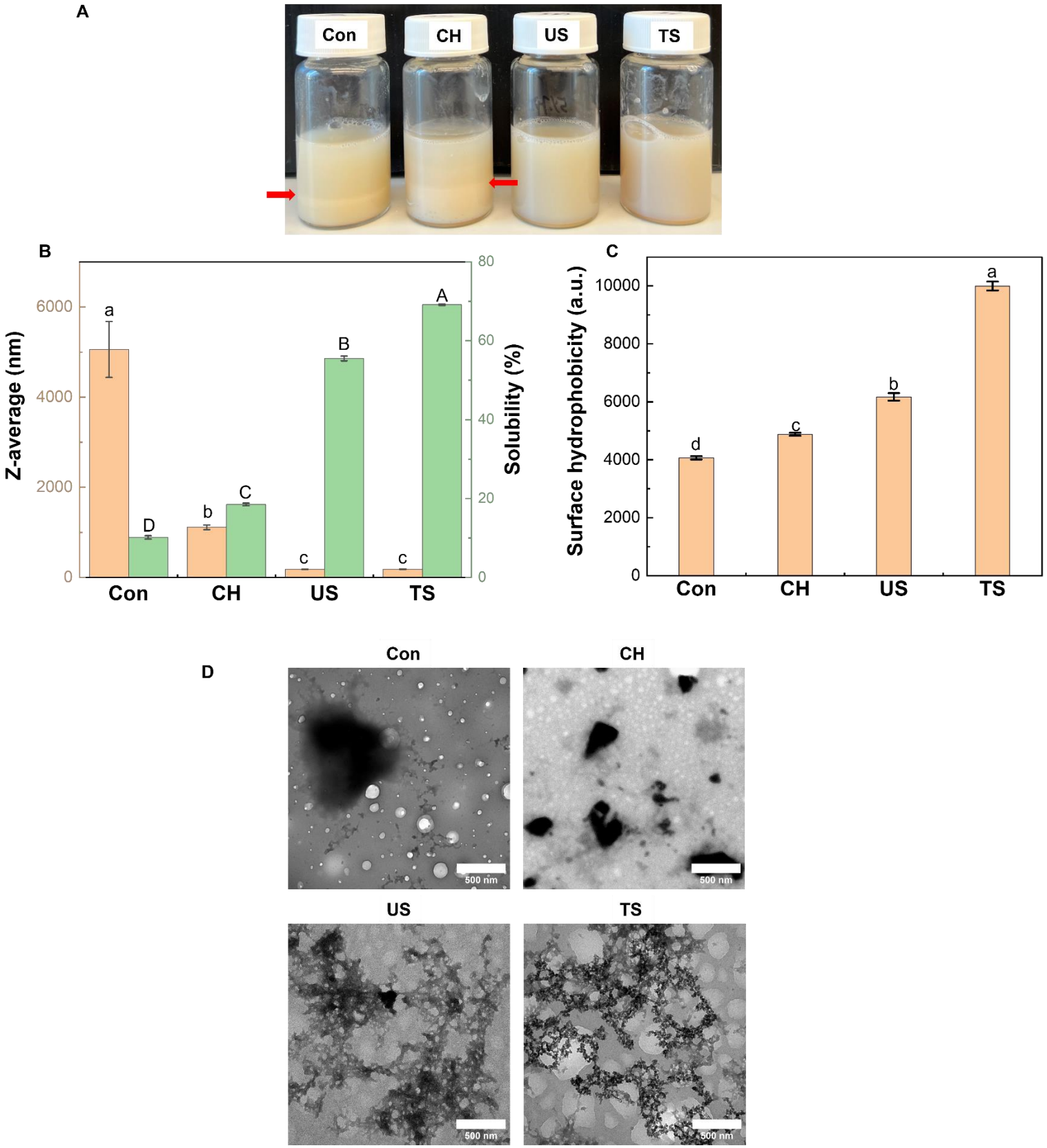

Fig. 6.2 (A) Visual appearance of 5 wt % faba bean protein isolate (FPI) samples before and after conventional heat treatment (CH), ultrasonication (US), or thermosonication (TS) at pH 7. (B) Particle size (Z-average) and solubility of control and CH-, US-, or

TS-treated FPI dispersions at pH 7. (C) Surface hydrophobicity of control and CH-, US-, or TS-treated FPI dispersions at pH 7. (D) TEM images of control and CH-, US-, or TS-treated FPI dispersions at pH 7 (scale bar: 500 nm). In B and C, different letters above the columns indicate significant differences ($P < 0.05$).

6.3.2.2 Particles sizes and solubilities of FPI after treatments

Fig. 6.2B shows the particle size and solubility of FPI dispersions before and after CH-, US-, and TS-treatment (5 wt %, pH 7). Overall, the control sample exhibited the largest particle size (~5057 nm) and the lowest solubility (~10.2%) compared to other samples. This finding is consistent with previous studies, indicating that native (untreated) plant proteins typically exhibited the largest particle size and lowest solubility. Similar findings have been reported in other native plant protein isolates such as quinoa protein isolates (QPI) (Luo, Yang, et al., 2022) and FPI (Hu, Cheng, Gilbert, Lee, et al., 2024). FPI dispersions after CH treatment showed a reduced particle size, decreasing from ~5057 to ~1114 nm) (**Fig. 6.2B**). This reduction could be attributed to the partial protein dissociation at high temperatures, as reported in soybean protein isolate (SPI) (90 °C for 20 min) (O′ Flynn, et al., 2021) and egg white proteins (Sponton, et al., 2017) after heat treatment at 80 °C for 5-20 min. US treatment resulted in a significant reduction in particle size, decreasing from ~5057 nm (Control) to ~180 nm (US). Similarly, TS treatment reduced FPI particle sizes to ~185 nm (TS) at pH 7 (**Fig. 6.2B**), which is the smallest particle size among all treatments. This reduction can be attributed to the disruption of certain protein interactions such as hydrophobic interactions and hydrogen bonds, during sonication and/or the combination of heating and sonication, leading to smaller particle size (Frydenberg, et al., 2016; Zhu, et al., 2023).

As for the solubility, the CH-treated FPI samples exhibited an increased in solubility to ~19% (**Fig. 6.2B**), which aligns well with the particle size results for the CH samples. This finding is also consistent with a previous study on heat treatment of FPI at pH 7 (Hu, Cheng, Gilbert, Lee, et al., 2024). The increase in solubility could be due to the reduction in protein particle size and alterations in various non-covalent and covalent interactions after CH treatment, which impacted protein conformations and their hydration ability (O′ Flynn, et al., 2021; Zhao, et al., 2020). In addition, the solubility of FPI dramatically increased from ~10% (Con) to ~56% (US) and ~69% (TS) (**Fig. 6.2B**). The reduction in particle sizes after sonication, as discussed earlier, would also result in larger surface areas for water accessibility, contributing to the increased solubility (Luo, Yang, et al., 2022). Regarding the highest solubility observed with TS treatment, Jiang, et al. (2017) suggested that this enhancement in protein solubility was due to TS facilitating the formation of more hydrogen bonds between water and protein

molecules, further improving protein solubilisation. In general, the TS treatment which, synergistically combines effects of thermal energy input and ultrasound induced cavitation is the most effective in modification FPI dispersions.

6.3.2.3 Surface hydrophobicity

The surface hydrophobicity of proteins is an important characteristic related to their stability, conformation, emulsifying and foaming abilities (Kato & Nakai, 1980). Therefore, the surface hydrophobicity of untreated (Con), CH-, US- and TS-treated FPI samples were determined, and results are shown in **Fig. 6.2C**. Compared to the control sample, surface hydrophobicity increased significantly after the various treatments, rising from ~4067 to ~4879 after CH, ~6170 after US, and ~9996 after TS. CH treatment could lead to an increase in surface hydrophobicity due to the unfolding proteins and limited exposure of hydrophobic groups (Voutsinas, et al., 1983; Zhao, et al., 2020). Similar findings have been reported in previous studies on soybean proteins (Wang, et al., 2014) and pea proteins (Hall & Moraru, 2021). FPI samples after US exhibited the second largest increase in surface hydrophobicity, likely due to exposure of hydrophobic groups and the enhanced solubility (Hernoux Villière, et al., 2013; Hu, Wu, et al., 2013; Jiang, et al., 2017). Among all treatments, the TS treated samples showed the most significant increase in surface hydrophobicity, which can be attributed to the substantial exposure of interior hydrophobic groups of FPI after TS treatment due to the smallest particle size (Hernoux Villière, et al., 2013; Hu, Cheng, Gilbert, Lee, et al., 2024). Similar results have been reported in previous studies, such as mung bean proteins after TS treatment at pH 7 (Zhong & Xiong, 2020).

6.3.2.4 Morphology of FPI aggregates as revealed by TEM

TEM images of untreated (Con) and treated FPI (US, CH, or TS) samples are shown in **Fig. 6.2D**. The native FPI samples (Con) displayed submicron-scale particle aggregates. After CH treatment, FPI formed slightly smaller but denser aggregates compared to the native state, which is consistent with the particle size results. Similar microstructures have been reported in FPI dispersions following CH treatment (Jo, et al., 2020). After US treatment for 30 min, the FPI aggregates appeared much smaller compared to both Con and CH samples, and the FPI protein network showed an extended structure. In the case of TS-treated FPI samples, the most expanded with strand-like interconnected

aggregate network was observed. According to Hu, Cheng, Gilbert, Lee, et al. (2024), TS treatment of FPI at pH 7 leads to the formation of amorphous aggregates with smaller sizes due to extensive FPI denaturation and aggregation, Additionally, FPI aggregates underwent structural rearrangement, forming amorphous aggregates with strand-like shapes (Chen, Ettelaie, et al., 2019; Kong & Yu, 2007).

6.3.3 Physicochemical properties of emulsions prepared from untreated and treated FPI

6.3.3.1 Oil droplet size distributions

Effects of different treatments

The oil droplet size distribution within emulsions is a critical factor that affects the stability, texture, and whipping performance of emulsified systems. **Fig. 6.3A** and **B** show the effects of various FPI treatments, at a fixed concentration of 5 wt%, on the oil droplet size distribution within cream emulsions. The D [4,3] value, representing the volume-weighted mean diameter, is the largest (~8.6 μm) in emulsions stabilised by native FPI (Control) at pH 7. This aligns with oil droplet size distributions in **Fig. 6.3B**, where the control sample exhibited a prominent peak at ~10 μm. CH treatment slightly reduced the D [4,3] to ~8.0 μm, while US- and TS-treated FPI significantly decrease the oil droplet size to ~7.5 μm and ~6.6 μm, respectively. This is consistent with the solubility and particle size results of FPI after various treatments (**Fig. 6.2B**), indicating that higher protein solubility with smaller particle size is strongly linked to the small oil droplet sizes of emulsions, reflecting better emulsification ability (Damodaran, 2017).

Similar correlations between plant protein solubility/particle size and emulsification capability have been observed in FPI (Hu, et al., 2023), quinoa protein isolates (QPI) (Zhang, Cheng, et al., 2021), pea globulins (Koyoro & Powers, 1987), and soy bean protein isolate (Liang & Tang, 2013). Protein with greater solubility and smaller particle sizes can migrate more quickly to the oil-water interface, reducing lower interfacial tension and resulting in smaller oil droplet sizes (Hu, et al., 2023; Zhu, Chen, et al., 2018). In addition to solubility, oil droplet size is also influenced by surface hydrophobicity of FPI. The surface hydrophobicity of proteins, which is linked to the exposure of hydrophobic amino acid residues at the oil-water interface, affects the

protein ability to absorb at the interface (Jiang, Cheng, et al., 2020). Indeed, the order of oil droplet sizes mirrors the surface hydrophobicity trends shown in **Fig. 6.2C**, suggesting a positive correlation between the surface hydrophobicity and protein emulsifying properties (Damodaran, 2017). Finally, the smallest oil droplet size observed in the emulsions stabilised by TS treated FPI can be attributed to its strand-like and extended microstructures. Previous emulsification studies on kidney pea protein fibrillar aggregates have also drawn similar conclusions (Wu, Zhang, et al., 2023).

Effects of FPI concentrations

As TS treatment exhibited the best emulsification performance among all treatments, the effects of FPI concentration on the oil droplet size distributions was further studied in TS samples, with results shown in **Fig. 6.3C and D**. The cream emulsion stabilised by 1 wt% FPI displayed a distribution with a predominant peak at ~11 μm. As the FPI concentration increased to 5wt%, the peaks progressively shifted towards smaller sizes of ~8 μm (**Fig. 6.3D**). **Fig. 6.3C** illustrates the changes in D [4,3] as a function of FPI concentration, indicating that higher concentrations result in smaller oil droplet sizes. Specifically, D [4,3] decreased from ~17.5 μm (1% FPI) to ~7.9 μm and ~7.5 μm as the FPI concentration increased from 3 wt% to 5 wt%.

The increase in protein concentration enhances the adsorption and surface coverage capabilities of proteins on oil droplets, contributing to the stabilisation of larger interfacial surface areas, which in turn reduces the oil droplets size (Sun & Gunasekaran, 2009). However, it is noteworthy of D [4,3] values only slightly decreased when the FPI concentration was increased from 3 wt% to 5 wt %. This suggests that the fact that FPI concentration (5 wt %) was nearly in excess at the O/W interface while stabilising the emulsion with oil volume fraction (ϕ) of 0.3, indicating TS-treated FPI was an effective emulsifier (Hu, Cheng, Gilbert, Lee, et al., 2024).

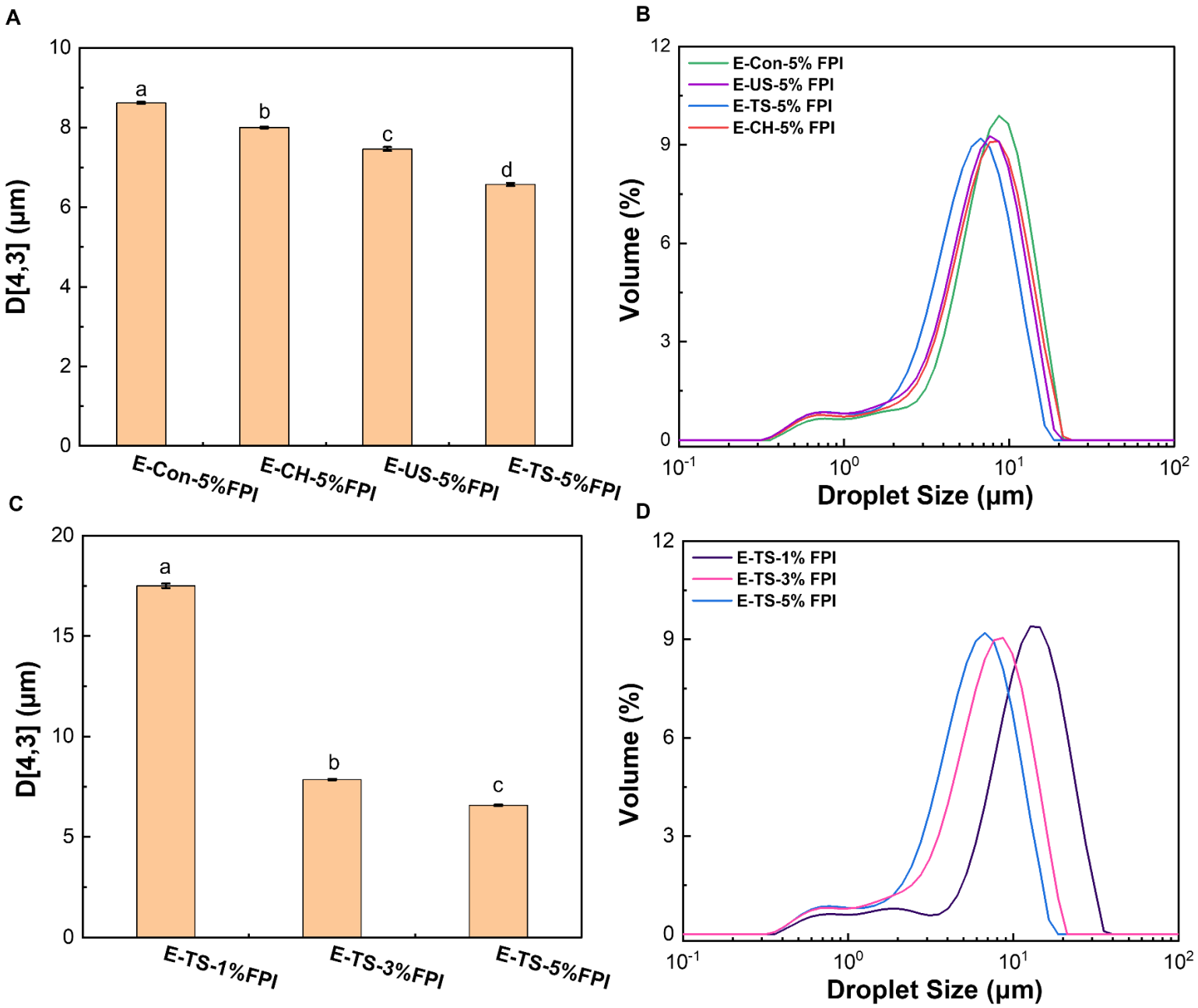

Fig. 6.3 Volume mean diameter (D [4,3]) of oil droplets (A) and oil droplet size distribution (B) in various cream emulsions stabilised by untreated and treated FPI. Volume mean diameter (D [4,3]) of oil droplets (C) and oil droplet size distribution (D) in various cream emulsions stabilised by TS treated FPI at different concentrations (1 wt%, 3 wt%, and 5 wt%). Different letters above the columns denote significant differences ($P < 0.05$) among cream emulsions stabilised by FPI after different treatments or concentrations. E-Con, E-CH, E-US, and E-TS represent the oil-in-water emulsions stabilised by FPI particles subjected to different physical treatments.

6.3.3.2 Microstructures of cream emulsions

Confocal laser scanning microscopy (CLSM) was used to observe the microstructures of cream emulsions stabilised by different treated FPI samples. Oil droplets and protein aggregates were stained as red and green, respectively as shown in **Fig. 6.4**. In native FPI-stabilised cream emulsions (**Fig. 6.4A**), it seems that oil droplets are stabilised by the absorbed FPI, and inhomogeneous protein aggregates are dispersed in the aqueous phase. This observation aligns well with a previous study (Hu, Cheng, Gilbert, Lee, et al., 2024). After CH treatment (**Fig. 6.4C**), larger protein aggregates appear between the oil droplets due to the denaturation and aggregation of FPI (Jiang, et al., 2016; Kimura, et al., 2008). Moreover, emulsions stabilised by US and TS treated FPI exhibited smaller oil droplet sizes, which agrees well with oil droplet size distribution results (**Fig. 6.3**). Among all the samples, the protein network structure in emulsions stabilised by TS treated FPI are the most continuous and homogenous, with small and uniform oil droplets embedded within it. This could be due to the denaturation, interactions, and entanglements of FPI aggregates after TS treatment, leading to a higher surface hydrophobicity in the aqueous phase and resulting in the bridging of FPI aggregates with oil droplets (Bai, et al., 2018; Mozafarpour, et al., 2022; Tang & Ghosh, 2021).

Regarding to TS treated FPI, the increasing FPI concentration from 1 wt% to 5 wt%) results in the formation of smaller oil droplets, which agrees with the oil droplet size results (**Fig. 6.3**). This observation is likely due to the higher protein concentration stabilising a larger interfacial area, resulting in smaller oil droplet size (Tang & Ghosh, 2021). The oil droplets also appear more compact and densely packed with higher FPI concentrations (**Fig. 6.4B, D and F**).

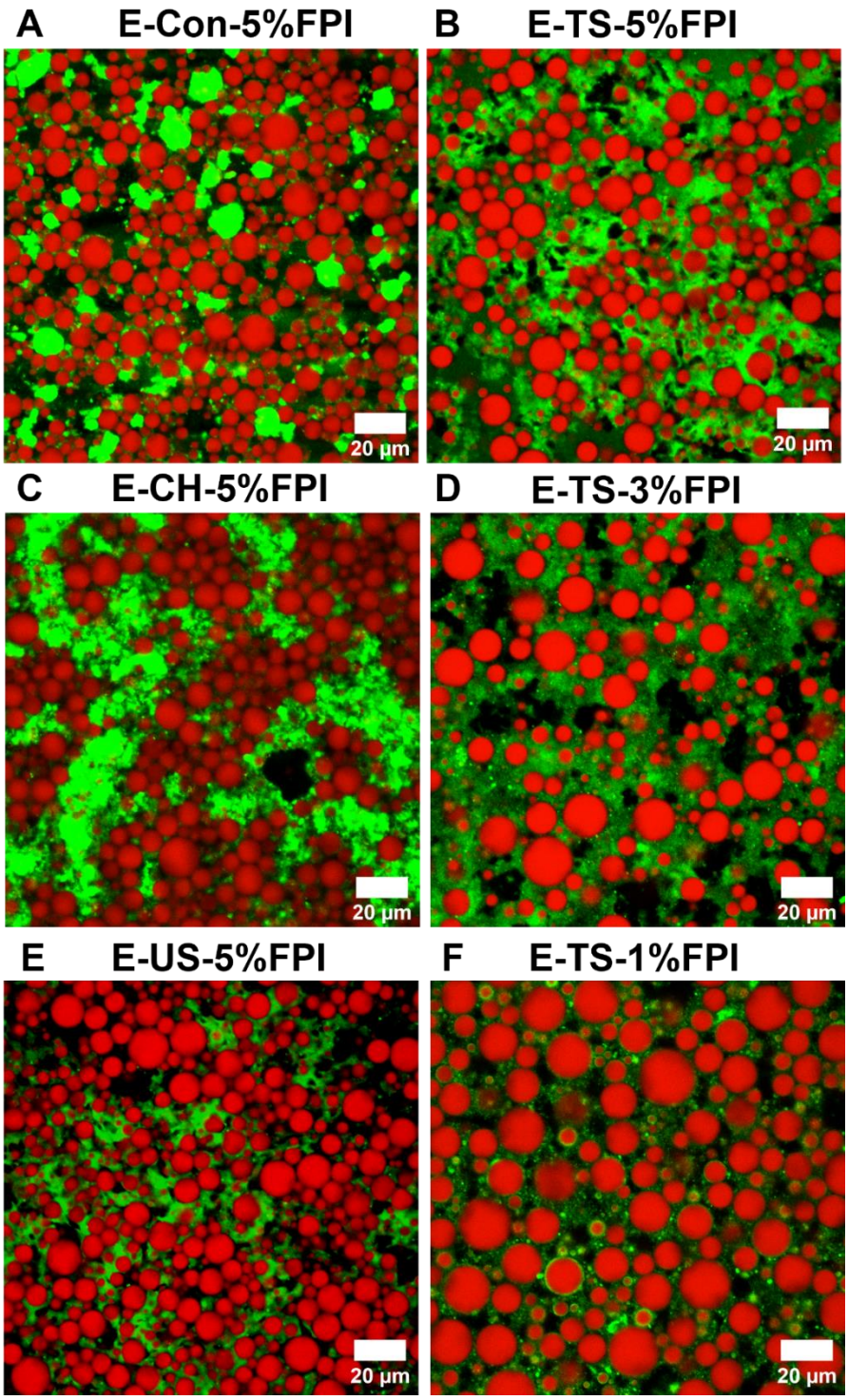

Fig. 6.4 Confocal micrographs of the cream emulsion samples stablised by (A, B, C, and E) differently treated 5 wt% FPI samples at pH 7; and (B, D, and F) cream emulsions stabilised by 1, 3, and 5 wt% of TS-treated FPI at pH 7. Scale bar = 20 μm). E-Con, E-CH, E-US, and E-TS represent the oil-in-water emulsions stabilised by FPI particles subjected to different physical treatments.

6.3.3.3 Apparent viscosity of cream emulsions

The measurement of apparent viscosity is crucial for characterising cream emulsions. For creating samples with a foamy texture, viscosity of plant-based cream emulsions must be reached at appropriate levels to effectively entrap air (Rezvani, et al., 2020). The viscosity of the cream emulsions is presented in **Fig. 6.5**. All cream emulsion samples exhibited shear-thinning behaviour, with viscosity decreasing as the shear rate increased. This behaviour has been widely observed in plant protein stabilised-cream emulsions, including soybean protein isolate (SPI) (Ningtyas, Bhandari, et al., 2021) and kidney bean proteins (Zhou, et al., 2019). As the shear rate increases, the greater hydrodynamic forces deform the flocs, leading a reduction in viscosity (Ningtyas, Bhandari, et al., 2021).

For better comparison of apparent viscosity among the cream emulsions, the apparent viscosity values at 1 s^{-1} are plotted in **Fig. 6.5B**. Emulsions stabilised by TS treated FPI exhibited the highest viscosity (~34 Pa·s), which could be due to its smallest oil droplet size and dense protein network formation in the aqueous phase promoted by entanglement of protein molecules. Cream emulsions stabilised by FPI after other treatments displayed significantly lower viscosities: ~4 Pa·s (Con), ~5 Pa·s (CH), and ~7 Pa·s (US) This finding aligns well with the results of oil droplet sizes and CLSM analysis (**Fig. 6.3 and 6.4**). In addition, increasing the concentration of TS-treated FPI resulted in a rise in viscosity, with viscosity values rising from (~0.18 Pa·s) at 1 wt% FPI to ~34 Pa·s at 5 wt% FPI (**Fig. 6.5D**). This could be attributed to greater FPI aggregate formation with a denser and compacter structure as revealed by CLSM (**Fig. 6.4**).

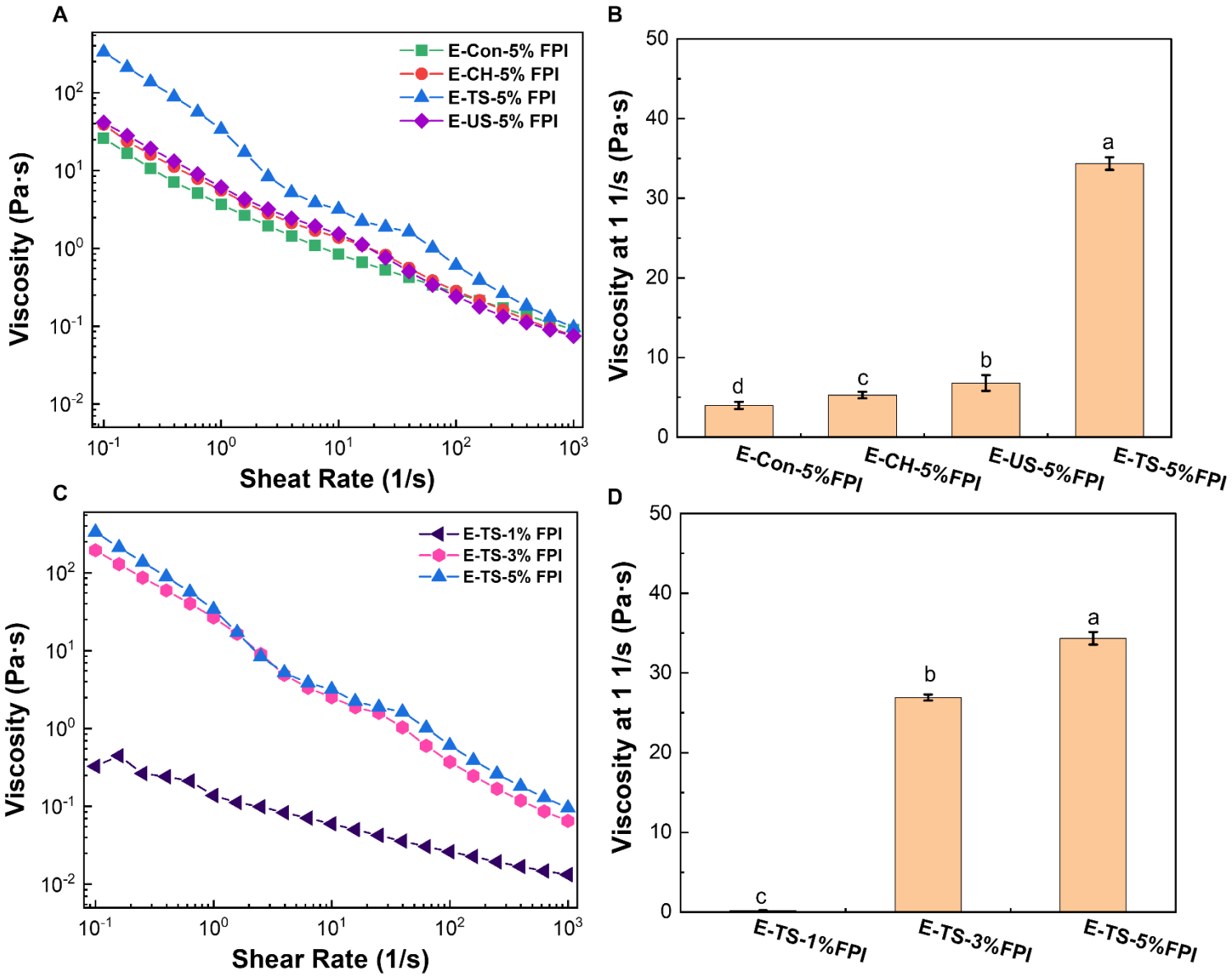

Fig. 6.5 Viscosity as a function of shear rate (A) and the appreant viscosity at 1/s (B) for various cream emulsions stabilised by untreated and treated faba bean protein isolate (FPI); Viscosity as a function of shear rate (C) and the appreant viscosity at 1/s (D) for for various cream emulsions stabilised by TS treated FPI at different concentrations (1 wt%, 3 wt%, and 5 wt%). Different letters above the column denote significant differences ($P < 0.05$). E-Con, E-CH, E-US, and E-TS represent the oil-in-water emulsions stabilised by FPI particles subjected to different physical treatments.

6.3.3.4 Small and large deformation viscoelastic properties of cream emulsions

The viscoelastic properties of various FPI-stabilised cream emulsions as a function of frequency are illustrated in **Fig. 6.6**. All samples exhibited parallel G' and G'' patterns with only slight dependence on frequency, indicating that all cream emulsions were dominated by an elastic behaviour, which can be classified as emulsion gels (Hu, et al., 2023). To better compare the mechanical strength between samples, the G' at 1 Hz is plotted (**Fig. 6.6 B and F**). Cream emulsions stabilised by TS-treated FPI demonstrated the highest G' (~163 Pa), surpassing all other samples. This can be attributed to the smaller oil droplet size, compact interactions between adjacent oil droplets, and entanglement of FPI molecules, as observed in **Fig. 6.4** (Hu, Cheng, Gilbert, Lee, et al., 2024). Similarly, higher FPI concentrations led to increased gel strength, with values ranging from ~12 Pa (1 wt% FPI) to ~163 Pa (5 wt% FPI) as shown in **Fig. 6.6F**. In general, the viscoelastic behaviour of emulsion gels aligns well with the viscosity results, with the 5wt% TS treated FPI- stabilised emulsions exhibiting the greatest mechanical strength. This highlights the superior gel-forming and stabilising properties of TS-treated FPI, reinforcing its effectiveness in enhancing emulsion's structural integrity and mechanical properties.

The G' and G'' of cream emulsions as a function of strain amplitude are shown in **Fig. 6.6C and G**. For all samples, G' and G'' remained independent of strain amplitude within the linear viscoelastic region (LVR), with G' consistently greater than G''. This further confirms the gel-like network structure of cream emulsions observed during the frequency sweep (Zou, et al., 2018). After the strain amplitude increased beyond the LVR, the G' values for all samples decreased dramatically, indicating structural disintegration of cream emulsions. With further increases in applied strain, crossover G' and G'' occurred, with the corresponding stress (σ_b) at this crossover point defined as breaking stress. Beyond the crossover point, G'' exceeds G', suggesting that the structure is disintegrated, and samples begin to flow.

Breaking stress (σ_b) values of all cream emulsion samples are shown in **Fig. 6.6D and H**. Emulsions stabilised by TS-treated FPI exhibited significantly higher σ_b values (~45.1 Pa) compared to emulsions stabilised FPI treated by other methods (ranging

from ~6.8 to ~8.1 Pa). This indicates that a stronger emulsion gel was formed with TS treatment. Furthermore, when the concentration of FPI increased from 1 to 5 wt%, σ_b substantially increased from ~5.4~45.1 Pa, which aligns with small deformation rheological results.

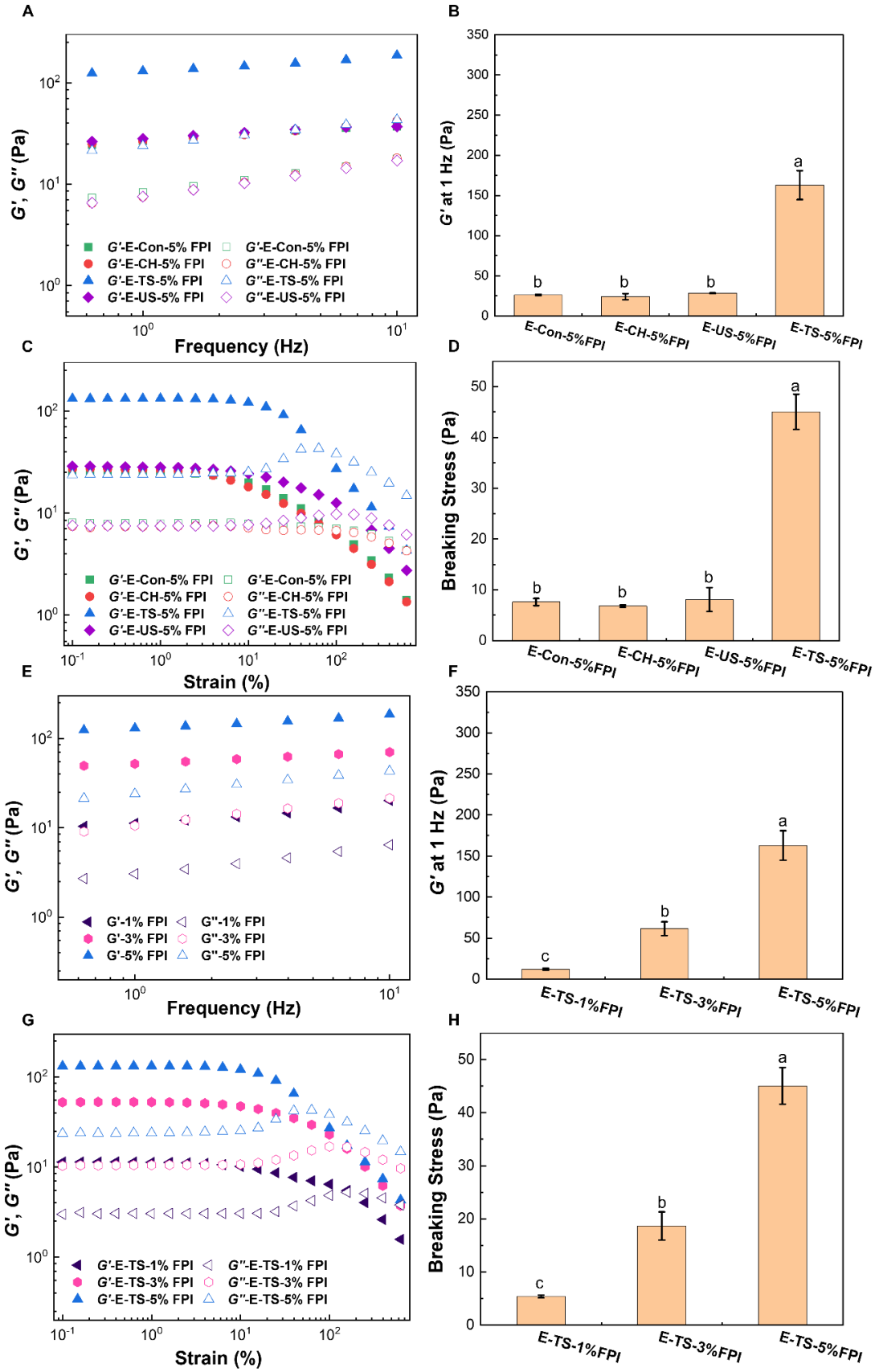

Fig. 6.6 Storage modulus (G', solid symbols) and loss modulus (G'', empty symbols) as a function of frequency (A) and strain amplitude (C) for various cream emulsions

stabilised by untreated and treated faba bean protein isolate (FPI). G' at 1 Hz (B) and breaking stress (D) for for various cream emulsions stabilised by untreated and treated faba bean protein isolate (FPI). Storage modulus (G', solid symbols) and loss modulus (G'', empty symbols) as a function of frequency (E) and strain amplitude (G) for various cream emulsions stabilised by TS treated FPI at different concentrations (1 wt%, 3 wt%, and 5 wt%). G' at 1 Hz (F) and breaking stress (H) for various cream emulsions stabilised by TS treated FPI at different concentrations (1 wt%, 3 wt%, and 5 wt%). In (B, D, F, and H) different letters above the column denote significant differences ($P < 0.05$). E-Con, E-CH, E-US, and E-TS represent the oil-in-water emulsions stabilised by FPI particles subjected to different physical treatments.

6.3.4 Characteristics of whipped creams

6.3.4.1 Visual appearance

The visual appearance of whipped cream composed of FPI is shown in **Fig. 6.7**. At a sample FPI concentration of 5 wt%, a noticeable difference can be seen among the various whipped creams. The TS-treated FPI produced a self-standing whipped cream with a significantly sharper surface compared to the others. This enhancement can be attributed to the stable three-dimensional network structure formed by strand-like, entangled FPI aggregates (Hu, Cheng, Gilbert, Lee, et al., 2024). The aggregates created through TS treatment not only improve emulsification performance at the oil/water interface, but also exhibit superior network formation capabilities, to achieving appropriate mechanical strength that enhance surface coverage and prevents air bubble collapsing (Dickinson, 2019; Murray, 2020). It has been suggested that an extremely high viscosity can hinder air entrance, while the extremely low viscosity may lead to the merge of air bubbles to produce larger bubbles (Indrawati, et al., 2008; Rezvani, et al., 2020). In addition, compared to control sample, CH and US treatment improved the whipping performance to some extent, as these treatments facilitated formation of protein aggregates with enhance emulsification capability and better network formations.

As the concentration of TS-treated FPI increased, the shape of whipped cream became progressively sharper; however, this effect was less pronounced when the FPI concentration rose from 3 wt % to 5 wt%. This observation agrees well with the results of the oil droplet sizes (**Fig. 6.3C**). As shown in **Fig. 6.4**, higher FPI concentrations resulted in more protein aggregates in the aqueous phase of the emulsions, which interconnected to formed local networks that support the foam structure (Han, et al., 2023; Zhang, et al., 2024).

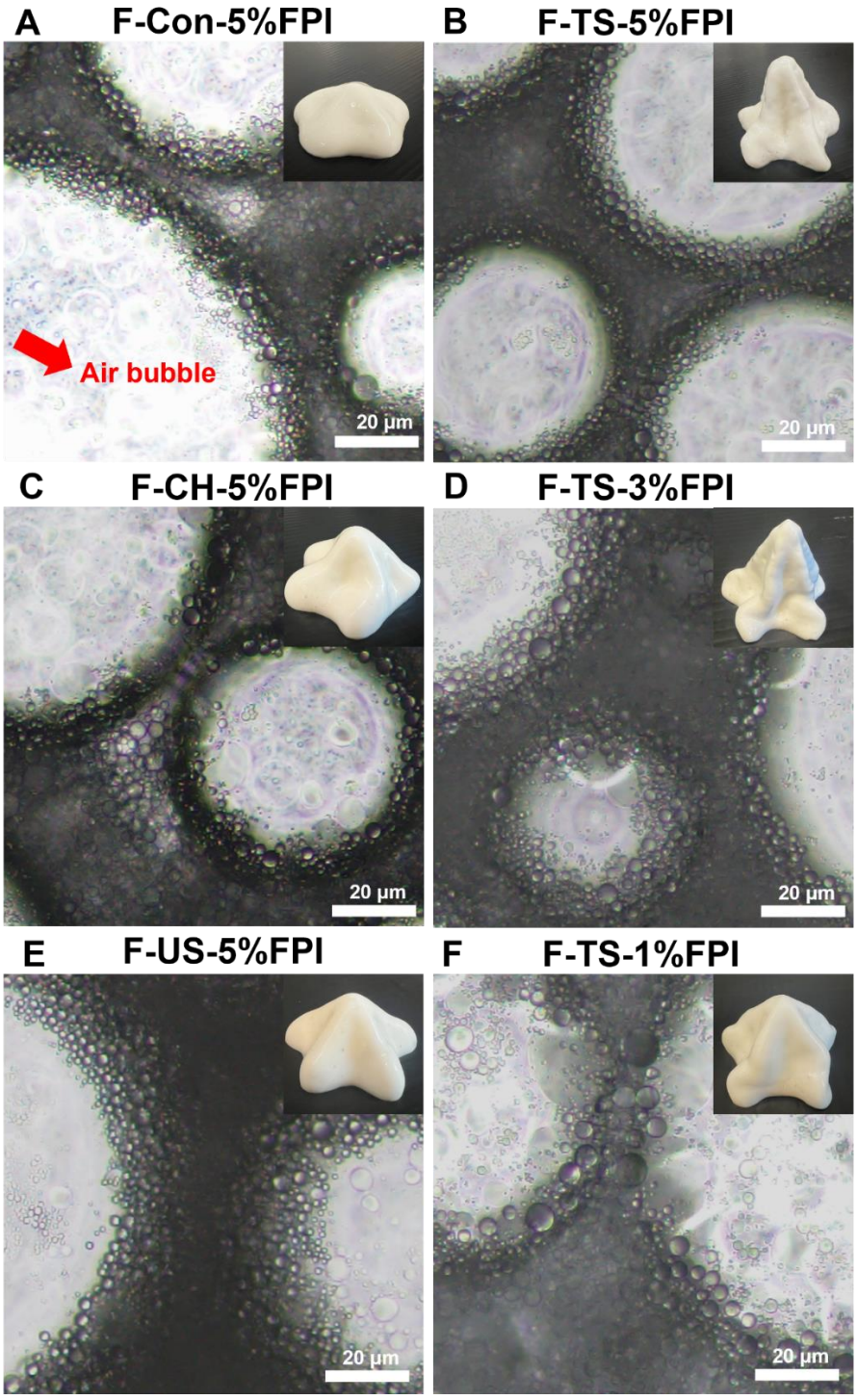

Fig. 6.7 Light micrographs and visual apprearence (Insets) of whipped cream samples made from various cream emulsions stablised by untreated and treated FPI (A, B, C, and E) or various emulsions stabilised by TS treated FPI at different concentrations (1 wt%, 3 wt%, and 5 wt%) (B, D, and F). Scale bar = 20 μm. F-Con, F-CH, F-US, and F-TS represent the whipped oil-in-water emulsions stabilised by FPI particles subjected to different physical treatments.

6.3.4.2 Microstructure of whipped creams

The microstructure of different types of whipped creams illustrated in **Fig. 6.7**. It is evident that whipped cream samples were formed by air bubbles stabilised by oil droplets and aqueous phase. As shown in **Fig. 6.7B**, TS treatment facilities the formation of small and uniform oil droplets absorbed on the air bubbles. The three-dimensional network structure is sufficiently strong to trap air bubbles and prevent their further coalescence. Additionally, as observed in **Fig. 6.7B, D, and F**, and in alignment with the findings presented in **Figs. 6.3** and **6.4**, the size of the oil droplets adsorbed onto the surfaces of the air bubbles decreased as the FPI concentration increased from 1 wt% to 5 wt%.

6.3.4.3 Apparent viscosity of whipped cream

The viscosity of whipped cream is a key characteristic, closely linked to its overall mouth feeling, which is critical for consumer acceptance (Szczesniak, 2002). Higher viscosity increases the resistance to movement of cream within the mouth, potentially leading to a sticky sensation on the palate (Laguna, et al., 2021). In **Fig. 6.8**, all samples exhibited a shear thinning behaviour, with viscosity decreasing as shear rate increased. This phenomenon occurs due to the alignment of individual macromolecules in the direction of shear and the disentanglement of the cream's polymer network, resulting in recued viscosity (Wu, Zhang, et al., 2023). Similar observations have been found in whipped creams made from other plant proteins such as kidney bean proteins (Wu, Zhang, et al., 2023) and faba bean protein microgels (Zhang, et al., 2024).

As shown in **Fig. 6.8B**, at a fixed FPI concentration of 5 wt%, TS treatment significantly enhanced the apparent viscosity at 1 s^{-1} (~19 Pa·s), compared to other treatments (~4 Pa·s for Con and CH; ~7 Pa·s for US). Similar to the viscosity results of cream emulsions shown in **Fig. 6.5D**, increasing FPI also contributed to higher viscosity, with values rising from ~9 Pa·s (1 wt% FPI) to ~19 Pa·s (5 wt% FPI) in **Fig. 6.8D**. In general, higher viscosity contributes to more stable whipped cream, as increased viscosity inhibits the escape of air bubbles and helps stabilise the foam structure, ensuring that the whipped cream maintains its form and texture (Wu, Zhang, et al., 2023; Zhao, et al., 2013).

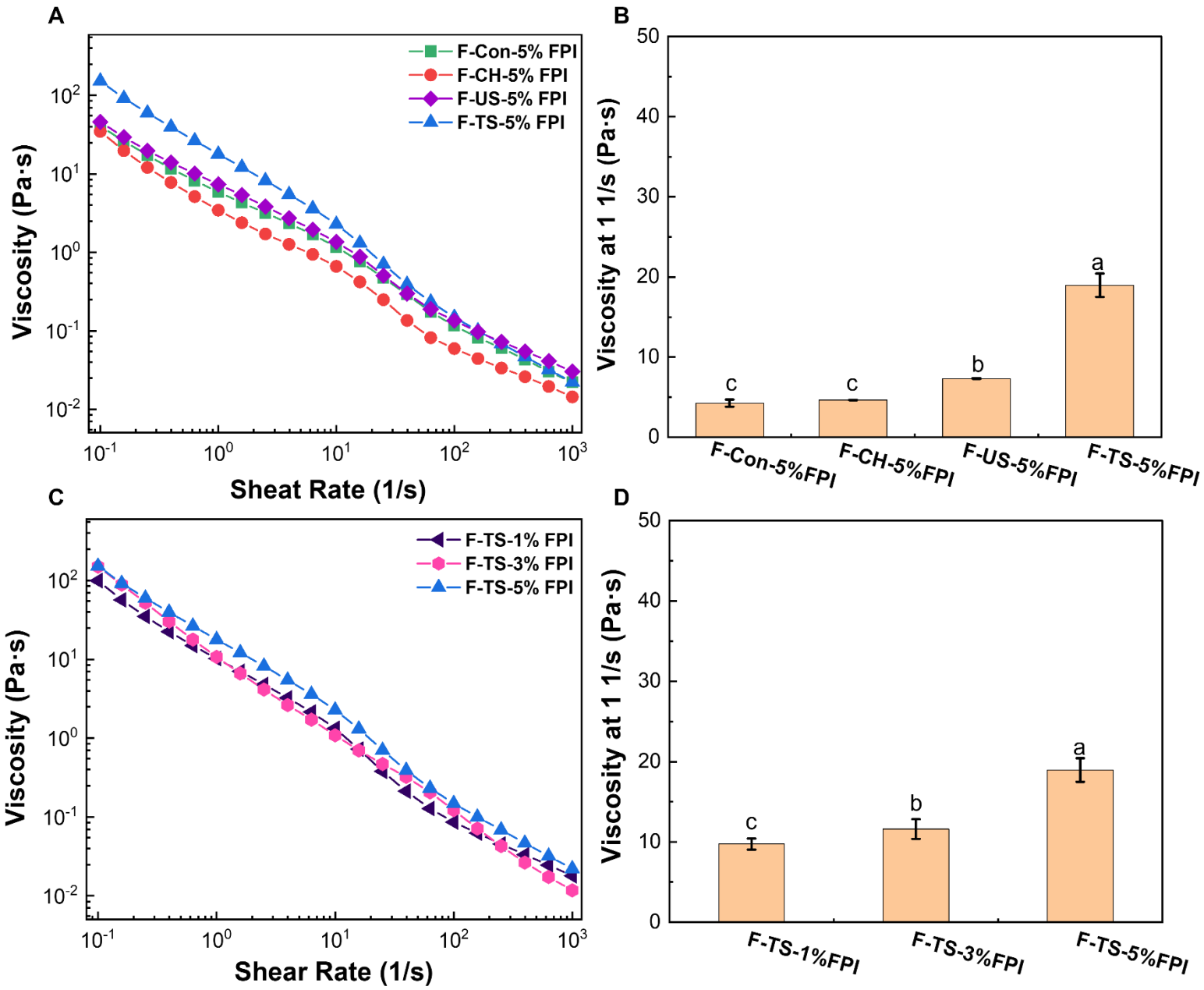

Fig. 6.8 Viscosity as a function of shear rate (A) and the appreant viscosity at 1/s (B) for various whipped creams stabilised by untreated and treated faba bean protein isolate (FPI); Viscosity as a function of shear rate (C) and the appreant viscosity at 1/s (D) for for various whipped creams stabilised by TS treated FPI at different concentrations (1 wt%, 3 wt%, and 5 wt%). Different letters above the column denote significant differences ($P < 0.05$). F-Con, F-CH, F-US, and F-TS represent the whipped oil-in-water emulsions stabilised by FPI particles subjected to different physical treatments.

3.4.4 Small and large deformation rheological properties of whipped cream

The frequency sweep of whipped cream is shown in **Fig. 6.9**. In the probed frequency range, G' and G'' remained independent of the frequency increase. This observation aligns with previous studies research on viscoelastic properties of whipped cream, confirming that whipped creams exhibited the characteristics of a typical solid-like system (Fu, et al., 2020; Rezvani, et al., 2020; Wu, Zhang, et al., 2023). Among at the samples with 5 wt% FPI, whipped cream prepared with TS-treated FPI showed the highest value of G' at 1 Hz (~65 Pa) as seen in **Fig. 6.9B**. Moreover, as the concentration of TS-treated FPI increased from 1 wt% to 5 wt%, gel strength at 1 Hz improved accordingly (from ~40 Pa to ~65 Pa), consistent with the viscosity results. The increase of mechanical strength plays a crucial role in inhibiting the movement and coalescence of air bubbles, which helps stabilise the foam and prevent collapse (Grossi, et al., 2024; Zhang, et al., 2024).

The strain dependent rheological characteristics of whipped creams are shown in **Fig. 6.9C** and **G**. Within the LVR, the values of G' and G'' remained independent of the strain amplitude, with G' consistently larger than G'', confirming the weak gel-like network structure of whipped creams as shown in frequency sweep (Tao, et al., 2023; Zou, et al., 2018). Beyond the LVR, as the strain amplitude increased, G' values for all samples decreased substantially, indicating structural disintegration (Yang, de Campo, et al., 2022). Further increases in strain led to a crossover point where G'' became smaller than G'. At 5 wt% FPI, whipped cream stabilised by TS-treated FPI exhibited the highest σ_b (~13 Pa), whereas whipped cream prepared with other treatments had significantly lower σ_b values (ranging from ~6 Pa to ~9 Pa), as shown in **Fig. 6.9D**. Similarly, increasing the FPI concentration from 1 wt% to 5 wt% led to a corresponding increase in σ_b values, from ~6 Pa to ~13 Pa (**Fig. 6.9H**). This trend aligns well with the results of the viscosity and frequency sweeps, confirming that higher FPI concentrations improve the mechanical strength of whipped creams.

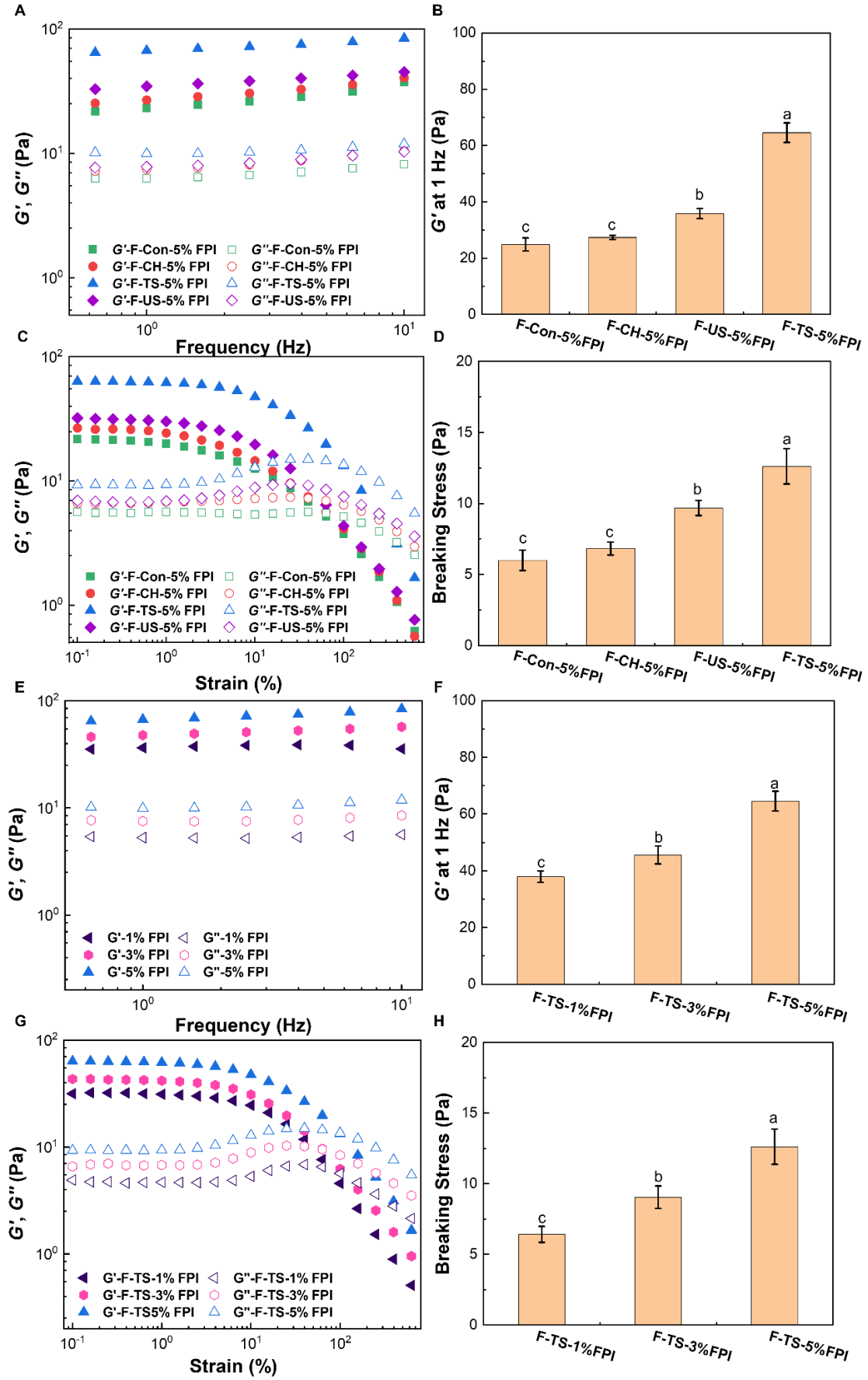

Fig. 6.9 Storage modulus (G', solid symbols) and loss modulus (G'', empty symbols) as

a function of frequency (A) and strain amplitude (C) for various whipped creams stabilised by untreated and treated faba bean protein isolate (FPI). G' at 1 Hz (B) and breaking stress (D) for for various cream emulsions stabilised by untreated and treated faba bean protein isolate (FPI). Storage modulus (*G′*, solid symbols) and loss modulus (*G″*, empty symbols) as a function of frequency (E) and strain amplitude (G) for various whipped creams stabilised by TS treated FPI at different concentrations (1 wt%, 3 wt%, and 5 wt%). G' at 1 Hz (F) and breaking stress (H) for various whipped creams stabilised by TS treated FPI at different concentrations (1 wt%, 3 wt%, and 5 wt%). In (B, D, F, and H) different letters above the column denote significant differences ($P < 0.05$). F-Con, F-CH, F-US, and F-TS represent the whipped oil-in-water emulsions stabilised by FPI particles subjected to different physical treatments.

6.3.4.5 Overrun and stability of whipped cream

The overrun results for various whipped cream samples are shown in **Fig. 6.10**. As illustrated in **Fig. 6.10A**, the overrun of TS-treated FPI samples was the highest (~375%) among all samples, indicating the three-dimensional network formed by FPI after TS treatment creates a stronger network structure compared to native (~80%), CH-treated (~135%) and US-treated (~34%) samples. This enhanced structure network effectively stabilises and retains more air during whipping (Wang, et al., 2021). Furthermore, **Fig. 6.10C** reveals that the overruns of 5 wt % TS-treated FPI samples were significantly greater than those of 3 wt % FPI (~280%) and 1 wt % FPI (~194%) samples., This suggests that a higher concentration of FPI leads to increased protein aggregates and improved whipping ability. The higher viscosity associated with increased FPI concentration likely contributed to this enhancement by facilitating the entrapment and stabilisation of air bubbles (Wu, Zhang, et al., 2023; Zhao, et al., 2013).

The stability of cream refers to its ability to resist the partial loss of cream serum during storage (Athari, et al., 2021; Rezvani, et al., 2020). In this study, the stability of whipped cream was evaluated over 2 h, reflecting typical consumption behaviour, as fresh whipped cream is usually consumed within a few hours (Liu, Cao, et al., 2022). As shown in **Fig. 6.10B**, whipped cream made from TS-treated FPI stabilised emulsions exhibited the highest stability (~22%). In contrast, the stability of other samples ranged from ~92% to ~98%), a finding that correlates well with the rheological results. The superior stability of TS treated samples can be attributed to their significantly higher viscosity and viscoelasticity compared to other samples (Fu, et al., 2020; Hotrum, et al., 2004). Furthermore, stability is improved with increasing FPI concentration; syneresis values decreased from ~95% for 1 wt% FPI to ~22% for 5 wt% FPI. This suggests that higher FPI concentration enhances the stability of whipped cream by improving the rheological properties, which in turn leads to better foam stability and greater resistance to serum separation. Finally, the whipping performance of FPI stabilised emulsion was compared with commercial dairy cream based on overrun and syneresis as shown in **Fig. S6.1**. The highest overrun and minimal syneresis observed in the dairy whipping cream could be attributed to the crystallisation and partial coalesces of milk fat globules, which enhanced air bubble entrapment and structural stability (Fu, et al., 2020; Rezvani,

et al., 2020).

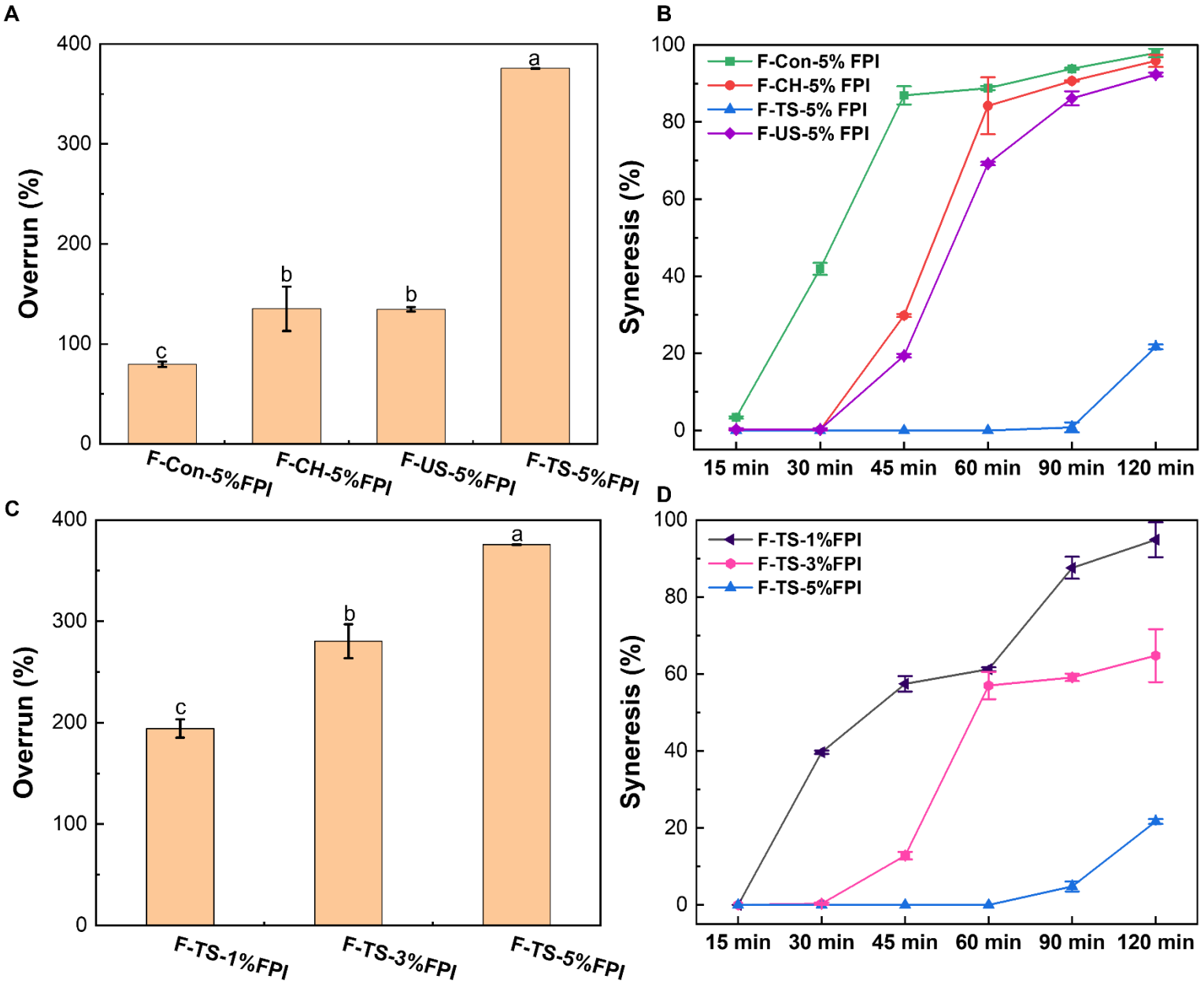

Fig. 6.10 The overrun (left) and syneresis (right) of whipped creams made from (A and B) untreated and treated FPI; (C and D) TS treated FPI at different concentrations (1 wt%, 3 wt%, and 5 wt%). The different letters above the column denote significant differences ($P < 0.05$). F-Con, F-CH, F-US, and F-TS represent the whipped oil-in-water emulsions stabilised by FPI particles subjected to different physical treatments.

6.3.5 Possible stabilisation mechanisms of whipped cream stabilised by various FPI aggregates

Based on experimental findings, a potential mechanism for the stabilisation of whipped cream using various untreated and treated FPI aggregates is proposed (**Fig. 6.11**). Compared to untreated FPI (control), different treatments resulted in the formation of distinct FPI aggregate morphologies, which, in turn, affected their emulsification and whipping performances. Heat treatment (CH) induced protein denaturation and unfolding, leading to the formation of irregular FPI microparticulate. These microparticulate enhanced the mechanical properties of the emulsions through a space-filling effect, thereby improving the whipping performance to some extent (Zhang, Cheng, et al., 2021). In contrast, thermosonication (TS) promoted extensive protein unfolding and structural rearrangement, resulting in the formation of strand-like protein aggregates. Due to their high aspect ratio and flexibility, these aggregates were more effective at stabilising interfaces by forming an interfacial layer, which helped prevent the merging of air bubbles and contributed to the stability of the whipped cream (Murray, 2020; Stanley, et al., 1996). Additionally, excess TS-treated FPI aggregates entangled and interacted within the aqueous phase, forming three-dimensional network structures. This further facilitated the entrapment and stabilisation of air bubbles. The concentration of FPI also plays a critical role in whipped cream formation. Higher FPI concentrations lead to the creation of smaller oil droplets and stronger emulsion networks, thereby enhancing both whipping capacity and stability (Zhang, et al., 2024).

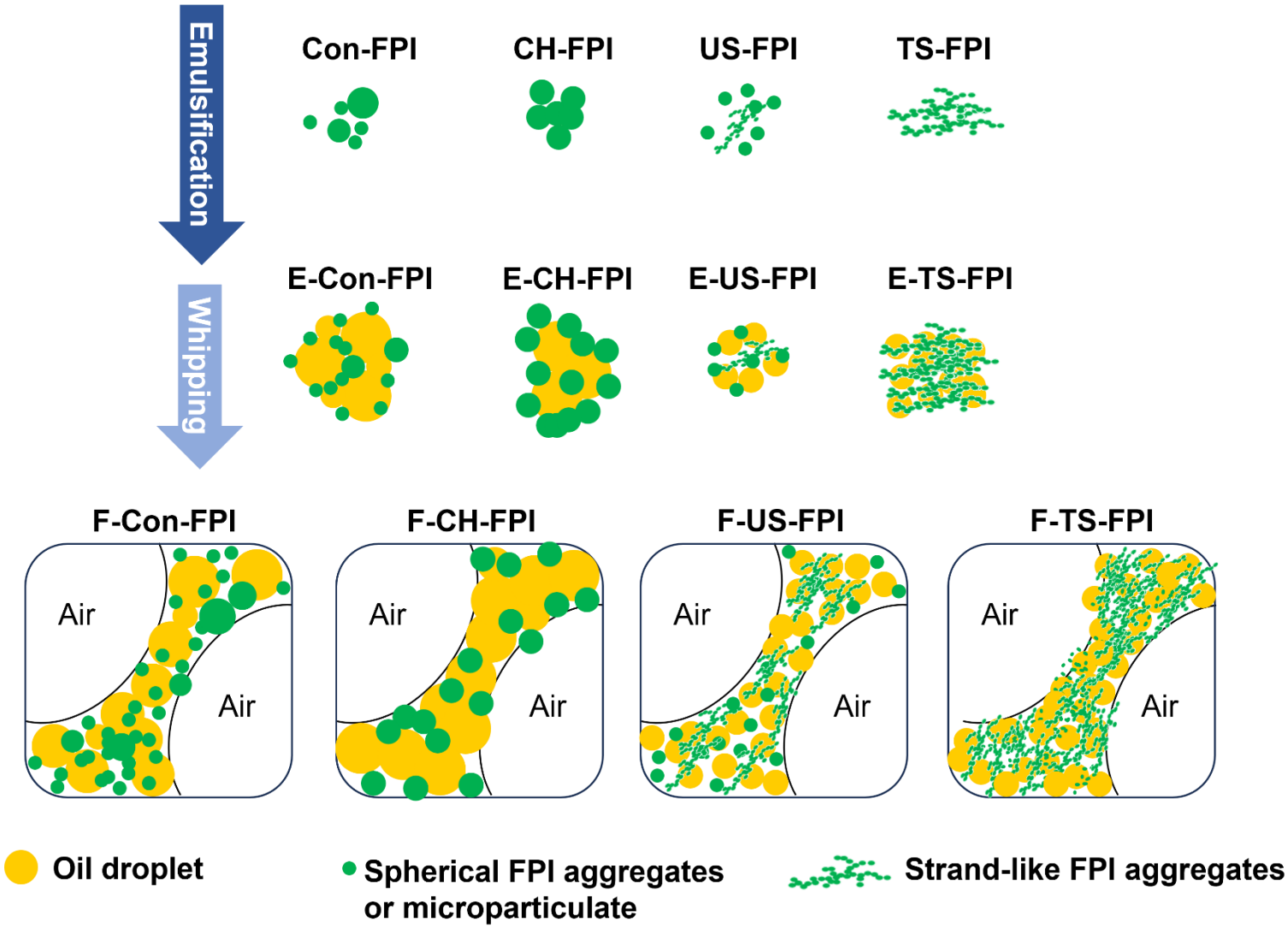

Fig. 6.11 Schematic diagrams of whipped creams stabilised by various untreated and treated FPI particles. E-Con, E-CH, E-US, and E-TS represent the oil-in-water emulsions stabilised by FPI particles subjected to different physical treatments. F-Con, F-CH, F-US, and F-TS represent the whipped oil-in-water emulsions stabilised by FPI particles subjected to different physical treatments.

6.4 Conclusions

This research systematically investigated the effects of various physical treatment namely conventional heating (CH), ultrasonication (US), and thermosonication (TS) on physicochemical properties and microstructural characteristics of FPI dispersions and their applications in formulating whipped creams. The results demonstrated that TS treatment was the most effective in reducing particle size and improving solubility. Exposure to ultrasonication and high temperature caused significant unfolding of FPI protein molecules, increasing surface hydrophobicity and forming strand-like protein aggregates. In addition, FPI aggregates obtained from TS treatment proved most suitable for the preparation of whipped cream based on soybean oil in water emulsions, providing viable alternative to animal fat or hydrogenated vegetable oil. Whipped cream made from TS treated FPI exhibited the highest overrun and least serum release during 2 h storage. This could be due to its superior emulsification capability and network-forming ability, which provided sufficient mechanical strength to entrap and stabilise air bubbles. Furthermore, higher FPI concentration resulted in a better whipping performance, which is likely due to the formation of smaller oil droplets and a more rigid structure network from the entanglement and interactions of unabsorbed FPI aggregates in the aqueous phase. This study highlights the significant potential of using TS- treated FPI in the development of clean-label and plant-based whipped creams.

Acknowledgements

The author Yinxuan Hu would like to thank Massey University, New Zealand, for awarding a doctoral scholarship. We also extend our thanks to the Manawatu Microscopy and Imaging Centre (MMIC) at Massey University, Palmerston North, for their generous support and assistance.

Supplementary Information

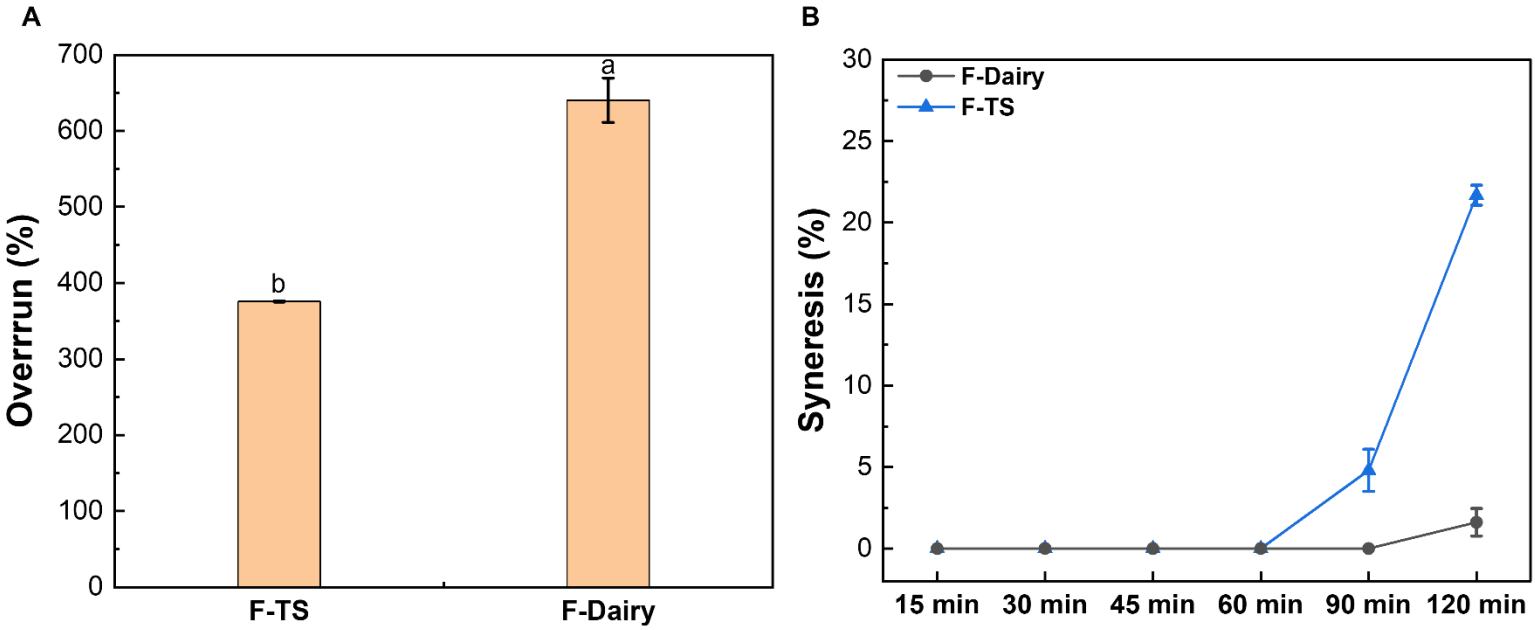

Fig. S6.1 The overrun (A) and syneresis (B) of whipped creams made from commercial dairy whipped cream and thermosonication (TS) treated FPI at 5 wt%. The different letters above the column denote significant differences ($P < 0.05$)

Chapter 7 Overall conclusions and future recommendations

7.1 Overall Conclusions

The overall goal of this project was to study the formation, stability, and functionality of plant protein aggregates, focusing on faba bean protein isolate (FPI). Various methods, including heat treatment, thermosonication and sonication, were employed in the preparation of these aggregates. Several model food systems (e.g. gels, emulsions and creams) were developed using FPI aggregates as the main ingredient after treatment under different conditions, including pH adjustments and variations in ionic strength.

This research encompasses four main studies, each investigating different aspects of FPI aggregates and applications, including 3D printing capabilities, emulsifying abilities, and foaming properties. A series of advanced experiments were conducted to characterise the physicochemical properties and microstructures of FPI aggregates, including FPI particle sizes, secondary structures, microstructures, and solubility. The functionalities of FPI aggregates, such as gelation behaviour, emulsifying abilities, and oil droplet interactions within the emulsion during long-term storage and/or heat treatment, were also investigated.

This project innovatively demonstrated the 3D printing performances of FPI-stabilised concentrated emulsions in **Chapter 3**. FPI aggregates were induced by pH adjustments (pH 3-pH 9), salt addition (NaCl and $CaCl_2$), both of which significantly affected the net charge (ζ-potential), solubility, and interfacial tension of native FPI particles. The results showed that concentrated emulsions stabilised by FPI aggregates at pH 7 and pH 9 exhibited excellent three-dimensional stability and printing precision, which maintained well-defined and self-supporting structures.

The rheological properties of the samples at pH 7 and pH 9, including high gel strength and large linear viscoelastic regions, were critical factors for enhancing printing precision. The concentration of FPI aggregates was also another key factor of the desirable rheological properties of the concentrated emulsions. As FPI concentrations increased from 1 wt% to 5 wt%, the mechanical strength of the emulsion gels improved, and the oil droplet sizes decreased. The presence of salts, such as NaCl and $CaCl_2$,

further improved gel strength and structural integrity.

Applying heat treatment at 90 °C for 30 min further enhanced the mechanical stiffness and printability of all emulsion samples, due to protein denaturation and further aggregation of FPI. These findings demonstrate the significant potential of FPI aggregates induced by pH adjustments, salt addition, and heat treatment, and the concentrated emulsions formed from various FPI aggregates had different performances in 3D food printing applications.

In **Chapter 4**, the study investigated the effects of thermosonication (TS) and conventional heating (CH) on FPI dispersions at pH 2 to form fibrils with a high aspect ratio. The TS treatment significantly accelerated the formation of FPI fibrils with high β-sheet content, as confirmed by TEM observation and SANS. The conversion rate of FPI fibrils formed after 30 min of TS treatment (~47%) was comparable to that formed after 4 h of heat treatment (~53%). LC-MS/MS analysis identified 47 and 67 unique peptides from the 30 min TS treatment and/or 4 h CH treatment, respectively. Additionally, TS-induced FPI dispersions had a distinctive gelation behaviour with a thermoreversible viscoelastic gel network, which exhibited significantly higher breaking strain compared to CH-induced FPI fibrillar gels. The improved physicochemical properties of TS-induced FPI fibrils had an enhanced emulsification capability, which made it successfully form HIPEs (ϕ = 0.75) with smaller oil droplet sizes, greater mechanical strength, and more compactly packed oil droplets than those HIPEs formed by native FPI particles. This work showed that the TS treatment was effective in the formation of plant protein fibrils, offering a range of potential applications as gelling and emulsifying agents.

Chapter 5 examined the properties of FPI aggregates formed by TS at pH 7, comparing them to those formed by CH. This was important because an extremely low pH value of FPI can affect its further applications. TS treatment resulted in FPI aggregates rich in β-sheet structures, as evidenced by ThT fluorescence, CD spectra, TEM, and SANS results. These FPI aggregates exhibited smaller particle sizes and increased solubility.

The formation of a thermoreversible viscoelastic gel network was also observed in TS-

treated FPI dispersions at 10 wt%. Subsequently, different FPI dispersion concentrations after 30 min of TS (1, 3, and 5 wt%) were used to stabilise O/W emulsions at various oil volume fractions (ϕ = 0.2, 0.5, and 0.7) compared to native FPI. The results showed that the emulsions formed by TS-30 induced FPI aggregates had smaller oil droplet sizes, greater mechanical strength, denser oil droplet microstructure, and greater storage stability. The formation of these new FPI aggregates indicates their potential as texturing and emulsifying agents in food, cosmetic, and pharmaceutical products.

Based on the finding that the FPI aggregates formed by the TS treatment exhibited outstanding physicochemical and functional properties, **Chapter 6** focused on developing plant based whipped cream using these protein aggregates. The TS-treated FPI protein aggregates displayed improved visual appearance, overrun, and stability compared to those treated with CH and ultrasonication (US). Microstructural analysis indicated that the protein aggregates formed by TS treatment were more flexible and could form thicker interfacial layers, which facilitated in stabilising the whipped cream by preventing air bubble coalescence and oil droplet crystallisation. Thus, the mechanical strength of whipped cream prepared by TS-treated FPI was also greater. This study provided valuable insights into producing high-quality plant-based whipped cream using TS-treated FPI, offering a potential promising approach to replace animal fats and hydrogenated vegetable oils.

Overall, the structure and interfacial properties of FPI aggregates played a crucial role in the formation and stability of emulsions, gels, and foams. By controlling the formation of different FPI aggregates through pH adjustments, modifying FPI concentration and applying treatments, such as heat treatment and thermosonication, the functional properties of FPI aggregates were significantly improved, especially in emulsions, foams, and gels.

This research contributes to the development of high-quality, plant-based food products with enhanced stability, mechanical strength, and application potential (e.g. 3D printing). The findings suggest new possibilities for plant protein aggregates in customised diets, high protein beverages, and whipped creams, promoting the use of

plant protein aggregates in innovative and sustainable food systems. The information gained from this project will contribute to the development of sustainable functional food products using plant protein aggregates with advanced functionalities.

7.2 Recommendations for future work

The fabrication of plant protein aggregates as functional ingredients in food products remains an active area of research, with several trends and limitations that need further exploration. One significant challenge is understanding the mechanisms underlying the different methods of plant protein aggregation. The complexity of plant proteins, which are typically mixtures of different types, makes it difficult to generalize findings across all plant proteins. For instance, while Chapter 4 of this study extensively investigates the aggregation behaviour of faba bean protein isolate (FPI) fibrillar aggregates, these results cannot be universally applied to all plant proteins. This indicates a need for deeper and more comprehensive research to develop hypotheses that could be applicable to a broader range of plant proteins.

For example, heat treatment is a common method used to form plant protein aggregates, however, there is a need for more research from a processing perspective. Investigating heat-induced plant protein aggregates using different heat sources, methods of heat transfer, and their efficiencies could provide valuable insights. Additionally, the techno-functional properties of plant protein aggregates formed under various temperature conditions—mild, moderate, and severe—remain underexplored. The combination of different methods, such as thermosonication, has shown potential for forming β-sheet structures at neutral pH, but the effects of biochemical methods such as enzymatic hydrolysis on these β-sheet-rich protein dispersions, especially in the fabrication of fibrillar aggregates without further heating, are still unclear and require further study. Moreover, the exploration of novel methods, such as the use of radiation, in forming plant protein aggregates also holds promise but is yet to be fully investigated.

Another area that requires more attention is the effect of other food components on plant protein aggregation. Currently, there is insufficient research on how components like animal proteins, varying fat content, and polysaccharides influence plant protein aggregation. The existing database on the effects of various food components on plant

protein aggregation is inadequate, necessitating the collection of more data to uncover the interactions between different components. The application of novel technologies, such as artificial intelligence, big data analytics, and modelling, could be instrumental in building a more comprehensive database and understanding these interactions.

Furthermore, the relationship between plant protein aggregation and nutrition and health is not well understood. The effects of plant protein aggregates on human digestion, metabolism and other physiological systems remain unclear, highlighting the importance of research that mimics the digestion, absorption, and bioavailability of plant proteins within the human body. Additionally, the connection between plant protein aggregates and human nutrition needs to be explored more thoroughly to develop a comprehensive understanding of their impact on health.

Finally, there is a need for the development of more stable and suitable devices for the industrial-scale production of plant protein aggregates. The industrialisation of food processing technologies is crucial, but many novel technologies currently used to form plant protein aggregates may negatively impact the longevity of processing equipment, thereby hindering their industrial application. Developing devices that can efficiently induce plant protein aggregation without compromising their durability is essential for the successful industrialisation of these functional ingredients.

References

Abd El-Salam, M., El-Shibiny, S., & Salem, A. (2009). Factors affecting the functional properties of whey protein products: A review. *Food Reviews International, 25*(3), 251-270.

Adal, E. (2024). Modification of faba bean protein isolate by high-intensity ultrasound treatment: screening of physicochemical, thermal, and structural properties. *Journal of Food Measurement and Characterization, 12*(1), 1-12.

Afkhami, R., Varidi, M. J., Varidi, M., & Hadizadeh, F. (2024). Boosting emulsion properties: The role of β-sheet content and fibril length in soy protein isolate emulsions. *Food Hydrocolloids, 149*, 109513.

Aggeli, A., Nyrkova, I. A., Bell, M., Harding, R., Carrick, L., McLeish, T. C., Semenov, A. N., & Boden, N. (2001). Hierarchical self-assembly of chiral rod-like molecules as a model for peptide β-sheet tapes, ribbons, fibrils, and fibers. *Proceedings of the National Academy of Sciences, 98*(21), 11857-11862.

Ahmad, T., Butt, M. Z., Aadil, R. M., Inam-ur-Raheem, M., Abdullah, Bekhit, A. E. D., Guimarães, J. T., Balthazar, C. F., Rocha, R. S., & Esmerino, E. A. (2019). Impact of nonthermal processing on different milk enzymes. *International Journal of Dairy Technology, 72*(4), 481-495.

Ahmadifard, N., Murueta, J. H. C., Abedian-Kenari, A., Motamedzadegan, A., & Jamali, H. (2016). Comparison the effect of three commercial enzymes for enzymatic hydrolysis of two substrates (rice bran protein concentrate and soy-been protein) with SDS-PAGE. *Journal of Food Science and Technology, 53*, 1279-1284.

Akharume, F. U., Aluko, R. E., & Adedeji, A. A. (2021). Modification of plant proteins for improved functionality: A review. *Comprehensive Reviews in Food Science and Food Safety, 20*(1), 198-224.

Akıllıoğlu, H. G., & Gökmen, V. (2016). Kinetic evaluation of the inhibition of protein glycation during heating. *Food Chemistry, 196*, 1117-1124.

Akkermans, C., Van der Goot, A., Venema, P., Gruppen, H., Vereijken, J., Van der Linden, E., & Boom, R. (2007). Micrometer-sized fibrillar protein aggregates from soy glycinin and soy protein isolate. *Journal of Agricultural and Food Chemistry, 55*(24), 9877-9882.

Akyazi, T., Goti, A., Oyarbide, A., Alberdi, E., & Bayon, F. (2020). A guide for the food industry to meet the future skills requirements emerging with industry 4.0. *Foods, 9*(4), 492.

Alavi, F., Chen, L., & Emam-Djomeh, Z. (2021). Effect of ultrasound-assisted alkaline treatment on functional property modifications of faba bean protein. *Food Chemistry, 354*, 129494.

Alavi, F., Chen, L., Wang, Z., & Emam-Djomeh, Z. (2021). Consequences of heating under alkaline pH alone or in the presence of maltodextrin on solubility, emulsifying and foaming properties of faba bean protein. *Food Hydrocolloids, 112*, 106335.

Alavi, F., Emam-Djomeh, Z., Mohammadian, M., Salami, M., & Moosavi-Movahedi, A. A. (2020). Physico-chemical and foaming properties of nanofibrillated egg white protein and its functionality in meringue batter. *Food Hydrocolloids, 101*, 105554.

Alghamdi, S. S. (2009). Chemical composition of faba bean (Vicia faba L.) genotypes under various water regimes. *Pakistan Journal of Nutrition, 8*(4), 477-482.

Alleoni, A. C. C. (2006). Albumen protein and functional properties of gelation and

foaming. *Scientia Agricola, 63*, 291-298.

Alrosan, M., Tan, T.-C., Koh, W. Y., Easa, A. M., Gammoh, S., & Alu'datt, M. H. (2023). Overview of fermentation process: structure-function relationship on protein quality and non-nutritive compounds of plant-based proteins and carbohydrates. *Critical Reviews in Food Science and Nutrition, 63*(25), 7677-7691.

Aluko, R. E., & Monu, E. (2003). Functional and bioactive properties of quinoa seed protein hydrolysates. *Journal of Food Science, 68*(4), 1254-1258.

Amagliani, L., & Schmitt, C. (2017). Globular plant protein aggregates for stabilization of food foams and emulsions. *Trends in Food Science & Technology, 67*, 248-259.

Amagliani, L., van de Langerijt, T. M., Morgenegg, C., Bovetto, L., & Schmitt, C. (2022). Influence of charged and non-charged co-solutes on the heat-induced aggregation of soy and pea proteins at pH 7.0. *Food Hydrocolloids*, 108392.

Amagliani, L., van de Langerijt, T. M., Morgenegg, C., Bovetto, L., & Schmitt, C. (2023). Influence of charged and non-charged co-solutes on the heat-induced aggregation of soy and pea proteins at pH 7.0. *Food Hydrocolloids, 137*, 108392.

Amiri, S., Nezamdoost-Sani, N., Mostashari, P., McClements, D. J., Marszałek, K., & Mousavi Khaneghah, A. (2024). Effect of the molecular structure and mechanical properties of plant-based hydrogels in food systems to deliver probiotics: an updated review. *Critical Reviews in Food Science and Nutrition, 64*(8), 2130-2156.

Andreescu, S., & Vasilescu, A. (2021). Advances in electrochemical detection for probing protein aggregation. *Current Opinion in Electrochemistry, 30*, 100820.

Ansarifar, E., Shahidi, F., Mohebbi, M., Ramezanian, N., Koocheki, A., & Mohamadian, A. (2019). Optimization of limonene microencapsulation based on native and fibril soy protein isolate by VIKOR method. *LWT, 115*, 107884.

Arbach, C. T., Alves, I. A., Serafini, M. R., Stephani, R., Perrone, Í. T., & de Carvalho da Costa, J. (2021). Recent patent applications in beverages enriched with plant proteins. *NPJ Science of Food, 5*(1), 28.

Armelin, E., Martí, M., Rudé, E., Labanda, J., Llorens, J., & Alemán, C. (2006). A simple model to describe the thixotropic behavior of paints. *Progress in Organic Coatings, 57*(3), 229-235.

Arrondo, J. L. R., Muga, A., Castresana, J., & Goñi, F. M. (1993). Quantitative studies of the structure of proteins in solution by Fourier-transform infrared spectroscopy. *Progress in Biophysics and Molecular Biology, 59*(1), 23-56.

Asioli, D., Aschemann-Witzel, J., Caputo, V., Vecchio, R., Annunziata, A., Næs, T., & Varela, P. (2017). Making sense of the "clean label" trends: A review of consumer food choice behavior and discussion of industry implications. *Food Research International, 99*, 58-71.

Athari, B., Nasirpour, A., Saeidy, S., & Esehaghbeygi, A. (2021). Physicochemical properties of whipped cream stabilized with electrohydrodynamic modified cellulose. *Journal of Food Processing and Preservation, 45*(9), e15688.

Augustin, M., & Cole, M. (2022). Towards a sustainable food system by design using faba bean protein as an example. *Trends in Food Science & Technology, 125*, 1-11.

Austin, L., Wickramaarachchi, P., Mannino, N. C., & Chen, D. (2024). Softening fat-free cream cheese by incorporating aggregates of pea protein hydrolysates. *Food Hydrocolloids, 147*, 109317.

Avelar, Z., Vicente, A. A., Saraiva, J. A., & Rodrigues, R. M. (2021). The role of

emergent processing technologies in tailoring plant protein functionality: New insights. *Trends in Food Science & Technology, 113*, 219-231.

Avilés-Gaxiola, S., Chuck-Hernández, C., del Refugio Rocha-Pizaña, M., García-Lara, S., López-Castillo, L. M., & Serna-Saldívar, S. O. (2018). Effect of thermal processing and reducing agents on trypsin inhibitor activity and functional properties of soybean and chickpea protein concentrates. *LWT, 98*, 629-634.

Badar, I. H., Wang, Z., Liu, H., Chen, Q., Xia, X., Liu, Q., & Kong, B. (2023). Future prospects of high internal phase pickering emulsions stabilized by natural modified biopolymers as a potential fat substitute in meat products. *Trends in Food Science & Technology*, 104176.

Bai, L., Huan, S., Xiang, W., & Rojas, O. J. (2018). Pickering emulsions by combining cellulose nanofibrils and nanocrystals: Phase behavior and depletion stabilization. *Green Chemistry, 20*(7), 1571-1582.

Banc, A., Charbonneau, C., Dahesh, M., Appavou, M.-S., Fu, Z., Morel, M.-H., & Ramos, L. (2016). Small angle neutron scattering contrast variation reveals heterogeneities of interactions in protein gels. *Soft Matter, 12*(24), 5340-5352.

Banerjee, S., & Bhattacharya, S. (2012). Food gels: gelling process and new applications. *Critical Reviews in Food Science and Nutrition, 52*(4), 334-346.

Barnes, H. A. (1994). Rheology of Emulsions—A Review. *Colloids and Surfaces A: Physicochemical and Engineering Aspects, 91*, 89-95.

Basak, S., & Annapure, U. S. (2022). Recent trends in the application of cold plasma for the modification of plant proteins-A review. *Future Foods, 5*, 100119.

Beck, S. M., Knoerzer, K., Sellahewa, J., Emin, M. A., & Arcot, J. (2017). Effect of different heat-treatment times and applied shear on secondary structure, molecular weight distribution, solubility and rheological properties of pea protein isolate as investigated by capillary rheometry. *Journal of Food Engineering, 208*, 66-76.

Beegum, P. S., Pandiselvam, R., Ramesh, S., Thube, S. H., Pandian, T. P., Khanashyam, A. C., Manikantan, M., & Hebbar, K. (2022). A critical appraisal on the antimicrobial, oral protective, and anti-diabetic functions of coconut and its derivatives. *Quality Assurance and Safety of Crops & Foods, 14*(2), 86-100.

Bély, M., & Makovitzky, J. (2006). Sensitivity and specificity of Congo red staining according to Romhanyi. Comparison with Puchtler's or Bennhold's methods. *Acta Histochemica, 108*(3), 175-180.

Benetti, J. V. M., do Prado Silva, J. T., & Nicoletti, V. R. (2019). SPI microgels applied to Pickering stabilization of O/W emulsions by ultrasound and high-pressure homogenization: rheology and spray drying. *Food Research International, 122*, 383-391.

Berrazaga, I., Message, J., Laleg, K., Salles, J., Guillet, C., Patrac, V., Giraudet, C., Le Bacquer, O., Boirie, Y., & Micard, V. (2019). Formulation, process conditions, and biological evaluation of dairy mixed gels containing fava bean and milk proteins: Effect on protein retention in growing young rats. *Journal of Dairy Science, 102*(2), 1066-1082.

Berry, J. D., Neeson, M. J., Dagastine, R. R., Chan, D. Y., & Tabor, R. F. (2015). Measurement of surface and interfacial tension using pendant drop tensiometry. *Journal of Colloid and Interface Science, 454*, 226-237.

Biancalana, M., & Koide, S. (2010). Molecular mechanism of Thioflavin-T binding to amyloid fibrils. *Biochimica et Biophysica Acta (BBA)-Proteins and Proteomics, 1804*(7), 1405-1412.

Bigi, F., Maurizzi, E., Quartieri, A., De Leo, R., Gullo, M., & Pulvirenti, A. (2023). Non-thermal techniques and the “hurdle” approach: How is food technology evolving? *Trends in Food Science & Technology, 132*, 11-39.

Blankart, M., Hasenfuss, S., Rupprecht, A., Oellig, C., Schwack, W., Granvogl, M., & Hinrichs, J. (2021). The effect of emulsifier by-products and storage conditions on the techno-functional properties of model aerosol whipping cream. *International Dairy Journal, 119*, 104989.

Blazek, J., & Gilbert, E. P. (2011). Application of small-angle X-ray and neutron scattering techniques to the characterisation of starch structure: A review. *Carbohydrate Polymers, 85*(2), 281-293.

Boland, M. J., Rae, A. N., Vereijken, J. M., Meuwissen, M. P., Fischer, A. R., van Boekel, M. A., Rutherfurd, S. M., Gruppen, H., Moughan, P. J., & Hendriks, W. H. (2013). The future supply of animal-derived protein for human consumption. *Trends in Food Science & Technology, 29*(1), 62-73.

Bolder, S. G., Hendrickx, H., Sagis, L. M., & Van der Linden, E. (2006). Ca2+-induced cold-set gelation of whey protein isolate fibrils. *Applied Rheology, 16*(5), 258-264.

Bolder, S. G., Sagis, L. M., Venema, P., & van der Linden, E. (2007). Thioflavin T and birefringence assays to determine the conversion of proteins into fibrils. *Langmuir, 23*(8), 4144-4147.

Boukari, H., Lin, J., & Harris, M. (1997). Small-angle X-ray scattering study of the formation of colloidal silica particles from alkoxides: primary particles or not? *Journal of Colloid and Interface Science, 194*(2), 311-318.

Boye, J., Zare, F., & Pletch, A. (2010). Pulse proteins: Processing, characterization, functional properties and applications in food and feed. *Food Research International, 43*(2), 414-431.

Brinkman, H. C. (1952). The viscosity of concentrated suspensions and solutions. *The Journal of Chemical Physics, 20*(4), 571-571.

Bučko, S., Katona, J., Popović, L., Petrović, L., & Milinković, J. (2016). Influence of enzymatic hydrolysis on solubility, interfacial and emulsifying properties of pumpkin (Cucurbita pepo) seed protein isolate. *Food Hydrocolloids, 60*, 271-278.

Bühler, J. M., Dekkers, B. L., Bruins, M. E., & Van Der Goot, A. J. (2020). Modifying faba bean protein concentrate using dry heat to increase water holding capacity. *Foods, 9*(8), 1077.

Burger, T. G., & Zhang, Y. (2019). Recent progress in the utilization of pea protein as an emulsifier for food applications. *Trends in Food Science & Technology, 86*, 25-33.

Cabra, V., Arreguin, R., Vazquez-Duhalt, R., & Farres, A. (2007). Effect of alkaline deamidation on the structure, surface hydrophobicity, and emulsifying properties of the Z19 α-zein. *Journal of Agricultural and Food Chemistry, 55*(2), 439-445.

Campbell, N. F., Shih, F. F., & Marshall, W. E. (1992). Enzymic phosphorylation of soy protein isolate for improved functional properties. *Journal of Agricultural and Food Chemistry, 40*(3), 403-406.

Cao, B., Fang, L., Liu, C., Min, W., & Liu, J. (2018). Effects of high hydrostatic pressure on the functional and rheological properties of the protein fraction extracted from pine nuts. *Food Science and Technology International, 24*(1), 53-66.

Cao, Y., & Mezzenga, R. (2019). Food protein amyloid fibrils: Origin, structure,

formation, characterization, applications and health implications. *Advances in colloid and interface science, 269*, 334-356.

Carrió, M., González-Montalbán, N., Vera, A., Villaverde, A., & Ventura, S. (2005). Amyloid-like properties of bacterial inclusion bodies. *Journal of Molecular Biology, 347*(5), 1025-1037.

Cen, K., Huang, C., Yu, X., Gao, C., Yang, Y., Tang, X., & Feng, X. (2023). Quinoa protein Pickering emulsion: a promising cryoprotectant to enhance the freeze-thaw stability of fish myofibril gels. *Food Chemistry, 407*, 135139.

Cen, K., Yu, X., Gao, C., Yang, Y., Tang, X., & Feng, X. (2022). Effects of quinoa protein Pickering emulsion on the properties, structure and intermolecular interactions of myofibrillar protein gel. *Food Chemistry, 394*, 133456.

Cerda-Costa, N., Esteras-Chopo, A., Aviles, F., Serrano, L., & Villegas, V. (2007). Early kinetics of amyloid fibril formation reveals conformational reorganisation of initial aggregates. *Journal of Molecular Biology, 366*(4), 1351-1363.

Chang, C., Tu, S., Ghosh, S., & Nickerson, M. (2015). Effect of pH on the inter-relationships between the physicochemical, interfacial and emulsifying properties for pea, soy, lentil and canola protein isolates. *Food Research International, 77*, 360-367.

Chao, D., & Aluko, R. E. (2018). Modification of the structural, emulsifying, and foaming properties of an isolated pea protein by thermal pretreatment. *CyTA-Journal of Food, 16*(1), 357-366.

Chao, D., Jung, S., & Aluko, R. E. (2018). Physicochemical and functional properties of high pressure-treated isolated pea protein. *Innovative Food Science & Emerging Technologies, 45*, 179-185.

Chatani, E., Lee, Y.-H., Yagi, H., Yoshimura, Y., Naiki, H., & Goto, Y. (2009). Ultrasonication-dependent production and breakdown lead to minimum-sized amyloid fibrils. *Proceedings of the National Academy of Sciences, 106*(27), 11119-11124.

Chavrier, F., Chapelon, J., Gelet, A., & Cathignol, D. (2000). Modeling of high-intensity focused ultrasound-induced lesions in the presence of cavitation bubbles. *The Journal of the Acoustical Society of America, 108*(1), 432-440.

Chen, D., Fang, F., Federici, E., Campanella, O., & Jones, O. G. (2020). Rheology, microstructure and phase behavior of potato starch-protein fibril mixed gel. *Carbohydrate Polymers, 239*, 116247.

Chen, J., Mu, T., Zhang, M., & Goffin, D. (2019). Effect of high hydrostatic pressure on the structure, physicochemical and functional properties of protein isolates from cumin (Cuminum cyminum) seeds. *International Journal of Food Science & Technology, 54*(3), 752-761.

Chen, L., Ettelaie, R., & Akhtar, M. (2019). Improved enzymatic accessibility of peanut protein isolate pre-treated using thermosonication. *Food Hydrocolloids, 93*, 308-316.

Chen, N., Zhao, M., Chassenieux, C., & Nicolai, T. (2016). Thermal aggregation and gelation of soy globulin at neutral pH. *Food Hydrocolloids, 61*, 740-746.

Chen, N., Zhao, M., Niepceron, F., Nicolai, T., & Chassenieux, C. (2017). The effect of the pH on thermal aggregation and gelation of soy proteins. *Food Hydrocolloids, 66*, 27-36.

Chen, S., Goode, A. E., Skepper, J. N., Thorley, A. J., Seiffert, J. M., Chung, K. F., Tetley, T. D., Shaffer, M. S., Ryan, M. P., & Porter, A. E. (2016). Avoiding artefacts during electron microscopy of silver nanomaterials exposed to

biological environments. *Journal of Microscopy, 261*(2), 157-166.

Chen, X., Yang, J., Shen, M., Chen, Y., Yu, Q., & Xie, J. (2022). Structure, function and advance application of microwave-treated polysaccharide: A review. *Trends in Food Science & Technology, 123*, 198-209.

Cheng, L., De Leon-Rodriguez, L. M., Gilbert, E. P., Loo, T., Petters, L., & Yang, Z. (2024). Self-assembly and hydrogelation of a potential bioactive peptide derived from quinoa proteins. *International Journal of Biological Macromolecules, 259*, 129296.

Cheng, L., Ye, A., Yang, Z., Gilbert, E. P., Knott, R., de Campo, L., Storer, B., Hemar, Y., & Singh, H. (2022). Small-angle X-ray scattering (SAXS) and small-angle neutron scattering (SANS) study on the structure of sodium caseinate in dispersions and at the oil-water interface: Effect of calcium ions. *Food Structure, 32*, 100276.

Cheng, Y., Fu, Y., Ma, L., Yap, P. L., Losic, D., Wang, H., & Zhang, Y. (2022). Rheology of edible food inks from 2D/3D/4D printing, and its role in future 5D/6D printing. *Food Hydrocolloids*, 107855.

Chuang, C.-C., Ye, A., Anema, S. G., & Loveday, S. M. (2021). Hemp globulin forms colloidal nanocomplexes with sodium caseinate during pH-cycling. *Food Research International, 150*, 110810.

Clarke, C. (2004). *The Science of Ice Cream*. Royal Society of Chemistry.

Coker, O. J., Shand, P. J., & Ghosh, S. (2024). The effect of heat treatment and high-pressure homogenization on the dispersibility and interfacial behavior of faba bean protein isolate and concentrate. *Sustainable Food Proteins*.

Contamine, R. F., Wilhelm, A., Berlan, J., & Delmas, H. (1995). Power measurement in sonochemistry. *Ultrasonics Sonochemistry, 2*(1), S43-S47.

Cosson, A., Correia, L. O., Descamps, N., Saint-Eve, A., & Souchon, I. (2022). Identification and characterization of the main peptides in pea protein isolates using ultra high-performance liquid chromatography coupled with mass spectrometry and bioinformatics tools. *Food Chemistry, 367*, 130747.

Costa, M. G. M., Fonteles, T. V., de Jesus, A. L. T., Almeida, F. D. L., de Miranda, M. R. A., Fernandes, F. A. N., & Rodrigues, S. (2013). High-intensity ultrasound processing of pineapple juice. *Food and Bioprocess Technology, 6*, 997-1006.

Couto, S. R., & Sanromán, M. A. (2006). Application of solid-state fermentation to food industry—a review. *Journal of Food Engineering, 76*(3), 291-302.

D'Alessio, G., Flamminii, F., Faieta, M., Prete, R., Di Michele, A., Pittia, P., & Di Mattia, C. D. (2023). High pressure homogenization to boost the technological functionality of native pea proteins. *Current Research in Food Science, 6*, 100499.

da Silva, A. M. M., Almeida, F. S., & Sato, A. C. K. (2021). Functional characterization of commercial plant proteins and their application on stabilization of emulsions. *Journal of Food Engineering, 292*, 110277.

Dabade, A., Kahar, S., Acharjee, A., Bhushette, P., & Annapure, U. (2023). Effect of atmospheric pressure non-thermal pin to plate cold plasma on structural and functional properties of soy protein isolate. *Journal of Agriculture and Food Research, 12*, 100538.

Dai, C., Hou, Y., Xu, H., Huang, L., Dabbour, M., Mintah, B. K., He, R., & Ma, H. (2022). Effect of solid-state fermentation by three different Bacillus species on composition and protein structure of soybean meal. *Journal of the Science of Food and Agriculture, 102*(2), 557-566.

Dai, C., Zhao, G., Zhao, M., & You, Q. (2012). Preparation of dispersed particle gel (DPG) through a simple high speed shearing method. *Molecules, 17*(12), 14484-14489.

Dai, S., Lian, Z., Qi, W., Chen, Y., Tong, X., Tian, T., Lyu, B., Wang, M., Wang, H., & Jiang, L. (2022). Non-covalent interaction of soy protein isolate and catechin: Mechanism and effects on protein conformation. *Food Chemistry, 384*, 132507.

Damodaran, S. (2005). Protein stabilization of emulsions and foams. *Journal of Food Science, 70*(3), R54-R66.

Damodaran, S. (2008). Amino acids, peptides and proteins. *Fennema's Food Chemistry, 4*, 425-439.

Damodaran, S. (2017). Protein-stabilized foams and emulsions. In A. Damodaran & A Paraf, (Ed.), *Food proteins and their applications* (pp. 57-110): CRC Press.

Dankar, I., Haddarah, A., El Omar, F., Sepulcre, F., & Pujolà, M. (2018). Assessing the microstructural and rheological changes induced by food additives on potato puree. *Food Chemistry, 240*, 304-313.

Davis, P., & Williams, S. (1998). Protein modification by thermal processing. *Allergy, 53*, 102-105.

De Angelis, D., Pasqualone, A., Squeo, G., Caponio, F., & Summo, C. (2023). Amino acid and fatty acid compositions of texturized vegetable proteins: Composizione di proteine vegetali testurizzate. *Italian Journal of Food Science, 35*(1), 19-25.

De Kort, D. W., Veen, S. J., Van As, H., Bonn, D., Velikov, K. P., & Van Duynhoven, J. P. (2016). Yielding and flow of cellulose microfibril dispersions in the presence of a charged polymer. *Soft Matter, 12*(21), 4739-4744.

de la Rosa-Millán, J., Orona-Padilla, J. L., Flores-Moreno, V. M., & Serna-Saldívar, S. O. (2018). Physicochemical, functional and ATR-FTIR molecular analysis of protein extracts derived from starchy pulses. *International Journal of Food Science & Technology, 53*(6), 1414-1424.

De Marchi, M., Costa, A., Pozza, M., Goi, A., & Manuelian, C. L. (2021). Detailed characterization of plant-based burgers. *Scientific Reports, 11*(1), 2049.

de Oliveira, F. C., Coimbra, J. S. d. R., de Oliveira, E. B., Zuñiga, A. D. G., & Rojas, E. E. G. (2016). Food protein-polysaccharide conjugates obtained via the Maillard reaction: A review. *Critical Reviews in Food Science and Nutrition, 56*(7), 1108-1125.

del Mar Yust, M., Pedroche, J., del Carmen Millán-Linares, M., Alcaide-Hidalgo, J. M., & Millán, F. (2010). Improvement of functional properties of chickpea proteins by hydrolysis with immobilised Alcalase. *Food Chemistry, 122*(4), 1212-1217.

Deng, R., Mars, M., Van Der Sman, R. G., Smeets, P. A., & Janssen, A. E. (2020). The importance of swelling for in vitro gastric digestion of whey protein gels. *Food Chemistry, 330*, 127182.

Derkach, S. R. (2009). Rheology of emulsions. *Advances in Colloid and Interface Science, 151*(1-2), 1-23.

Dhull, S. B., Kidwai, M. K., Noor, R., Chawla, P., & Rose, P. K. (2022). A review of nutritional profile and processing of faba bean (Vicia faba L.). *Legume Science, 4*(3), e129.

Di Carlo, M. G., Minicozzi, V., Foderà, V., Militello, V., Vetri, V., Morante, S., & Leone, M. (2015). Thioflavin T templates amyloid β (1–40) conformation and aggregation pathway. *Biophysical Chemistry, 206*, 1-11.

Dickinson, E. (2017). Biopolymer-based particles as stabilizing agents for emulsions and foams. *Food Hydrocolloids, 68*, 219-231.

Dickinson, E. (2019). Strategies to control and inhibit the flocculation of protein-stabilized oil-in-water emulsions. *Food Hydrocolloids, 96*, 209-223.

Dille, M. J., Knutsen, S. H., & Draget, K. I. (2022). Gels and gelled emulsions prepared by acid-induced gelation of mixtures of faba bean (Vicia faba) protein concentrate and λ-carrageenan. *Applied Food Research, 2*(2), 100174.

Doost, A. S., Nasrabadi, M. N., Kassozi, V., Dewettinck, K., Stevens, C. V., & Van der Meeren, P. (2019). Pickering stabilization of thymol through green emulsification using soluble fraction of almond gum–Whey protein isolate nano-complexes. *Food Hydrocolloids, 88*, 218-227.

Drakos, A., Doxastakis, G., & Kiosseoglou, V. (2007). Functional effects of lupin proteins in comminuted meat and emulsion gels. *Food Chemistry, 100*(2), 650-655.

Du, H., Lin, Y., Stanton, C., Daniloski, D., Zannini, E., Ross, R. P., & Miao, S. (2023). Characterization and functional properties of pH-and heated time-induced aggregates from red lentil protein. *Food Structure, 37*, 100342.

Du, L., Li, S., & Meng, Z. (2024). Fat analogue emulsions stabilized by peanut protein microgel particles: microscale and nanoscale structure and stabilization process analysis. *Journal of the Science of Food and Agriculture, 104*(6), 3788-3797.

Du, L., & Meng, Z. (2024). Carrageenan-induced conjugated oat protein isolate microgel particles as structure modulators in fat analogues and their digestion behaviors. *Journal of Colloid and Interface Science*.

Dudkiewicz, A., Tiede, K., Loeschner, K., Jensen, L. H. S., Jensen, E., Wierzbicki, R., Boxall, A. B., & Molhave, K. (2011). Characterization of nanomaterials in food by electron microscopy. *TrAC Trends in Analytical Chemistry, 30*(1), 28-43.

Dufrêne, Y. F., Ando, T., Garcia, R., Alsteens, D., Martinez-Martin, D., Engel, A., Gerber, C., & Müller, D. J. (2017). Imaging modes of atomic force microscopy for application in molecular and cell biology. *Nature nanotechnology, 12*(4), 295-307.

Eckert, E., Han, J., Swallow, K., Tian, Z., Jarpa-Parra, M., & Chen, L. (2019). Effects of enzymatic hydrolysis and ultrafiltration on physicochemical and functional properties of faba bean protein. *Cereal Chemistry, 96*(4), 725-741.

Eivazzadeh-Keihan, R., Radinekiyan, F., Maleki, A., Salimi Bani, M., Hajizadeh, Z., & Asgharnasl, S. (2019). A novel biocompatible core-shell magnetic nanocomposite based on cross-linked chitosan hydrogels for in vitro hyperthermia of cancer therapy. *International Journal of Biological Macromolecules, 140*, 407-414.

El-Adawy, T. A. (2000). Functional properties and nutritional quality of acetylated and succinylated mung bean protein isolate. *Food Chemistry, 70*(1), 83-91.

Enfield, R. E., Pandya, J. K., Lu, J., McClements, D. J., & Kinchla, A. J. (2022). The future of 3D food printing: Opportunities for space applications. *Critical Reviews in Food Science and Nutrition*, 1-14.

Fang, Z., Cai, X., Wu, J., Zhang, L., Fang, Y., & Wang, S. (2021). Effect of simultaneous treatment combining ultrasonication and pH-shifting on SPI in the formation of nanoparticles and encapsulating resveratrol. *Food Hydrocolloids, 111*, 106250.

Fasman, G. D. (2013). *Circular dichroism and the conformational analysis of biomolecules*: Springer Science & Business Media.

Felix, M., Romero, A., Carrera-Sanchez, C., & Guerrero, A. (2019). Assessment of interfacial viscoelastic properties of Faba bean (Vicia faba) protein-adsorbed O/W layers as a function of pH. *Food Hydrocolloids, 90*, 353-359.

Feng, S., Zhang, S., Jiang, M., Liu, F., Chen, K., & Zhang, Y. (2023). Effects of glycation methods on the interfacial behavior and emulsifying performance of soy protein isolate-gum Arabic conjugates. *International Journal of Biological Macromolecules, 233*, 123554.

Feng, T., Fan, C., Wang, X., Wang, X., Xia, S., & Huang, Q. (2022). Food-grade Pickering emulsions and high internal phase Pickering emulsions encapsulating cinnamaldehyde based on pea protein-pectin-EGCG complexes for extrusion 3D printing. *Food Hydrocolloids, 124*, 107265.

Ferjancic-Biagini, A., Giardina, T., & Puigserver, A. (1998). Acylation of food proteins and hydrolysis by digestive enzymes: A review. *Journal of Food Biochemistry, 22*(4), 331-345.

Fernandez-Escamilla, A.-M., Rousseau, F., Schymkowitz, J., & Serrano, L. (2004). Prediction of sequence-dependent and mutational effects on the aggregation of peptides and proteins. *Nature Biotechnology, 22*(10), 1302-1306.

Fernandez-Flores, A. (2011). A review of amyloid staining: methods and artifacts. *Biotechnic & Histochemistry, 86*(5), 293-301.

Figueroa-González, J. J., Lobato-Calleros, C., Vernon-Carter, E. J., Aguirre-Mandujano, E., Alvarez-Ramirez, J., & Martínez-Velasco, A. (2022). Modifying the structure, physicochemical properties, and foaming ability of amaranth protein by dual pH-shifting and ultrasound treatments. *LWT, 153*, 112561.

Fitzpatrick, J. J., & Ahrné, L. (2005). Food powder handling and processing: Industry problems, knowledge barriers and research opportunities. *Chemical Engineering and Processing: Process Intensification, 44*(2), 209-214.

Flores-Jiménez, N. T., Ulloa, J. A., Urías-Silvas, J. E., Ramírez-Ramírez, J. C., Bautista-Rosales, P. U., & Gutiérrez-Leyva, R. (2022). Influence of high-intensity ultrasound on physicochemical and functional properties of a guamuchil Pithecellobium dulce (Roxb.) seed protein isolate. *Ultrasonics Sonochemistry, 84*, 105976.

Flores, M., & Piornos, J. A. (2021). Fermented meat sausages and the challenge of their plant-based alternatives: A comparative review on aroma-related aspects. *Meat Science, 182*, 108636.

Foegeding, E. A., & Davis, J. P. (2011). Food protein functionality: A comprehensive approach. *Food Hydrocolloids, 25*(8), 1853-1864.

Franco, J., Partal, P., Ruiz-M Rquez, D., Conde, B., & Gallegos, C. (2000). Influence of pH and protein thermal treatment on the rheology of pea protein-stabilized oil-in-water emulsions. *Journal of the American Oil Chemists' Society, 77*, 975-984.

Frydenberg, R. P., Hammershøj, M., Andersen, U., Greve, M. T., & Wiking, L. (2016). Protein denaturation of whey protein isolates (WPIs) induced by high intensity ultrasound during heat gelation. *Food Chemistry, 192*, 415-423.

Fu, L., He, Z., Zeng, M., Qin, F., & Chen, J. (2020). Effects of soy protein composition in recombined soy-based cream on the stability and physical properties of whipping cream. *Journal of the Science of Food and Agriculture, 100*(6), 2732-2741.

Fu, L., Wang, Z., He, Z., Zeng, M., Qin, F., & Chen, J. (2023). Effects of soluble aggregates sizes on rheological properties of soybean protein isolate under high temperature. *LWT, 182*, 114793.

Galazka, V. B., Dickinson, E., & Ledward, D. A. (2000). Influence of high pressure processing on protein solutions and emulsions. *Current Opinion in Colloid &*

Interface Science, 5(3-4), 182-187.
Galema, S. A. (1997). Microwave chemistry. *Chemical Society Reviews, 26*(3), 233-238.
Galvão, A. M. M. T., da Costa, G. F., Dos Santos, M., Pollonio, M. A. R., & Hubinger, M. D. (2024). Replacing the animal fat in Bologna sausages using high internal phase emulsion stabilized with lentil protein isolate (Lens culinaris). *Meat Science*, 109589.
Gao, K., Rao, J., & Chen, B. (2023). Plant protein solubility: A challenge or insurmountable obstacle. *Advances in Colloid and Interface Science*, 103074.
Gao, Z., Zhao, J., Huang, Y., Yao, X., Zhang, K., Fang, Y., Nishinari, K., Phillips, G. O., Jiang, F., & Yang, H. (2017). Edible Pickering emulsion stabilized by protein fibrils. Part 1: Effects of pH and fibrils concentration. *LWT, 76*, 1-8.
Gaspar, A. L. C., & de Góes-Favoni, S. P. (2015). Action of microbial transglutaminase (MTGase) in the modification of food proteins: A review. *Food Chemistry, 171*, 315-322.
Ge, J., Sun, C., Chang, Y., Sun, M., Zhang, Y., & Fang, Y. (2022). Heat-induced pea protein isolate gels reinforced by panda bean protein amyloid fibrils: Gelling properties and formation mechanism. *Food Research International, 162*, 112053.
Georget, E., Miller, B., Callanan, M., Heinz, V., & Mathys, A. (2014). (Ultra) high pressure homogenization for continuous high pressure sterilization of pumpable foods–a review. *Frontiers in Nutrition, 1*, 15.
Gharibzahedi, S. M. T., & Smith, B. (2020). The functional modification of legume proteins by ultrasonication: A review. *Trends in Food Science & Technology, 98*, 107-116.
Gharsallaoui, A., Cases, E., Chambin, O., & Saurel, R. (2009). Interfacial and emulsifying characteristics of acid-treated pea protein. *Food Biophysics, 4*(4), 273-280.
Gilbert, E. P. (2019). Small-angle X-Ray and neutron scattering in food colloids. *Current Opinion in Colloid & Interface Science, 42*, 55-72.
Gilbert, E. P. (2023). Neutron techniques for food hydrocolloids. *Current Opinion in Colloid & Interface Science*, 101730.
Gilbert, E. P., Schulz, J. C., & Noakes, T. J. (2006). 'Quokka'—the small-angle neutron scattering instrument at OPAL. *Physica B: Condensed Matter, 385*, 1180-1182.
Giteru, S. G., Oey, I., & Ali, M. A. (2018). Feasibility of using pulsed electric fields to modify biomacromolecules: A review. *Trends in Food Science & Technology, 72*, 91-113.
Godoi, F. C., Bhandari, B. R., Prakash, S., & Zhang, M. (2018). *Fundamentals of 3D food printing and applications*: Academic press.
Goeden-Wood, N. L., Keasling, J. D., & Muller, S. J. (2003). Self-assembly of a designed protein polymer into β-sheet fibrils and responsive gels. *Macromolecules, 36*(8), 2932-2938.
Gogate, P. R., & Kabadi, A. M. (2009). A review of applications of cavitation in biochemical engineering/biotechnology. *Biochemical Engineering Journal, 44*(1), 60-72.
Goldstein, J. I., Newbury, D. E., Michael, J. R., Ritchie, N. W., Scott, J. H. J., & Joy, D. C. (2017). *Scanning electron microscopy and X-ray microanalysis*: springer.
Gouseti, O., Larsen, M. E., Amin, A., Bakalis, S., Petersen, I. L., Lametsch, R., & Jensen, P. E. (2023). Applications of enzyme technology to enhance transition

to plant proteins: a review. *Foods, 12*(13), 2518.
Greenfield, N. J. (2006). Using circular dichroism spectra to estimate protein secondary structure. *Nature Protocols, 1*(6), 2876-2890.
Grossi, M., Rao, J., & Chen, B. (2024). Tuning the properties of plant-based whipped cream through zein nanoparticles-sodium stearate complex. *Food Hydrocolloids, 155*, 110219.
Grossmann, L., & McClements, D. J. (2023). Current insights into protein solubility: A review of its importance for alternative proteins. *Food Hydrocolloids, 137*, 108416.
Gu, B. J., Masli, M. D. P., & Ganjyal, G. M. (2020). Whole faba bean flour exhibits unique expansion characteristics relative to the whole flours of lima, pinto, and red kidney beans during extrusion. *Journal of Food Science, 85*(2), 404-413.
Guimarães, J. T., Silva, E. K., Alvarenga, V. O., Costa, A. L. R., Cunha, R. L., Sant'Ana, A. S., Freitas, M. Q., Meireles, M. A. A., & Cruz, A. G. (2018). Physicochemical changes and microbial inactivation after high-intensity ultrasound processing of prebiotic whey beverage applying different ultrasonic power levels. *Ultrasonics Sonochemistry, 44*, 251-260.
Guinier, A., Fournet, G., Walker, C. B., & Vineyard, G. H. (1956). Small-angle scattering of X-rays. In: American Institute of Physics.
Guinier, A., Fournet, G., Walker, C. B., & Yudowitch, K. L. (1955). *Small-angle Scattering of X-rays*: Wiley New York.
Guliyeva, A. J., & Gasymov, O. K. (2020). ANS fluorescence: Potential to discriminate hydrophobic sites of proteins in solid states. *Biochemistry and Biophysics Reports, 24*, 100843.
Gülseren, İ., Güzey, D., Bruce, B. D., & Weiss, J. (2007). Structural and functional changes in ultrasonicated bovine serum albumin solutions. *Ultrasonics Sonochemistry, 14*(2), 173-183.
Gumus, C. E., Decker, E. A., & McClements, D. J. (2017a). Formation and stability of ω-3 oil emulsion-based delivery systems using plant proteins as emulsifiers: Lentil, pea, and faba bean proteins. *Food Biophysics, 12*(2), 186-197.
Gumus, C. E., Decker, E. A., & McClements, D. J. (2017b). Impact of legume protein type and location on lipid oxidation in fish oil-in-water emulsions: Lentil, pea, and faba bean proteins. *Food Research International, 100*, 175-185.
Guo, F., Xiong, Y. L., Qin, F., Jian, H., Huang, X., & Chen, J. (2015). Surface properties of heat-induced soluble soy protein aggregates of different molecular masses. *Journal of Food Science, 80*(2), C279-C287.
Hall, A. E., & Moraru, C. I. (2021). Structure and function of pea, lentil and faba bean proteins treated by high pressure processing and heat treatment. *LWT, 152*, 112349.
Hamada, J. S., & Swanson, B. (1994). Deamidation of food proteins to improve functionality. *Critical Reviews in Food Science & Nutrition, 34*(3), 283-292.
Hammouda, B., Ho, D. L., & Kline, S. (2004). Insight into clustering in poly (ethylene oxide) solutions. *Macromolecules, 37*(18), 6932-6937.
Han, Y. M., Zhu, L., Qi, X. G., Zhang, H., & Wu, G. C. (2023). Characteristics of low-fat whipped cream containing protein-based fat replacers. *International Journal of Dairy Technology, 76*(2), 276-290.
Harris, J. R. (2015). Transmission electron microscopy in molecular structural biology: a historical survey. *Archives of biochemistry and biophysics, 581*, 3-18.
He, Z., Li, W., Guo, F., Li, W., Zeng, M., & Chen, J. (2015). Foaming characteristics of

commercial soy protein isolate as influenced by heat-induced aggregation. *International Journal of Food Properties, 18*(8), 1817-1828.

Hei, X., Li, S., Liu, Z., Wu, C., Ma, X., Jiao, B., Hu, H., Zhu, J., Adhikari, B., & Wang, Q. (2024). Characteristics of Pickering emulsions stabilized by microgel particles of five different plant proteins and their application. *Food Chemistry, 449*, 139187.

Hellebois, T., Gaiani, C., Planchon, S., Renaut, J., & Soukoulis, C. (2021). Impact of heat treatment on the acid induced gelation of brewers' spent grain protein isolate. *Food Hydrocolloids, 113*, 106531.

Herneke, A., Karkehabadi, S., Lu, J., Lendel, C., & Langton, M. (2023). Protein nanofibrils from mung bean: The effect of pH on morphology and the ability to form and stabilise foams. *Food Hydrocolloids, 136*, 108315.

Herneke, A., Lendel, C., Johansson, D., Newson, W., Hedenqvist, M., Karkehabadi, S., Jonsson, D., & Langton, M. (2021). Protein nanofibrils for sustainable food–characterization and comparison of fibrils from a broad range of plant protein isolates. *ACS Food Science & Technology, 1*(5), 854-864.

Herneke, A., Lendel, C., Karkehabadi, S., Lu, J., & Langton, M. (2023). Protein nanofibrils from fava bean and its major storage proteins: formation and ability to generate and stabilise foams. *Foods, 12*(3), 521.

Hernoux Villière, A., Lassi, U., & Lévêque, J. M. (2013). An original ultrasonic reaction with dual coaxial frequencies for biomass processing. *Ultrasonics Sonochemistry, 20*(6), 1341-1344.

Herreman, L., Nommensen, P., Pennings, B., & Laus, M. C. (2020). Comprehensive overview of the quality of plant-And animal-sourced proteins based on the digestible indispensable amino acid score. *Food science & nutrition, 8*(10), 5379-5391.

Hettiarachchi, C. A., Melton, L. D., Gerrard, J. A., & Loveday, S. M. (2012). Formation of β-lactoglobulin nanofibrils by microwave heating gives a peptide composition different from conventional heating. *Biomacromolecules, 13*(9), 2868-2880.

Higa, F. A., & Nickerson, M. T. (2023). Plant protein-carbohydrate conjugates: A review of their production, functionality and nutritional attributes. *Food Reviews International, 39*(2), 750-771.

Hite, B. H. (1899). *The effect of pressure in the preservation of milk: a preliminary report* (Vol. 58): The Station.

Hong, D.-P., Han, S., L Fink, A., & N Uversky, V. (2011). Characterization of the non-fibrillar α-synuclein oligomers. *Protein and Peptide Letters, 18*(3), 230-240.

Hotrum, N. E., Cohen Stuart, M. A., van Vliet, T., & van Aken, G. A. (2004). Spreading of partially crystallized oil droplets on an air/water interface. *Colloids and Surfaces A: Physicochemical and Engineering Aspects, 240*(1), 83-92.

Housmans, J. A., Wu, G., Schymkowitz, J., & Rousseau, F. (2023). A guide to studying protein aggregation. *The FEBS Journal, 290*(3), 554-583.

Hu, A., & Li, L. (2021). Effect mechanism of ultrasound pretreatment on fibrillation Kinetics, physicochemical properties and structure characteristics of soy protein isolate nanofibrils. *Ultrasonics Sonochemistry, 78*, 105741.

Hu, H., Cheung, I. W., Pan, S., & Li-Chan, E. C. (2015). Effect of high intensity ultrasound on physicochemical and functional properties of aggregated soybean β-conglycinin and glycinin. *Food Hydrocolloids, 45*, 102-110.

Hu, H., Li-Chan, E. C., Wan, L., Tian, M., & Pan, S. (2013). The effect of high intensity

ultrasonic pre-treatment on the properties of soybean protein isolate gel induced by calcium sulfate. *Food Hydrocolloids, 32*(2), 303-311.

Hu, H., Wu, J., Li-Chan, E. C., Zhu, L., Zhang, F., Xu, X., Fan, G., Wang, L., Huang, X., & Pan, S. (2013). Effects of ultrasound on structural and physical properties of soy protein isolate (SPI) dispersions. *Food Hydrocolloids, 30*(2), 647-655.

Hu, Y., Cheng, L., Gilbert, E. P., Lee, S. J., & Yang, Z. (2024). Impact of thermosonication at neutral pH on the structural characteristics of faba bean protein isolate dispersions and their physicochemical and techno-functional properties. *Food Hydrocolloids*, 110140.

Hu, Y., Cheng, L., Gilbert, E. P., Loo, T. S., Lee, S. J., Harrison, J., & Yang, Z. (2024). Fibrillisation of faba bean protein isolate by thermosonication for process efficacy: microstructural characteristics, assembly behaviour, and physicochemical properties. *Food Hydrocolloids*, 110127.

Hu, Y., Cheng, L., Lee, S. J., & Yang, Z. (2023). Formation and characterisation of concentrated emulsion gels stabilised by faba bean protein isolate and its applications for 3D food printing. *Colloids and Surfaces A: Physicochemical and Engineering Aspects*, 131622.

Hu, Y., He, C., Woo, M. W., Xiong, H., Hu, J., & Zhao, Q. (2019). Formation of fibrils derived from whey protein isolate: Structural characteristics and protease resistance. *Food & Function, 10*(12), 8106-8115.

Huang, Z.-X., Lin, W.-F., Zhang, Y., & Tang, C.-H. (2022). Freeze-thaw-stable high internal phase emulsions stabilized by soy protein isolate and chitosan complexes at pH 3.0 as promising mayonnaise replacers. *Food Research International, 156*, 111309.

Hudson, S. A., Ecroyd, H., Kee, T. W., & Carver, J. A. (2009). The thioflavin T fluorescence assay for amyloid fibril detection can be biased by the presence of exogenous compounds. *The FEBS Journal, 276*(20), 5960-5972.

Husband, F., Wilde, P., Clark, D., Rawel, H., & Muschiolik, G. (1994). Foaming properties of modified faba bean protein isolates. *Food Hydrocolloids, 8*(5), 455-468.

Hyun, K., Kim, S. H., Ahn, K. H., & Lee, S. J. (2002). Large amplitude oscillatory shear as a way to classify the complex fluids. *Journal of Non-Newtonian Fluid Mechanics, 107*(1-3), 51-65.

Indrawati, L., Wang, Z., Narsimhan, G., & Gonzalez, J. (2008). Effect of processing parameters on foam formation using a continuous system with a mechanical whipper. *Journal of Food Engineering, 88*(1), 65-74.

Islam, M. A., Amin, M. N., Siddiqui, S. A., Hossain, M. P., Sultana, F., & Kabir, M. R. (2019). Trans fatty acids and lipid profile: A serious risk factor to cardiovascular disease, cancer and diabetes. *Diabetes & Metabolic Syndrome: Clinical Research & Reviews, 13*(2), 1643-1647.

Jackson, C. L., Chanzy, H. D., Booy, F. P., Drake, B. J., Tomalia, D. A., Bauer, B. J., & Amis, E. J. (1998). Visualization of dendrimer molecules by transmission electron microscopy (TEM): Staining methods and cryo-TEM of vitrified solutions. *Macromolecules, 31*(18), 6259-6265.

Jambrak, A. R., Mason, T. J., Lelas, V., Herceg, Z., & Herceg, I. L. (2008). Effect of ultrasound treatment on solubility and foaming properties of whey protein suspensions. *Journal of Food Engineering, 86*(2), 281-287.

Jeske, S., Zannini, E., & Arendt, E. K. (2018). Past, present and future: The strength of plant-based dairy substitutes based on gluten-free raw materials. *Food*

Rresearch International, 110, 42-51.

Ji, F., Xu, J., Ouyang, Y., Mu, D., Li, X., Luo, S., Shen, Y., & Zheng, Z. (2021). Effects of NaCl concentration and temperature on fibrillation, structure, and functional properties of soy protein isolate fibril dispersions. *LWT, 149*, 111862.

Ji, H., Dong, S., Han, F., Li, Y., Chen, G., Li, L., & Chen, Y. (2018). Effects of dielectric barrier discharge (DBD) cold plasma treatment on physicochemical and functional properties of peanut protein. *Food and Bioprocess Technology, 11*, 344-354.

Jiang, H., Zheng, L., Zou, Y., Tong, Z., Han, S., & Wang, S. (2019). 3D food printing: Main components selection by considering rheological properties. *Critical Reviews in Food Science and Nutrition, 59*(14), 2335-2347.

Jiang, J., Wang, Q., & Xiong, Y. L. (2018). A pH shift approach to the improvement of interfacial properties of plant seed proteins. *Current Opinion in Food Science, 19*, 50-56.

Jiang, S., Ding, J., Andrade, J., Rababah, T. M., Almajwal, A., Abulmeaty, M. M., & Feng, H. (2017). Modifying the physicochemical properties of pea protein by pH-shifting and ultrasound combined treatments. *Ultrasonics Sonochemistry, 38*, 835-842.

Jiang, S., Yildiz, G., Ding, J., Andrade, J., Rababahb, T. M., Almajwalc, A., Abulmeatyc, M. M., & Feng, H. (2019). Pea protein nanoemulsion and nanocomplex as carriers for protection of cholecalciferol (vitamin D3). *Food and Bioprocess Technology, 12*, 1031-1040.

Jiang, Y.-H., Cheng, J.-H., & Sun, D.-W. (2020). Effects of plasma chemistry on the interfacial performance of protein and polysaccharide in emulsion. *Trends in Food Science & Technology, 98*, 129-139.

Jiang, Z., Wang, J., Stoddard, F., Salovaara, H., & Sontag-Strohm, T. (2020). Preparation and characterization of emulsion gels from whole faba bean flour. *Foods, 9*(6), 755.

Jiang, Z., Pulkkinen, M., Wang, Y., Lampi, A. M., Stoddard, F. L., Salovaara, H., Piironen, V., & Sontag-Strohm, T. (2016). Faba bean flavour and technological property improvement by thermal pre-treatments. *LWT, 68*, 295-305.

Jiao, B., Shi, A., Wang, Q., & Binks, B. P. (2018). High-internal-phase pickering emulsions stabilized solely by peanut-protein-isolate microgel particles with multiple potential applications. *Angewandte Chemie International Edition, 57*(30), 9274-9278.

Jin, J., Okagu, O. D., Yagoub, A. E. A., & Udenigwe, C. C. (2021). Effects of sonication on the in vitro digestibility and structural properties of buckwheat protein isolates. *Ultrasonics Sonochemistry, 70*, 105348.

Jin, W., Wang, Z., Peng, D., Shen, W., Zhu, Z., Cheng, S., Li, B., & Huang, Q. (2020). Effect of pulsed electric field on assembly structure of α-amylase and pectin electrostatic complexes. *Food Hydrocolloids, 101*, 105547.

Jo, Y.-J., Huang, W., & Chen, L. (2020). Fabrication and characterization of lentil protein gels from fibrillar aggregates and the gelling mechanism study. *Food & Function, 11*(11), 10114-10125.

Josefsson, L., Ye, X., Brett, C. J., Meijer, J., Olsson, C., Sjögren, A., Sundlöf, J., Davydok, A., Langton, M., & Emmer, Å. (2019). Potato protein nanofibrils produced from a starch industry sidestream. *ACS Sustainable Chemistry & Engineering, 8*(2), 1058-1067.

Ju, Q., Yuan, Y., Wu, C., Hu, Y., Zhou, S., & Luan, G. (2023). Heat-induced aggregation

of subunits/polypeptides of soybean protein: Structural and physicochemical properties. *Food Chemistry, 405*, 134774.

Kamada, A., Rodriguez-Garcia, M., Ruggeri, F. S., Shen, Y., Levin, A., & Knowles, T. P. (2021). Controlled self-assembly of plant proteins into high-performance multifunctional nanostructured films. *Nature Communications, 12*(1), 3529.

Karabulut, G., Goksen, G., & Khaneghah, A. M. (2024). Plant-based protein modification strategies towards challenges. *Journal of Agriculture and Food Research*, 101017.

Karaca, A. C., Low, N., & Nickerson, M. (2011). Emulsifying properties of chickpea, faba bean, lentil and pea proteins produced by isoelectric precipitation and salt extraction. *Food Research International, 44*(9), 2742-2750.

Karataş, S. Ç., Günay, D., & Sayar, S. (2017). In vitro evaluation of whole faba bean and its seed coat as a potential source of functional food components. *Food Chemistry, 230*, 182-188.

Karolkowski, A., Martin, C., Bouzidi, E., Albouy, J.-F., Levavasseur, L., Briand, L., & Salles, C. (2022). Heat Treatment, Cultivar and Formulation Modify the Sensory Properties and Consumer Acceptability of Gels Containing Faba Bean (Vicia faba L. minor) Protein Concentrates. *Foods, 11*(19), 3018.

Kaspchak, E., de Oliveira, M. A. S., Simas, F. F., Franco, C. R. C., Silveira, J. L. M., Mafra, M. R., & Igarashi-Mafra, L. (2017). Determination of heat-set gelation capacity of a quinoa protein isolate (Chenopodium quinoa) by dynamic oscillatory rheological analysis. *Food Chemistry, 232*, 263-271.

Kato, A., & Nakai, S. (1980). Hydrophobicity determined by a fluorescence probe method and its correlation with surface properties of proteins. *Biochimica et Biophysica Acta (BBA)-Protein Structure, 624*(1), 13-20.

Keivaninahr, F., Gadkari, P., Benis, K. Z., Tulbek, M., & Ghosh, S. (2021). Prediction of emulsification behaviour of pea and faba bean protein concentrates and isolates from structure–functionality analysis. *RSC Advances, 11*(20), 12117-12135.

Keppler, J. K., Schwarz, K., & van der Goot, A. J. (2020). Covalent modification of food proteins by plant-based ingredients (polyphenols and organosulphur compounds): A commonplace reaction with novel utilization potential. *Trends in Food Science & Technology, 101*, 38-49.

Kew, B., Holmes, M., Liamas, E., Ettelaie, R., Connell, S. D., Dini, D., & Sarkar, A. (2023). Transforming sustainable plant proteins into high performance lubricating microgels. *Nature Communications, 14*(1), 4743.

Khatkar, A. B., Kaur, A., & Khatkar, S. K. (2020). Restructuring of soy protein employing ultrasound: Effect on hydration, gelation, thermal, in-vitro protein digestibility and structural attributes. *LWT, 132*, 109781.

Kim, T.-K., Yong, H.-I., Jung, S., Kim, Y.-B., & Choi, Y.-S. (2020). Effects of replacing pork fat with grape seed oil and gelatine/alginate for meat emulsions. *Meat Science, 163*, 108079.

Kim, W., Wang, Y., & Selomulya, C. (2020). Dairy and plant proteins as natural food emulsifiers. *Trends in Food Science & Technology, 105*, 261-272.

Kimura, A., Fukuda, T., Zhang, M., Motoyama, S., Maruyama, N., & Utsumi, S. (2008). Comparison of Physicochemical Properties of 7S and 11S Globulins from Pea, Fava Bean, Cowpea, and French Bean with Those of Soybean□ French Bean 7S Globulin Exhibits Excellent Properties. *Journal of Agricultural and Food Chemistry, 56*(21), 10273-10279.

Kline, S. R. (2006). Reduction and analysis of SANS and USANS data using IGOR Pro. *Journal of Applied Crystallography, 39*(6), 895-900.

Klupsaite, D., Juodeikiene, G., Zadeike, D., Bartkiene, E., Maknickiene, Z., & Liutkute, G. (2017). The influence of lactic acid fermentation on functional properties of narrow-leaved lupine protein as functional additive for higher value wheat bread. *LWT, 75*, 180-186.

Kong, J., & Yu, S. (2007). Fourier transform infrared spectroscopic analysis of protein secondary structures. *Acta Biochimica et Biophysica Sinica, 39*(8), 549-559.

Kornet, C., Venema, P., Nijsse, J., van der Linden, E., van der Goot, A. J., & Meinders, M. (2020). Yellow pea aqueous fractionation increases the specific volume fraction and viscosity of its dispersions. *Food Hydrocolloids, 99*, 105332.

Kornet, R., Shek, C., Venema, P., van der Goot, A. J., Meinders, M., & van der Linden, E. (2021). Substitution of whey protein by pea protein is facilitated by specific fractionation routes. *Food Hydrocolloids, 117*, 106691.

Kornet, R., Sridharan, S., Venema, P., Sagis, L. M., Nikiforidis, C. V., van der Goot, A. J., Meinders, M. B., & van der Linden, E. (2022). Fractionation methods affect the gelling properties of pea proteins in emulsion-filled gels. *Food Hydrocolloids, 125*, 107427.

Kornet, R., Veenemans, J., Venema, P., van der Goot, A. J., Meinders, M., Sagis, L., & van der Linden, E. (2021). Less is more: Limited fractionation yields stronger gels for pea proteins. *Food Hydrocolloids, 112*, 106285.

Koyoro, H., & Powers, J. (1987). Functional properties of pea globulin fractions. *Cereal Chemistry, 64*(2), 97-101.

Krieger, I. M., & Dougherty, T. J. (1959). A mechanism for non-Newtonian flow in suspensions of rigid spheres. *Transactions of the Society of Rheology, 3*(1), 137-152.

Krüger, M., Oosterhoff, L. A., van Wolferen, M. E., Schiele, S. A., Walther, A., Geijsen, N., De Laporte, L., van der Laan, L. J., Kock, L. M., & Spee, B. (2020). Cellulose nanofibril hydrogel promotes hepatic differentiation of human liver organoids. *Advanced Healthcare Materials, 9*(6), 1901658.

Kuijk, A., Koppert, R., Versluis, P., van Dalen, G., Remijn, C., Hazekamp, J., Nijsse, J., & Velikov, K. P. (2013). Dispersions of attractive semiflexible fiberlike colloidal particles from bacterial cellulose microfibrils. *Langmuir, 29*(47), 14356-14360.

Kutzli, I., Zhou, J., Li, T., Baier, S. K., & Mezzenga, R. (2023). Formation and characterization of plant-based amyloid fibrils from hemp seed protein. *Food Hydrocolloids, 137*, 108307.

Laemmli, U. K. (1970). Cleavage of structural proteins during the assembly of the head of bacteriophage T4. *Nature, 227*(5259), 680-685.

Laguna, L., Fiszman, S., & Tarrega, A. (2021). Saliva matters: Reviewing the role of saliva in the rheology and tribology of liquid and semisolid foods. Relation to in-mouth perception. *Food Hydrocolloids, 116*, 106660.

Langton, M., Ehsanzamir, S., Karkehabadi, S., Feng, X., Johansson, M., & Johansson, D. P. (2020). Gelation of faba bean proteins-Effect of extraction method, pH and NaCl. *Food Hydrocolloids, 103*, 105622.

Lattanzi, V., André, I., Gasser, U., Dubackic, M., Olsson, U., & Linse, S. (2021). Amyloid β 42 fibril structure based on small-angle scattering. *Proceedings of the National Academy of Sciences, 118*(48), e2112783118.

Lee, H., Yildiz, G., Dos Santos, L., Jiang, S., Andrade, J., Engeseth, N., & Feng, H. (2016). Soy protein nano-aggregates with improved functional properties

prepared by sequential pH treatment and ultrasonication. *Food Hydrocolloids, 55*, 200-209.

Lee, S.-H., Shahbaz, H. M., Jeong, S.-H., Hong, S.-Y., & Lee, D.-U. (2022). Effect of pulsed electric field treatment on cell-membrane permeabilization of potato tissue and the quality of French fries. *Italian Journal of Food Science, 34*(3), 13-24.

Lee, Y., Li, D. S., Ilavsky, J., Kuzmenko, I., Jeng, G., O'Donnell, M., & Pozzo, L. D. (2019). Ultrasound-based formation of nano-Pickering emulsions investigated via in-situ SAXS. *Journal of Colloid and Interface Science, 536*, 281-290.

Lefevre, T., & Subirade, M. (2000). Molecular differences in the formation and structure of fine-stranded and particulate β-lactoglobulin gels. *Biopolymers: Original Research on Biomolecules, 54*(7), 578-586.

Lefèvre, T., & Subirade, M. (2003). Formation of intermolecular β-sheet structures: a phenomenon relevant to protein film structure at oil–water interfaces of emulsions. *Journal of Colloid and Interface Science, 263*(1), 59-67.

Leng, X., Cheng, S., Wu, H., Nian, Y., Zeng, X., & Hu, B. (2022). High internal phase emulsions stabilized with polyphenol-amyloid fibril supramolecules for encapsulation and protection of lutein. *Journal of Agricultural and Food Chemistry, 70*(7), 2328-2338.

Levy, R., Okun, Z., Davidovich-Pinhas, M., & Shpigelman, A. (2021). Utilization of high-pressure homogenization of potato protein isolate for the production of dairy-free yogurt-like fermented product. *Food Hydrocolloids, 113*, 106442.

Levy, R., Okun, Z., & Shpigelman, A. (2021). High-pressure homogenization: Principles and applications beyond microbial inactivation. *Food Engineering Reviews, 13*, 490-508.

Li, C., Dai, T., Jiang, D., Geng, Q., Deng, L., Li, T., Zhong, J., Liu, C., & Chen, J. (2024). Acid-induced pea protein gels pretreated with media milling: Gelling properties and the formation mechanism. *Food Chemistry, 449*, 139110.

Li, S., Jiao, B., Meng, S., Fu, W., Faisal, S., Li, X., Liu, H., & Wang, Q. (2022). Edible mayonnaise-like Pickering emulsion stabilized by pea protein isolate microgels: Effect of food ingredients in commercial mayonnaise recipe. *Food Chemistry, 376*, 131866.

Li, T., Wang, L., Geng, H., Zhang, X., & Chen, Z. (2021). Formation, structural characteristics, foaming and emulsifying properties of rice glutelin fibrils. *Food Chemistry, 354*, 129554.

Li, T., Wang, L., Zhang, X., Geng, H., Xue, W., & Chen, Z. (2021). Assembly behavior, structural characterization and rheological properties of legume proteins based amyloid fibrils. *Food Hydrocolloids, 111*, 106396.

Li, T., Yang, Y., Lv, D., Wang, G., Guo, J., Wan, Z., & Yang, X. (2024). Formation of a transparent soy protein hydrogel: Controlled thermal aggregation of protein using glutaminase. *Food Hydrocolloids*, 110202.

Li, T., Zhou, J., Peydayesh, M., Yao, Y., Bagnani, M., Kutzli, I., Chen, Z., Wang, L., & Mezzenga, R. (2023). Plant protein amyloid fibrils for multifunctional sustainable materials. *Advanced Sustainable Systems, 7*(4), 2200414.

Li, T., Zhou, J., Wu, Q., Zhang, X., Chen, Z., & Wang, L. (2023). Modifying functional properties of food amyloid-based nanostructures from rice glutelin. *Food Chemistry, 398*, 133798.

Li, X., Fan, L., Liu, Y., & Li, J. (2021). New insights into food O/W emulsion gels: Strategies of reinforcing mechanical properties and outlook of being applied to

food 3D printing. *Critical Reviews in Food Science and Nutrition*, 1-23.

Li, X., Xu, X., Song, L., Bi, A., Wu, C., Ma, Y., Du, M., & Zhu, B. (2020). High internal phase emulsion for food-grade 3D printing materials. *ACS Applied Materials & Interfaces, 12*(40), 45493-45503.

Li, X., Ye, C., Tian, Y., Pan, S., & Wang, L. (2018). Effect of ohmic heating on fundamental properties of protein in soybean milk. *Journal of Food Process Engineering, 41*(3), e12660.

Li, X. L., Liu, W. J., Xu, B. C., & Zhang, B. (2022). Simple method for fabrication of high internal phase emulsions solely using novel pea protein isolate nanoparticles: Stability of ionic strength and temperature. *Food Chemistry, 370*, 130899.

Li, Y., Cheng, Y., Zhang, Z., Wang, Y., Mintah, B. K., Dabbour, M., Jiang, H., He, R., & Ma, H. (2020). Modification of rapeseed protein by ultrasound-assisted pH shift treatment: Ultrasonic mode and frequency screening, changes in protein solubility and structural characteristics. *Ultrasonics Sonochemistry, 69*, 105240.

Li, Z., & Ngai, T. (2013). Microgel particles at the fluid–fluid interfaces. *Nanoscale, 5*(4), 1399-1410.

Liamas, E., Connell, S. D., & Sarkar, A. (2023). Frictional behaviour of plant proteins in soft contacts: unveiling nanoscale mechanisms. *Nanoscale Advances, 5*(4), 1102-1114.

Liang, H.-N., & Tang, C.-H. (2013). pH-dependent emulsifying properties of pea [Pisum sativum (L.)] proteins. *Food Hydrocolloids, 33*(2), 309-319.

Liang, Y., & Kristinsson, H. G. (2007). Structural and foaming properties of egg albumen subjected to different pH-treatments in the presence of calcium ions. *Food Research International, 40*(6), 668-678.

Liu, C., Pei, R., & Heinonen, M. (2022). Faba bean protein: A promising plant-based emulsifier for improving physical and oxidative stabilities of oil-in-water emulsions. *Food Chemistry, 369*, 130879.

Liu, F., Li, M., Wang, Q., Yan, J., Han, S., Ma, C., Ma, P., Liu, X., & McClements, D. J. (2023). Future foods: Alternative proteins, food architecture, sustainable packaging, and precision nutrition. *Critical Reviews in Food Science and Nutrition, 63*(23), 6423-6444.

Liu, F., & Tang, C.-H. (2011). Cold, gel-like whey protein emulsions by microfluidisation emulsification: Rheological properties and microstructures. *Food Chemistry, 127*(4), 1641-1647.

Liu, F., & Tang, C.-H. (2013). Soy protein nanoparticle aggregates as pickering stabilizers for oil-in-water emulsions. *Journal of Agricultural and Food Chemistry, 61*(37), 8888-8898.

Liu, L., Miao, Y., Hu, C., Gao, L., He, W., Chu, H., Zhang, T., Li, C., & Guo, W. (2024). Effect of ultrasonic frequency on the structural and functional properties of pea protein isolation. *Journal of the Science of Food and Agriculture, 104*(3), 1431-1440.

Liu, Q., Yang, Q., Wang, Y., Jiang, Y., & Chen, H. (2023). Formation and structural characteristics of pea globulin amyloid-like fibrils pretreated with low-frequency magnetic field. *Food Hydrocolloids*, 109331.

Liu, W., Gao, H., McClements, D. J., Zhou, L., Wu, J., & Zou, L. (2019). Stability, rheology, and β-carotene bioaccessibility of high internal phase emulsion gels. *Food hydrocolloids, 88*, 210-217.

Liu, X., Guo, J., Wan, Z.-L., Liu, Y.-Y., Ruan, Q.-J., & Yang, X.-Q. (2018). Wheat

gluten-stabilized high internal phase emulsions as mayonnaise replacers. *Food Hydrocolloids, 77*, 168-175.

Liu, Y., Zhang, W., Wang, K., Bao, Y., Regenstein, J. M., & Zhou, P. (2019). Fabrication of gel-like emulsions with whey protein isolate using microfluidization: Rheological properties and 3D printing performance. *Food and Bioprocess Technology, 12*(12), 1967-1979.

Liu, Y., Zhang, Y., Guo, Z., Wang, C., Kang, H., Li, J., Wang, W., Li, Y., Lu, F., & Liu, Y. (2021). Enhancing the functional characteristics of soy protein isolate via cross-linking catalyzed by Bacillus subtilis transglutaminase. *Journal of the Science of Food and Agriculture, 101*(10), 4154-4160.

Liu, Z., Cao, Z., Zhao, M., Zhang, H., Wang, J., & Sun, B. (2022). Synergistic influence of protein particles and low-molecular-weight emulsifiers on the stability of a milk fat-based whippable oil-in-water emulsion. *Food Hydrocolloids, 127*, 107520.

Liu, Z., Zhang, M., Bhandari, B., & Yang, C. (2018). Impact of rheological properties of mashed potatoes on 3D printing. *Journal of Food Engineering, 220*, 76-82.

Louros, N., Orlando, G., De Vleeschouwer, M., Rousseau, F., & Schymkowitz, J. (2020). Structure-based machine-guided mapping of amyloid sequence space reveals uncharted sequence clusters with higher solubilities. *Nature Communications, 11*(1), 3314.

Loveday, S. M. (2019). Food proteins: technological, nutritional, and sustainability attributes of traditional and emerging proteins. *Annual Review of Food Science and Technology, 10*, 311-339.

Loveday, S. M., & Halim, C. (2024). Protein isolates made in the laboratory versus the factory: A case study with mung bean and chickpea. *Sustainable Food Proteins, 2*(2), 89-98.

Lu, Y., Mao, L., Hou, Z., Miao, S., & Gao, Y. (2019). Development of emulsion gels for the delivery of functional food ingredients: From structure to functionality. *Food Engineering Reviews, 11*(4), 245-258.

Lu, Z., He, J., Zhang, Y., & Bing, D. (2020). Composition, physicochemical properties of pea protein and its application in functional foods. *Critical Rreviews in Food Science and Nutrition, 60*(15), 2593-2605.

Luo, L., Cheng, L., Zhang, R., & Yang, Z. (2022). Impact of high-pressure homogenization on physico-chemical, structural, and rheological properties of quinoa protein isolates. *Food Structure, 32*, 100265.

Luo, L., Yang, Z., Wang, H., Ashokkumar, M., & Hemar, Y. (2022). Impacts of sonication and high hydrostatic pressure on the structural and physicochemical properties of quinoa protein isolate dispersions at acidic, neutral and alkaline pHs. *Ultrasonics Sonochemistry, 91*, 106232.

Luo, L., Zhang, R., Palmer, J., Hemar, Y., & Yang, Z. (2021). Impact of high hydrostatic pressure on the gelation behavior and microstructure of quinoa protein isolate dispersions. *ACS Food Science & Technology, 1*(11), 2144-2151.

Lv, P., Wang, D., Dai, L., Wu, X., Gao, Y., & Yuan, F. (2020). Pickering emulsion gels stabilized by high hydrostatic pressure-induced whey protein isolate gel particles: Characterization and encapsulation of curcumin. *Food Research International, 132*, 109032.

Lyu, Z., Sala, G., & Scholten, E. (2022). Water distribution in maize starch-pea protein gels as determined by a novel confocal laser scanning microscopy image analysis method and its effect on structural and mechanical properties of

composite gels. *Food Hydrocolloids, 133*, 107942.

Ma, Q., Ma, S., Liu, J., Pei, Y., Tang, K., Qiu, J., Wan, J., Zheng, X., & Zhang, J. (2023). Preparation and application of natural protein polymer-based Pickering emulsions. *e-Polymers, 23*(1), 20230001.

Makroo, H., Rastogi, N., & Srivastava, B. (2020). Ohmic heating assisted inactivation of enzymes and microorganisms in foods: A review. *Trends in Food Science & Technology, 97*, 451-465.

Malterre, N., Bot, F., Lerda, E., Arendt, E. K., Zannini, E., & O'Mahony, J. A. (2024). Enhancing the Techno-Functional Properties of Lentil Protein Isolate Dispersions Using In-Line High-Shear Rotor-Stator Mixing. *Foods, 13*(2), 283.

Mantovani, R. A., de Figueiredo Furtado, G., Netto, F. M., & Cunha, R. L. (2018). Assessing the potential of whey protein fibril as emulsifier. *Journal of Food Engineering, 223*, 99-108.

Martin, A. H., Castellani, O., de Jong, G. A., Bovetto, L., & Schmitt, C. (2019). Comparison of the functional properties of RuBisCO protein isolate extracted from sugar beet leaves with commercial whey protein and soy protein isolates. *Journal of the Science of Food and Agriculture, 99*(4), 1568-1576.

Martínez-Velasco, A., Lobato-Calleros, C., Hernández-Rodríguez, B. E., Román-Guerrero, A., Alvarez-Ramirez, J., & Vernon-Carter, E. J. (2018). High intensity ultrasound treatment of faba bean (Vicia faba L.) protein: Effect on surface properties, foaming ability and structural changes. *Ultrasonics Sonochemistry, 44*, 97-105.

Masalova, I., Foudazi, R., & Malkin, A. Y. (2011). The rheology of highly concentrated emulsions stabilized with different surfactants. *Colloids and Surfaces A: Physicochemical and Engineering Aspects, 375*(1-3), 76-86.

Mason, T., Bibette, J., & Weitz, D. (1995). Elasticity of compressed emulsions. *Physical Review Letters, 75*(10), 2051.

Mason, T. O., Chirgadze, D. Y., Levin, A., Adler-Abramovich, L., Gazit, E., Knowles, T. P., & Buell, A. K. (2014). Expanding the solvent chemical space for self-assembly of dipeptide nanostructures. *ACS Nano, 8*(2), 1243-1253.

Matsumiya, K., & Murray, B. S. (2016). Soybean protein isolate gel particles as foaming and emulsifying agents. *Food Hydrocolloids, 60*, 206-215.

Maurer-Stroh, S., Debulpaep, M., Kuemmerer, N., De La Paz, M. L., Martins, I. C., Reumers, J., Morris, K. L., Copland, A., Serpell, L., & Serrano, L. (2010). Exploring the sequence determinants of amyloid structure using position-specific scoring matrices. *Nature Methods, 7*(3), 237-242.

McCarthy, N. A., Kennedy, D., Hogan, S. A., Kelly, P. M., Thapa, K., Murphy, K. M., & Fenelon, M. A. (2016). Emulsification properties of pea protein isolate using homogenization, microfluidization and ultrasonication. *Food Research International, 89*, 415-421.

McClements, D. J. (2004a). *Food Emulsions: Principles, Practices, and Techniques*: CRC press.

McClements, D. J. (2004b). Protein-stabilized emulsions. *Current Opinion in Colloid & Interface Science, 9*(5), 305-313.

McClements, D. J. (2007). Critical review of techniques and methodologies for characterization of emulsion stability. *Critical Reviews in Food Science and Nutrition, 47*(7), 611-649.

McClements, D. J., & Grossmann, L. (2021). The science of plant-based foods: Constructing next-generation meat, fish, milk, and egg analogs. *Comprehensive*

Reviews in Food Science and Food Safety, 20(4), 4049-4100.

Mehr, H. M., & Koocheki, A. (2020). Effect of atmospheric cold plasma on structure, interfacial and emulsifying properties of Grass pea (Lathyrus sativus L.) protein isolate. *Food Hydrocolloids, 106*, 105899.

Meng, X., Li, T., Song, T., Chen, C., Venkitasamy, C., Pan, Z., & Zhang, H. (2019). Solubility, structural properties, and immunomodulatory activities of rice dreg protein modified with sodium alginate under microwave heating. *Food Science & Nutrition, 7*(8), 2556-2564.

Meng, Y., Wei, Z., & Xue, C. (2022). Protein fibrils from different food sources: A review of fibrillation conditions, properties, applications and research trends. *Trends in Food Science & Technology, 121*, 59-75.

Messens, W., Van Camp, J., & Huyghebaert, A. (1997). The use of high pressure to modify the functionality of food proteins. *Trends in Food Science & Technology, 8*(4), 107-112.

Meyer, E. (2003). *Atomic force microscopy: fundamentals to most advanced applications*: Springer.

Micklitsch, C. M., Medina, S. H., Yucel, T., Nagy-Smith, K. J., Pochan, D. J., & Schneider, J. P. (2015). Influence of hydrophobic face amino acids on the hydrogelation of β-hairpin peptide amphiphiles. *Macromolecules, 48*(5), 1281-1288.

Miedzianka, J., Walkowiak, K., Zielińska-Dawidziak, M., Zambrowicz, A., Wolny, S., & Kita, A. (2023). The functional and physicochemical properties of rice protein concentrate subjected to acetylation. *Molecules, 28*(2), 770.

Mihara, H., Matsumura, S., & Takahashi, T. (2005). Construction and control of self-assembly of amyloid and fibrous peptides. *Bulletin of the Chemical Society of Japan, 78*(4), 572-590.

Mir, N. A., Riar, C. S., & Singh, S. (2020). Structural modification in album (Chenopodium album) protein isolates due to controlled thermal modification and its relationship with protein digestibility and functionality. *Food Hydrocolloids, 103*, 105708.

Miranda, C. G., Rodrigues, R. M., Pereira, R. N., Speranza, P., Kurozawa, L. E., Vicente, A. A., & Sato, A. C. K. (2023). Influence of ohmic heating on lentil protein structure and protein-pectin interactions. *Innovative Food Science & Emerging Technologies, 87*, 103413.

Moll, P., Salminen, H., Schmitt, C., & Weiss, J. (2021). Impact of microfluidization on colloidal properties of insoluble pea protein fractions. *European Food Research and Technology, 247*(3), 545-554.

Monteiro, S. H., Silva, E. K., Alvarenga, V. O., Moraes, J., Freitas, M. Q., Silva, M. C., Raices, R. S., Sant'Ana, A. S., Meireles, M. A. A., & Cruz, A. G. (2018). Effects of ultrasound energy density on the non-thermal pasteurization of chocolate milk beverage. *Ultrasonics Sonochemistry, 42*, 1-10.

Mozafarpour, R., Koocheki, A., & Nicolai, T. (2022). Modification of grass pea protein isolate (Lathyrus sativus L.) using high intensity ultrasound treatment: Structure and functional properties. *Food Research International, 158*, 111520.

Mu, D., Li, H., Li, X., Zhu, J., Qiao, M., Wu, X., Luo, S., Yang, P., Zhao, Y., & Liu, F. (2020). Enhancing laccase-induced soybean protein isolates gel properties by microwave pretreatment. *Journal of Food Processing and Preservation, 44*(4), e14386.

Munialo, C. D., Martin, A. H., Van Der Linden, E., & De Jongh, H. H. (2014). Fibril

formation from pea protein and subsequent gel formation. *Journal of Agricultural and Food Chemistry, 62*(11), 2418-2427.

Murillo, J. S., Osen, R., Hiermaier, S., & Ganzenmüller, G. (2019). Towards understanding the mechanism of fibrous texture formation during high-moisture extrusion of meat substitutes. *Journal of Food Engineering, 242*, 8-20.

Murray, B. S. (2007). Stabilization of bubbles and foams. *Current Opinion in Colloid & Interface Science, 12*(4-5), 232-241.

Murray, B. S. (2020). Recent developments in food foams. *Current Opinion in Colloid & Interface Science, 50*, 101394.

Naiki, H., Higuchi, K., Hosokawa, M., & Takeda, T. (1989). Fluorometric determination of amyloid fibrils in vitro using the fluorescent dye, thioflavine T. *Analytical Biochemistry, 177*(2), 244-249.

Nakajima, K., Nishioka, D., Hirao, M., So, M., Goto, Y., & Ogi, H. (2017). Drastic acceleration of fibrillation of insulin by transient cavitation bubble. *Ultrasonics Sonochemistry, 36*, 206-211.

Nakajima, K., Toda, H., Yamaguchi, K., So, M., Ikenaka, K., Mochizuki, H., Goto, Y., & Ogi, H. (2021). Half-time heat map reveals ultrasonic effects on morphology and kinetics of amyloidogenic aggregation reaction. *ACS Chemical Neuroscience, 12*(18), 3456-3466.

Napieraj, M., Brûlet, A., Lutton, E., Randrianarisoa, U., Boire, A., & Boué, F. (2022). Monitoring food structure in plant protein gels during digestion: Rheometry and Small Angle Neutron Scattering studies. *Food Structure, 32*, 100270.

Nasrabadi, M. N., Doost, A. S., & Mezzenga, R. (2021). Modification approaches of plant-based proteins to improve their techno-functionality and use in food products. *Food Hydrocolloids, 118*, 106789.

Nawaz, M. A., Singh, T. K., Stockmann, R., Jegasothy, H., & Buckow, R. (2021). Quality attributes of ultra-high temperature-treated model beverages prepared with faba bean protein concentrates. *Foods, 10*(6), 1244.

Nawaz, M. A., Tan, M., Øiseth, S., & Buckow, R. (2022). An emerging segment of functional legume-based beverages: A review. *Food Reviews International, 38*(5), 1064-1102.

Ndoye, F. T., Erabit, N., Flick, D., & Alvarez, G. (2013). In-line characterization of a whey protein aggregation process: Aggregates size and rheological measurements. *Journal of Food Engineering, 115*(1), 73-82.

Nechyporchuk, O., Belgacem, M. N., & Pignon, F. (2016). Current progress in rheology of cellulose nanofibril suspensions. *Biomacromolecules, 17*(7), 2311-2320.

Nelson, R., Sawaya, M. R., Balbirnie, M., Madsen, A. Ø., Riekel, C., Grothe, R., & Eisenberg, D. (2005). Structure of the cross-β spine of amyloid-like fibrils. *Nature, 435*(7043), 773-778.

Nicolai, T. (2019). Gelation of food protein-protein mixtures. *Advances in Colloid and Interface Science, 270*, 147-164.

Nicolai, T., & Durand, D. (2013). Controlled food protein aggregation for new functionality. *Current Opinion in Colloid & Interface Science, 18*(4), 249-256.

Nilsson, M. R. (2004). Techniques to study amyloid fibril formation in vitro. *Methods, 34*(1), 151-160.

Ningtyas, D. W., Bhandari, B., & Prakash, S. (2021). Modulating the fat globules of plant-based cream emulsion: Influence of the source of plant proteins. *Innovative Food Science & Emerging Technologies, 74*, 102852.

Ningtyas, D. W., Tam, B., Bhandari, B., & Prakash, S. (2021). Effect of different types

and concentrations of fat on the physico-chemical properties of soy protein isolate gel. *Food Hydrocolloids, 111*, 106226.

Nissen, S. H., Schmidt, J. M., Gregersen, S., Hammershøj, M., Møller, A. H., Danielsen, M., Stødkilde, L., Nebel, C., & Dalsgaard, T. K. (2021). Increased solubility and functional properties of precipitated Alfalfa protein concentrate subjected to pH shift processes. *Food Hydrocolloids, 119*, 106874.

Nivala, O., Mäkinen, O. E., Kruus, K., Nordlund, E., & Ercili-Cura, D. (2017). Structuring colloidal oat and faba bean protein particles via enzymatic modification. *Food Chemistry, 231*, 87-95.

Nivala, O., Nordlund, E., Kruus, K., & Ercili-Cura, D. (2021). The effect of heat and transglutaminase treatment on emulsifying and gelling properties of faba bean protein isolate. *LWT, 139*, 110517.

O′ Flynn, T. D., Hogan, S. A., Daly, D. F., O′ Mahony, J. A., & McCarthy, N. A. (2021). Rheological and solubility properties of soy protein isolate. *Molecules, 26*(10), 3015.

Oboroceanu, D., Wang, L., Magner, E., & Auty, M. A. (2014). Fibrillization of whey proteins improves foaming capacity and foam stability at low protein concentrations. *Journal of Food Engineering, 121*, 102-111.

Ohhashi, Y., Kihara, M., Naiki, H., & Goto, Y. (2005). Ultrasonication-induced amyloid fibril formation of β2-microglobulin. *Journal of Biological Chemistry, 280*(38), 32843-32848.

Olatunde, O. O., Hewage, A., Dissanayake, T., Aluko, R. E., Karaca, A. C., Shang, N., & Bandara, N. (2023). Cold atmospheric plasma-induced protein modification: Novel nonthermal processing technology to improve protein quality, functionality, and allergenicity reduction. *Comprehensive Reviews in Food Science and Food Safety, 22*(3), 2197-2234.

Otegui, I., Fernández-Quintela, A., Diego, A. D., Cid, C., Macarulla, M., & Partearroyo, M. (1997). Properties of spray-dried and freeze-dried faba bean protein concentrates. *International Journal of Food Science & Technology, 32*(6), 439-443.

Paciulli, M., Littardi, P., Carini, E., Paradiso, V. M., Castellino, M., & Chiavaro, E. (2020). Inulin-based emulsion filled gel as fat replacer in shortbread cookies: Effects during storage. *LWT, 133*, 109888.

Padial-Domínguez, M., Espejo-Carpio, F. J., García-Moreno, P. J., Jacobsen, C., & Guadix, E. M. (2020). Protein derived emulsifiers with antioxidant activity for stabilization of omega-3 emulsions. *Food chemistry, 329*, 127148.

Pan, X., Fang, Y., Wang, L., Xie, M., Hu, B., Zhu, Y., Zhao, E., Pei, F., Shen, F., & Li, P. (2019). Effect of enzyme types on the stability of oil-in-water emulsions formed with rice protein hydrolysates. *Journal of the Science of Food and Agriculture, 99*(15), 6731-6740.

Pang, S., Shao, P., Sun, Q., Pu, C., & Tang, W. (2020). Relationship between the emulsifying properties and formation time of rice bran protein fibrils. *LWT, 122*, 108985.

Patel, A. R. (2017). *Edible oil structuring*: Royal Society of Chemistry.

Pathak, R., Bhangu, S. K., Martin, G. J., Separovic, F., & Ashokkumar, M. (2022). Ultrasound-induced protein restructuring and ordered aggregation to form amyloid crystals. *European Biophysics Journal, 51*(4-5), 335-352.

Peng, J., Calabrese, V., Veen, S. J., Versluis, P., Velikov, K. P., Venema, P., & van der Linden, E. (2018). Rheology and microstructure of dispersions of protein fibrils

and cellulose microfibrils. *Food Hydrocolloids, 82*, 196-208.

Peng, W., Kong, X., Chen, Y., Zhang, C., Yang, Y., & Hua, Y. (2016). Effects of heat treatment on the emulsifying properties of pea proteins. *Food Hydrocolloids, 52*, 301-310.

Penha, C. B., Santos, V. D. P., Speranza, P., & Kurozawa, L. E. (2021). Plant-based beverages: Ecofriendly technologies in the production process. *Innovative Food Science & Emerging Technologies, 72*, 102760.

Péron, N., Mészáros, R., Varga, I., & Gilányi, T. (2007). Competitive adsorption of sodium dodecyl sulfate and polyethylene oxide at the air/water interface. *Journal of Colloid and Interface Science, 313*(2), 389-397.

Phoon, P. Y., San Martin-Gonzalez, M. F., & Narsimhan, G. (2014). Effect of hydrolysis of soy β-conglycinin on the oxidative stability of O/W emulsions. *Food Hydrocolloids, 35*, 429-443.

Pickering, S. U. (1907). Cxcvi.—emulsions. *Journal of the Chemical Society, Transactions, 91*, 2001-2021.

Pogostin, B. H., Linse, S., & Olsson, U. (2019). Fibril charge affects α-synuclein hydrogel rheological properties. *Langmuir, 35*(50), 16536-16544.

Priyadarshini, A., Tiwari, B. K., & Rajauria, G. (2022). Assessing the environmental and economic sustainability of functional food ingredient production process. *Processes, 10*(3), 445.

Promeyrat, A., Bax, M.-L., Traore, S., Aubry, L., Santé-Lhoutellier, V., & Gatellier, P. (2010). Changed dynamics in myofibrillar protein aggregation as a consequence of heating time and temperature. *Meat Science, 85*(4), 625-631.

Queirós, R. P., Saraiva, J. A., & da Silva, J. A. L. (2018). Tailoring structure and technological properties of plant proteins using high hydrostatic pressure. *Critical Reviews in Food Science and Nutrition, 58*(9), 1538-1556.

Rahate, K. A., Madhumita, M., & Prabhakar, P. K. (2021). Nutritional composition, anti-nutritional factors, pretreatments-cum-processing impact and food formulation potential of faba bean (Vicia faba L.): A comprehensive review. *Lwt, 138*, 110796.

Rahman, M. M., Hojilla-Evangelista, M. P., & Lamsal, B. P. (2022). Impact of high-power sonication on yield, molecular structure, and functional properties of soy protein isolate. *Innovative Food Science & Emerging Technologies, 79*, 103034.

Rao, A., Shallo, H., Ericson, A., & Thomas, R. (2002). Characterization of soy protein concentrate produced by membrane ultrafiltration. *Journal of Food Science, 67*(4), 1412-1418.

Relucenti, M., Familiari, G., Donfrancesco, O., Taurino, M., Li, X., Chen, R., Artini, M., Papa, R., & Selan, L. (2021). Microscopy methods for biofilm imaging: focus on SEM and VP-SEM pros and cons. *Biology, 10*(1), 51.

Rezvani, F., Abbasi, H., & Nourani, M. (2020). Effects of protein–polysaccharide interactions on the physical and textural characteristics of low-fat whipped cream. *Journal of Food Processing and Preservation, 44*(10), e14743.

Rigacci, S., Bucciantini, M., Relini, A., Pesce, A., Gliozzi, A., Berti, A., & Stefani, M. (2008). The (1–63) region of the p53 transactivation domain aggregates in vitro into cytotoxic amyloid assemblies. *Biophysical journal, 94*(9), 3635-3646.

Riha III, W. E., Izzo, H. V., Zhang, J., & Ho, C. T. (1996). Nonenzymatic deamidation of food proteins. *Critical Reviews in Food Science & Nutrition, 36*(3), 225-255.

Rodriguez, L. M. D. L., Hemar, Y., Cornish, J., & Brimble, M. A. (2016). Structure–mechanical property correlations of hydrogel forming β-sheet peptides.

Chemical Society Reviews, 45(17), 4797-4824.

Rojas, A., Liwo, A., Browne, D., & Scheraga, H. A. (2010). Mechanism of fiber assembly: treatment of Aβ peptide aggregation with a coarse-grained united-residue force field. *Journal of Molecular Biology, 404*(3), 537-552.

Rojas, M. L., Kubo, M. T., Miano, A. C., & Augusto, P. E. (2022). Ultrasound processing to enhance the functionality of plant-based beverages and proteins. *Current Opinion in Food Science, 48*, 100939.

Rosa-Sibakov, N., Heiniö, R.-L., Cassan, D., Holopainen-Mantila, U., Micard, V., Lantto, R., & Sozer, N. (2016). Effect of bioprocessing and fractionation on the structural, textural and sensory properties of gluten-free faba bean pasta. *LWT, 67*, 27-36.

Ross-Murphy, S. B. (1994). *Physical techniques for the study of food biopolymers*: Springer Science & Business Media.

Rubinov, B., Wagner, N., Matmor, M., Regev, O., Ashkenasy, N., & Ashkenasy, G. (2012). Transient fibril structures facilitating nonenzymatic self-replication. *ACS Nano, 6*(9), 7893-7901.

Ruggeri, F. S., Charmet, J., Kartanas, T., Peter, Q., Chia, S., Habchi, J., Dobson, C. M., Vendruscolo, M., & Knowles, T. P. (2018). Microfluidic deposition for resolving single-molecule protein architecture and heterogeneity. *Nature Communications, 9*(1), 1-12.

Ryan, K. N., & Foegeding, E. A. (2015). Formation of soluble whey protein aggregates and their stability in beverages. *Food Hydrocolloids, 43*, 265-274.

Samaei, S. P., Ghorbani, M., Tagliazucchi, D., Martini, S., Gotti, R., Themelis, T., Tesini, F., Gianotti, A., Toschi, T. G., & Babini, E. (2020). Functional, nutritional, antioxidant, sensory properties and comparative peptidomic profile of faba bean (Vicia faba, L.) seed protein hydrolysates and fortified apple juice. *Food Chemistry, 330*, 127120.

Sari, Y. W., Mulder, W. J., Sanders, J. P., & Bruins, M. E. (2015). Towards plant protein refinery: review on protein extraction using alkali and potential enzymatic assistance. *Biotechnology Journal, 10*(8), 1138-1157.

Sarkar, A., Kamaruddin, H., Bentley, A., & Wang, S. (2016). Emulsion stabilization by tomato seed protein isolate: Influence of pH, ionic strength and thermal treatment. *Food Hydrocolloids, 57*, 160-168.

Schlegel, K., Leidigkeit, A., Eisner, P., & Schweiggert-Weisz, U. (2019). Technofunctional and sensory properties of fermented lupin protein isolates. *Foods, 8*(12), 678.

Schmelter, L., Rohm, H., & Struck, S. (2021). Gluten-free bakery products: Cookies made from different Vicia faba bean varieties. *Future Foods, 4*, 100038.

Schmitt, C., Bovetto, L., Buczkowski, J., Reis, G. D. O., Pibarot, P., Amagliani, L., & Dombrowski, J. (2021). Plant proteins and their colloidal state. *Current Opinion in Colloid & Interface Science, 56*, 101510.

Schmitt, C., & Wanasundara, J. P. (2024). Functionality of plant proteins and importance of aggregation state. In *Functionality of Plant Proteins* (pp. 47-66): Elsevier.

Schwenke, K. (2001). Reflections about the functional potential of legume proteins A Review. *Food/Nahrung, 45*(6), 377-381.

Scurlock, P. G. (1986). Production of cream from ultrafiltered milk. *Journal of Dairy Research, 53*(3), 431-438.

Sethi, S., Tyagi, S. K., & Anurag, R. K. (2016). Plant-based milk alternatives an

emerging segment of functional beverages: a review. *Journal of Food Science and Technology, 53*, 3408-3423.

Shahbal, N., Jing, X., Bhandari, B., Dayananda, B., & Prakash, S. (2023). Effect of enzymatic hydrolysis on solubility and surface properties of pea, rice, hemp, and oat proteins: implication on high protein concentrations. *Food Bioscience, 53*, 102515.

Shahbazi, M., Jäger, H., Ahmadi, S. J., & Lacroix, M. (2020). Electron beam crosslinking of alginate/nanoclay ink to improve functional properties of 3D printed hydrogel for removing heavy metal ions. *Carbohydrate Polymers, 240*, 116211.

Shahbazi, M., Jäger, H., Chen, J., & Ettelaie, R. (2021). Construction of 3D printed reduced-fat meat analogue by emulsion gels. Part II: Printing performance, thermal, tribological, and dynamic sensory characterization of printed objects. *Food Hydrocolloids, 121*, 107054.

Shao, J., Peng, D., Yang, J., Huang, F., Jin, W., Xiao, J., Sun, S., Li, F., Li, T., & Deng, Q. (2024). Improvement of foaming and emulsifying properties of SPI via weak-base synchronized membrane separation: Insight from tuning the interfacial flexibility. *Food Hydrocolloids, 154*, 110110.

Sharif, H. R., Williams, P. A., Sharif, M. K., Abbas, S., Majeed, H., Masamba, K. G., Safdar, W., & Zhong, F. (2018). Current progress in the utilization of native and modified legume proteins as emulsifiers and encapsulants–A review. *Food Hydrocolloids, 76*, 2-16.

Shen, Y., Du, Z., Wu, X., & Li, Y. (2022). Modulating molecular interactions in pea protein to improve its functional properties. *Journal of Agriculture and Food Research, 8*, 100313.

Shen, Y., & Li, Y. (2021). Acylation modification and/or guar gum conjugation enhanced functional properties of pea protein isolate. *Food Hydrocolloids, 117*, 106686.

Shiferaw Terefe, N., & Augustin, M. A. (2020). Fermentation for tailoring the technological and health related functionality of food products. *Critical Reviews in Food Science and Nutrition, 60*(17), 2887-2913.

Shin, J.-A., Hong, Y.-J., & Lee, K.-T. (2021). Development and physicochemical properties of low saturation alternative fat for whipping cream. *Molecules, 26*(15), 4586.

Shirsath, S., Sonawane, S., & Gogate, P. (2012). Intensification of extraction of natural products using ultrasonic irradiations—A review of current status. *Chemical Engineering and Processing: Process Intensification, 53*, 10-23.

Singh, T. P., Siddiqi, R. A., & Sogi, D. S. (2019). Statistical optimization of enzymatic hydrolysis of rice bran protein concentrate for enhanced hydrolysate production by papain. *LWT, 99*, 77-83.

Singhal, A., Karaca, A. C., Tyler, R., & Nickerson, M. (2016). Pulse proteins: from processing to structure-function relationships. *Grain Legumes, 55*.

Singhania, R. R., Patel, A. K., Soccol, C. R., & Pandey, A. (2009). Recent advances in solid-state fermentation. *Biochemical Engineering Journal, 44*(1), 13-18.

So, M., Yagi, H., Sakurai, K., Ogi, H., Naiki, H., & Goto, Y. (2011). Ultrasonication-dependent acceleration of amyloid fibril formation. *Journal of Molecular Biology, 412*(4), 568-577.

Speroni, F., Beaumal, V., de Lamballerie, M., Anton, M., Añón, M., & Puppo, M. (2009). Gelation of soybean proteins induced by sequential high-pressure and thermal

treatments. *Food Hydrocolloids, 23*(5), 1433-1442.

Spiegel, T., & Huss, M. (2002). Whey protein aggregation under shear conditions–effects of pH-value and removal of calcium. *International Journal of Food Science & Technology, 37*(5), 559-568.

Sponton, O. E., Perez, A. A., Ramel, J. V., & Santiago, L. G. (2017). Protein nanovehicles produced from egg white. Part 1: Effect of pH and heat treatment time on particle size and binding capacity. *Food Hydrocolloids, 73*, 67-73.

Stanley, C. B., Perevozchikova, T., & Berthelier, V. (2011). Structural formation of huntingtin exon 1 aggregates probed by small-angle neutron scattering. *Biophysical Journal, 100*(10), 2504-2512.

Stanley, D., Goff, H., & Smith, A. (1996). Texture-structure relationships in foamed dairy emulsions. *Food Research International, 29*(1), 1-13.

Stathopulos, P. B., Scholz, G. A., Hwang, Y. M., Rumfeldt, J. A., Lepock, J. R., & Meiering, E. M. (2004). Sonication of proteins causes formation of aggregates that resemble amyloid. *Protein Science, 13*(11), 3017-3027.

Stryer, L. (1965). The interaction of a naphthalene dye with apomyoglobin and apohemoglobin: a fluorescent probe of non-polar binding sites. *Journal of Molecular Biology, 13*(2), 482-495.

Su, J., Ma, Q., Cai, Y., Li, H., Yuan, F., Ren, F., Wang, P., & Van der Meeren, P. (2023). Incorporating surfactants within protein-polysaccharide hybrid particles for high internal phase emulsions (HIPEs): Toward plant-based mayonnaise. *Food Hydrocolloids, 136*, 108211.

Su, Y., Jiang, L., Chen, D., Yu, H., Yang, F., Guo, Y., Xie, Y., & Yao, W. (2022). In vitro and in silico approaches to investigate antimicrobial and biofilm removal efficacies of combined ultrasonic and mild thermal treatment against Pseudomonas fluorescens. *Ultrasonics Sonochemistry, 83*, 105930.

Sun, C., Fu, J., Tan, Z., Zhang, G., Xu, X., & Song, L. (2022). Improved thermal and oxidation stabilities of pickering high internal phase emulsions stabilized using glycated pea protein isolate with glycation extent. *LWT, 162*, 113465.

Sun, C., & Gunasekaran, S. (2009). Effects of protein concentration and oil-phase volume fraction on the stability and rheology of menhaden oil-in-water emulsions stabilized by whey protein isolate with xanthan gum. *Food Hydrocolloids, 23*(1), 165-174.

Sun, C., Wang, C., Xiong, Z., & Fang, Y. (2021). Properties of binary complexes of whey protein fibril and gum arabic and their functions of stabilizing emulsions and simulating mayonnaise. *Innovative Food Science & Emerging Technologies, 68*, 102609.

Sun, W., Zhou, F., Zhao, M., Yang, B., & Cui, C. (2011). Physicochemical changes of myofibrillar proteins during processing of Cantonese sausage in relation to their aggregation behaviour and in vitro digestibility. *Food Chemistry, 129*(2), 472-478.

Suriboot, J., Marmo, A. C., Ngo, B. K. D., Nigam, A., Ortiz-Acosta, D., Tai, B. L., & Grunlan, M. A. (2021). Amphiphilic, thixotropic additives for extrusion-based 3D printing of silica-reinforced silicone. *Soft Matter, 17*(15), 4133-4142.

Szczesniak, A. S. (2002). Texture is a sensory property. *Food Quality and Preference, 13*(4), 215-225.

Tadros, T. F. (1994). Fundamental principles of emulsion rheology and their applications. *Colloids and Surfaces A: Physicochemical and Engineering Aspects, 91*, 39-55.

Taha, A., Hu, T., Zhang, Z., Bakry, A. M., Khalifa, I., Pan, S., & Hu, H. (2018). Effect of different oils and ultrasound emulsification conditions on the physicochemical properties of emulsions stabilized by soy protein isolate. *Ultrasonics Sonochemistry, 49*, 283-293.

Tamang, N., Shrestha, P., Khadka, B., Mondal, M. H., Saha, B., & Bhattarai, A. (2021). A review of biopolymers' utility as emulsion stabilizers. *Polymers, 14*(1), 127.

Tan, M., Nawaz, M. A., & Buckow, R. (2023). Functional and food application of plant proteins–a review. *Food Reviews International, 39*(5), 2428-2456.

Tang, C.-H. (2020a). Globular proteins as soft particles for stabilizing emulsions: Concepts and strategies. *Food Hydrocolloids, 103*, 105664.

Tang, C. (2020b). Globular proteins as soft particles for stabilizing emulsions: Concepts and strategies. *Food Hydrocolloids, 103*, 105664.

Tang, C., & Liu, F. (2013). Cold, gel-like soy protein emulsions by microfluidization: Emulsion characteristics, rheological and microstructural properties, and gelling mechanism. *Food Hydrocolloids, 30*(1), 61-72.

Tang, C., Wang, S., & Huang, Q. (2012). Improvement of heat-induced fibril assembly of soy β-conglycinin (7S Globulins) at pH 2.0 through electrostatic screening. *Food Research International, 46*(1), 229-236.

Tang, Q., Roos, Y. H., & Miao, S. (2024). Structure, gelation mechanism of plant proteins versus dairy proteins and evolving modification strategies. *Trends in Food Science & Technology*, 104464.

Tang, Q., Roos, Y. H., Vahedikia, N., & Miao, S. (2024). Evaluation on pH-dependent thermal gelation performance of chickpea, pea protein, and casein micelles. *Food Hydrocolloids, 149*, 109618.

Tang, Y., Stone, A., Wang, Y., Zhou, L., Kimmel, J., House, J., & Nickerson, M. (2023). Effect of a pH shift treatment on the functional properties of individual and blended commercial plant protein ingredients. *European Food Research and Technology, 249*(8), 1969-1977.

Tang, Y. R., & Ghosh, S. (2021). Stability and rheology of canola protein isolate-stabilized concentrated oil-in-water emulsions. *Food Hydrocolloids, 113*, 106399.

Tang, Z. X., Ying, R. F., & Shi, L. E. (2021). Physicochemical and functional characteristics of proteins treated by a pH-shift process: a review. *International Journal of Food Science & Technology, 56*(2), 515-529.

Tanger, C., Mertens, J., & Kulozik, U. (2022). Influence of extraction method on the aggregation of pea protein during thermo-mechanical treatment. *Food Hydrocolloids, 127*, 107514.

Tanger, C., Quintana Ramos, P., & Kulozik, U. (2021). Comparative assessment of thermal aggregation of whey, potato, and pea protein under shear stress for microparticulation. *ACS Food Science & Technology, 1*(5), 975-985.

Tanger, C., Schmidt, F., Utz, F., Kreissl, J., Dawid, C., & Kulozik, U. (2021). Pea protein microparticulation using extrusion cooking: Influence of extrusion parameters and drying on microparticle characteristics and sensory by application in a model milk dessert. *Innovative Food Science & Emerging Technologies, 74*, 102851.

Tao, H., Lu, F., Zhu, X.-F., Wang, H.-L., & Xu, X.-M. (2023). Freezing-induced loss of wheat starch granule-associated proteins affected dough quality: From water distribution, rheological properties, microstructure, and gluten development. *Journal of Cereal Science, 109*, 103606.

Tcholakova, S., Lesov, I., Golemanov, K., Denkov, N. D., Judat, S., Engel, R., & Danner, T. (2011). Efficient emulsification of viscous oils at high drop volume fraction. *Langmuir, 27*(24), 14783-14796.

Tian, T., Liu, S., Li, L., Wang, S., Cheng, L., Feng, J., Wang, Z., Tong, X., Wang, H., & Jiang, L. (2023). Soy protein fibrils–β-carotene interaction mechanisms: Toward high nutrient plant-based mayonnaise. *LWT, 184*, 114870.

Tranter, G. (2017). Protein structure analysis by CD, FTIR, and Raman spectroscopies. *Mol Sci Chem Eng*(12).

Tungland, B., & Meyer, D. (2002). Nondigestible oligo-and polysaccharides (Dietary Fiber): their physiology and role in human health and food. *Comprehensive Reviews in Food Science and Food Safety, 1*(3), 90-109.

Velez-Erazo, E. M., Bosqui, K., Rabelo, R. S., Kurozawa, L. E., & Hubinger, M. D. (2020). High internal phase emulsions (HIPE) using pea protein and different polysaccharides as stabilizers. *Food Hydrocolloids, 105*, 105775.

Verkade, P. (2012). Electron Microscopy (TEM and SEM). *Essential Guide to Reading Biomedical Papers: Recognising and Interpreting Best Practice*, 59-65.

Veronika, H., & Samantha, B. (2021). Plant-based foods market to hit $162 billion in next decade, projects bloomberg intelligence. In: Bloomberg Intelligence.

Viejo, C. G., Harris, N., & Fuentes, S. (2024). Assessment of changes in sensory perception, biometrics and emotional response for space exploration by simulating microgravity positions. *Food Research International, 175*, 113827.

Villamiel, M., & de Jong, P. (2000). Influence of high-intensity ultrasound and heat treatment in continuous flow on fat, proteins, and native enzymes of milk. *Journal of Agricultural and Food Chemistry, 48*(2), 472-478.

Villarino, C. B. J., Jayasena, V., Coorey, R., Chakrabarti-Bell, S., & Johnson, S. K. (2016). Nutritional, health, and technological functionality of lupin flour addition to bread and other baked products: Benefits and challenges. *Critical Reviews in Food Science and Nutrition, 56*(5), 835-857.

Visser, D., Loo, T., Norris, G., & Parry, D. A. (2023). Potential implications of the glycosylation patterns in collagen α1 (I) and α2 (I) chains for fibril assembly and growth. *Journal of Structural Biology, 215*(1), 107938.

Vogelsang-O'Dwyer, M., Petersen, I. L., Joehnke, M. S., Sørensen, J. C., Bez, J., Detzel, A., Busch, M., Krueger, M., O'Mahony, J. A., & Arendt, E. K. (2020). Comparison of Faba bean protein ingredients produced using dry fractionation and isoelectric precipitation: Techno-functional, nutritional and environmental performance. *Foods, 9*(3), 322.

Voutsinas, L. P., Cheung, E., & Nakai, S. (1983). Relationships of hydrophobicity to emulsifying properties of heat denatured proteins. *Journal of Food Science, 48*(1), 26-32.

Wang, C., Guan, X., Sang, J., Zhou, J., Wang, C., Ngai, T., & Lin, W. (2023). General liquid vegetable oil structuring via high internal phase Pickering emulsion stabilized by soy protein isolate nanoparticles. *Journal of Food Engineering, 356*, 111595.

Wang, M.-P., Chen, X.-W., Guo, J., Yang, J., Wang, J.-M., & Yang, X.-Q. (2019). Stabilization of foam and emulsion by subcritical water-treated soy protein: Effect of aggregation state. *Food Hydrocolloids, 87*, 619-628.

Wang, P., Chen, C., Guo, H., Zhang, H., Yang, Z., & Ren, F. (2018). Casein gel particles as novel soft Pickering stabilizers: The emulsifying property and packing behaviour at the oil-water interface. *Food Hydrocolloids, 77*, 689-698.

Wang, S., Xie, Y., Ding, Y., Huo, Z., Li, J., Song, J., Huo, Y., Zhao, L., Zhang, J., & Wang, S. (2023). Fibrillation of whey protein isolate by radio frequency heating for process efficiency: Assembly behavior, structural characteristics, and in-vitro digestion. *Innovative Food Science & Emerging Technologies, 88*, 103436.

Wang, X., Cheng, L., Wang, H., & Yang, Z. (2022). Limited Alcalase hydrolysis improves the thermally-induced gelation of quinoa protein isolate (QPI) dispersions. *Current Research in Food Science, 5*, 2061-2069.

Wang, X., Ma, D., Liu, Y., Wang, Y., Qiu, C., & Wang, Y. (2022). Physical properties of oleogels fabricated by the combination of diacylglycerols and monoacylglycerols. *Journal of the American Oil Chemists' Society, 99*(11), 1007-1018.

Wang, X., Tang, C., Li, B., Yang, X., Li, L., & Ma, C. (2008). Effects of high-pressure treatment on some physicochemical and functional properties of soy protein isolates. *Food Hydrocolloids, 22*(4), 560-567.

Wang, Y., Hartel, R. W., & Zhang, L. (2021). The stability of aerated emulsions: Effects of emulsifier synergy on partial coalescence and crystallization of milk fat. *Journal of Food Engineering, 291*, 110257.

Wang, Y., Li, S., Zaheer, A., & Song, Q. (2010). Extraction of broad bean protein and effects of NaCl concentration and pH value on its solubility and emulsibility. *Transactions of the Chinese Society of Agricultural Engineering, 26*(1), 380-384.

Wang, Y., Shen, Y., Qi, G., Li, Y., Sun, X. S., Qiu, D., & Li, Y. (2020). Formation and physicochemical properties of amyloid fibrils from soy protein. *International Journal of Biological Macromolecules, 149*, 609-616.

Wang, Z., Li, Y., Jiang, L., Qi, B., & Zhou, L. (2014). Relationship between secondary structure and surface hydrophobicity of soybean protein isolate subjected to heat treatment. *Journal of Chemistry, 2014*.

Wei, L., Song, K., Shao, D., Dong, C., Wang, L., & Jiang, J. (2023). The effect of endogenous phenol and gallic acid on structure and functionalities of mung bean protein in aerated emulsion system. *Food Hydrocolloids, 143*, 108942.

Wei, Z., Cheng, J., & Huang, Q. (2019). Food-grade Pickering emulsions stabilized by ovotransferrin fibrils. *Food Hydrocolloids, 94*, 592-602.

Wei, Z., & Huang, Q. (2020). Impact of covalent or non-covalent bound epigallocatechin-3-gallate (EGCG) on assembly, physicochemical characteristics and digestion of ovotransferrin fibrils. *Food Hydrocolloids, 98*, 105314.

Wen, C., Zhang, J., Yao, H., Zhou, J., Duan, Y., Zhang, H., & Ma, H. (2019). Advances in renewable plant-derived protein source: The structure, physicochemical properties affected by ultrasonication. *Ultrasonics Sonochemistry, 53*, 83-98.

White, D., Fisk, I., Mitchell, J., Wolf, B., Hill, S., & Gray, D. (2008). Sunflower-seed oil body emulsions: rheology and stability assessment of a natural emulsion. *Food Hydrocolloids, 22*(7), 1224-1232.

Willett, W., Rockström, J., Loken, B., Springmann, M., Lang, T., Vermeulen, S., Garnett, T., Tilman, D., DeClerck, F., & Wood, A. (2019). Food in the Anthropocene: the EAT–Lancet Commission on healthy diets from sustainable food systems. *The Lancet, 393*(10170), 447-492.

Wittek, P., Walther, G., Karbstein, H. P., & Emin, M. A. (2021). Comparison of the rheological properties of plant proteins from various sources for extrusion applications. *Foods, 10*(8), 1700.

Wood, J., & Enser, M. (2017). Manipulating the fatty acid composition of meat to improve nutritional value and meat quality. *New Aspects of Meat Quality*, 501-535.

Wood, K., Mata, J. P., Garvey, C. J., Wu, C.-M., Hamilton, W. A., Abbeywick, P., Bartlett, D., Bartsch, F., Baxter, P., & Booth, N. (2018). QUOKKA, the pinhole small-angle neutron scattering instrument at the OPAL Research Reactor, Australia: design, performance, operation and scientific highlights. *Journal of Applied Crystallography, 51*(2), 294-314.

Wouters, A. G., Rombouts, I., Fierens, E., Brijs, K., & Delcour, J. A. (2016). Relevance of the functional properties of enzymatic plant protein hydrolysates in food systems. *Comprehensive Reviews in Food Science and Food Safety, 15*(4), 786-800.

Wright, D. J., & Boulter, D. (1974). Purification and subunit structure of legumin of Vicia faba L.(broad bean). *Biochemical Journal, 141*(2), 413-418.

Wu, C., Liu, Z., Zhi, L., Jiao, B., Hu, H., Ma, X., Zhu, J., Pignitter, M., Wang, Q., & Shi, A. (2023). Effect of oil content and protein particles concentration on non-dairy whip topping based on Pickering emulsion system and their 3D printing properties. *Food Hydrocolloids, 144*, 109012.

Wu, C., Wang, T., Ren, C., Ma, W., Wu, D., Xu, X., Wang, L. S., & Du, M. (2021). Advancement of food-derived mixed protein systems: Interactions, aggregations, and functional properties. *Comprehensive Reviews in Food Science and Food Safety, 20*(1), 627-651.

Wu, G., Fanzo, J., Miller, D. D., Pingali, P., Post, M., Steiner, J. L., & Thalacker-Mercer, A. E. (2014). Production and supply of high-quality food protein for human consumption: sustainability, challenges, and innovations. *Annals of the New York Academy of Sciences, 1321*(1), 1-19.

Wu, H., Nian, Y., Liu, Y., Zhang, Y., & Hu, B. (2022). Formation of pea protein amyloid fibrils to stabilize high internal phase emulsions for encapsulation of lutein. *Journal of Functional Foods, 94*, 105110.

Wu, S., Zhang, Z., Liu, C., & Ma, T. (2023). Effect of pH-shifting and sonication-assisted treatment on properties and stability of vegetable oil-based whipped cream stabilized by kidney bean protein aggregates. *Food Hydrocolloids, 141*, 108736.

Wynnychuk, C., Jo, Y.-J., Chu, Y., & Chen, L. (2021). Long-term stable emulsions prepared from lentil protein fibrillar aggregates. *Food Structure, 29*, 100204.

Xia, N., Lu, X. X., Zheng, Z., Mu, D. D., Zhong, X. Y., Luo, S. Z., & Zhao, Y. Y. (2021). Study on preparation of acylated soy protein and stability of emulsion. *Journal of the Science of Food and Agriculture, 101*(12), 4959-4968.

Xia, W., Siu, W. K., & Sagis, L. M. (2021). Linear and non-linear rheology of heat-set soy protein gels: Effects of selective proteolysis of β-conglycinin and glycinin. *Food Hydrocolloids, 120*, 106962.

Xiang, S., Zou, H., Liu, Y., & Ruan, R. (2020). Effects of microwave heating on the protein structure, digestion properties and Maillard products of gluten. *Journal of Food Science and Technology, 57*, 2139-2149.

Xiao, J., Gonzalez, A. J. P., & Huang, Q. (2016). Kafirin nanoparticles-stabilized Pickering emulsions: Microstructure and rheological behavior. *Food Hydrocolloids, 54*, 30-39.

Xiao, J., Li, Y., & Huang, Q. (2016). Recent advances on food-grade particles stabilized Pickering emulsions: Fabrication, characterization and research trends. *Trends*

in Food Science & Technology, 55, 48-60.

Xiong, T., Xiong, W., Ge, M., Xia, J., Li, B., & Chen, Y. (2018). Effect of high intensity ultrasound on structure and foaming properties of pea protein isolate. *Food Research International, 109*, 260-267.

Xu, B., Feng, M., Chitrakar, B., Cheng, J., Wei, B., Wang, B., Zhou, C., & Ma, H. (2023). Multi-frequency power thermosonication treatments of clear strawberry juice: Impact on color, bioactive compounds, flavor volatiles, microbial and polyphenol oxidase inactivation. *Innovative Food Science & Emerging Technologies, 84*, 103295.

Xu, W., Sun, H., Jia, Y., Jia, Y., Ning, Y., Wang, Y., Jiang, L., Luo, D., & Shah, B. R. (2023). Pickering emulsions synergistic stabilized with konjac glucomannan and xanthan gum/lysozyme nanoparticles: Structure, protection and gastrointestinal digestion. *Carbohydrate Polymers, 305*, 120507.

Xu, X., Fan, L., & Li, J. (2024). Freeze–thaw stability of high-internal-phase emulsion stabilized by chickpea protein microgel particles and its application in surimi. *Journal of the Science of Food and Agriculture*.

Xu, Y., Ma, C.-m., Yang, Y., Bian, X., Liu, X.-f., Wang, Y., & Zhang, N. (2023). Food-derived protein amyloid-like fibrils: Fibrillation mechanism, structure, and recent advances for the stabilization of emulsions. *Food Hydrocolloids*, 109146.

Xu, Y., Tang, C., Liu, T., & Liu, R. (2018). Ovalbumin as an outstanding Pickering nanostabilizer for high internal phase emulsions. *Journal of Agricultural and Food Chemistry, 66*(33), 8795-8804.

Xu, Z., Shan, G., Hao, N., Li, L., Lan, T., Dong, Y., Wen, J., Tian, R., Zhang, Y., & Jiang, L. (2022). Structure remodeling of soy protein-derived amyloid fibrils mediated by epigallocatechin-3-gallate. *Biomaterials, 283*, 121455.

Xu, Z., Wang, X., Gao, Y., Zhang, Y., Jiang, L., & Sui, X. (2023). Structural insights into acidic heating-induced amyloid fibrils derived from soy protein as a function of protein concentration. *Food Hydrocolloids, 145*, 109085.

Yagi, H., Hasegawa, K., Yoshimura, Y., & Goto, Y. (2013). Acceleration of the depolymerization of amyloid β fibrils by ultrasonication. *Biochimica et Biophysica Acta (BBA)-Proteins and Proteomics, 1834*(12), 2480-2485.

Yakupova, E. I., Bobyleva, L. G., Vikhlyantsev, I. M., & Bobylev, A. G. (2019). Congo Red and amyloids: history and relationship. *Bioscience Reports, 39*(1), BSR20181415.

Yan, J., Zhao, S., Xu, X., & Liu, F. (2024). Enhancing pea protein isolate functionality: A comparative study of high-pressure homogenization, ultrasonic treatment, and combined processing techniques. *Current Research in Food Science, 8*, 100653.

Yan, S., Xu, J., Zhang, S., & Li, Y. (2021). Effects of flexibility and surface hydrophobicity on emulsifying properties: Ultrasound-treated soybean protein isolate. *LWT, 142*, 110881.

Yan, X., Bai, X., Liu, X., & Liu, F. (2024). Enhanced functional properties of pea protein isolate microgel particles modified with sodium alginate: Mixtures and conjugates. *Food Chemistry, 441*, 138358.

Yang, J., Duan, Y., Geng, F., Cheng, C., Wang, L., Ye, J., Zhang, H., Peng, D., & Deng, Q. (2022). Ultrasonic-assisted pH shift-induced interfacial remodeling for enhancing the emulsifying and foaming properties of perilla protein isolate. *Ultrasonics Sonochemistry, 89*, 106108.

Yang, J., Kornet, R., Ntone, E., Meijers, M. G., van den Hoek, I. A., Sagis, L. M.,

Venema, P., Meinders, M. B., Berton-Carabin, C. C., & Nikiforidis, C. V. (2024). Plant protein aggregates induced by extraction and fractionation processes: Impact on techno-functional properties. *Food Hydrocolloids*, 110223.

Yang, J., Liu, G., Zeng, H., & Chen, L. (2018). Effects of high pressure homogenization on faba bean protein aggregation in relation to solubility and interfacial properties. *Food Hydrocolloids, 83*, 275-286.

Yang, J., & Sagis, L. M. (2021). Interfacial behavior of plant proteins—novel sources and extraction methods. *Current Opinion in Colloid & Interface Science, 56*, 101499.

Yang, J., Zhu, B., Lu, K., Dou, J., Ning, Y., Wang, H., Li, Y., Qi, B., & Jiang, L. (2023). Construction and characterization of Pickering emulsions stabilized by soy protein hydrolysate microgel particles and quercetin-loaded performance in vitro digestion. *Food Research International, 169*, 112844.

Yang, J. T., Wu, C. S. C., & Martinez, H. M. (1986). Calculation of protein conformation from circular dichroism. In *Methods in Enzymology* (Vol. 130, pp. 208-269): Elsevier.

Yang, Y., Jiao, Q., Wang, L., Zhang, Y., Jiang, B., Li, D., Feng, Z., & Liu, C. (2022). Preparation and evaluation of a novel high internal phase Pickering emulsion based on whey protein isolate nanofibrils derived by hydrothermal method. *Food Hydrocolloids, 123*, 107180.

Yang, Z., & Cheng, L. (2024). Impact of ultrasound emulsification on the physicochemical properties of emulsions stabilised by quinoa protein isolates at different pHs. *Food Biophysics, 19*(1), 160-171.

Yang, Z., Cheng, L., de Campo, L., Gilbert, E. P., Mittelbach, R., Luo, L., Ye, A., Li, S., & Hemar, Y. (2023). Microstructural evolution during acid induced gelation of cow, goat, and sheep milk probed by time-resolved (ultra)-small angle neutron scattering. *Food Hydrocolloids, 137*, 108381.

Yang, Z., de Campo, L., Gilbert, E. P., Knott, R., Cheng, L., Storer, B., Lin, X., Luo, L., Patole, S., & Hemar, Y. (2022). Effect of NaCl and CaCl2 concentration on the rheological and structural characteristics of thermally-induced quinoa protein gels. *Food Hydrocolloids, 124*, 107350.

Yang, Z., Hemar, Y., Hilliou, L., Gilbert, E. P., McGillivray, D. J., Williams, M. A., & Chaieb, S. (2016). Nonlinear behavior of gelatin networks reveals a hierarchical structure. *Biomacromolecules, 17*(2), 590-600.

Yang, Z., Yang, H., & Yang, H. (2018). Effects of sucrose addition on the rheology and microstructure of κ-carrageenan gel. *Food Hydrocolloids, 75*, 164-173.

Ye, J., Deng, L., Wang, Y., McClements, D. J., Luo, S., & Liu, C. (2021). Impact of rutin on the foaming properties of soybean protein: Formation and characterization of flavonoid-protein complexes. *Food Chemistry, 362*, 130238.

Ye, X., Lendel, C., Langton, M., Olsson, R. T., & Hedenqvist, M. S. (2019). Protein nanofibrils: Preparation, properties, and possible applications in industrial nanomaterials. In *Industrial Applications of Nanomaterials* (pp. 29-63): Elsevier.

Yi, J., He, Q., Peng, G., & Fan, Y. (2022). Improved water solubility, chemical stability, antioxidant and anticancer activity of resveratrol via nanoencapsulation with pea protein nanofibrils. *Food Chemistry, 377*, 131942.

Yildiz, G., Andrade, J., Engeseth, N. E., & Feng, H. (2017). Functionalizing soy protein nano-aggregates with pH-shifting and mano-thermo-sonication. *Journal of Colloid and Interface Science, 505*, 836-846.

Yu, Z., Li, N., Liu, Y., Zhang, B., Zhang, M., Wang, X., & Wang, X. (2024). Formation, structure and functional characteristics of amyloid fibrils formed based on soy protein isolates. *International Journal of Biological Macromolecules, 254*, 127956.

Yue, J., Yao, X., Gou, Q., Li, D., Liu, N., Yang, D., Gao, Z., Midgley, A., Katsuyoshi, N., & Zhao, M. (2022). Recent advances of interfacial and rheological property based techno-functionality of food protein amyloid fibrils. *Food Hydrocolloids, 132*, 107827.

Zhang, C., Yang, Y., Zhao, X., Zhang, L., Li, Q., Wu, C., Ding, X., & Qian, J. (2021). Assessment of impact of pulsed electric field on functional, rheological and structural properties of vital wheat gluten. *LWT, 147*, 111536.

Zhang, F., Roosen-Runge, F., Skoda, M. W., Jacobs, R. M., Wolf, M., Callow, P., Frielinghaus, H., Pipich, V., Prevost, S., & Schreiber, F. (2012). Hydration and interactions in protein solutions containing concentrated electrolytes studied by small-angle scattering. *Physical Chemistry Chemical Physics, 14*(7), 2483-2493.

Zhang, J., Liu, Q., Chen, Q., Sun, F., Liu, H., & Kong, B. (2022). Synergistic modification of pea protein structure using high-intensity ultrasound and pH-shifting technology to improve solubility and emulsification. *Ultrasonics Sonochemistry, 88*, 106099.

Zhang, J., Zhao, S., Liu, Q., Chen, Q., Liu, H., & Kong, B. (2023). High internal phase emulsions stabilized by pea protein isolate modified by ultrasound and pH-shifting: Effect of chitosan self-assembled particles. *Food Hydrocolloids, 141*, 108715.

Zhang, J., Zhu, R., & Meng, Z. (2024). Whipped cream stabilized by faba bean protein isolate microgel particles substituted for sodium caseinate: Whipping performance and foam stabilization analysis. *Food Hydrocolloids*, 110388.

Zhang, J. Y., Pandya, J. K., McClements, D. J., Lu, J., & Kinchla, A. J. (2021). Advancements in 3D food printing: A comprehensive overview of properties and opportunities. *Critical Reviews in Food Science and Nutrition*, 1-18.

Zhang, J. Y., Pandya, J. K., McClements, D. J., Lu, J., & Kinchla, A. J. (2022). Advancements in 3D food printing: A comprehensive overview of properties and opportunities. *Critical Reviews in Food Science and Nutrition, 62*(17), 4752-4768.

Zhang, Q., Li, L., Lan, Q., Li, M., Wu, D., Chen, H., Liu, Y., Lin, D., Qin, W., & Zhang, Z. (2019). Protein glycosylation: A promising way to modify the functional properties and extend the application in food system. *Critical Reviews in Food Science and Nutrition, 59*(15), 2506-2533.

Zhang, R., Cheng, L., Luo, L., Hemar, Y., & Yang, Z. (2021). Formation and characterisation of high-internal-phase emulsions stabilised by high-pressure homogenised quinoa protein isolate. *Colloids and Surfaces A: Physicochemical and Engineering Aspects, 631*, 127688.

Zhang, R., Luo, L., Yang, Z., Ashokkumar, M., & Hemar, Y. (2021). Formation by high power ultrasound of aggregated emulsions stabilised with milk protein concentrate (MPC70). *Ultrasonics Sonochemistry, 81*, 105852.

Zhang, S., Holmes, M., Ettelaie, R., & Sarkar, A. (2020). Pea protein microgel particles as Pickering stabilisers of oil-in-water emulsions: Responsiveness to pH and ionic strength. *Food Hydrocolloids, 102*, 105583.

Zhang, S., Huang, W., Feizollahi, E., Roopesh, M., & Chen, L. (2021). Improvement of pea protein gelation at reduced temperature by atmospheric cold plasma and the

gelling mechanism study. *Innovative Food Science & Emerging Technologies, 67*, 102567.

Zhang, W., Taheri-Ledari, R., Ganjali, F., Mirmohammadi, S. S., Qazi, F. S., Saeidirad, M., KashtiAray, A., Zarei-Shokat, S., Tian, Y., & Maleki, A. (2023). Effects of morphology and size of nanoscale drug carriers on cellular uptake and internalization process: a review. *RSC advances, 13*(1), 80-114.

Zhang, X., Lei, Y., Luo, X., Wang, Y., Li, Y., Li, B., & Liu, S. (2021). Impact of pH on the interaction between soybean protein isolate and oxidized bacterial cellulose at oil-water interface: Dilatational rheological and emulsifying properties. *Food Hydrocolloids, 115*, 106609.

Zhang, X., Xie, W., Liang, Q., Jiang, X., Zhang, Z., & Shi, W. (2023). High inner phase emulsion of fish oil stabilized with rutin-grass carp (Ctenopharyngodon idella) myofibrillar protein: Application as a fat substitute in surimi gel. *Food Hydrocolloids, 145*, 109115.

Zhang, X., Zhang, S., Zhong, M., Qi, B., & Li, Y. (2022). Soy and whey protein isolate mixture/calcium chloride thermally induced emulsion gels: Rheological properties and digestive characteristics. *Food Chemistry, 380*, 132212.

Zhang, X., Zuo, Z., Ma, W., Yu, P., Li, T., & Wang, L. (2021). Assemble behavior of ultrasound-induced quinoa protein nanoparticles and their roles on rheological properties and stability of high internal phase emulsions. *Food Hydrocolloids, 117*, 106748.

Zhang, Y.-H., & Huang, L.-H. (2014). Effect of heat-induced formation of rice bran protein fibrils on morphological structure and physicochemical properties in solutions and gels. *Food Science and Biotechnology, 23*, 1417-1423.

Zhang, Y.-H., Huang, L.-H., & Wei, Z.-C. (2014). Effects of additional fibrils on structural and rheological properties of rice bran albumin solution and gel. *European Food Research and Technology, 239*(6), 971-978.

Zhang, Y., & Dee, D. R. (2023). Morphology, formation kinetics and core composition of pea and soy 7S and 11S globulin amyloid fibrils. *Journal of Agricultural and Food Chemistry, 71*(11), 4755-4765.

Zhang, Y., Liang, S., Zhang, J., Chi, Y., Tian, B., Li, L., Jiang, B., Li, D., Feng, Z., & Liu, C. (2020). Preparation of whey protein isolate nanofibrils by microwave heating and its application as carriers of lipophilic bioactive substances. *LWT, 125*, 109213.

Zhang, Y., Lu, Y., Zhang, R., Gao, Y., & Mao, L. (2021). Novel high internal phase emulsions with gelled oil phase: Preparation, characterization and stability evaluation. *Food Hydrocolloids, 121*, 106995.

Zhao, D., Li, L., Xu, D., Sheng, B., Qin, D., Chen, J., Li, B., & Zhang, X. (2018). Application of ultrasound pretreatment and glycation in regulating the heat-induced amyloid-like aggregation of β-lactoglobulin. *Food Hydrocolloids, 80*, 122-129.

Zhao, J., Tian, Z., & Chen, L. (2010). Effects of deamidation on structure and functional properties of barley hordein. *Journal of Agricultural and Food Chemistry, 58*(21), 11448-11455.

Zhao, L., Zhang, M., Chitrakar, B., & Adhikari, B. (2021). Recent advances in functional 3D printing of foods: A review of functions of ingredients and internal structures. *Critical Reviews in Food Science and Nutrition, 61*(21), 3489-3503.

Zhao, M., Xiong, W., Chen, B., Zhu, J., & Wang, L. (2020). Enhancing the solubility

and foam ability of rice glutelin by heat treatment at pH12: Insight into protein structure. *Food Hydrocolloids, 103*, 105626.

Zhao, Q., Kuang, W., Long, Z., Fang, M., Liu, D., Yang, B., & Zhao, M. (2013). Effect of sorbitan monostearate on the physical characteristics and whipping properties of whipped cream. *Food Chemistry, 141*(3), 1834-1840.

Zhao, R., Fu, W., Chen, Y., Li, B., Liu, S., & Li, Y. (2022). Structural modification of whey protein isolate by cinnamaldehyde and stabilization effect on β-carotene-loaded emulsions and emulsion gels. *Food Chemistry, 366*, 130602.

Zhao, W., Tang, Y., Lu, L., Chen, X., & Li, C. (2014). Pulsed electric fields processing of protein-based foods. *Food and Bioprocess Technology, 7*, 114-125.

Zhao, Y., Tian, R., Xu, Z., Jiang, L., & Sui, X. (2023). Recent advances in soy protein extraction technology. *Journal of the American Oil Chemists' Society, 100*(3), 187-195.

Zhong, Z., & Xiong, Y. L. (2020). Thermosonication-induced structural changes and solution properties of mung bean protein. *Ultrasonics Sonochemistry, 62*, 104908.

Zhou, H., Tan, Y., & McClements, D. J. (2023). Applications of the INFOGEST in vitro digestion model to foods: A review. *Annual Review of Food Science and Technology, 14*(1), 135-156.

Zhou, J., Li, T., Peydayesh, M., Usuelli, M., Lutz-Bueno, V., Teng, J., Wang, L., & Mezzenga, R. (2022). Oat plant amyloids for sustainable functional materials. *Advanced Science, 9*(4), 2104445.

Zhou, Q., Lv, S., Wang, W., Zhu, S., Xu, J., Zheng, M., Liu, Y., Zhou, Y., Sui, X., & Xiao, Y. (2024). Remodeling mechanism of gel network structure of soy protein isolate amyloid fibrils mediated by cellulose nanocrystals. *Carbohydrate Polymers*, 121919.

Zhou, X., Dong, R., & Gao, Y. (2019). Effects of pH-shifting combined with mild heating processes on structural and functional properties of broad bean protein isolates. *Food and Fermentation Industries, 45*(1), 100-108.

Zhou, Y., Smith, D., Leong, B. J., Brännström, K., Almqvist, F., & Chapman, M. R. (2012). Promiscuous cross-seeding between bacterial amyloids promotes interspecies biofilms. *Journal of Biological Chemistry, 287*(42), 35092-35103.

Zhu, L., Li, Y., Yu, J., Liu, H., Li, H., Liu, X., Chen, L., Wang, G., Liu, X., & Ding, W. (2023). Interfacial behavior and emulsifying property of thermosonication-treated soy glycinin. *LWT, 187*, 115368.

Zhu, P., Huang, W., & Chen, L. (2022). Develop and characterize thermally reversible transparent gels from pea protein isolate and study the gel formation mechanisms. *Food Hydrocolloids, 125*, 107373.

Zhu, P., Yang, J., & Chen, L. (2024). Protein–water–protein interaction: viscosity and gelation. In J. P. D. Wanasundara, C. Schmitt & B. P. Lamsal (Eds.), *Functionality of Plant Proteins* (pp. 115-150): Academic Press.

Zhu, Y. Q., Chen, X., McClements, D. J., Zou, L., & Liu, W. (2018). Pickering-stabilized emulsion gels fabricated from wheat protein nanoparticles: Effect of pH, NaCl and oil content. *Journal of Dispersion Science and Technology, 39*(6), 826-835.

Zhu, Z., Bassey, A. P., Cao, Y., Ma, Y., Huang, M., & Yang, H. (2022). Food protein aggregation and its application. *Food Research International, 160*, 111725.

Zhu, Z., Zhu, W., Yi, J., Liu, N., Cao, Y., Lu, J., Decker, E. A., & McClements, D. J. (2018). Effects of sonication on the physicochemical and functional properties

of walnut protein isolate. *Food Research International, 106*, 853-861.

Zink, J., Wyrobnik, T., Prinz, T., & Schmid, M. (2016). Physical, chemical and biochemical modifications of protein-based films and coatings: An extensive review. *International Journal of Molecular Sciences, 17*(9), 1376.

Zou, Y., Yang, X., & Scholten, E. (2018). Rheological behavior of emulsion gels stabilized by zein/tannic acid complex particles. *Food Hydrocolloids, 77*, 363-371.

Appendix

Appendix A: Permissions for reuse published articles

Permission form for reprinting **Fig.2.1A**

ELSEVIER LICENSE TERMS AND CONDITIONS	
Jan 14, 2025	
This Agreement between Yinxuan Hu ("You") and Elsevier ("Elsevier") consists of your license details and the terms and conditions provided by Elsevier and Copyright Clearance Center.	
License Number	5947471450557
License Date	Jan 14, 2025
Licensed Content Publisher	Elsevier
Licensed Content Publication	Trends in Food Science & Technology
Licensed Content Title	Structure, function and advance application of microwave-treated polysaccharide: A review
Licensed Content Author	Xianxiang Chen,Jun Yang,Mingyue Shen,Yi Chen,Qiang Yu,Jianhua Xie
Licensed Content Date	May 1, 2022
Licensed Content Volume	123
Licensed Content Issue	n/a
Licensed Content Pages	12
Start Page	198
End Page	209
Type of Use	reuse in a thesis/dissertation
Portion	figures/tables/illustrations
Number of figures/tables/illustrations	1
Format	both print and electronic
Are you the author of this Elsevier article?	No
Will you be translating?	No
Title of new work	Fabrication, characterisation, and application of functional protein aggregates derived from faba bean protein isolates
Institution name	Massey University
Expected presentation date	Mar 2025
Portions	Fig. 2.1A
The Requesting Person / Organization to Appear on the License	Yinxuan Hu
Requestor Location	Mr. YINXUAN HU 38A Schnapper Rock Road Schnapper Rock, Auckland, Auckland 0632 New Zealand
Publisher Tax ID	GB 494 6272 12

Permission form for reprinting **Fig.2.3**

ELSEVIER LICENSE TERMS AND CONDITIONS	
Jan 14, 2025	
This Agreement between Yinxuan Hu ("You") and Elsevier ("Elsevier") consists of your license details and the terms and conditions provided by Elsevier and Copyright Clearance Center.	
License Number	5947480165580
License Date	Jan 14, 2025
Licensed Content Publisher	Elsevier
Licensed Content Publication	Food Hydrocolloids
Licensed Content Title	Current insights into protein solubility: A review of its importance for alternative proteins
Licensed Content Author	Lutz Grossmann,David Julian McClements
Licensed Content Date	Apr 1, 2023
Licensed Content Volume	137
Licensed Content Issue	n/a
Licensed Content Pages	1
Start Page	108416
End Page	0
Type of Use	reuse in a thesis/dissertation
Portion	figures/tables/illustrations
Number of figures/tables/illustrations	1
Format	both print and electronic
Are you the author of this Elsevier article?	No
Will you be translating?	No
Title of new work	Fabrication, characterisation, and application of functional protein aggregates derived from faba bean protein isolates
Institution name	Massey University
Expected presentation date	Mar 2025
Portions	Fig. 2.3
The Requesting Person / Organization to Appear on the License	Yinxuan Hu
Requestor Location	Mr. YINXUAN HU 38A Schnapper Rock Road Schnapper Rock, Auckland, Auckland 0632 New Zealand
Publisher Tax ID	GB 494 6272 12

Permission form for reprinting **Fig.2.4**

ELSEVIER LICENSE TERMS AND CONDITIONS	
Jan 14, 2025	
This Agreement between Yinxuan Hu ("You") and Elsevier ("Elsevier") consists of your license details and the terms and conditions provided by Elsevier and Copyright Clearance Center.	
License Number	5947480438355
License Date	Jan 14, 2025
Licensed Content Publisher	Elsevier
Licensed Content Publication	Food Research International
Licensed Content Title	Food protein aggregation and its application
Licensed Content Author	Zongshuai Zhu,Anthony Pius Bassey,Yaqi Cao,Yanlan Ma,Ming Huang,Hongshun Yang
Licensed Content Date	Oct 1, 2022
Licensed Content Volume	160
Licensed Content Issue	n/a
Licensed Content Pages	1
Start Page	111725
End Page	0
Type of Use	reuse in a thesis/dissertation
Portion	figures/tables/illustrations
Number of figures/tables/illustrations	1
Format	both print and electronic
Are you the author of this Elsevier article?	No
Will you be translating?	No
Title of new work	Fabrication, characterisation, and application of functional protein aggregates derived from faba bean protein isolates
Institution name	Massey University
Expected presentation date	Mar 2025
Portions	Fig. 2.4
The Requesting Person / Organization to Appear on the License	Yinxuan Hu
Requestor Location	Mr. YINXUAN HU 38A Schnapper Rock Road Schnapper Rock, Auckland, Auckland 0632 New Zealand
Publisher Tax ID	GB 494 6272 12

Permission form for reprinting **Fig.2.5**

ELSEVIER LICENSE TERMS AND CONDITIONS	
Jan 14, 2025	
This Agreement between Yinxuan Hu ("You") and Elsevier ("Elsevier") consists of your license details and the terms and conditions provided by Elsevier and Copyright Clearance Center.	
License Number	5947480678576
License Date	Jan 14, 2025
Licensed Content Publisher	Elsevier
Licensed Content Publication	Current Opinion in Colloid & Interface Science
Licensed Content Title	Small-angle X-Ray and neutron scattering in food colloids
Licensed Content Author	Elliot Paul Gilbert
Licensed Content Date	Aug 1, 2019
Licensed Content Volume	42
Licensed Content Issue	n/a
Licensed Content Pages	18
Start Page	55
End Page	72
Type of Use	reuse in a thesis/dissertation
Portion	figures/tables/illustrations
Number of figures/tables/illustrations	1
Format	both print and electronic
Are you the author of this Elsevier article?	No
Will you be translating?	No
Title of new work	Fabrication, characterisation, and application of functional protein aggregates derived from faba bean protein isolates
Institution name	Massey University
Expected presentation date	Mar 2025
Portions	Fig. 2.5A
The Requesting Person / Organization to Appear on the License	Yinxuan Hu
Requestor Location	Mr. YINXUAN HU 38A Schnapper Rock Road Schnapper Rock, Auckland, Auckland 0632 New Zealand
Publisher Tax ID	GB 494 6272 12

Permission form for reprinting **Fig.2.5B**

ELSEVIER LICENSE TERMS AND CONDITIONS	
Jan 14, 2025	
This Agreement between Yinxuan Hu ("You") and Elsevier ("Elsevier") consists of your license details and the terms and conditions provided by Elsevier and Copyright Clearance Center.	
License Number	5947480944010
License Date	Jan 14, 2025
Licensed Content Publisher	Elsevier
Licensed Content Publication	Food Hydrocolloids
Licensed Content Title	Effect of NaCl and CaCl2 concentration on the rheological and structural characteristics of thermally-induced quinoa protein gels
Licensed Content Author	Zhi Yang,Liliana de Campo,Elliot Paul Gilbert,Robert Knott,Lirong Cheng,Ben Storer,Xiaoling Lin,Lan Luo,Shubham Patole,Yacine Hemar
Licensed Content Date	Mar 1, 2022
Licensed Content Volume	124
Licensed Content Issue	n/a
Licensed Content Pages	1
Start Page	107350
End Page	0
Type of Use	reuse in a thesis/dissertation
Portion	figures/tables/illustrations
Number of figures/tables/illustrations	1
Format	both print and electronic
Are you the author of this Elsevier article?	No
Will you be translating?	No
Title of new work	Fabrication, characterisation, and application of functional protein aggregates derived from faba bean protein isolates
Institution name	Massey University
Expected presentation date	Mar 2025
Portions	Fig. 2.5B
The Requesting Person / Organization to Appear on the License	Yinxuan Hu
Requestor Location	Mr. YINXUAN HU 38A Schnapper Rock Road Schnapper Rock, Auckland, Auckland 0632 New Zealand
Publisher Tax ID	GB 494 6272 12

Permission form for reprinting **Fig.2.6B**

ELSEVIER LICENSE TERMS AND CONDITIONS	
Jan 14, 2025	
This Agreement between Yinxuan Hu ("You") and Elsevier ("Elsevier") consists of your license details and the terms and conditions provided by Elsevier and Copyright Clearance Center.	
License Number	5947481072940
License Date	Jan 14, 2025
Licensed Content Publisher	Elsevier
Licensed Content Publication	Journal of Food Engineering
Licensed Content Title	Functional characterization of commercial plant proteins and their application on stabilization of emulsions
Licensed Content Author	Aurenice Maria Mota da Silva,Flavia Souza Almeida,Ana Carla Kawazoe Sato
Licensed Content Date	Mar 1, 2021
Licensed Content Volume	292
Licensed Content Issue	n/a
Licensed Content Pages	1
Start Page	110277
End Page	0
Type of Use	reuse in a thesis/dissertation
Portion	figures/tables/illustrations
Number of figures/tables/illustrations	1
Format	both print and electronic
Are you the author of this Elsevier article?	No
Will you be translating?	No
Title of new work	Fabrication, characterisation, and application of functional protein aggregates derived from faba bean protein isolates
Institution name	Massey University
Expected presentation date	Mar 2025
Portions	Fig. 2.6B
The Requesting Person / Organization to Appear on the License	Yinxuan Hu
Requestor Location	Mr. YINXUAN HU 38A Schnapper Rock Road Schnapper Rock, Auckland, Auckland 0632 New Zealand
Publisher Tax ID	GB 494 6272 12